

Loop corrections in supersymmetry

*Inclusive cross-section for slepton pair production at
hadron colliders*

Tore Klungland



Thesis submitted for the degree of
Master in Theoretical Physics
60 credits

Department of Physics
Faculty of mathematics and natural sciences

UNIVERSITY OF OSLO

Spring 2022

Loop corrections in supersymmetry

*Inclusive cross-section for slepton pair production at
hadron colliders*

Tore Klungland

© 2022 Tore Klungland

Loop corrections in supersymmetry

<http://www.duo.uio.no/>

Printed: Reprosentralen, University of Oslo

Sammendrag

I søk etter supersymmetriske partikler ved hadron-akseleratorer trengs presise teoretiske prediksjoner for produksjonstverrsnittet deres. I praksis innebærer dette at flest mulige høyere ordens effekter inkluderes, slik at avhengigheten av ufysiske parametere, og dermed den teoretiske usikkerheten, reduseres; videre vil man, ved å holde parameterene til modellen ubestemte, gjøre det mulig å gjøre et mer komplett søk over parameterrommet. Med dette som mål har vi regnet ut det inklusive tverrsnittet for slepton-parproduksjon ved hadron-akseleratorer til andre orden i kvantekromodynamikk (QCD), inkludert korreksjoner fra supersymmetriske partikler, i tillegg til å inkludere resummerte resultater til andre logaritmiske orden.

Sistnevnte er nødvendig siden kanselleringen av divergenser i perturbasjonsteori etterlater logaritmiske ledd, som kan bli store dersom gluoner med lav energi emitteres. Vi viser at ved hjelp av Wilson-linjer kan de logaritmiske bidragene resummeres, slik at de blir inkludert til alle ordener i perturbasjonsteori.

Siden slepton-parproduksjon er en ren elektrosvak prosess til første orden, viser numerisk implementasjon av beregningene en betydelig økning i tverrsnittet når QCD-effekter inkluderes. Når de resummerte bidragene legges til er økningen i tverrsnittet ikke like stor; hovedeffekten til disse bidragene er at den teoretiske usikkerheten minskes, ved at avhengigheten av ufysiske parametere reduseres.

I tillegg til resultater for tverrsnittet, sammenligner vi implementasjonen vår med standard numeriske verktøy for supersymmetri-beregninger, og demonstrerer en forbedring i både presisjon og fart. Sistnevnte er særlig verdifullt, da det muliggjør et mer effektivt søk over parameterrommet til teorien.

Abstract

In searches for supersymmetric particles at hadron colliders, high-precision theoretical predictions for their production cross-section are needed. In practice this means including as many higher-order effects as possible, to reduce the dependence upon unphysical parameters and thus the theoretical uncertainty; furthermore, by keeping the parameters of the model undetermined, one allows for a more comprehensive scan over the parameter space. To this end, we have calculated the inclusive cross-section for slepton pair production at hadron colliders, to next-to-leading order in QCD, including loop corrections from supersymmetric particles, as well as adding resummed results to the next-to-leading logarithmic order.

The latter is needed since the canceling of divergences at the next-to-leading order leaves logarithmic terms, that can grow large when low-energy, “soft” gluons are emitted. We show that by the use of Wilson lines these logarithmic contributions can be resummed, so that they are included to all orders in perturbation theory.

Since slepton pair production is purely an electroweak process at tree-level, numerical implementation of our calculations show a significant enhancement to the cross-section from including QCD effects. When adding resummed results to the fixed-order ones the increase in the cross-section is smaller; the main effect of these contributions is lowering the theoretical uncertainty by reducing the dependence upon unphysical parameters.

In addition to the cross-section results, we also compare our implementation to standard numerical tools for supersymmetry calculations, demonstrating an improvement in both precision and speed. The latter is in particular valuable, as it allows for a more efficient search of the parameter space of the theory.

Acknowledgments

First and foremost I want to thank my supervisor, Are Raklev, for his support throughout my work on this thesis. He has given me both the freedom to pursue the areas of research I find most interesting, and guidance and advice whenever needed.

I also wish to thank the rest of the “xsec” group at the Theory section at UiO for providing a welcoming and encouraging environment for these past years. I am particularly grateful to Lasse Braseth for many valuable discussions, and for his constant encouragement.

Lastly, I owe a very special thanks to my parents and the rest of my family. Working on a master’s degree during a pandemic has not always been easy, and would not have been possible without their support.

Contents

Sammendrag	i
Abstract	iii
Acknowledgments	v
Introduction	1
1 Perturbative quantum field theory	5
1.1 Standard Model	5
1.1.1 Basic principles	5
1.1.2 Yang-Mills theory	6
1.1.3 Higgs mechanism	8
1.1.4 Field content and Lagrangian	9
1.2 Regularization and renormalization	12
1.2.1 Dimensional regularization	12
1.2.2 Loop integrals in d dimensions	14
1.2.3 Renormalized perturbation theory	17
1.2.4 Renormalization schemes	19
1.2.5 The renormalization group	20
1.2.6 Renormalizability	23
1.2.7 Infrared divergences	24
1.3 Passarino-Veltman reduction	25
2 Supersymmetry	29
2.1 Superfields	29
2.1.1 Super-Poincaré algebra	29
2.1.2 Representations	31
2.2 Minimal Supersymmetric Standard Model	33
2.2.1 Supersymmetric Lagrangians	34
2.2.2 Supergauge invariance	35
2.2.3 Minimal field content	35
2.2.4 Superpotential and R -parity	37
2.2.5 Breaking supersymmetry	38
2.3 Theoretical advantages of the MSSM	39
2.3.1 Hierarchy problem	39
2.3.2 Electroweak symmetry breaking	41
2.4 Phenomenology of the MSSM	42
2.4.1 Supersymmetric particles	42

2.4.2	Slepton pair production at hadron colliders	43
3	Quantum chromodynamics	45
3.1	Structure of the $SU(3)$ gauge group	45
3.1.1	Color sums	46
3.2	Asymptotic freedom and color confinement	47
3.2.1	Renormalization of the strong coupling	47
3.2.2	Jets	50
3.3	Factorization and parton distribution functions	50
3.3.1	Integrating over PDFs	52
3.4	Renormalized PDFs	53
4	Slepton pair production in QCD	57
4.1	Kinematics and factorization	57
4.2	Leading-order cross-section	62
4.3	Standard Model corrections at NLO	63
4.3.1	Virtual loop correction	63
4.3.2	Renormalizing the virtual diagram	65
4.3.3	Real gluon emission	66
4.3.4	Real quark emission	69
4.4	Supersymmetry correction	70
4.4.1	Self-energy counterterm	73
4.5	Hadronic cross-section at NLO	75
4.6	Cross-section in Mellin space	76
4.6.1	Quark-gluon scattering	77
4.6.2	Quark-antiquark scattering	78
4.7	Resummation of large logarithms	79
4.7.1	Wilson lines and the eikonal approximation	80
4.7.2	Drell-Yan cross-section with Wilson lines	83
4.7.3	1-loop correction	84
4.7.4	Exponentiation	87
4.7.5	Resummed cross-section at NLL	87
4.7.6	Matching with fixed-order calculations	88
4.7.7	Evaluating the inverse Mellin transform	89
4.8	Generalizing to other particles	91
5	Numerical results	93
5.1	Conventions and technical details	93
5.2	Verification and comparisons	95
5.2.1	Comparisons to other sources	95
5.2.2	Inverse Mellin transform	99
5.3	Scale dependence	100
5.4	Dependence upon MSSM parameters	102
5.4.1	Final-state masses and PDF uncertainty	102
5.4.2	Mass mixing	103
5.4.3	Squark and gluino masses	105
5.4.4	Weak boson widths	107
	Conclusion	111

Appendices	113
A Dirac algebra in d dimensions	115
A.1 Contraction identities	115
A.2 Trace relations	116

Introduction

The Standard Model of particle physics is a highly successful theory, effectively describing three of the four fundamental interactions in nature from just a few starting principles — Yang-Mills theory for non-Abelian gauge symmetry [1], and the Higgs mechanism for the breaking of such symmetries [2–4]. It has been extensively tested and several important predictions of the theory have been confirmed experimentally, notably the existence of the massive weak-interaction gauge bosons W^\pm and Z , and more recently the existence of the Higgs boson, discovered at the Large Hadron Collider (LHC) in 2012 [5].

There remain, however, observed phenomena that are not explained by the theory, as well as theoretical shortcomings; for example, it provides no explanation for dark matter, for which there is strong experimental evidence; it does not include any description of gravity; the construction of the Higgs mechanism is somewhat *ad hoc*, in the sense that there is no obvious origin of the Higgs potential that leads to the breaking of the electroweak symmetry; and its couplings have Landau poles, meaning that the theory breaks down at sufficiently high or low energies.

The latter is not necessarily a problem if one considers the theory to be an effective field theory, with a completion at higher energy scales than currently experimentally accessible, but this does lead to another issue: The masses of scalar particles such as the Higgs boson are highly sensitive to corrections from particles that appear at such high energy scales. The fact that the observed Higgs boson mass is on the same scale as the other electroweak particles would then require a remarkable cancellation between terms at a far higher scale, and some significant fine-tuning of the parameters in the theory. This is known as the hierarchy problem.

All of this points towards the conclusion that the Standard Model cannot be a complete theory, and that if one wishes to approach a unified description of nature, an extension of the Standard Model is required. One possible extension is the Minimal Supersymmetric Standard Model (MSSM), in which by expanding the Poincaré symmetry group of the Standard Model to include a symmetry between bosonic and fermionic degrees of freedom, one introduces a set of new particles called *superpartners* to the Standard Model particles.

This model can potentially remedy some of the aforementioned problems of the Standard Model; if one imposes the conservation of a quantity called R -parity, which is usually done to keep the theory as consistent with experimental observations as possible, these new supersymmetric particles can only be created and destroyed in pairs. Thus the lightest supersymmetric particle is a possible dark matter candidate. The theory also gives a potential solution to the hierarchy problem, through interactions between the Higgs boson and supersymmetric particles. Furthermore, if one assumes equality of supersymmetric particle masses at some high energy scale (which would be desirable in the high-energy completion of the theory, as there is no clear origin for differing masses), the Higgs potential at the electroweak scale can automatically, by radiative corrections, take the form required to break the electroweak symmetry.

In order to test any new theory, one must compare its predictions to experimental results from particle colliders like the LHC, e.g. to look for evidence of new particles. As the experimental

precision is steadily improving, the theoretical calculations must be performed to high precision as well in order to properly compare the two. This means including higher-order contributions to the theoretical calculations; such contributions decrease the dependence on unphysical quantities like the renormalization and factorization scales, making the theoretical uncertainty smaller. In this way comparison between theory and experiment can be made more precise.

Further, as the MSSM contains a multitude of parameters that can affect its predictions, efficient numerical evaluation is necessary for a comprehensive study of the theory; thus, to implement high-precision calculations efficiently, these must be made analytical to the extent that it is possible. This also makes it more straightforward to generalize results to other processes, by avoiding simplifications that may only be valid in specific situations.

One of the simplest, and most useful, observables to study in the MSSM is the cross-section for the pair-production of sleptons, the superpartners of the Standard Model leptons, at hadron colliders. Since this process contains no strong interactions to the leading order in perturbation theory, it is a comparatively uncomplicated process to study at higher orders, but it still contains many of the same corrections as other processes involving supersymmetric particles. As a consequence, such a process makes a useful starting point in a study of the theory.

To this end, we will in this thesis calculate the cross-section for slepton pair production at the LHC to next-to-leading order in perturbation theory, using quantum chromodynamics and including loop corrections from interactions with supersymmetric particles. At fixed order in perturbation theory, the emission of soft (low-energy) gluons can lead to large logarithmic corrections; this is dealt with by expressing the soft part of the interaction in terms of geometrical objects called Wilson lines, which allows the cross-section to be resummed. Including resummed contributions is expected to further reduce the dependence on unphysical parameters, lowering the theoretical uncertainty. This in turn makes comparisons of theoretical results to data more precise, and allows one to be more stringent in excluding regions of the parameter space of the model.

We also implement our calculations numerically, to see explicitly how the aforementioned theoretical uncertainty is affected by higher order corrections and how the results depend on MSSM parameters. This also allows us to test our calculations, for both precision and speed, against some standard numerical packages, specifically RESUMMINO and PROSPINO.

The thesis is structured as follows: In Chapter 1 we briefly comment on the structure of gauge theories and the contents of the Standard Model, to make the transition to the MSSM clearer, as well as some technicalities with perturbative calculations in quantum field theory. Specifically, we discuss the regularization and renormalization techniques required to keep quantities finite, and their theoretical basis; and how the momentum integrals that appear at higher orders in perturbation theory can be categorized and kept track of using Passarino-Veltman functions.

In Chapter 2 we transition from the Standard Model to the Minimal Supersymmetric Standard Model, by first looking at the theoretical structure of supersymmetry as an extension of the Poincaré group; we then comment on the construction of the simplest possible supersymmetric theory consistent with experiments, and the new particles this gives rise to. We then discuss the phenomenology of this model; we look at the mass spectrum of the model and how the various particles can be produced and (indirectly) observed at particle colliders, focusing in particular on slepton pair production at hadron colliders.

In Chapter 3 we discuss some of the technical aspects of quantum chromodynamics (QCD) that will be relevant when studying slepton pair production at higher orders. Due to the principle of color confinement, particles with color charge are only observed in bound states called hadrons; therefore, the particles colliding at a hadron collider can be any of the constituents of the hadron, depending on probability distributions in their momenta called parton distribution functions (PDFs). This complicates QCD calculations, in particular since these distributions are determined by low-energy

strong interactions, which are not calculable perturbatively. Luckily the factorization theorems for QCD state that the short- and long-range parts of interactions essentially decouple, making it possible to extract these PDFs experimentally, while the short-range part can be calculated in perturbation theory. As we will see, this will allow us to remove some divergences, as these distributions themselves, like the various couplings in the theory, can be renormalized.

In Chapter 4, we use the theory of the previous chapters to calculate the inclusive cross-section for slepton pair production at the LHC. For completeness, and to establish the notation and structure of the calculation, we first show the calculation to leading order, before moving on to QCD corrections. The next-to-leading order (NLO) calculation is shown in detail, including the various divergences appearing and how they are dealt with. The last part of the chapter focuses on resummation as a way of dealing with the large logarithmic terms that appear in the NLO cross-section. We briefly discuss how Wilson loops can be used to represent cross-sections involving soft gluons, showing explicitly how higher order corrections can appear in this formalism. We then sketch how exponentiation of these objects can lead to a resummed expression for the logarithmic corrections, to next-to-leading logarithmic order.

In Chapter 5 we implement these results numerically for a collection of MSSM parameters. We first make some simple tests to verify the calculations, both to test the inverse Mellin transform required to evaluate the resummed results, and to compare to existing packages for supersymmetry calculations. We then investigate the effect that higher-order corrections have on how the cross-section depends on unphysical parameters, before seeing how the results depend on the various parameters appearing in the calculations.

Finally, we make our conclusions and some propositions for further work on this subject.

Chapter 1

Perturbative quantum field theory

In this chapter we review some of the general field theoretical background for the calculations to be made in the thesis. The reader is assumed to be familiar with the basics of quantum field theory (QFT), so this is not intended as a complete introduction to quantum field theory and the Standard Model (SM) from first principles; rather, we briefly review some general concepts that will become useful in later chapters.

First, we summarize the logic behind the construction of the Standard Model Lagrangian and its field content; this is mainly to be used as a reference when transitioning to supersymmetry in the next chapter, so we will only comment on the most important points.

We then move on to look at some technical aspects of perturbative quantum field theory. Higher-order corrections generically contain divergences which must be kept track of and eventually removed from observable quantities by re-defining the theory; this requires techniques called regularization and renormalization, respectively. These techniques, and the specific methods and conventions used are covered here.

We also look at a convenient method of categorizing the momentum integrals that appear, which greatly simplify the calculations, called Passarino-Veltman reduction; with this technique, exploiting the Lorentz invariant nature of the theory, the initially complicated integrals can be decomposed into generic functions that are efficiently calculable numerically.

1.1 Standard Model

To begin, we give a short summary of the logic behind the construction of the Standard Model Lagrangian. As mentioned above the reader is assumed to be acquainted with basic quantum field theory, so we will not go into concepts like quantization; a thorough introduction to the basics of QFT can be found in references like [6] or [7].

We will instead focus mainly on the content of the theory, which will be useful when later constructing the Minimal Supersymmetric Standard Model (MSSM); since this is an *extension* to the Standard Model, the MSSM Lagrangian must naturally also contain the Standard Model Lagrangian, so its construction must follow the same structure. This section will therefore make a useful reference later.

1.1.1 Basic principles

In its most basic sense, the Standard Model can be seen as a theory describing fermions, i.e. regular matter. All other fields, meaning gauge bosons and the Higgs boson, appear by necessity in the construction of the theory.

The SM Lagrangian is based on two underlying principles: Invariance under local gauge transformations in Yang-Mills theory [1], described by the gauge group

$$\mathrm{SU}(3)_C \times \mathrm{SU}(2)_L \times \mathrm{U}(1)_Y, \quad (1.1)$$

and the spontaneous breaking of one of part of this symmetry by the Higgs mechanism [2–4].

The $\mathrm{SU}(3)_C$ group describes the transformation of fermions carrying color charge, called quarks. These are arranged in so-called color triplets, and transform in the fundamental representation of the group; as we discuss in Sec. 1.1.2, demanding these transformations to be local gives rise to an octuplet of massless¹ vector gauge fields g_μ^a , referred to as gluons.

Fermions fields ψ_L with left-handed chirality, meaning that they satisfy $P_L \psi_L = \frac{1}{2}(1 - \gamma^5)\psi_L = \psi_L$, are arranged in doublets transforming in the fundamental representation of $\mathrm{SU}(2)_L$;² and all fermions carrying hypercharge Y transform under $\mathrm{U}(1)_Y$, again in the fundamental representation. Together these two form the electroweak symmetry group, and the locality of this symmetry requires in total four massive electroweak gauge bosons.

These are not the electroweak bosons we observe physically, however, as the electroweak symmetry is broken spontaneously by the introduction of a complex scalar Higgs doublet, also transforming under the electroweak group; as we will discuss in Sec. 1.1.3, the potential of this field can be constructed in such a way that the vacuum state (or any state at a sufficiently low energy scale) violates the electroweak symmetry, leaving only the familiar electromagnetic $\mathrm{U}(1)_{\mathrm{EM}}$ symmetry, under which particles with a charge $Q = T^3 + Y$ transform.³ After this symmetry breaking the electroweak bosons mix, leaving four physically observed mass eigenstates; three of them — the so-called weak bosons W^\pm and Z — are massive, while the last, the photon, is massless. This way of intertwining the observed weak and electromagnetic forces is called the Glashow [8]–Weinberg [9]–Salam [10] (GWS) theory for electroweak unification.

We will now look in some more detail at how the various terms in the Lagrangian arise from these principles.

1.1.2 Wilson lines and Yang-Mills theory

A general Lagrangian for an N -tuple of Dirac fermions ψ_i , $i = 1, 2, \dots, N$, is given by

$$\mathcal{L} = \bar{\psi}_i (i\not{\partial} - m) \psi_i, \quad (1.2)$$

where a sum over i is implicit, and $\not{\partial} \equiv \gamma^\mu \partial_\mu$. This is invariant under a global non-Abelian $\mathrm{SU}(N)$ transformation given by

$$\psi_i(x) \rightarrow \exp(i\alpha^a T^a)_{ij} \psi_j(x), \quad (1.3)$$

where T^a are group generators and α^a are constants. In a physical theory, the concept of locality — meaning that what happens at separate spacetime points is independent — is desirable. Thus we want this transformation to become local, i.e. to take $\alpha^a \rightarrow \alpha^a(x)$.

This complicates things considerably, however, as now the difference between fields ψ_i at separate spacetime points — including, significantly, the derivative — is no longer well-defined, as the fields at separate points transform differently under the gauge transformations. Explicitly, the difference between fields $\psi_i(y)$ and $\psi_i(x)$ transforms as

$$\psi_i(y) - \psi_i(x) \rightarrow \left(e^{i\alpha^a(y)T^a} \right)_{ij} \psi_j(y) - \left(e^{i\alpha^a(x)T^a} \right)_{ij} \psi_j(x). \quad (1.4)$$

¹As we will see in Sec. 1.1.2, mass terms for gauge fields are not gauge invariant, excluding them from a gauge invariant theory.

²Right-handed fields ψ_R , with $P_R \psi_R = \frac{1}{2}(1 + \gamma^5)\psi_R = \psi_R$, are $\mathrm{SU}(2)_L$ singlets.

³Here $T^3 = \frac{1}{2}\sigma^3 = \frac{1}{2}\begin{pmatrix} 1 & 0 \\ 0 & -1 \end{pmatrix}$.

We can solve this problem by the introduction of objects called Wilson lines $W_P(x, y)$.^{4,5} If these are defined to transform under the gauge transformations as

$$W_P(x, y) \rightarrow e^{i\alpha^a(x)T^a} W_P(x, y) e^{-i\alpha^a(y)T^a}, \quad (1.5)$$

they allow us to compare the fields $\psi_i(x)$ and $\psi_j(y)$ in a consistent manner, by re-defining their difference as $W_P(x, y)_{ij} \psi_j(y) - \psi_i(x)$; with this modification, both terms now transform in the same way.

Similarly, we can change the derivative in Eq. (1.2) to a *covariant derivative* D_μ , defined by

$$D_\mu \psi_i(x) \equiv \lim_{\delta x^\mu \rightarrow 0} \frac{W_P(x, x + \delta x)_{ij} \psi_j(x + \delta x) - \psi_i(x)}{\delta x^\mu}, \quad (1.6)$$

so that $D_\mu \psi_i(x) \rightarrow (e^{i\alpha^a(x)T^a})_{ij} D_\mu \psi_j(x)$.

A Wilson line connecting the points y and x by a path P can be expressed explicitly in terms of the *gauge field* $\mathbf{A}_\mu^a \equiv A_\mu^a T^a$, as

$$W_P(x, y) = P \left\{ \exp \left(ig \int_y^x A_\mu^a(z) T^a dz^\mu \right) \right\}, \quad (1.7)$$

where P is a path-ordering operator. It ensures that when Taylor expanding the exponential, the gauge field “latest” on the path, i.e. closest to the endpoint x , is always placed furthest to the left in each term. This is important in non-Abelian gauge theories as the gauge fields at different spacetime points do not in general commute; this follows from the algebra of the $SU(N)$ generators,

$$[T^a, T^b] = if^{abc} T^c, \quad (1.8)$$

where the structure constants $f^{abc} \neq 0$. The constant g in Eq. (1.7) is just a number, referred to as the coupling strength of the theory.

We now see the origin of the gauge fields in the Standard Model; they appear when we want to take covariant derivatives of fermion fields transforming under a local gauge symmetry. In fact, by Taylor expanding Eq. (1.7) and inserting it into Eq. (1.6), keeping only the linear term of the expansion since $\delta x^\mu \rightarrow 0$, we find that

$$D_\mu \psi_i(x) = \partial_\mu \psi_i(x) - ig A_\mu^a T_{ij}^a \psi_j(x), \quad (1.9)$$

meaning that \mathbf{A}_μ works as a *connection* on the geometry of gauge transformations.⁶

Since the Wilson lines transform under $SU(N)$, so do the gauge fields; by again Taylor-expanding Eq. (1.7) and inserting it into Eq. (1.5) we find that infinitesimally ($\alpha^a \ll 1$), the components of \mathbf{A}_μ transform as

$$\begin{aligned} A_\mu^a &\rightarrow A_\mu^a(x) + \frac{1}{g} \partial_\mu \alpha^a(x) - f^{abc} \alpha^b(x) A_\mu^c(x) \\ &= A_\mu^a(x) + \frac{1}{g} D_\mu \alpha^a(x), \end{aligned} \quad (1.10)$$

⁴These were originally introduced by Wilson [11] in an attempt to explain color confinement in quantum chromodynamics, as will be discussed in Chapter 3.

⁵This is not the most straightforward nor conventional approach; however, it has a nice geometrical interpretation, and introduces the concept of Wilson lines, which will be useful in Chapter 4.

⁶We will not go into much detail on this here; for more on connections and covariant derivatives, see a textbook on general relativity, e.g. Ref. [12].

where $D_\mu \alpha^a = \partial_\mu \alpha^a + g f^{abc} A_\mu^b \alpha_c$ is the covariant derivative of a field transforming in the adjoint representation. This means that while the fermions transform in the fundamental representation of $SU(N)$, the gauge bosons transform in the adjoint representation.

Note that the transformation property of the gauge field forbids any mass term $\sim m^2 \mathbf{A}^\mu \mathbf{A}_\mu$ in a gauge invariant theory, since

$$\mathbf{A}^\mu \mathbf{A}_\mu \rightarrow \mathbf{A}'^\mu \mathbf{A}'_\mu \neq \mathbf{A}^\mu \mathbf{A}_\mu, \quad (1.11)$$

under the transformations.

Abelian gauge invariance For the Abelian group $U(1)$ the analysis is mostly identical, with the obvious simplification that there is only one generator $T = \mathbb{1}$, meaning that all $f^{abc} = 0$.

1.1.3 Higgs mechanism and electroweak unification

As mentioned in Sec. 1.1.1, following the logic of the previous section, imposing $SU(2)_L \times U(1)_Y$ gauge symmetry leads to the appearance of four massless vector bosons; a triplet W_μ^a , $a = 1, 2, 3$, transforming in the adjoint representation of $SU(2)_L$, plus a single B_μ from the Abelian group. However, since we observe that three of these bosons are in fact massive, this symmetry must be broken at our energy scale.

This is done by postulating a complex, left-handed⁷ scalar doublet H with hypercharge $\frac{1}{2}$, that transforms under these gauge groups as

$$H(x) \rightarrow \exp \left(ig\alpha^a(x)\tau^a + \frac{1}{2}ig'\beta(x) \right) H(x), \quad (1.12)$$

where g and g' are $SU(2)_L$ and $U(1)_Y$ couplings, respectively, and $\tau^a \equiv \frac{1}{2}\sigma^a$, σ^a being the Pauli matrices.

The Lagrangian for this field is in general given by

$$\mathcal{L}_H = |D_\mu H|^2 - V(H), \quad (1.13)$$

with $D_\mu H = \partial_\mu H - igW_\mu^a \tau^a H - \frac{1}{2}ig'B_\mu H$. The electroweak symmetry in the vacuum state is broken by setting the Higgs potential $V(H)$ so that it has a minimum for $H \neq 0$; its value at this point is called its vacuum expectation value, or vev.

A simple choice of potential is that of complex ϕ^4 theory (with “ ϕ ” renamed to H), given by

$$V(H) = -\mu^2 H^\dagger H + \lambda (H^\dagger H)^2, \quad (1.14)$$

where μ^2 and λ can in principle take any (real) values, positive or negative. This potential has a finite minimum at non-zero field value as long as $\mu^2 > 0$ and $\lambda > 0$. The minimum is located at

$$H_0 = \frac{1}{\sqrt{2}} \begin{pmatrix} 0 \\ v \end{pmatrix}, \quad (1.15)$$

with $v = \sqrt{\mu^2/\lambda}$.⁸ Expanding H around this minimum by setting

$$H(x) = \frac{1}{\sqrt{2}} \begin{pmatrix} 0 \\ v + h(x) \end{pmatrix}, \quad (1.16)$$

⁷The Higgs field is only “left-handed” in the sense that it transforms under $SU(2)_L$ transformations; being a scalar, it does not have any relation to chirality operators like left-handed fermions do.

⁸This form of H_0 is chosen for simplicity, but without loss of generality; the potential is $SU(2)$ invariant, and we also have a $U(1)$ symmetry to remove any complex phase.

and inserting this into the $|D_\mu H|^2$ term of the Lagrangian, we find that it contains mass terms for three linear combinations of the $SU(2)_L \times U(1)_Y$ gauge bosons. These are given by [9]

$$W_\mu^\pm = \frac{1}{\sqrt{2}}(W_\mu^1 \mp iW_\mu^2), \quad (1.17)$$

with electric charge $Q = \pm 1$ and mass $m_W = \frac{1}{2}vg$; and

$$Z_\mu = \cos \theta_W W_\mu^3 - \sin \theta_W B_\mu, \quad (1.18)$$

where $\tan \theta_W \equiv g'/g$, which is electrically neutral but has mass $m_Z = m_W / \cos \theta_W$. The remaining mass eigenstate is the photon, which remains massless:

$$A_\mu = \cos \theta_W B_\mu + \sin \theta_W W_\mu^3. \quad (1.19)$$

This demonstrates the power of this theory, as it manages to describe massive gauge bosons in a gauge-invariant Lagrangian, even though mass terms for these particles are explicitly forbidden by gauge invariance. It also combines this with a description of electromagnetism, since the vacuum state retains a $U(1)_{\text{EM}}$ symmetry as we mentioned in Sec. 1.1.1; belonging to this symmetry is the photon, coupling to particles with electric charge $Q = T^3 + Y$ with the standard electromagnetic coupling strength $e = g \sin \theta_W$.

There is a catch, however, in that setting the Higgs potential so that the Higgs field obtains a vev, as in Eq. (1.14) with $\mu^2 > 0$, is arguably rather ad hoc; we typically want to describe as much of physics as possible from a single set of principles, e.g. in some high-energy Grand Unification Theory where observed phenomena at our lower energy scale follow from renormalization properties of the theory. However, there is no clear mechanism for how such a symmetry-breaking potential would arise, so we essentially have to assume that it “just happens” to have this form. In Chapter 2 we will see how this can happen automatically in the MSSM, through the renormalization of the parameters in the Higgs potential.

1.1.4 Field content and Lagrangian

Having summarized how gauge fields and the Higgs field appear in the theory as an effect of the postulated gauge symmetry and the breaking thereof, we now want to write down a Lagrangian containing all possible renormalizable terms that do not violate gauge invariance. The inclusion of every possible term can be motivated from renormalization, to be discussed in Sec. 1.2; even if the “bare” Lagrangian were missing some terms, it might get contributions from higher-order corrections.

First, we need to consider what fields are included. From experiment we have three generations of quarks and leptons; the left-handed ones are organized into $SU(2)$ doublets⁹ given by

$$L^i = \left\{ \begin{pmatrix} \nu_{eL} \\ e_L \end{pmatrix}, \begin{pmatrix} \nu_{\mu L} \\ \mu_L \end{pmatrix}, \begin{pmatrix} \nu_{\tau L} \\ \tau_L \end{pmatrix} \right\}, \quad Q^i = \left\{ \begin{pmatrix} u_L \\ d_L \end{pmatrix}, \begin{pmatrix} c_L \\ s_L \end{pmatrix}, \begin{pmatrix} t_L \\ b_L \end{pmatrix} \right\}. \quad (1.20)$$

The right-handed components are singlets under $SU(2)_L$, and are denoted by

$$\begin{aligned} \nu_R^i &= \{\nu_{eR}, \nu_{\mu R}, \nu_{\tau R}\}, & \ell_R^i &= \{e_R, \mu_R, \tau_R\}, \\ u_R^i &= \{u_R, c_R, t_R\}, & d_R^i &= \{d_R, s_R, b_R\}. \end{aligned} \quad (1.21)$$

⁹Each quark is also an $SU(3)$ color triplet, but this is left implicit as this fact does not affect anything other than the color interactions in the Lagrangian.

Table 1.1: Charges of the Standard Model fermions and Higgs field under the gauge groups. F denotes that the field transforms in the fundamental representation of the relevant group; the hypercharges Y in the last line are inferred from the electric charges by the relation $Q = T^3 + Y$.

Field	L^i	ℓ_R^i	ν_R^i	Q^i	u_R^i	d_R^i	H
$\text{SU}(3)_C$	0	0	0	F	F	F	0
$\text{SU}(2)_L$	F	0	0	F	0	0	F
$\text{U}(1)_Y$	$-\frac{1}{2}$	-1	0	$\frac{1}{6}$	$\frac{2}{3}$	$-\frac{1}{3}$	$\frac{1}{2}$

Right-handed neutrinos are not traditionally included in the Standard Model; we have included them here mainly for symmetry with the quark sector, in particular when we later in this section discuss the mixing of mass and gauge eigenstates for quarks and neutrinos. The exact properties of neutrinos remains an open question in physics; in particular whether or not they are Dirac or Majorana in nature, and the origin of their extremely low masses relative to other SM particles.

Finally there is, as we discussed in Sec. 1.1.3, the complex scalar Higgs doublet H .

A summary of the fields and their charges under the various gauge groups can be found in Tab. 1.1.

We now have all the ingredients to write down all of the kinetic terms for the fermions and Higgs field; following Sec. 1.1.2, we have (as usual, a sum over i is implicit)

$$\begin{aligned}
\mathcal{L}_k = & i\bar{Q}^i \left(\not{\partial} - ig_s \not{g}^a T^a - ig \not{W}^a \tau^a - \frac{1}{6} ig' \not{B} \right) Q^i \\
& + i\bar{u}_R^i \left(\not{\partial} - ig_s \not{g}^a T^a - \frac{2}{3} ig' \not{B} \right) u_R^i + i\bar{d}_R^i \left(\not{\partial} - ig_s \not{g}^a T^a + \frac{1}{3} ig' \not{B} \right) d_R^i \\
& + i\bar{L}^i \left(\not{\partial} - ig \not{W}^a \tau^a + \frac{1}{2} ig' \not{B} \right) L^i + i\bar{\ell}_R^i (\not{\partial} + ig' \not{B}) \ell_R^i + i\bar{\nu}_R^i \not{\partial} \nu_R^i \\
& + \left| \partial_\mu H - ig W_\mu^a \tau^a H - \frac{1}{2} ig' B_\mu H \right|^2,
\end{aligned} \tag{1.22}$$

where g_μ^a is the octet gluon field, and T^a and τ^a are the generators of $\text{SU}(3)$ and $\text{SU}(2)$, respectively, in the fundamental representation. g_s is the $\text{SU}(3)_C$ coupling.

Note the important fact that we cannot, while satisfying gauge invariance, add fermion mass terms.¹⁰ First, mass terms with same-chirality fields like $\bar{E}E$ or $\bar{e}_R e_R$ (with $E = L^1$, $e_R = \ell_R^1$) vanish. This can be seen since any chiral field satisfies $\psi_{L/R} = P_{L/R} \psi_{L/R}$, with $P_{L/R} = \frac{1}{2}(1 \mp \gamma^5)$. Then, with $P_{L/R} P_{R/L} = 0$, $(\gamma^5)^\dagger = \gamma^5$, and $\{\gamma^\mu, \gamma^5\} = 0$, we have

$$\begin{aligned}
\overline{(P_{L/R} \psi_{L/R})} P_{L/R} \psi_{L/R} &= \psi_{L/R}^\dagger P_{L/R} \gamma^0 P_{L/R} \psi_{L/R} \\
&= \bar{\psi}_{L/R} P_{R/L} P_{L/R} \psi_{L/R} = 0.
\end{aligned} \tag{1.23}$$

Meanwhile, terms like $\bar{e}_R E$ violate gauge invariance, as the left- and right-handed spinors carry different charges and thus transform differently.

What we can add instead are Yukawa terms, i.e. interactions between the Higgs field and two

¹⁰The one exception is the right-handed neutrino; since it is uncharged under all gauge groups one might include a Majorana mass term like $iM_{ij}(\nu_R^i)^T \sigma^2 \nu_R^j$, where ν_R^i is a Weyl spinor [6, p. 600]. However, since the right-handed neutrino does not couple to anything its properties, including mass terms, are not very relevant for our purposes.

fermions. The most general gauge invariant terms that can be written down are

$$\begin{aligned}\mathcal{L}_Y = & -Y_{ij}^\ell \bar{L}^i H \ell_R^j - Y_{ij}^\nu \bar{L}^i H^C \nu_R^j \\ & - Y_{ij}^d \bar{Q}^i H d_R^j - Y_{ij}^u \bar{Q}^i H^C u_R^j + \text{h.c.},\end{aligned}\quad (1.24)$$

where $H^C \equiv i\sigma^2 H^*$ is defined to keep terms SU(2) invariant. When H is expanded around its vacuum expectation value like in Sec. 1.1.3 this generates mass matrices for the fermions.

Note that the Yukawa matrices Y_{ij} are not in general diagonal; non-zero off-diagonal terms in these matrices indicate a discrepancy between the gauge interaction eigenstates and mass eigenstates. Such phenomena are indeed observed, and can be described by the CKM [13, 14] and PMNS [15] matrices for the down-type quarks (d, s, b) and neutrinos respectively. The gauge invariance can be exploited so as to keep the mass and gauge eigenstates identical for leptons and up-type quarks (u, c, t).

For the Higgs boson, masses (and self-interactions) are added easily through the potential given in Eq. (1.14):

$$\mathcal{L}_H = -V(H). \quad (1.25)$$

Finally, there remain kinetic terms for the gauge bosons. These are written in terms of field strength tensors; for a general non-Abelian gauge group like the one discussed in Sec. 1.1.2, it can be defined by¹¹

$$\mathbf{F}_{\mu\nu} \equiv \frac{i}{g}[D_\mu, D_\nu], \quad (1.26)$$

where $\mathbf{F}_{\mu\nu} = F_{\mu\nu}^a T^a$. From Eq. (1.9), its components are given by

$$F_{\mu\nu}^a = \partial_\mu A_\nu^a - \partial_\nu A_\mu^a + gf^{abc} A_\mu^b A_\nu^c. \quad (1.27)$$

For an Abelian theory, with $f^{abc} = 0$ both $F_{\mu\nu}$ and, naturally, its square $(F_{\mu\nu})^2 = F_{\mu\nu} F^{\mu\nu}$ are gauge invariant; this is not the case for non-Abelian SU(N). However, we can write down a gauge-invariant term by taking the trace in generator space, which when using properties of SU(N) generators gives

$$\text{tr}(\mathbf{F}_{\mu\nu})^2 = \frac{1}{2}(F_{\mu\nu}^a)^2, \quad (1.28)$$

with an implicit sum over a . Then, the kinetic gauge terms of the Lagrangian are given by

$$\mathcal{L}_g = -\frac{1}{4}(g_{\mu\nu}^a)^2 - \frac{1}{4}(W_{\mu\nu}^a)^2 - \frac{1}{4}(B_{\mu\nu})^2, \quad (1.29)$$

where $g_{\mu\nu}^a$, $W_{\mu\nu}^a$, and $B_{\mu\nu}$ are the SU(3), SU(2), and U(1) field strengths, respectively.

These are all the terms that are possible to add under the restriction of Lorentz invariance and renormalizability, since the latter restricts the couplings of each term to have a non-negative mass dimension (more on this in Sec. 1.2.6), and the fermionic and bosonic fields have mass dimensions $\frac{3}{2}$ and 1, respectively, while the Lagrangian has dimension 4. We could also add a term proportional to $\epsilon^{\mu\nu\alpha\beta} F_{\mu\nu}^a F_{\alpha\beta}^a$; this would, however, lead to violation of the so-called CP symmetry in the strong interactions, and this is not seen experimentally. The absence of such a term, given that we argued previously that all renormalizable terms compatible with gauge invariance should be included, is called the strong CP problem [16].

To summarize, the Standard Model Lagrangian is given by

$$\mathcal{L}_{\text{SM}} = \mathcal{L}_k + \mathcal{L}_Y + \mathcal{L}_H + \mathcal{L}_g, \quad (1.30)$$

with the various terms defined in Eqs. (1.22), (1.24), (1.25), and (1.29).

¹¹It can also be constructed from an infinitesimal *Wilson loop*, which is a Wilson line over a closed path.

1.2 Regularization and renormalization

When calculating higher-order corrections in quantum field theory, divergences are all but unavoidable. Obviously this does not invalidate the theory or make these calculations impossible, or else perturbative QFT would essentially be useless; instead they are dealt with in two steps.

The first is called regularization, which is essentially a generalization of the expression, making it analytical in every point but the physical one. An example is when a momentum integral, integrated over all momenta diverges for large momenta; one can then introduce an ultraviolet cutoff Λ . The expression will still diverge when taking the limit $\Lambda \rightarrow \infty$, which is the physically relevant case, but the regularization makes the divergence manifest and possible to deal with mathematically.

In a sense, regularization can be seen as a way of postponing the problem of the divergence, keeping track of it while performing the rest of the calculation. The hope is that eventually, another similar divergence will arise in the calculation and that the two will cancel. As we will discuss in Sec. 1.2.7, and see in practice in Chapter 4, this is often the case for infrared divergences, which appear in the low-energy limit of calculations.

Not all divergences cancel by themselves in calculations, however; in such cases, renormalization of the theory is necessary. Renormalization is a technique where one uses that the parameters in the Lagrangian are not themselves directly measurable, only physical observables such as scattering cross-sections. Thus the Lagrangian parameters can be redefined, in terms of physically measurable quantities, to absorb the divergences arising in the calculations, leaving a finite result.

For theories to be predictive, it is crucial that one can define the theory in terms of a *finite* number of parameters, each fixed by experiment, so that just a few measurements can be used to predict a potentially infinite number of observables. This is determined by a property called renormalizability; we already used this to argue which terms could be included in the Standard Model Lagrangian, and we will soon see how it is defined, as well as some technical aspects of renormalization. First, however, we introduce the method of regularization that we will be using in our later calculations.

1.2.1 Dimensional regularization

Above, we mentioned ultraviolet cutoffs as a possible method for regularization. Though this is intuitive, it is not very convenient in practice nor mathematically sound. The most naive approach, imposing a hard cutoff to only include energies $k < \Lambda$ explicitly breaks Lorentz invariance; a more sophisticated method, due to Pauli and Villars [17], is introducing unphysical particles with mass Λ , which makes results finite outside of $\Lambda \rightarrow \infty$. This cannot be used in Yang-Mills theories, however, as it includes introducing massive gauge bosons, which is forbidden by gauge invariance.

Instead, we will in the rest of this thesis be using a less intuitive, though more practical, method, called dimensional regularization (DR), as first introduced by t'Hooft and Veltman [18]. In DR, the number of spacetime dimensions is analytically continued from 4 to

$$d = 4 - 2\epsilon; \tag{1.31}$$

this makes divergences appear as poles in ϵ , typically of the form $\frac{1}{\epsilon}$ or $\frac{1}{\epsilon^2}$.

This is apparently not as well-motivated as the aforementioned regulators, as it is not immediately clear how it is related to any infrared or ultraviolet phenomena that would lead to divergences, but since it respects the symmetries of the theory it turns out to be more useful.

The motivation for this approach becomes clearer when looking at the loop integrals that generically appear in higher-order calculations; for example, the integral

$$\int \frac{d^d k}{(2\pi)^d} \frac{1}{(k^2 - \Delta + i\epsilon)^2}, \tag{1.32}$$

is divergent for $d \geq 4$, but not for $d < 4$. In other words, we can regularize this integral by setting $d = 4 - 2\epsilon$ with $\epsilon > 0$. We will discuss these integrals in more detail in Sec. 1.2.2.

Note that this is an example of an ultraviolet divergence since it appears for $d \geq 4$; by power-counting, if we use a high-energy cutoff Λ as a regulator, for large Λ it behaves as

$$\int \frac{d^d k}{(2\pi)^d} \frac{1}{(k^2 - \Delta + i\epsilon)^2} \sim \begin{cases} \Lambda^{d-4} & d \neq 4, \\ \ln \Lambda & d = 4. \end{cases} \quad (1.33)$$

Similarly, an expression is infrared divergent if it diverges for $d \leq 4$, since it will go like $1/\Lambda^{4-d}$, where Λ is now a low-energy cutoff.

To keep the action $S = \int d^d x \mathcal{L}$ dimensionless, the mass dimension of the Lagrangian must be shifted to d ; we thus need to redefine the mass dimensions of the couplings and fields of the Lagrangian. As an example, consider the Lagrangian of a non-Abelian gauge theory,

$$\mathcal{L} = -\frac{1}{4} \left(\partial_\mu A_\nu^a - \partial_\nu A_\mu^a + g f^{abc} A_\mu^b A_\nu^c \right)^2 + i \bar{\psi} (\not{\partial} - ig \not{A}^a T^a - m) \psi. \quad (1.34)$$

In order to keep $[\mathcal{L}] = d$,¹² keeping in mind that $[\partial_\mu] = [m] = 1$, we must have

$$[\psi] = \frac{d-1}{2}, \quad [A_\mu^a] = \frac{d-2}{2}, \quad [g] = \frac{4-d}{2}. \quad (1.35)$$

The latter means that the coupling has obtained dimensions, which can be cumbersome to deal with in calculations; it is therefore conventional to instead redefine the coupling by taking

$$g \rightarrow \mu^{\frac{4-d}{2}} g, \quad (1.36)$$

where μ is an arbitrary energy scale. This does have the downside of introducing an unphysical parameter into the calculations, but it can actually be useful; since it must drop out of physically observable quantities by virtue of being an unphysical quantity, imposing independence of μ upon observables can give expressions for the parameters of the theory as functions of μ . This leads to the renormalization group, as will be discussed in Sec. 1.2.5.

The scale μ can also give some measure of the uncertainty of a theoretical calculation due to truncating the perturbation series at a certain order; at this order the expression will still have some μ dependence, but the exact result must be independent of it. Thus we can use the dependence of our truncated result upon μ to get a measure of the information lost in higher orders.

This is conventionally, and somewhat absurdly, done by varying the scale between 2μ and $\mu/2$, μ being the arbitrary central scale, and defining the theoretical uncertainty as the difference between the results at the two scales. Of course, this has no connection to actual statistical uncertainties in that it has no relation to confidence levels, etc.; furthermore, this approach can drastically underestimate the higher-order contributions when they contain large couplings that were not present at the lower order, e.g. when considering QCD corrections to processes that are purely QED at the leading order. Nonetheless, as it is the standard procedure, we will do the same in our later calculations in this thesis.

The advantage, practically, of using dimensional regularization is that the algebra in the calculations is mostly unchanged, with some generalizations from 4- to d -dimensional space. Perhaps the most notable example of this is the treatment of Dirac matrices, which inevitably show up in calculations with fermions; the Dirac algebra is unchanged,

$$\{\gamma^\mu, \gamma^\nu\} = 2g^{\mu\nu} \mathbb{1}_{4 \times 4}, \quad (1.37)$$

but in d spacetime dimensions this leads to some differences in trace and contraction identities. This is covered in Appendix A.

¹²Technically this should be written as m^d , but with $\hbar = c = 1$ there are no other units than mass/energy.

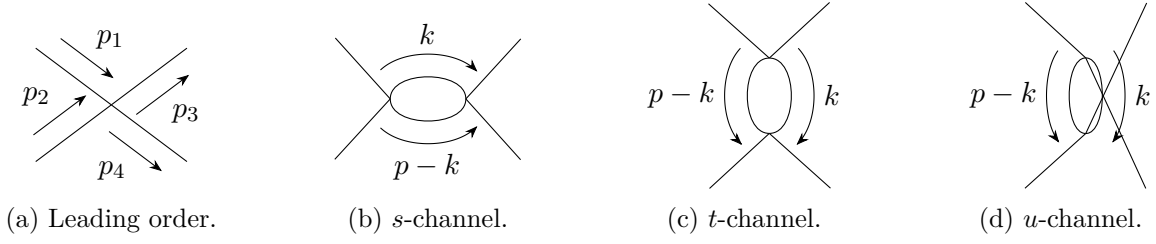


Figure 1.1: Leading order and 1-loop contributions to $2 \rightarrow 2$ scattering in scalar ϕ^4 theory. The momentum p in the loop diagrams is defined, from left to right, as $p = p_1 + p_2$, $p = p_1 - p_3$, and $p = p_1 - p_4$. The external momenta in the 1-loop diagrams are the same as at the leading order.

1.2.2 Loop integrals in d dimensions

Higher-order calculations in quantum field theory typically involve the evaluation of momentum integrals; in a Feynman diagram, all internal momenta that are not exactly determined by momentum conservation must be integrated over. The analytic continuation from 4 to d dimensions makes these slightly more complicated, but it does allow us to make the divergences manifest in ϵ , which is very useful for renormalization purposes.

To see an example of how divergences arise in these integrals, and to present some techniques for how these are solved, we will look in detail at a simple loop calculation, namely $2 \rightarrow 2$ scattering in massless, real ϕ^4 theory. The Lagrangian of such a theory is given by

$$\mathcal{L} = \frac{1}{2}(\partial_\mu \phi_0)^2 - \frac{\lambda_0}{4!}\phi_0^4, \quad (1.38)$$

written in terms of “bare” quantities ϕ_0 and λ_0 , in anticipation of the renormalization discussion to follow in the coming sections. The tree-level matrix element, shown in Fig. 1.1a, is easily evaluated to

$$i\mathcal{M}_1 = -i\lambda_0. \quad (1.39)$$

Note that we do not need to make the replacement $\lambda_0 \rightarrow \mu^{(4-d)/2}\lambda_0$ in the leading-order matrix element; as long as the matrix element is not multiplied by anything divergent, any ϵ -dependent terms will vanish in the limit $\epsilon \rightarrow 0$.

The next-to-leading order (NLO) diagrams, all shown in Fig. 1.1, all have a similar form; with the momentum p defined as either $p_1 + p_2$, $p_1 - p_3$, or $p_1 - p_4$, each of them has the form

$$i\mathcal{M}_2(p) = \mu^{4-d} \frac{(-i\lambda_0)^2}{2} \int \frac{d^d k}{(2\pi)^d} \frac{i^2}{(k^2 + i\epsilon)((p-k)^2 + i\epsilon)}. \quad (1.40)$$

The factor $1/2$ is a symmetry factor due to the bosonic nature of scalars; the two propagators in the loop can be swapped without changing the result, so we must divide by this symmetry factor to avoid double-counting identical states.

We will evaluate this momentum integral in two steps. First, we use a technique called Feynman parametrization to rewrite the integrand; this will allow us to make a change of variables, making the integrand spherically symmetric. This is done by using the identity [7]

$$\frac{1}{A_1 A_2 \cdots A_n} = \int_0^1 dx_1 \cdots dx_n \delta\left(\sum x_i - 1\right) \frac{(n-1)!}{[x_1 A_1 + x_2 A_2 + \cdots + x_n A_n]}. \quad (1.41)$$

With this, we can write the NLO matrix element as¹³

$$i\mathcal{M}_2(p) = \frac{\lambda_0^2}{2} \mu^{4-d} \int_0^1 dx \int \frac{d^d k}{(2\pi)^d} \frac{1}{D^2}, \quad (1.42)$$

where

$$\begin{aligned} D &= x((p-k)^2 + i\varepsilon) + (1-x)(k^2 + i\varepsilon) \\ &= (k-xp)^2 - \Delta + i\varepsilon, \end{aligned} \quad (1.43)$$

with $\Delta = -p^2 x(1-x)$. We can now make a variable transformation in the integral, taking $k \rightarrow k + xp$, to get

$$i\mathcal{M}_2(p) = \frac{\lambda_0^2}{2} \mu^{4-d} \int_0^1 dx \int \frac{d^d k}{(2\pi)^d} \frac{1}{(k^2 - \Delta + i\varepsilon)^2}. \quad (1.44)$$

The integral is now spherically symmetric, but still on a form that is cumbersome to evaluate, given the Lorentz signature $k^2 = (k_0)^2 - \mathbf{k}^2$. We can fix this by using our second step, called Wick rotation, wherein we use the Feynman “ $+i\varepsilon$ ” prescription of the propagators; in the complex k^0 plane, the poles of the integrand are located at

$$k_0 = \pm \sqrt{\mathbf{k}^2 + \Delta} \mp i\varepsilon. \quad (1.45)$$

Therefore, we can define a closed integration contour for k^0 where we integrate along the real axis from $-\infty$ to ∞ ; in a quarter-circle from ∞ to $i\infty$; along the imaginary axis from $i\infty$ to $-i\infty$; and in another quarter-circle from $-i\infty$ to $-\infty$. Since the integrand has no poles within this contour, the integral is zero, which again means that the integrals along the real and imaginary axes exactly cancel since the quarter-circle parts, being infinitely far away, do not contribute.

In other words, we get exactly the same result by changing the integration limits on y^0 from $(-\infty, \infty)$ to $(-i\infty, i\infty)$. We can then make a variable change to the *Euclidean* momentum $k_E = (k_E^0, \mathbf{k}_E) \equiv (-ik_0, \mathbf{k})$, so that $d^d k = i d^d k_E$ and $k^2 = -k_E^2 = -(k_E^0)^2 - \mathbf{k}_E^2$.

After changing variables our expression is on the form of a spherically symmetric integral:

$$i\mathcal{M}_2(p) = \frac{i\lambda_0^2}{2} \mu^{4-d} \int_0^1 dx \int \frac{d^d k_E}{(2\pi)^d} \frac{1}{(k_E^2 + \Delta - i\varepsilon)^2}. \quad (1.46)$$

We keep the $i\varepsilon$ regulator in the denominator even though its main purpose has been served in defining a prescription to avoid the poles in k^0 , as it will still be needed to regulate the integral over the Feynman parameter x later.

Euclidean, spherically symmetric integrals on this form are fairly straightforward to evaluate; the integration measure can be decomposed as

$$d^d k_E = d\Omega_d k_E^{d-1} dk_E, \quad (1.47)$$

with

$$d\Omega_d = \sin^{d-2} \phi_{d-1} \sin^{d-3} \phi_{d-2} \cdots \sin \phi_2 d\phi_1 \cdots d\phi_{d-1}. \quad (1.48)$$

The integration limits on the various angles are $\phi_1 \in [0, 2\pi)$, $\phi_i \in [0, \pi)$ for $i > 1$. Since the integrand only depends on the magnitude k_E , these can be integrated out by defining $x_i = \sin^2 \phi_i$

¹³We can interchange the orders of the integrations as the regularization makes the loop integral finite.

to give

$$\begin{aligned}\Omega_d &= \int d\Omega_d = 2\pi \prod_{i=2}^{d-1} \left(\int_0^\pi d\phi_i \sin^{i-1} \phi_i \right) = 2\pi \prod_{i=2}^{d-1} \left(\int_0^1 dx x^{\frac{i}{2}-1} (1-x)^{-\frac{1}{2}} \right) \\ &= 2\pi \prod_{i=2}^{d-1} \left(\frac{\Gamma(\frac{i}{2})\Gamma(\frac{1}{2})}{\Gamma(\frac{i+1}{2})} \right) = \frac{2\pi^{\frac{d}{2}}}{\Gamma(\frac{d}{2})}.\end{aligned}\tag{1.49}$$

Here we used the formula for the Euler beta function, given by

$$B(a, b) = \frac{\Gamma(a)\Gamma(b)}{\Gamma(a+b)} = \int_0^1 dx x^{a-1} (1-x)^{b-1}.\tag{1.50}$$

The remaining integral over k_E is reasonably simple; we change variables to $z \equiv \Delta/(k_E^2 + \Delta)$, where for brevity we have absorbed the $-\epsilon$ term into Δ , obtaining another beta integral:

$$\begin{aligned}\int dk_E \frac{k_E^{d-1}}{(k_E^2 + \Delta)^2} &= \frac{1}{2} \Delta^{\frac{d-4}{2}} \int_0^1 dz (1-z)^{\frac{d-2}{2}} z^{\frac{2-d}{2}} \\ &= \frac{1}{2} \Delta^{\frac{d-4}{2}} \Gamma\left(\frac{d}{2}\right) \Gamma\left(\frac{4-d}{2}\right).\end{aligned}\tag{1.51}$$

Here we see the ultraviolet divergence arise: The last gamma function has a pole for $d = 4$; we can expand around this pole by setting $d = 4 - 2\epsilon$, $\epsilon > 0$:

$$\Gamma(\epsilon) = \frac{1}{\epsilon} - \gamma_E + \mathcal{O}(\epsilon),\tag{1.52}$$

where $\gamma_E \approx 0.577$ is the Euler-Mascheroni constant.

Finally, we are left with the integral over the Feynman parameter x , which is left undetermined for now:

$$\int_0^1 dx \Delta^{\frac{d-4}{2}} = p^{d-4} \int_0^1 dx [-x(1-x) - i\epsilon]^{\frac{d-4}{2}}.\tag{1.53}$$

Note that ϵ is just a regulator to be taken to zero at the end of the calculation, so rescaling it as we have done here does not change anything.

Collecting everything, the 1-loop amplitude is given by

$$i\mathcal{M}_2(p) = \frac{i\lambda_0^2}{2(4\pi)^{\frac{d}{2}}} \left(\frac{\mu^2}{p^2} \right)^{\frac{4-d}{2}} \Gamma\left(\frac{4-d}{2}\right) \int_0^1 dx [-x(1-x) - i\epsilon]^{\frac{d-4}{2}}.\tag{1.54}$$

We now Taylor expand around $\epsilon = 0$ using $a^\epsilon = 1 + \epsilon \ln a + \mathcal{O}(\epsilon^2)$, dropping all terms of order $\mathcal{O}(\epsilon)$ or higher, which leaves

$$i\mathcal{M}_2(p) = \frac{i\lambda_0^2}{32\pi^2} \left[\frac{1}{\bar{\epsilon}} + \ln \frac{\mu^2}{p^2} - \int_0^1 dx \ln [-x(1-x) - i\epsilon] \right],\tag{1.55}$$

where we have defined $1/\bar{\epsilon} \equiv 1/\epsilon - \gamma_E + \ln 4\pi$.

We can now perform the integration over the Feynman parameter x :

$$\begin{aligned}\int_0^1 dx \ln [-x(1-x) - i\epsilon] &= -i\pi + 2 \int_0^1 dx \ln (x + i\epsilon) \\ &= -i\pi - 2 + \mathcal{O}(\epsilon),\end{aligned}\tag{1.56}$$

after which we can safely take $\varepsilon \rightarrow 0$.

As an aside, we note that this means that \mathcal{M}_2 has an imaginary part, given by

$$\text{Im}\mathcal{M}_2 = \frac{\lambda_0^2}{32\pi}; \quad (1.57)$$

this is, not coincidentally, equal to $(p_1 + p_2)^2$ times the leading-order cross-section for $2 \rightarrow 2$ scattering; this shows an example of the optical theorem [7, p. 231].

Finally, adding together the three NLO diagrams (using the standard Lorentz-invariant Mandelstam variables $s = (p_1 + p_2)^2$, $t = (p_1 - p_3)^2$, and $u = (p_1 - p_4)^2$ with the leading-order result, we have to $\mathcal{O}(\lambda_0^2)$:

$$i\mathcal{M} = -i\lambda_0 + \frac{i\lambda_0^2}{32\pi^2} \left[\frac{3}{\varepsilon} + 6 + \ln \frac{\mu^2}{s} + \ln \frac{\mu^2}{t} + \ln \frac{\mu^2}{u} + 3i\pi \right] + \mathcal{O}(\lambda_0^3). \quad (1.58)$$

We still have a divergence in the limit $\varepsilon \rightarrow 0$; this is fixed by renormalization, to which we turn now.

1.2.3 Renormalized perturbation theory

To renormalize this amplitude, we note that the bare parameters of a Lagrangian, such as λ_0 , are not directly measurable; they are only determined indirectly, e.g. through cross-sections at particle accelerators. Therefore, attempting to define a theory in terms of these theoretical parameters is not very productive; it is much more practical to define it in terms of a few experimentally measured observables.

In other words, we define the *renormalized* parameters of the Lagrangian to fit to experiments; this procedure is what is referred to as renormalization, and if all amplitudes at each given order in perturbation theory can be made finite by the same finite set of renormalized parameters the theory is said to be *renormalizable*. The criteria for renormalizability is related to power-counting of terms in the Lagrangian, which we used to argue for the Standard Model Lagrangian in Sec. 1.1; we will see how this works shortly.

To this end, we define the *renormalized* coupling λ by the experimentally measured value¹⁴ for the amplitude at a given center-of-mass energy $\sqrt{s} = \sqrt{s_0}$:

$$\lambda \equiv -\mathcal{M}(s = s_0). \quad (1.59)$$

This is an example of a *renormalization condition*. We can now express λ_0 in terms of this quantity; assuming that it can be written as a perturbation series in λ , we have

$$\lambda_0 = \lambda + a\lambda^2 + \mathcal{O}(\lambda^3). \quad (1.60)$$

Inserting this into Eq. (1.58) for $s = s_0$, we find that

$$-\lambda = -(\lambda + a\lambda^2) + \frac{\lambda^2}{32\pi^2} \left[\frac{3}{\varepsilon} + 6 + \ln \frac{\mu^2}{s_0} + \ln \frac{\mu^2}{t} + \ln \frac{\mu^2}{u} + 3i\pi \right] + \mathcal{O}(\lambda^3), \quad (1.61)$$

and solving for a yields

$$\lambda_0 = \lambda + \frac{\lambda^2}{32\pi^2} \left[\frac{3}{\varepsilon} + 6 + \ln \frac{\mu^2}{s_0} + \ln \frac{\mu^2}{t} + \ln \frac{\mu^2}{u} + 3i\pi \right] + \mathcal{O}(\lambda^3). \quad (1.62)$$

¹⁴Supposing, for the sake of the example, that this toy model actually describes reality so that such an experiment actually exists.

Finally, we insert this into Eq. (1.58) for a general s , to obtain the finite result

$$\mathcal{M}(s) = -\lambda - \frac{\lambda^2}{32\pi^2} \ln \frac{s}{s_0} + \mathcal{O}(\lambda^3). \quad (1.63)$$

Thus we see how renormalizing the coupling in terms of an experimentally measured, finite, result, gives us finite predictions from loop calculations. Note that for a renormalizable theory, this same renormalized coupling will also give finite results for other amplitudes at the same order; thus fitting just one parameter to experiment allows us to calculate a multitude of different quantities. This is crucial for the predictivity of renormalizable theories.

Though the above procedure — performing the loop calculations with the bare parameters from the Lagrangian, and then fixing these in terms of measured quantities to get a finite result — is intuitive, it is not the most practical. Instead, we typically use what is referred to as *renormalized perturbation theory*.

In such a theory, all the bare parameters of the Lagrangian, i.e. the fields, masses, and coupling constants, are related to renormalized ones by multiplicative renormalization constants; for our ϕ^4 example, this would mean setting

$$\phi_0 \equiv \sqrt{Z_\phi} \phi, \quad \lambda_0 \equiv Z_\lambda \lambda. \quad (1.64)$$

Inserting this into Eq. (1.38), the Lagrangian can be written as

$$\mathcal{L} = \frac{1}{2} Z_\phi (\partial_\mu \phi)^2 - Z_{\phi^4} \frac{\lambda}{4!} \phi^4, \quad (1.65)$$

where we have defined $Z_{\phi^4} \equiv Z_\phi^2 Z_\lambda$. We can now expand the renormalization constants as $Z_\phi = 1 + \delta_\phi$, $Z_{\phi^4} = 1 + \delta_{\phi^4}$, so that

$$\mathcal{L} = \frac{1}{2} (\partial_\mu \phi)^2 - \frac{\lambda}{4!} \phi^4 + \frac{1}{2} \delta_\phi (\partial_\mu \phi)^2 - \frac{\delta_{\phi^4}}{4!} \phi^4. \quad (1.66)$$

The first two terms are exactly like the original Lagrangian, but now with renormalized quantities; the last two are called counterterms. In practice, the factors δ_ϕ and δ_{ϕ^4} take the role of the bare quantities we worked with previously, in that they are arbitrary, non-measurable factors that can be defined to fit our renormalized parameters to experiment.

When doing calculations in renormalized perturbation theory, we perform the loop calculations like we did above, but now with renormalized couplings, masses, etc., and add counterterm diagrams as necessary to remove divergences. The Feynman rules for the counterterm diagrams can be read off from Eq. (1.66) by considering the counterterms as interaction vertices in perturbation theory:

$$\text{---} \overset{p}{\circlearrowleft} \overset{p}{\circlearrowright} \text{---} = ip^2 \delta_\phi, \quad (1.67)$$

$$\text{---} \times \text{---} = -i\delta_{\phi^4}. \quad (1.68)$$

At 1-loop order in renormalized perturbation theory, following the calculations of the previous sections and including a vertex counterterm diagram, we then have

$$i\mathcal{M} = -i\lambda + \frac{i\lambda^2}{32\pi^2} \left[\frac{3}{\bar{\epsilon}} + 6 + \ln \frac{\mu^2}{s} + \ln \frac{\mu^2}{t} + \ln \frac{\mu^2}{u} + 3i\pi \right] - i\delta_{\phi^4} + \mathcal{O}(\lambda_0^3). \quad (1.69)$$

The result in Eq. (1.63) can then be obtained by setting the counterterm to

$$\delta_{\phi^4} = \frac{\lambda^2}{32\pi^2} \left[\frac{3}{\bar{\epsilon}} + 6 + \ln \frac{\mu^2}{s_0} + \ln \frac{\mu^2}{t} + \ln \frac{\mu^2}{u} + 3i\pi \right]. \quad (1.70)$$

1.2.4 Renormalization schemes

The expression in (1.70) is just one possible choice for the counterterm; as long as it cancels the divergence in the amplitude, the finite part can in principle be anything we want. How we define a counterterm defines what *renormalization scheme* we are using.

The simplest possible choice, though perhaps not the most well-motivated physically, is just removing the divergence and nothing else; this is called minimal subtraction (MS). The convenience of this is that we can just remove ultraviolet divergences from matrix element calculations, without having to do any further calculations to determine the finite part of the counterterm.

In practice, *modified* minimal subtraction ($\overline{\text{MS}}$) is more used; in this scheme we set the counterterm to remove not just the divergence, but the part proportional to

$$\frac{1}{\bar{\epsilon}} \equiv \frac{1}{\epsilon} - \gamma_E + \ln 4\pi, \quad (1.71)$$

or equivalently remove the pole in ϵ and rescale $\mu^2 \rightarrow \mu^2 e^{\gamma_E}/4\pi$. For our above ϕ^4 example this would mean taking

$$\delta_{\phi^4} = \frac{\lambda^2}{32\pi^2} \frac{3}{\bar{\epsilon}}. \quad (1.72)$$

Another possibility, which has a more immediate physical interpretation, is called on-shell renormalization. We will demonstrate this scheme through an example, namely quantum electrodynamics (QED), with a bare Lagrangian given by

$$\mathcal{L} = -\frac{1}{4}Z_3(\partial_\mu A_\nu - \partial_\nu A_\mu)^2 + Z_2\bar{\psi}(i\not{\partial} - Z_m m)\psi - eZ_1 A_\mu^a \bar{\psi}\gamma^\mu\psi. \quad (1.73)$$

Here we have defined $Z_m m = m_0$, $\sqrt{Z_2}\psi \equiv \psi_0$, $\sqrt{Z_3}A \equiv A_0$, $Z_e e \equiv e_0$, and $Z_1 \equiv Z_e Z_2 \sqrt{Z_3}$. All of the renormalization constants are expanded around 1 by counterterms, exactly like in the ϕ^4 example. In the on-shell scheme, the counterterms are set so that the renormalized parameters correspond exactly to the physically measured ones.¹⁵

This is done by considering the form of the total (i.e. taking into account all possible loop corrections) 2- and 3-point functions in the theory, as discussed for example in Refs. [6, 7].

The total fermion propagator can be written as

$$iG(\not{p}) = \frac{i}{\not{p} - m + \Sigma(\not{p})}, \quad (1.74)$$

where $\Sigma(\not{p})$ is the sum of all possible 1-particle irreducible (1PI)¹⁶ loop corrections to the propagator. In the on-shell scheme we want the renormalized mass m to correspond exactly to the physically measured m_P , called the pole mass. For this to be the case, $G(\not{p})$ must have a pole at $\not{p} = m_P$ with residue 1; this leads us to the first two on-shell renormalization conditions:

$$\Sigma(\not{p})\Big|_{\not{p}=m_P} = 0, \quad (1.75)$$

$$\frac{d}{d\not{p}}\Sigma(\not{p})\Big|_{\not{p}=m_P} = 0. \quad (1.76)$$

For later use, we specify what this means for massless fermions, with $m_P = 0$, which is approximately the case in high-energy scattering. In this case the first condition is automatically

¹⁵This is not necessarily the case in $\overline{\text{MS}}$, where for example the renormalized mass of a fermion is shifted from its physical value by a μ -dependent term.

¹⁶Meaning that all internal lines in the diagram have loop momentum running through them.

satisfied at all orders; when the fermion is taken to be massless in the Lagrangian, i.e. $m = 0$, the Lagrangian is symmetric under the chiral transformation (of the fermion fields)

$$\psi \rightarrow e^{i\alpha\gamma^5}\psi. \quad (1.77)$$

This symmetry will also be respected in loops, since the Feynman rules come from the Lagrangian. Thus a non-zero effective mass term, induced by loop effects, will not appear at any order as it would violate the chiral symmetry.

We must still set the residue, however; at 1-loop order,

$$\Sigma(\not{p}) = \Sigma_2(\not{p}) + \not{p}\delta_2 + \mathcal{O}(e^4), \quad (1.78)$$

where Σ_2 is the 1-loop correction, so that

$$\delta_2 = -\left.\frac{d}{d\not{p}}\Sigma_2(\not{p})\right|_{\not{p}=0}, \quad (1.79)$$

in the on-shell scheme.

Similarly, the photon 2-point function is given by

$$iG^{\mu\nu}(p) = -i\left(g^{\mu\nu} - \frac{p^\mu p^\nu}{p^2}\right)\frac{1}{p^2(1 + \Pi(p^2))}, \quad (1.80)$$

where $\Pi(p^2)$ is the sum of 1PI corrections to the function. Here only one condition is needed; since gauge invariance guarantees that the photon is massless at all orders, we only need to fix the residue by setting

$$\Pi(0) = 0. \quad (1.81)$$

Lastly we need to fix the charge e ; this is done by demanding that the all-order fermion-fermion-photon vertex, denoted by $\Gamma^\mu(p)$, satisfy

$$\Gamma^\mu(0) = \gamma^\mu. \quad (1.82)$$

What this means in practice is that e is defined to correspond to the elementary charge measured in low-energy experiments, in which we can take the limit $p^2 \rightarrow 0$.

In our later calculations we will mostly be using $\overline{\text{MS}}$ renormalization, with the exception of masses; since we will not encounter any propagator corrections at the order to which we are calculating, it is more convenient to use pole masses rather than their $\overline{\text{MS}}$ versions. This is due to the fact that the particles appearing in the calculations have (in principle) well-defined pole masses: All of the incoming quarks are assumed to be massless since the center-of-mass energy is so large — this refers to the physical pole mass, not $\overline{\text{MS}}$. Similarly, typical parameter sets for supersymmetric particles have their masses listed as pole masses. It will therefore be more convenient to consistently use on-shell masses rather than convert them to their $\overline{\text{MS}}$ values.

1.2.5 The renormalization group

As we alluded to above, couplings and masses in the $\overline{\text{MS}}$ renormalization scheme can depend on the unphysical parameter μ . Though this might initially seem undesirable, it can actually provide us with valuable information about how parameters depend on energy, by demanding that observables be independent of unphysical parameters. The resulting running of renormalized parameters is described by so-called *renormalization group equations* (RGEs).

We can see an example of how this works by returning to our ϕ^4 example. Recall that the bare coupling was defined in $d = 4 - 2\epsilon$ dimensions, to 1-loop order, as

$$\begin{aligned}\lambda_0 &= \mu^\epsilon Z_\lambda \lambda = \mu^\epsilon Z_{\phi^4} Z_\phi^{-2} \lambda \\ &= \mu^\epsilon (1 + \delta_{\phi^4} - 2\delta_\phi + \mathcal{O}(\lambda^4)) \lambda.\end{aligned}\tag{1.83}$$

Now, since this is a parameter of the bare Lagrangian, which has no μ dependence, λ_0 must be independent of μ , meaning that $\mu \frac{d\lambda_0}{d\mu} = 0$, or

$$0 = \mu \frac{d\lambda}{d\mu} + \epsilon \lambda + \lambda \mu \frac{d}{d\mu} (\delta_{\phi^4}).\tag{1.84}$$

Note that the δ_ϕ term has been dropped; this is due to the fact that at 1-loop level the only correction to the propagator, which would lead to a non-zero counterterm, is given by a scaleless integral $\int d^4k/k^2$. This integral vanishes in dimensional regularization; thus $\delta_\phi = 0$ to 1-loop order.

We can now solve Eq. (1.84) for the ϕ^4 β -function, defined as

$$\beta(\lambda) \equiv \mu \frac{d\lambda}{d\mu}\tag{1.85}$$

$$= -\epsilon \lambda - \lambda \mu \frac{d}{d\mu} (\delta_{\phi^4}).\tag{1.86}$$

We calculate this expression perturbatively in λ . At the lowest order, $\beta(\lambda) = -\epsilon \lambda$; we then use the chain rule to find

$$\mu \frac{d}{d\mu} \delta_{\phi^4} = \beta(\lambda) \frac{d}{d\lambda} \delta_{\phi^4} = -\frac{3\lambda}{16\pi^2} + \mathcal{O}(\epsilon),\tag{1.87}$$

where we inserted Eq. (1.70) and our leading-order β -function. Re-inserting this into Eq. (1.86), now taking the limit $\epsilon \rightarrow 0$, we find

$$\beta(\lambda) = \frac{3\lambda^2}{16\pi^2} + \mathcal{O}(\lambda^3).\tag{1.88}$$

Solving this equation, we find the RG running of λ , given by

$$\lambda(\mu) = -\frac{1}{\frac{3}{16\pi^2} \ln \frac{\mu}{\Lambda}},\tag{1.89}$$

where Λ is an integration constant. If we assume that λ has been measured at some scale so that $\lambda(\mu_0)$ is known, this can alternatively be written as

$$\lambda(\mu) = \frac{\lambda(\mu_0)}{1 - \frac{3\lambda(\mu_0)}{16\pi^2} \ln \frac{\mu}{\mu_0}}.\tag{1.90}$$

We observe that λ increases with momentum, and conversely decreases for low energies; such theories are called *infrared free*.

The usefulness of this expression is seen by inserting it into Eq. (1.39) in place of λ_0 ; expanding in $\lambda(\mu_0)$ we find

$$i\mathcal{M} = -i\lambda(\mu_0) = -i\lambda(\mu_0) - i \frac{3\lambda^2(\mu_0)}{32\pi^2} \ln \frac{\mu^2}{\mu_0^2} + \mathcal{O}(\lambda(\mu_0)^3).\tag{1.91}$$

This is exactly our renormalized 1-loop expression in Eq. (1.63), setting $\mu^2 = s$, $\mu_0^2 = s_0$, and $\lambda(\mu_0) = \lambda$, but it also automatically includes contributions to all orders in λ . We could also have

obtained this result by summing up an infinite series of diagrams with an arbitrary number of copies of the loop in Fig. 1.1b;¹⁷ instead we have found it from just a 1-loop calculation and the renormalization group.

Since we had to set $\mu^2 = s$ in order to reproduce our earlier result, this suggests that we should in general keep the arbitrary scale μ around the relevant energy scale of the process. μ is often referred to as the *renormalization scale*, as it serves as a proxy for the scale at which the theory is renormalized.

From Eq. (1.89), we see a potential problem: At very high energy scales, $\mu = \Lambda$, the coupling blows up, and above this scale perturbation theory breaks down. Such a point is called a Landau pole, and is common in quantum field theories. Another example is the running of the fine-structure constant $\alpha = e^2/4\pi$ in QED [6]:

$$\alpha(\mu) = \frac{2\pi}{\beta_0 \ln \frac{\mu}{\Lambda_{\text{QED}}}} = \frac{\alpha(m_Z)}{1 - \frac{\alpha(m_Z)}{3\pi} \ln \frac{\mu^2}{m_Z^2}}, \quad (1.92)$$

with $\beta_0 = -\frac{4}{3}$, and $\alpha(m_Z)^{-1} = 127.94$ [19]. The fact that QED, one of the most precisely and successfully tested theories in physics, breaks down at high energies (specifically at $\Lambda_{\text{QED}} \approx 10^{286}$ eV) is not as troublesome as it seems; it *does* mean that QED is not a complete theory, in that it cannot describe all of physics, but this is not surprising. Quantum field theory is already expected to break down at the Planck scale, where quantum gravity effects would become significant, and this scale is far below the Landau pole of QED.

Instead, it suggests that we look at quantum field theory and the Standard Model as an effective field theory, where some high-energy degrees of freedom have been integrated out. Such theories can be very useful at their appropriate energy scales, like the 4-Fermi theory of weak interactions, where the weak bosons can be integrated out for energies far below their masses; or even the theory of weak interactions, where whatever mechanism causes spontaneous electroweak symmetry breaking is not observed at our energy scales.

The above manipulations with counterterm is just one way of obtaining the RG running of parameters; another possibility is by the Callan-Symanzik [20, 21] equation.

This equation can be derived fairly easily, by considering Green's functions; as an example, we take a Green's function in massless ϕ^4 theory with n external particles. The bare Green's function (written in terms of bare fields) can be related to the renormalized one (written in terms of renormalized fields) as

$$G_n^0 = \langle \phi_0(x_1) \cdots \phi_0(x_n) \rangle = Z_\phi^{\frac{n}{2}} \langle \phi(x_1) \cdots \phi(x_n) \rangle = Z_\phi^{\frac{n}{2}} G_n. \quad (1.93)$$

Since the bare Green's function is written in terms of bare fields it must be independent of μ , meaning that

$$0 = \mu \frac{d}{d\mu} G_n^0 = \mu \frac{d}{d\mu} \left(Z_\phi^{\frac{n}{2}} G_n \right). \quad (1.94)$$

The renormalized Green's function can depend on μ both directly and through the coupling λ ; using the chain rule we find

$$\left(\mu \frac{\partial}{\partial \mu} + \frac{n}{2} \gamma_\phi + \beta(\lambda) \frac{\partial}{\partial \lambda} \right) G_n = 0, \quad (1.95)$$

where $\gamma_\phi \equiv \frac{\mu}{Z_\phi} \frac{dZ_\phi}{d\mu}$ is called the *anomalous dimension* of the theory. This equation is what is referred to as the Callan-Symanzik equation; it allows us to calculate the running coupling and anomalous dimension by considering the dependence of n -point functions upon the scale μ and the coupling λ .

¹⁷This is an example of resummation, which will be discussed more later.

1.2.6 Renormalizability

In order for a theory to be predictive, it is significant that the above renormalization can be performed using a finite number of counterterms. If this is the case, we can define the counterterms by fitting a few calculations to experiments, and use these to make predictions for any other process in the theory.

In general, there are three different categorizations for renormalizability [7]:

- In a *renormalizable* theory there is a finite number of UV-divergent amplitudes at any given order in perturbation theory, coming from 1-particle irreducible diagrams; thus all UV divergences at any order can be removed with counterterms corresponding to this finite number of amplitudes.
- In a *super-renormalizable* theory there is a finite number of UV-divergent *diagrams*; at sufficiently high order in perturbation theory we do not need any counterterms, as there are no UV divergences.
- In a *non-renormalizable* theory, all amplitudes at sufficiently high order in perturbation theory diverge. This means that to remove all divergences, we in principle need an infinite number of counterterms.

Note that this does not necessarily mean that non-renormalizable theories are useless, nor that super-renormalizable theories are more useful than just renormalizable ones; the infinite number of divergences in non-renormalizable theories are typically proportional to polynomials in external momenta, so in the low-energy limit most can be discarded, making the theory perfectly valid in these regions. Similarly, super-renormalizable theories can be useful in the high-energy regime, but may not have a sensible low-energy limit.

The degree of renormalizability can largely be determined by power-counting. To see this, we consider a quantity called the *superficial degree of (ultraviolet) divergence* D , which essentially just describes the mass dimension of a matrix element \mathcal{M} ; using a high-energy cutoff Λ to regulate loop integrals, we expect $\mathcal{M} \sim \Lambda^D$ for $D \neq 0$, and $\mathcal{M} \sim \ln \Lambda$ for $D = 0$.

Note that this behavior is not always the case, hence the prefix “superficial;” there may be certain symmetries restricting the form of loop corrections, which can reduce the degree of divergence of a diagram, or even make it finite. An example is the fermion two-point function. By simple power-counting it *should* be linearly divergent, i.e. proportional to Λ ; but from the arguments in Sec. 1.2.4 it must actually be proportional to the (renormalized) fermion mass m_f since $m_f = 0$ in the Lagrangian ensures that there are no loop corrections to the mass. Thus by power counting, the two-point function can at worst be logarithmically divergent.

If at any given order in perturbation theory there is a finite number of 1PI amplitudes with $D \geq 0$, the theory is renormalizable; this is due to the BPHZ theorem [22–24], which states that all divergences can be removed by counterterms corresponding to these 1PI amplitudes.

To see how the superficial degree of divergence relates to the mass dimension of couplings, we consider a completely general theory of fermions and bosons (either vectors or scalars; this makes no difference to the dimensional analysis), with an interaction term combining n_f fermions and n_b bosons. By dimensional analysis, now assuming spacetime dimension $d = 4$ for simplicity, the coupling constant g must satisfy $[g] = 4 - \frac{3}{2}n_f - n_b \equiv \delta$ since fermions and bosons have mass dimensions $\frac{3}{2}$ and 1, respectively.

For a general 1PI amplitude with L loop integrals, P_f internal fermion lines, P_b internal bosons, and n interaction vertices, D is given by

$$D = 4L - P_f - 2P_b, \quad (1.96)$$

since each loop requires a 4-dimensional loop integral with measure d^4k , and fermion and boson propagators are given by $\sim i/\not{k}$ and $\sim i/k^2$, respectively. This can be simplified; *a priori* all propagator momenta must be integrated over, but each vertex contains a momentum-conserving delta function which removes one integral. One delta function merely assures that the total momentum is conserved; thus we have

$$L = P_f + P_b - n + 1. \quad (1.97)$$

Further, since each vertex connects n_f fermions and n_b bosons, the number of vertices can be expressed as

$$n = \frac{1}{n_b}(2P_b + b) = \frac{1}{n_f}(2P_f + f), \quad (1.98)$$

where b and f are the number of external boson and fermion lines, respectively (internal lines are connected to two vertices while external ones are connected to one). This can be combined to give

$$D = 4 - \frac{3}{2}f - b - n\delta. \quad (1.99)$$

We can now connect the dimension of the coupling δ to the degree of renormalizability: For a renormalizable theory there is a finite number of divergent 1PI diagrams at each order, i.e. for any n above. From Eq. (1.99) this is only possible when $\delta = 0$. For a super-renormalizable theory, at sufficiently high orders, i.e. sufficiently high n , there are no UV divergences; this is achieved with $\delta > 0$. For non-renormalizable theories all diagrams diverge at sufficiently high orders; this means that $\delta < 0$.

This allows us to categorize renormalizability in a second way:

- In a renormalizable theory, no couplings have negative mass dimension, and at least one coupling has mass dimension zero.
- In a super-renormalizable theory, all couplings have positive mass dimensions.
- In a non-renormalizable theory, at least one coupling has negative mass dimension.

This explains why we restrict ourselves to Lagrangian terms with couplings of non-negative mass dimensions for renormalizable theories.

1.2.7 Infrared divergences

So far we have mainly concerned ourselves with ultraviolet divergences, which can be removed in the renormalization of the theory. Other divergences can appear too, however, which must be dealt with differently; these are referred to as infrared divergences, as they occur in the low-energy part of momentum integrals.

For ultraviolet divergences, we were able to exploit the fact that even though an amplitude might contain a divergence, the difference between amplitudes at different scales is finite; thus we could define our theory by fitting to a measurement at some scale μ_0 and get finite results at other scales by using μ_0 as a reference point.

This is closely related to the fact that UV divergences show up as simple poles in ϵ ; when using a UV cutoff Λ_{UV} these correspond to terms proportional to $\ln(\Lambda_{UV}^2/p^2)$, for some momentum scale p , which can be easily removed by subtracting the result at another scale p_1 .

For infrared divergences, this is different. As we will see explicitly in Sec. 4.3, when setting $d = 4 - 2\epsilon_{IR}$, where now $\epsilon_{IR} < 0$ to keep $d > 4$,¹⁸ we also get double poles of the form $1/\epsilon_{IR}^2$, which

¹⁸Recall that, as we discussed earlier, IR divergent terms typically behave like $1/\Lambda_{IR}^{4-d}$, where Λ_{IR} is a low-energy cutoff; thus such terms are regulated by setting $d > 4$.

correspond, when using an infrared cutoff, to terms proportional to $\ln^2(\Lambda_{\text{IR}}^2/Q^2)$; these cannot be removed by a simple subtraction.

Instead, these divergences must be removed by appealing to the nature of the experiments in which our predictions would be tested. Observationally, there is no way to distinguish the case of two high-energy final-state particles, from that of two high-energy particles and one that either has very low energy or momentum very close to one of the other particles. Thus we can only expect sensible predictions when we sum over all possible processes that contribute to the same observed state at each order in perturbation theory. If we do not include all such processes, our result will contain *soft* and/or *collinear* divergences, corresponding respectively to the two aforementioned cases where a 3-particle state is indistinguishable from a 2-particle one.

In practice this means that a theoretical $2 \rightarrow 2$ scattering cross-section, in order to get an infrared finite result, must also include the calculation of a $2 \rightarrow 3$ cross-section at the same order. Exactly how this is done depends on what result we actually want: If we insist on calculating the production cross-section for *only* two particles, we include the 3-particle final state only in the case where it is indistinguishable from 2 particles; this is done by cutoffs in the energy of the third emitted particle, or its angle to the other two, at the experimental resolution. In this way the theoretical resolution effectively works as an infrared cutoff.

Another possibility is including all processes that include the production of our desired 2-particle pair, alongside any arbitrary set of other particles; the resulting cross-section is called the *inclusive* cross-section. This is often easier but can be just as useful, in particular when searching for new physics; if we are looking for a process in which a pair of new particles are produced, it makes sense to include all possible such processes. This is especially the case at hadron colliders, where any observed final state can include a potentially large number of jets (see Chapter 3), and “filtering” these out of calculations can be impractical.

1.3 Systematics of loop integrals with Passarino-Veltman reduction

In Sec. 1.2.2 we showed how a loop integral can be calculated using dimensional regularization. Performing the loop integration explicitly for each diagram contributing to an amplitude can be cumbersome, especially when the propagating particles are massive, since the dependence on various scales then quickly becomes more complicated than our previous calculation.

Luckily, the form that these integrals can take turns out to be restricted by Lorentz invariance. In fact, at 1-loop level, all such integrals can be reduced, by a procedure called Passarino-Veltman reduction, to functions of scalar 1-loop n -point functions [25], which are simpler to calculate, and more importantly, do not have to be calculated explicitly for each diagram. These scalar functions are in turn restricted to only depend on external momenta and the masses of the particles in the loop.

Up to 3-point functions, they are given by (in $d = 4 - 2\epsilon$ dimensions)

$$A_0(m^2) \equiv \frac{(4\pi)^{\frac{d}{2}} \mu^{4-d}}{ir_\Gamma} \int \frac{d^d k}{(2\pi)^d} \frac{1}{k^2 - m^2}, \quad (1.100)$$

$$B_0(p^2, m_1^2, m_2^2) \equiv \frac{(4\pi)^{\frac{d}{2}} \mu^{4-d}}{ir_\Gamma} \int \frac{d^d k}{(2\pi)^d} \frac{1}{(k^2 - m_1^2)((k+p)^2 - m_2^2)}, \quad (1.101)$$

$$\begin{aligned} C_0(p_1^2, p_2^2, (p_1 + p_2)^2, m_1^2, m_2^2, m_3^2) &\equiv \frac{(4\pi)^{\frac{d}{2}} \mu^{4-d}}{ir_\Gamma} \int \frac{d^d k}{(2\pi)^d} \\ &\times \frac{1}{(k^2 - m_1^2)((k+p_1)^2 - m_2^2)((k+p_1+p_2)^2 - m_3^2)}, \end{aligned} \quad (1.102)$$

following the LoopTools [26, 27] conventions for the normalization and the definitions of momenta, all of which are defined to run into the loop. The factor r_Γ is defined as

$$r_\Gamma \equiv \frac{\Gamma^2(1-\epsilon)\Gamma(1+\epsilon)}{\Gamma(1-2\epsilon)}. \quad (1.103)$$

A generic loop integral of the type we will consider in this thesis, appearing in a Yang-Mills n -point function with $n \in \{2, 3\}$, can also have up to 2 factors of k^μ in its numerator, originating from fermion propagators.¹⁹ Otherwise these are identical to the scalar functions listed above, and they are denoted by B^μ , $B^{\mu\nu}$, C^μ , and $C^{\mu\nu}$.

The aim is now to express these tensor integrals as functions of the scalar ones. This is done by exploiting the Lorentz structure of the integrals; since they are (rank 1 or 2) tensors, the result of the integrals must also be written as a linear combination of symmetric (since $k^\mu k^\nu$ is symmetric) tensors with the same rank, with scalar coefficients. The list of such tensors is short; since k^μ is integrated over, the only available ones are products of the external momenta and the metric $g_{\mu\nu}$. Explicitly, again following the momentum conventions of LoopTools where $q_n \equiv \sum_{i=1}^n p_i$ in the three-point functions, the integrals can be parametrized as

$$B^\mu = p^\mu B_1, \quad (1.104)$$

$$B^{\mu\nu} = g^{\mu\nu} B_{00} + p^\mu p^\nu B_{11}, \quad (1.105)$$

$$C^\mu = q_1^\mu C_1 + q_2^\mu C_2, \quad (1.106)$$

$$C^{\mu\nu} = g^{\mu\nu} C_{00} + q_1^\mu q_1^\nu C_{11} + q_2^\mu q_2^\nu C_{22} + (q_1^\mu q_2^\nu + q_2^\mu q_1^\nu) C_{12}, \quad (1.107)$$

suppressing the arguments of the scalar coefficient functions. The ‘‘Passarino-Veltman coefficients’’ B_1 , B_{ij} , C_i , and C_{ij} are (a priori) unknown functions of the same scalars as their corresponding integrals, namely masses and dot products of external momenta. By contracting both sides of these equations with the available tensors we obtain linear systems of equations, the left-hand sides of which can be reduced to functions of the known scalar functions A_0 , B_0 , and C_0 , making it possible to solve for the unknown functions in terms of the known ones.

¹⁹In general a 1-loop n -point diagram can have up to n internal fermion lines, but a diagram with a three-fermion loop would need to have at least three external gauge bosons, and we will not need to consider such diagrams here. Note also that this is not the case for the 1-point function, as the integral of $k^\mu/(k^2 - m^2)$ would be zero by symmetry, so A_0 is the most general 1-point function that can appear.

As a simple example, we contract both sides of Eq. (1.104) with p_μ . This leaves $p_\mu B^\mu = p^2 B_1$, where

$$p_\mu B^\mu = \frac{(4\pi)^{\frac{d}{2}} \mu^{4-d}}{ir_\Gamma} \int \frac{d^d k}{(2\pi)^d} \frac{p \cdot k}{(k^2 - m_1^2)((k+p)^2 - m_2^2)}. \quad (1.108)$$

Now we can rewrite the numerator of this expression, using

$$p \cdot k = \frac{1}{2} \left[((k+p)^2 - m_2^2) - (k^2 - m_1^2) - (p^2 + m_1^2 - m_2^2) \right]. \quad (1.109)$$

The first two terms then each cancel one factor in the denominator, leaving just A_0 integrals, while the third can be factored out, leaving a B_0 integral. This allows us to solve for B_1 , obtaining (now explicitly stating the arguments for clarity)

$$B_1(p^2, m_1^2, m_2^2) = \frac{1}{2p^2} [A_0(m_1^2) - A_0(m_2^2) - (p^2 + m_1^2 - m_2^2) B_0(p^2, m_1^2, m_2^2)]. \quad (1.110)$$

The same procedure similarly leads to expressions for the remaining functions in terms of the scalar integrals. We will not do this explicitly here; the important point is that this procedure allows us to express potentially complicated tensor integrals as combinations of external tensors, with coefficients that can in turn be expressed in terms of (reasonably) simple scalar integrals, which have been extensively studied [28]. These integrals, and functions thereof, e.g. the Passarino-Veltman coefficients, can be calculated efficiently in numerical packages such as LoopTools [26, 27]; thus, we will content ourselves with expressing 1-loop contributions to cross-sections etc. as functions of these Passarino-Veltman coefficients.

Chapter 2

Supersymmetry

In this chapter we present the Minimal Supersymmetric Standard Model (MSSM) as a possible extension to the Standard Model, and discuss its predictions and how these may be tested experimentally.

First we discuss the basic idea behind supersymmetry as an extension to the Poincaré symmetry group of the special theory of relativity. We will see that it is possible to postulate a symmetry between fermionic and bosonic degrees of freedom, and that the representations of this symmetry group can be expressed as so-called superfields.

Next, we use these superfields to construct a Lagrangian. Here we use the previous discussion of the Standard Model as a reference for what fields must be included and how the Lagrangian must be constructed; the minimal model (in terms of the number of superfields) that fulfills these conditions is the MSSM.

We finish the chapter by discussing the properties of the model; both how it can potentially solve some of the unanswered questions of the Standard Model, as we mentioned in the introduction, and the new particles it predicts. We focus in particular on sleptons, the scalar partners to the Standard Model leptons, and experiments relevant for their potential discovery. Such particles could in theory be produced at particle colliders such as the Large Hadron Collider (LHC) or electron-positron colliders; we will look at the mechanism for production at such colliders, what signatures one might expect in experiments depending on the parameters of the MSSM, and which observables must be calculated theoretically to compare to experiment.

2.1 Superfields

2.1.1 Super-Poincaré algebra

The Special Theory of Relativity is largely based on invariance of physics under coordinate transformations between arbitrary inertial frames, as described by the Poincaré group P . These transformations can in general be written as

$$x^\mu \rightarrow x'^\mu = \Lambda^\mu{}_\nu x^\nu + a^\mu, \quad (2.1)$$

where Λ is any 4×4 matrix satisfying $\Lambda^T g \Lambda = g$, g being the metric tensor in Minkowski space, and a^μ is an arbitrary 4-vector. Note that the Poincaré group P can be expressed as a semi-direct product of the Lorentz group $L = O(1,3)$, describing the matrices Λ , and the translation group $T(1,3)$ in 4-dimensional Minkowski space, so that

$$P = O(1,3) \ltimes T(1,3). \quad (2.2)$$

Restricting ourselves to the *proper orthochronous* Poincaré group $SO^+(1, 3)$, where $\det \Lambda = +1$ and $\Lambda^0_0 \geq +1$,¹ the Poincaré Lie algebra is described by the relations [29]

$$[M_{\mu\nu}, M_{\rho\sigma}] = -i(g_{\mu\rho}M_{\nu\sigma} - g_{\mu\sigma}M_{\nu\rho} - g_{\nu\rho}M_{\mu\sigma} + g_{\nu\sigma}M_{\mu\rho}), \quad (2.3a)$$

$$[M_{\mu\nu}, P_\rho] = -i(g_{\mu\rho}P_\nu - g_{\nu\rho}P_\mu), \quad (2.3b)$$

$$[P_\mu, P_\nu] = 0, \quad (2.3c)$$

where $M_{\mu\nu} = -M_{\nu\mu}$ and $P_\mu = -i\partial_\mu$ are the generators of the (proper orthochronous) Lorentz group and the translation group, respectively.

So far we have only discussed the coordinate symmetries of special relativity. What we would ideally want now is to extend this symmetry group to also include the *internal* symmetries of the Standard Model, namely the gauge groups discussed in Sec. 1.1.1. Unfortunately, per Coleman and Mandula [30], any such extended symmetry group would be isomorphic to the direct product of the gauge groups and the Poincaré group; in other words there can be no interaction between the two groups, making the construction rather unhelpful.

Instead, following Haag, Lopuszanski, and Sohnius [31], we construct a *superalgebra*. A superalgebra, or a graded Lie algebra, is a direct sum of two vector spaces² $L = L_0 \oplus L_1$, defined along with a product $\circ : L \times L \rightarrow L$, such that for all $x_i, y_i, z_i \in L_i$, $i = 0, 1$, we have:

- *Grading:*

$$x_i \circ y_j \in L_{i+j \bmod 2}. \quad (2.4)$$

- *Supersymmetrization:*

$$x_i \circ y_j = -(-1)^{ij} y_j \circ x_i. \quad (2.5)$$

- *Generalized Jacobi identity:*

$$x_k \circ (y_l \circ z_m)(-1)^{km} + y_l \circ (z_m \circ x_k)(-1)^{lk} + z_m \circ (x_k \circ y_l)(-1)^{ml} = 0. \quad (2.6)$$

In this way, L is a generalized Lie algebra, where some of the elements are given anticommutation relations instead of commutation relations, as determined by Eq. (2.5). For this reason these \mathbb{Z}_2 graded Lie algebras, wherein we combine only two vector spaces, cannot be used to combine the Poincaré algebra with the gauge groups, as both of these are defined with commutation relations.³ However, these constructions are still interesting in their own right, as we shall see.

With these definitions, we can define the *super-Poincaré algebra* by extending Eq. (2.3) with four generators Q_a ; together these form a Majorana spinor, which can also be described by two-component Weyl spinors Q_A and $\bar{Q}_{\dot{A}}$ (left-handed and right-handed, respectively). In terms of these Weyl spinors, the super-Poincaré algebra is defined by the Poincaré algebra with the additional

¹This excludes time and space inversions, leaving only continuous transformations. The other parts of the group can be accessed by performing these inversions.

²This is for the case of a so-called \mathbb{Z}_2 graded Lie algebra; it is possible to add more vector spaces.

³If we allow for more than two vector spaces to be combined, i.e. by adding two vector spaces to the Poincaré generators, it is possible for one of the new sets of generators to be defined with commutation relations. In this way one can potentially combine the Lie algebra with gauge groups, along with another set of generators.

relations [29]

$$\{Q_A, Q_B\} = 0, \quad (2.7a)$$

$$\{\bar{Q}_{\dot{A}}, \bar{Q}_{\dot{B}}\} = 0, \quad (2.7b)$$

$$\{Q_A, \bar{Q}_{\dot{B}}\} = 2(\sigma^\mu)_{A\dot{B}} P_\mu, \quad (2.7c)$$

$$[Q_A, M^{\mu\nu}] = (\sigma^{\mu\nu})_A{}^B Q_B, \quad (2.7d)$$

$$[Q_A, P_\mu] = 0, \quad (2.7e)$$

$$[\bar{Q}_{\dot{A}}, P_\mu] = 0, \quad (2.7f)$$

where $\sigma^i = -\bar{\sigma}^i$ are the Pauli matrices, $\sigma^0 = \bar{\sigma}^0 = \mathbf{1}_{2 \times 2}$, and $\sigma^{\mu\nu} \equiv \frac{i}{4}(\sigma^\mu \bar{\sigma}^\nu - \sigma^\nu \bar{\sigma}^\mu)$. In this definition the original Poincaré generators correspond to the L_0 vector field as described above, while the new Weyl spinor generators make up L_1 . The product \circ describes the commutator or anti-commutator, determined by Eq. (2.5).

With this, we can parametrize a general supersymmetry transformation, under the super-Poincaré group, as an exponential map given by

$$g = \exp \left[i a^\mu P_\mu + i \alpha^A Q_A + i \bar{\alpha}_{\dot{A}} \bar{Q}^{\dot{A}} + \frac{i}{2} \omega_{\rho\sigma} M^{\rho\sigma} \right]. \quad (2.8)$$

Here a^μ and $\omega_{\rho\sigma} = -\omega_{\sigma\rho}$ are the parameters of regular Poincaré transformations, while α^A and $\bar{\alpha}_{\dot{A}}$ are anticommuting Grassmann numbers. Note that contractions with Weyl spinors and anticommuting numbers such as these are defined as

$$\psi\chi = \psi^A \chi_A = \epsilon_{AB} \psi^A \chi^B = \psi^2 \chi^1 - \psi^1 \chi^2, \quad (2.9a)$$

$$\bar{\psi}\bar{\chi} = \bar{\psi}_{\dot{A}} \bar{\chi}^{\dot{A}} = \epsilon^{\dot{A}\dot{B}} \bar{\psi}_{\dot{A}} \bar{\chi}_{\dot{B}} = \bar{\psi}_{\dot{1}} \bar{\chi}_{\dot{2}} - \bar{\psi}_{\dot{2}} \bar{\chi}_{\dot{1}}. \quad (2.9b)$$

By acting on a function $f(x^\mu, \theta^A, \bar{\theta}_{\dot{A}})$ we can express the new super-Poincaré generators explicitly as [29]

$$Q_A = -i(\partial_A - i(\sigma^\mu \bar{\theta})_A \partial_\mu), \quad (2.10)$$

$$\bar{Q}^{\dot{A}} = -i(\bar{\partial}^{\dot{A}} - i(\bar{\sigma}^\mu \theta)^{\dot{A}} \partial_\mu), \quad (2.11)$$

where the Grassmann derivatives are defined as $\partial_A \equiv \frac{\partial}{\partial \theta^A}$, $\bar{\partial}^{\dot{A}} \equiv \frac{\partial}{\partial \bar{\theta}_{\dot{A}}}$.

2.1.2 Representations

Having developed the supersymmetric extension to the Poincaré algebra, we can now define objects that transform under the operations belonging to the corresponding group. These are called superfields, and are generic functions of the four-vector x^μ and the sets of Grassmann numbers θ^A and $\bar{\theta}_{\dot{A}}$, $A, \dot{A} \in \{0, 1\}$.

The general form of a superfield is actually rather straightforward to write down; since Grassmann numbers anticommute, the highest powers that can appear in any function are, following Eq. (2.9), $\theta\theta \equiv \theta^A \theta_A = -2\theta^1 \theta^2$ and $\bar{\theta}\bar{\theta} \equiv \bar{\theta}_{\dot{A}} \bar{\theta}^{\dot{A}} = 2\bar{\theta}_{\dot{1}} \bar{\theta}_{\dot{2}}$. Thus we can write a generic superfield as a power series expansion in θ and $\bar{\theta}$, including powers up to just two of each of them.

In total, there are then 9 possible terms. The coefficient of each term is a complex function of x^μ , called a component field; its transformation properties under the Lorentz group can be deduced by

demanding that the superfield transform as a scalar or pseudoscalar under Lorentz transformations. Thus we can write down a generic superfield $\Phi(x, \theta, \bar{\theta})$ as

$$\begin{aligned} \Phi(x, \theta, \bar{\theta}) = & f(x) + \theta^A \phi_A(x) + \bar{\theta}_{\dot{A}} \bar{\chi}^{\dot{A}}(x) + (\theta\theta)m(x) + (\bar{\theta}\bar{\theta})n(x) \\ & + (\theta\sigma^\mu\bar{\theta})V_\mu(x) + (\theta\theta)\bar{\theta}_{\dot{A}}\bar{\lambda}^{\dot{A}}(x) + (\bar{\theta}\bar{\theta})\theta^A\psi_A(x) + (\theta\theta)(\bar{\theta}\bar{\theta})d(x), \end{aligned} \quad (2.12)$$

where the various component fields transform under Lorentz transformations as:

$$\begin{aligned} f(x), m(x), n(x): & \text{ Scalars or pseudo-scalars,} \\ \psi_A(x), \phi_A(x): & \text{ Left-handed Weyl spinors,} \\ \bar{\chi}^{\dot{A}}(x), \bar{\lambda}^{\dot{A}}(x): & \text{ Right-handed Weyl spinors,} \\ V_\mu(x): & \text{ Four-vector,} \\ d(x): & \text{ Scalar.} \end{aligned}$$

The specific properties of a superfield are determined by the representation of the super-Poincaré algebra in which it transforms. It can be shown that any irreducible representation of the super-algebra can be labeled by two numbers: $m^2 \in \mathbb{R}$, corresponding to mass, and j , a generalized spin quantum number. We will concern ourselves with the representations with $j = 0$, called scalar superfields, and $j = \frac{1}{2}$, called vector superfields.⁴

To see the physical relevance of these representations, we can construct so-called Clifford vacua $|\Omega\rangle$ that satisfy $Q^A|\Omega\rangle = 0$. Acting on these states with $\bar{Q}^{\dot{1}}$ and/or $\bar{Q}^{\dot{2}}$ one can construct three additional states with the same m^2, j quantum numbers, but potentially with different spins. Specifically, it can be shown [29] that the $j = 0$ representation contains two scalar (spin-0) and two fermion (spin- $\frac{1}{2}$) states; while the $j = \frac{1}{2}$ representation contains four fermion states, three vector (spin-1) states, and one scalar state.

In general, each representation of the super-algebra contains an equal number of fermionic and bosonic states, all with the same mass m ; thus we see that extending the Poincaré algebra as we have done here imposes an additional symmetry between bosonic and fermionic degrees of freedom. In practice this means that when we construct a supersymmetric theory that is supposed to include the established Standard Model, each Standard Model particle will obtain at least one supersymmetric partner particle (“sparticle”), with opposite statistics.

We now return to Eq. (2.12), to try to recover these representations in superfield form; these superfields will later be used to construct a supersymmetric Lagrangian. The scalar superfields can be constructed by imposing $\bar{D}_{\dot{A}}\Phi(x, \theta, \bar{\theta}) = 0$ for left-handed scalar superfields Φ , and $D_A\Phi^\dagger(x, \theta, \bar{\theta}) = 0$ for right-handed superfields Φ^\dagger . Here D_A and $\bar{D}_{\dot{A}}$ are covariant derivatives, defined so that they commute with supersymmetry transformations (analogously to how gauge covariant derivatives commute with gauge transformations, as discussed in Sec. 1.1.2); explicitly [29]

$$D_A \equiv \partial_A + i(\sigma^\mu\bar{\theta})_A\partial_\mu, \quad (2.13)$$

$$\bar{D}_{\dot{A}} \equiv -\bar{\partial}_{\dot{A}} - i(\theta\sigma^\mu)_{\dot{A}}\partial_\mu. \quad (2.14)$$

Through a variable transformation it can be shown that the only allowed component fields in a left-handed scalar superfield are those that do not multiply any powers of $\bar{\theta}$ in Eq. (2.12). Following standard conventions these are given slightly different names from those we have used so far; the possible component fields are denoted by $A(x) \equiv f(x)$ and $F(x) \equiv m(x)$, which are complex scalars, and $\psi_A(x) \equiv \phi_A(x)$, a left-handed complex Weyl spinor. Applying the Euler-Lagrange equations of

⁴The reason for these names will be made clearer shortly.

motion, we can cancel unphysical degrees of freedom,⁵ leaving two fermionic and two scalar degrees of freedom. Thus as desired, the scalar superfield corresponds to the $j = 0$ representation of the super-Poincaré algebra.

Similarly, right-handed scalar superfields contain two complex scalars and a complex right-handed Weyl spinor, which after equations of motion reduce to the same number of degrees of freedom as in the left-handed case.

The $j = \frac{1}{2}$ representation is recovered in two steps. First we define a vector superfield Φ by $\Phi = \Phi^\dagger$; from Eq. (2.12) this implies

$$f(x), d(x), V_\mu(x) \in \mathbb{R}, \quad (2.15)$$

$$n(x) = m^*(x), \quad (2.16)$$

$$\bar{\chi}^{\dot{A}}(x) = \bar{\phi}^{\dot{A}}(x), \quad (2.17)$$

$$\bar{\lambda}^{\dot{A}}(x) = \bar{\psi}^{\dot{A}}(x). \quad (2.18)$$

This still leaves us with too many degrees of freedom compared to the $j = \frac{1}{2}$ representation as discussed above. This is actually analogous to the situation for vector fields in gauge theories, where due to gauge invariance the vector fields have unphysical degrees of freedom; these can be integrated out, when quantizing the theory, by making a choice of gauge.

The solution here is similar; by defining *supergauge* transformations on the superfields, which we will discuss in Sec. 2.2.2, we recover the physical degrees of freedom corresponding to the $j = \frac{1}{2}$ representation in what is called Wess-Zumino gauge. After applying equations of motion this further reduces the degrees of freedom to two (massless) vector and two fermion degrees of freedom corresponding to a left-handed Weyl spinor λ and its right-handed conjugate $\bar{\lambda}$.

2.2 Minimal Supersymmetric Standard Model

Now that we have briefly explained the theoretical background for the super-Poincaré algebra and how its representations can be expressed as superfields, we can go about constructing a Lagrangian consisting of these superfields. We have two basic criteria for this model: It must contain at least all of the established Standard Model, as it is supposed to be an *extension* thereof; and it must contain terms that break supersymmetry.

The latter may seem counterproductive; we are after all trying to construct a supersymmetric theory, so having to break supersymmetry in the same theory appears to rather defeat the purpose. However, if supersymmetry were not broken, from the discussion in Sec. 2.1.2 all of the new supersymmetric particles would be mass-degenerate to their Standard Model counterparts;⁶ from experiment this is clearly not the case, so supersymmetry must be broken at our energy scales. This logic is similar to that of electroweak theory, where the theory is based on gauge invariance, but that invariance is broken at our energy scales.

We will discuss the breaking of supersymmetry at the end of this section; first, we will construct a supersymmetric extension to the Standard Model by following the same logic as in Sec. 1.1.

⁵This includes the entire F field; having no derivatives it is a so-called *auxiliary* field, for which we can solve in terms of other, physical degrees of freedom.

⁶Since each representation is labeled by the number j and a *single* mass m .

2.2.1 Supersymmetric Lagrangians

The action in a supersymmetric theory is defined as

$$S \equiv \int d^4x \int d^4\theta \mathcal{L}, \quad (2.19)$$

where the Grassmann volume element is defined as [29]

$$d^4\theta \equiv d^2\theta d^2\bar{\theta}, \quad (2.20)$$

$$d^2\theta \equiv -\frac{1}{4}d\theta^A d\theta_A, \quad (2.21)$$

$$d^2\bar{\theta} \equiv -\frac{1}{4}d\bar{\theta}_{\dot{A}} d\bar{\theta}^{\dot{A}}, \quad (2.22)$$

so that $\int d^4\theta (\theta\theta)(\bar{\theta}\bar{\theta}) \equiv 1$, and all lesser powers of θ vanish under the integration.

With these definitions only the highest-order terms in the Lagrangian survive the integration over the Grassmann coordinates. This is important for the action to remain invariant under supersymmetry transformations; for a vector superfield the $\theta\theta\bar{\theta}\bar{\theta}$ component changes by a total derivative $\sim \partial_\mu f^\mu(x)$, which vanishes under integration, keeping S unchanged. Similarly, for a scalar superfield the $\theta\theta$ component ($\bar{\theta}\bar{\theta}$ in the case of a right-handed superfield) has this property. The other component fields do not in general transform in this way; thus we must take care to only project out the highest order terms in a supersymmetric action.

Notice here that this gives supersymmetric Lagrangians a different mass dimension from “regular” ones; from Eq. (2.7c), $[Q^A] = \frac{1}{2}[P^\mu] = \frac{1}{2}$, and then from Eq. (2.8) we have $[\theta^A] = -[Q^A] = -\frac{1}{2}$ and $[d\theta] = \frac{1}{2}$. The overall dimension of the integrals in Eq. (2.19) is therefore -2 . Thus, to keep the action dimensionless, we must have $[\mathcal{L}] = 2$.

This means that to keep the mass dimensions of couplings non-negative, and hence the Lagrangian renormalizable, the Lagrangian can at most have operators of mass dimension 2. Furthermore, as we noted above we must project out only the highest-order component fields of scalar or vector superfields to keep the action supersymmetry-invariant. To do this, each term in the Lagrangian must actually transform like one of these types of field. Thus in a Lagrangian constructed out of scalar superfields, we can only include terms of the form $\Phi_i^\dagger \Phi_i$, which are vector superfields, or products of scalar superfields of the same handedness, which are also scalar superfields of that same handedness.

Then, taking into account that the action must be real and that scalar superfields have mass dimension 1,⁷ the most general renormalizable and supersymmetric Lagrangian written solely in terms of a set of scalar superfields $\Phi_i(x, \theta, \bar{\theta})$ is

$$\mathcal{L} = \Phi_i^\dagger \Phi_i + \bar{\theta}\bar{\theta}W[\Phi] + \theta\theta W^\dagger[\Phi^\dagger], \quad (2.23)$$

where the *superpotential* $W[\Phi]$, by renormalizability, can be written as

$$W[\Phi] = g_i \Phi_i + m_{ij} \Phi_i \Phi_j + \lambda_{ijk} \Phi_i \Phi_j \Phi_k. \quad (2.24)$$

The first term in Eq. (2.23) is referred to as the kinetic term.

⁷This can be seen from the first term in Eq. (2.12), since scalar fields have mass dimension 1.

2.2.2 Supergauge invariance

To make a supersymmetric extension of the Standard Model, we need to define the supersymmetric equivalent to gauge transformations. These are referred to as supergauge transformations. We will discuss the non-Abelian case here; the Abelian case, as in Sec. 1.1.2, can be obtained easily from this.

A non-Abelian supergauge transformation on a multiplet (left-handed) scalar superfield Φ , for a gauge group with generators T^a , is defined by [32]

$$\Phi \rightarrow \Phi' = e^{-igT^a\Lambda^a}\Phi, \quad (2.25)$$

where Λ^a , in order for Φ' to remain a left-handed scalar superfield, must themselves be left-handed scalar superfields. Defining $\Lambda \equiv g\Lambda^a T^a$, the kinetic term in Eq. (2.23) transforms as

$$\Phi^\dagger \Phi \rightarrow \Phi^\dagger e^{i\Lambda^\dagger} e^{-i\Lambda} \Phi. \quad (2.26)$$

We make this gauge invariant similarly to regular gauge theories; we replace the kinetic term by $\Phi^\dagger e^{\mathbf{V}} \Phi$, with $\mathbf{V} = gV^a T^a$; here V^a are vector superfields, which must transform as

$$e^{\mathbf{V}} \rightarrow e^{-i\Lambda^\dagger} e^{\mathbf{V}} e^{i\Lambda}. \quad (2.27)$$

Like in the Standard Model Lagrangian, see Eq. (1.29), we can also add a field strength term that is both gauge and supersymmetry invariant, as well as renormalizable; we define the supersymmetric field strength as

$$W_A \equiv -\frac{1}{4} \overline{D} \overline{D} (e^{-\mathbf{V}} D_A e^{\mathbf{V}}), \quad (2.28a)$$

$$\overline{W}^{\dot{A}} \equiv -\frac{1}{4} D D (e^{-\mathbf{V}} \overline{D}^{\dot{A}} e^{\mathbf{V}}). \quad (2.28b)$$

These can be shown to be left-handed and right-handed scalar superfields, respectively, in that $\overline{D}^{\dot{A}} W_A = 0$ and $D_A \overline{W}^{\dot{A}} = 0$.

The construction to create supergauge invariant Lagrangian terms out of these field strengths is similar to in Yang-Mills theory; depending on the representation R of the group generators T^a , we can add

$$\mathcal{L}_g = -\frac{1}{4T(R)g^2} \overline{\theta} \theta \text{tr}(W^A W_A) - \frac{1}{4T(R)g^2} \theta \theta \text{tr}(\overline{W}_{\dot{A}} \overline{W}^{\dot{A}}), \quad (2.29)$$

to the Lagrangian, with $\text{tr}(T^a T^b) = T(R) \delta^{ab}$.

2.2.3 Minimal field content

We now have all of the theoretical pieces necessary to construct a supersymmetric extension to the Standard Model (so far we assume the model to be exactly supersymmetric; the breaking of supersymmetry will be discussed in Sec. 2.2.5). First we must consider what superfields to include in the Lagrangian; in order for the number of predicted new particles to stay as low as possible, we will only include the bare minimum number of fields needed to contain all of the Standard Model fields discussed in Sec. 1.1.4. The model that follows from this principle is called the Minimal Supersymmetric Standard Model (MSSM).

Recall from Sec. 2.1.2 that a scalar superfields contains (excluding auxiliary fields) one Weyl spinor and one complex scalar. Thus for each Standard Model Dirac fermion⁸ we need one left-handed scalar superfield and a different right-handed one. For each of these fields we also get a scalar particle/antiparticle pair.

⁸With left- and right-handed chiralities summed over; $\psi = \psi_L + \psi_R$, $\psi_{R/L} = \frac{1}{2}(1 \pm \gamma^5)\psi$.

Table 2.1: Charges of the MSSM left-handed scalar superfields. The $SU(2)_L$ singlets have opposite hypercharges from those listed in Tab. 1.1; this is due to the fact the right-handed spinors listed there are obtained from the conjugate of the left-handed superfields in this table. As before, F means that the field transforms in the fundamental representation of a group.

Field	L_i	$\bar{\ell}_i$	Q_i	\bar{u}_i	\bar{d}_i	H_u	H_d
$SU(3)_C$	0	0	F	F	F	0	0
$SU(2)_L$	F	0	F	0	0	F	F
$U(1)_Y$	$-\frac{1}{2}$	1	$\frac{1}{6}$	$-\frac{2}{3}$	$\frac{1}{3}$	$\frac{1}{2}$	$-\frac{1}{2}$

These superfields are organized exactly like in the Standard Model case; left-handed superfields are arranged into $SU(2)_L$ doublets given by

$$L_i = \left\{ \begin{pmatrix} \nu_e \\ e \end{pmatrix}, \begin{pmatrix} \nu_\mu \\ \mu \end{pmatrix}, \begin{pmatrix} \nu_\tau \\ \tau \end{pmatrix} \right\}, \quad Q_i = \left\{ \begin{pmatrix} u \\ d \end{pmatrix}, \begin{pmatrix} c \\ s \end{pmatrix}, \begin{pmatrix} t \\ b \end{pmatrix} \right\}. \quad (2.30)$$

The right-handed superfields are $SU(2)_L$ singlets, given by

$$\bar{\ell}_i^\dagger = \left\{ \bar{e}^\dagger, \bar{\mu}^\dagger, \bar{\tau}^\dagger \right\}, \quad \bar{u}_i^\dagger = \left\{ \bar{u}^\dagger, \bar{c}^\dagger, \bar{t}^\dagger \right\}, \quad \bar{d}_i^\dagger = \left\{ \bar{d}^\dagger, \bar{s}^\dagger, \bar{b}^\dagger \right\}, \quad (2.31)$$

where $\bar{\ell}_i$, \bar{u}_i , and \bar{d}_i are *left-handed* superfields, with opposite hypercharges from those listed for the right-handed fields in Tab. 1.1. Note that we have not included any right-handed neutrino superfield here; this is purely conventional.

For the Higgs boson, the situation is now more complicated. For the Standard Model Yukawa terms in Eq. (1.24) we had to take the conjugate of the Higgs field in the terms with up-type particles, e.g. $-Y_{ij}^u \bar{Q}^i H^C u_R^j$ with $H^C = i\sigma^2 H^*$. Generalizing this to superfields would mean including terms in the Lagrangian that mix left- and right-handed superfields, which we cannot do. Thus we will need two Higgs doublet superfields, given by

$$H_u = \begin{pmatrix} H_u^+ \\ H_u^0 \end{pmatrix}, \quad H_d = \begin{pmatrix} H_d^0 \\ H_d^- \end{pmatrix}. \quad (2.32)$$

This will give four scalar Higgs particles (two electrically neutral, one positive and one negative) and one neutral pseudoscalar — the three remaining scalar degrees of freedom are used to give masses to the W^\pm and Z bosons — as well as fermion *Higgsinos*.

A summary of the (left-handed) scalar superfields we have included, with their respective charges under the gauge groups, can be found in Tab. 2.1.

Finally we need the supergauge fields; in terms of component fields, after eliminating auxiliary fields, these bring a massless vector and a pair of Weyl spinors λ and $\bar{\lambda}$. If the superfield is electrically uncharged, these Weyl spinors combine to form a Majorana fermion; if not they can combine with the Weyl spinors of a different vector superfield to form Dirac fermions.

The kinetic and gauge terms follow more or less automatically from our previous discussion; denoting the vector gauge superfields of $SU(3)_C$, $SU(2)_L$, and $U(1)_Y$ by g^a , W^a , and B , respectively, and using the charges in Tab. 2.1, we can write

$$\begin{aligned} \mathcal{L}_k = & Q_i^\dagger e^{g_s g^a T^a + g W^a \tau^a + \frac{1}{6} g' B} Q_i + \bar{u}_i^\dagger e^{g_s g^a T^a - \frac{2}{3} g' B} \bar{u}_i + \bar{d}_i^\dagger e^{g_s g^a T^a + \frac{1}{3} g' B} \bar{d}_i \\ & + L_i^\dagger e^{g W^a \tau^a + \frac{1}{2} g' B} L_i + \bar{\ell}_i^\dagger e^{g' B} \bar{\ell}_i + H_u^\dagger e^{g W^a \tau^a + \frac{1}{2} g' B} H_u + H_d^\dagger e^{g W^a \tau^a - \frac{1}{2} g' B} H_d. \end{aligned} \quad (2.33)$$

For the gauge terms, we get, using $T(R) = T_F = \frac{1}{2}$ in the fundamental representation of both $SU(3)$ and $SU(2)$,

$$\mathcal{L}_g = \frac{1}{2g_s^2} \bar{\theta}\theta \text{tr}(g^A g_A) + \frac{1}{2g^2} \bar{\theta}\theta \text{tr}(W^A W_A) + \frac{1}{4} \bar{\theta}\theta B^A B_A + \text{h.c.}, \quad (2.34)$$

where g^A , W^A , and B^A are the field strengths constructed from g^a , W^a , and B , respectively.⁹

2.2.4 Superpotential and R -parity

The last ingredient needed is finding the most general gauge invariant superpotential consisting of these fields. Recall that the superpotential contribution to the Lagrangian is

$$\mathcal{L}_W = \bar{\theta}\theta W[\Phi_i] + \text{h.c.}, \quad (2.35)$$

with

$$W[\Phi_i] = g_i \Phi_i + m_{ij} \Phi_i \Phi_j + \lambda_{ijk} \Phi_i \Phi_j \Phi_k. \quad (2.36)$$

Following the logic of Sec. 1.1.4 we would now write down all possible such terms consistent with gauge invariance. This quickly leads to trouble, however; for example, we might add a term like $\lambda_{ijk} L_i L_j \bar{\ell}_k$;¹⁰ this, and other similar terms, predict non-zero amplitudes for processes that violate lepton and baryon number conservation. For this to be consistent with experiment the couplings would have to be extremely small.

In order to avoid such interactions altogether, we postulate another symmetry of the theory, called conservation of R -parity. The R -parity of a particle with baryon number B , lepton number L , and spin s is defined as [32]

$$P_R \equiv (-1)^{3(B-L)+2s}. \quad (2.37)$$

For a multi-particle state, the total R -parity given by the product of the individual parities. With this definition all Standard Model particles (plus the additional Higgs scalars we had to introduce) have $P_R = +1$, while supersymmetric particles (sparticles) have $P_R = -1$.

The postulated conservation of R -parity in the Lagrangian forbids the problematic terms from the superpotential; physically, it means that sparticles must always be created or annihilated in even numbers, and in particular that the lightest supersymmetric particle (LSP) is completely stable since there is nothing it can decay to. As a consequence, a neutral¹¹ LSP in an R -parity conserving theory is a possible dark matter candidate; dark matter must be (at least very close to) stable as it would otherwise have decayed already, and this is satisfied by the LSP.

Now, postulating an additional symmetry like this is obviously undesirable, since for a theory to be as predictive as possible we typically want to start from as few basic principles as possible. However, in this situation, where the other alternative would be constructing a model that clearly breaks with observed phenomena, unless there is some significant fine-tuning of parameters, it is probably the lesser “evil.”

With R -parity conservation the most general superpotential of the MSSM is given by

$$W[\Phi_i] = Y_{ij}^\ell L_i H_d \bar{\ell}_j + Y_{ij}^d Q_i H_d \bar{d}_j + Y_{ij}^u Q_i H_u \bar{u}_j + \mu H_u H_d. \quad (2.38)$$

⁹For an abelian theory with a vector superfield B the field strength simplifies to $B_A = -\frac{1}{4} \bar{D}\bar{D}D_A B$, with no trace necessary to make the Lagrangian term gauge invariant.

¹⁰In this and the expressions to follow, we implicitly insert a factor $i\sigma^2$ in between all $SU(2)_L$ doublets to preserve $SU(2)_L$ gauge invariance.

¹¹A neutral particle has limited interaction with ordinary matter besides gravitation.

The Yukawa terms correspond to the Yukawa terms in the SM Lagrangian, with the same couplings (so that we reproduce the SM masses); thus μ is so far the only new Lagrangian parameter of the MSSM relative to the SM. This, along with Eqs. (2.33) and (2.34), exhausts the possible terms we can include in a supersymmetric, renormalizable, gauge invariant, and R -parity conserving Lagrangian consisting of our minimal number of superfields.

Notice that at surface-level, it would appear that this Lagrangian is missing a quartic Higgs boson interaction like the one in Eq. (1.14), which was what led to electroweak symmetry breaking. This is not the case, however; when applying equations of motion to solve for the auxiliary fields and eliminate them in favor of dynamical fields, we obtain a *scalar potential* that among other things contains quartic interactions of scalar component fields.

2.2.5 Breaking supersymmetry

The Lagrangian we have constructed so far is invariant under supersymmetry transformations, meaning that all of the new supersymmetric particles are mass degenerate to their Standard Model counterparts, badly contradicting experimental results. Thus supersymmetry must be broken at our energy scale.

Presumably, such a breaking of supersymmetry would happen through a mechanism similar to the Higgs mechanism, where the symmetry is spontaneously broken at some higher energy scale. The exact mechanism that causes this is unclear, however, so we will simply add terms to the Lagrangian that explicitly break supersymmetry.

This is similar to an “effective” theory in the Wilsonian picture of renormalization, in which we assume that the spontaneous symmetry breaking happens at an energy scale that is inaccessible experimentally. We can then integrate out these high-energy degrees of freedom, leaving effective, non-supersymmetric terms in the Lagrangian. This is analogous to the theory of weak interactions where high-energy degrees of freedom are integrated out, leaving a non-gauge invariant theory with massive vector bosons.

To avoid the quadratic divergences that lead to the hierarchy problem, as will be discussed in Sec. 2.3.1, we restrict ourselves to so-called “soft” terms, whose couplings have mass dimensions of at least one [33]; these still give divergences, but only logarithmic ones. Following the notation of Ref. [32], the possible soft terms in a supergauge theory are

$$\begin{aligned} \mathcal{L}_{\text{soft}} = & - \left(\frac{1}{4T(R)g^2} M_a \theta\theta\bar{\theta}\bar{\theta} \text{tr}(W_a^A W_{aA}) + \frac{1}{6} a_{ijk} \theta\theta\bar{\theta}\bar{\theta} \Phi_i \Phi_j \Phi_k \right. \\ & \left. + \frac{1}{2} b_{ij} \theta\theta\bar{\theta}\bar{\theta} \Phi_i \Phi_j + t_i \theta\theta\bar{\theta}\bar{\theta} \Phi_i \right) + \text{h.c.} - m_{ij}^2 \theta\theta\bar{\theta}\bar{\theta} \Phi_i^\dagger \Phi_j, \end{aligned} \quad (2.39)$$

or in terms of component fields,

$$\int d^4\theta \mathcal{L}_{\text{soft}} = - \left(\frac{1}{2} M_a \lambda_a^A \lambda_{aA} + \frac{1}{6} a_{ijk} \phi_i \phi_j \phi_k + \frac{1}{2} b_{ij} \phi_i \phi_j + t_i \phi_i \right) + \text{c.c.} - m_{ij}^2 \phi_i^\dagger \phi_j. \quad (2.40)$$

Here λ_a^A is the left-handed Weyl spinor component of the vector superfield V_a ; ϕ_i is the scalar component of a scalar superfield Φ_i . From this form we see that these terms have exactly the desired effect, giving extra mass terms to all of the sparticles.

Which of these soft-breaking terms are included in the MSSM Lagrangian is determined by enforcing gauge invariance and R -parity conservation, like before. This immediately excludes the tadpole term ($\propto t_i$) as we have no gauge singlet superfields. The a_{ijk} and b_{ij} terms are allowed for the same combinations of fields as in the superpotential, see Eq. (2.38); the field strength term is allowed for each of the three gauge groups; and the final mass term is allowed as long as ϕ_i^\dagger transforms in the complex conjugate representation of the gauge groups relative to ϕ_j .

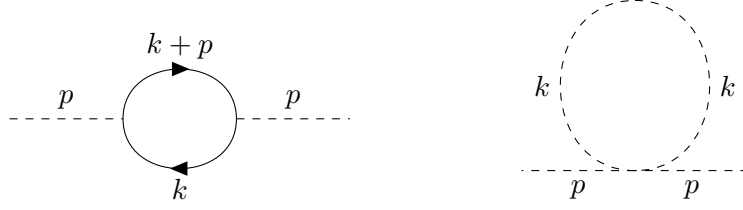


Figure 2.1: 1-loop fermionic (left) and scalar (right) contributions to the Higgs boson self-energy.

2.3 Theoretical advantages of the MSSM

As we alluded to in the Introduction there are several outstanding theoretical questions in the Standard Model, that may be solved in the MSSM. One of these was dark matter; and in Sec. 2.2.4 we briefly noted how the MSSM provides a possible dark matter candidate in the LSP. Now, we will demonstrate how loop effects can help answer more of these questions. We begin with perhaps the most historically important one, which has been one of the most significant arguments for supersymmetry, namely the Higgs boson hierarchy problem.

2.3.1 Hierarchy problem

The origin of the hierarchy problem can be understood by considering corrections to the Higgs boson propagator, and hence its $\overline{\text{MS}}$ mass, at one-loop level. Suppose that the Higgs boson can interact with a fermion ψ with mass m_f , and a scalar ϕ with mass m_s , as described by the Lagrangian terms

$$\mathcal{L} \supset -\lambda_f \bar{\psi} \psi H - \lambda_s \phi^\dagger \phi H^\dagger H. \quad (2.41)$$

These particles contribute to the Higgs self-energy through the loops shown in Fig. 2.1. Summing over the infinite series of insertions of these loops on the Higgs propagator, the total propagator, renormalized in the $\overline{\text{MS}}$ scheme, is given by

$$iG(p^2) = \frac{i}{p^2 - m_{\overline{\text{MS}}}^2 + \Sigma_{\overline{\text{MS}}}(p^2)}, \quad (2.42)$$

where, evaluating the loops in Fig. 2.1, the (unrenormalized) self-energy is given by

$$i\Sigma(p^2) = -|\lambda_f|^2 \mu^{4-d} \int \frac{d^d k}{(2\pi)^d} \frac{\text{Tr}[(\not{k} + m_f)(\not{k} + \not{p} + m_f)]}{(k^2 - m_f^2)((k+p)^2 - m_f^2)} + 2\lambda_s \mu^{\frac{4-d}{2}} \int \frac{d^d k}{(2\pi)^d} \frac{1}{k^2 - m_s^2}. \quad (2.43)$$

Evaluating the Dirac trace and using our previously discussed methods of Feynman parametrization and Wick rotation, this can be rewritten as

$$i\Sigma(p^2) = 4i|\lambda_f|^2 \mu^{4-d} \int_0^1 dx \int \frac{d\Omega_d}{(2\pi)^d} \int_0^\infty dk_E \frac{k_E^{d-1} (k_E^2 - \Delta)}{(k_E^2 + \Delta)^2} - 2i\lambda_s \int \frac{d\Omega_d}{(2\pi)^d} \int_0^\infty dk_E \frac{k_E^{d-1}}{k_E^2 + m_s^2}, \quad (2.44)$$

where $\Delta \equiv m_f^2 - p^2 x(1-x)$.

We evaluate this in two different ways. First we use a simple ultraviolet cutoff, i.e. changing the upper integration limit of k_E to Λ and setting $d = 4$, leaving

$$\Sigma_\Lambda(p^2) \simeq \frac{|\lambda_f|^2}{4\pi^2} \Lambda^2 - \frac{\lambda_s}{8\pi^2} \Lambda^2 \quad (2.45)$$

to highest order in Λ . We observe that the self-energy is quadratically divergent; if we assume that Λ has some physical meaning, e.g. as the highest energy scale at which the theory is viable, this suggests that the Higgs boson propagator and mass are extremely sensitive to corrections from these high energy scales. In other words, the Higgs mass is *UV sensitive*. The divergences can be removed through mass renormalization, but this still requires significant fine-tuning to cancel very large terms.

The quadratic divergence is not present in dimensional regularization, but the UV sensitivity remains; to see this, suppose that the masses of the interacting particles $m_f, m_s \gg m_h$, so that

$$\Sigma_d \simeq -\frac{|\lambda_f|^2}{4\pi^2} \left(\frac{3m_f^2}{\bar{\epsilon}} + m_f^2 \right) + \frac{\lambda_s}{8\pi^2} \left(\frac{m_s^2}{\bar{\epsilon}} + m_s^2 \right), \quad (2.46)$$

where $\frac{1}{\bar{\epsilon}} = \frac{1}{\epsilon} - \gamma_E + \ln 4\pi$. Then, defining the $\overline{\text{MS}}$ -renormalized version of the self-energy $\Sigma_{\overline{\text{MS}}}$ by simply removing the terms proportional to $1/\bar{\epsilon}$, the difference between the $\overline{\text{MS}}$ mass and physical pole mass m_h of the Higgs boson is given by

$$m_h^2 - m_{\overline{\text{MS}}}^2 = -\Sigma_{\overline{\text{MS}}}(m_h^2), \quad (2.47)$$

as determined by demanding that Eq. (2.42) have a pole at the physical mass m_h . Explicitly this means that

$$m_h^2 - m_{\overline{\text{MS}}}^2 \simeq \frac{|\lambda_f|^2}{4\pi^2} m_f^2 - \frac{\lambda_s}{8\pi^2} m_s^2. \quad (2.48)$$

Again we see that the Higgs mass is highly sensitive to contributions from higher scales; if we suppose that the Standard Model has some UV completion at a high energy,¹² e.g. at the Planck scale, and interactions between the Higgs boson and particles at this scale exist, the Higgs mass gets corrections proportional to this scale. The fact that the observed Higgs mass is still on the same energy scale as other electroweak particles is the *hierarchy problem* of the Higgs boson.

This problem vanishes in a supersymmetric theory. As we noted in Sec. 2.1.2, fermions and their scalar partners have the same mass as long as supersymmetry is not broken, i.e. $m_f = m_s$. Furthermore, from a Yukawa term $W_Y[\Phi] = -\lambda\Phi\Phi H$ in the superpotential, we get a contribution, in terms of component fields, of

$$\mathcal{L} \supset -\lambda\psi\psi h, \quad (2.49)$$

where ψ is the Weyl spinor component of Φ , and h is the scalar component of H . Eliminating auxiliary degrees of freedom by solving for auxiliary fields with the equations of motion, the Yukawa term contribution to the Lagrangian also includes a term [32]

$$\mathcal{L} \supset -\left| \frac{\partial W_Y}{\partial \phi} \right|^2 = -|\lambda|^2 \phi^\dagger \phi h^\dagger h, \quad (2.50)$$

where ϕ is the scalar component of Φ . This means that we also have $\lambda_s = |\lambda_f|^2$ in our above notation.

Finally, as we argued in Sec. 2.2.3, a Dirac fermion must be constructed out of two scalar superfields, meaning that there are two (complex) scalars ϕ for each Dirac fermion ψ . Taking all of this into account, we see that the fermion and scalar contributions, in both Eqs. (2.45) and (2.48), exactly cancel in a supersymmetric theory.

Naturally, this will not be the case in the MSSM, which contains terms that explicitly break supersymmetry. Still, as long as we limit these terms to so-called soft terms with mass dimensions

¹²Which we need to do in a complete theory, due to the Landau poles discussed in Sec. 1.2.5.

of at least 1 as we did in the previous section, the divergences in the Higgs self-energy are at worst logarithmic [33], not quadratic as they were above. From Eq. (2.40) and following the above calculation, we see that we will get a contribution proportional to $a_{ijk}^2/(4\pi)^2$ to the (squared) Higgs mass,¹³ and since $[a_{ijk}] = 1$, by dimensional analysis the cutoff dependence can then at most be logarithmic. To keep this correction on the same order as the Higgs mass itself, and avoid too much fine-tuning of parameters, we then at most want $a_{ijk} \sim m_{\text{soft}} \lesssim 1 \text{ TeV}$.

Thus, as long as the new particles are not much heavier than 1 TeV, we can still avoid the hierarchy problem in the MSSM.

2.3.2 Electroweak symmetry breaking

In Sec. 1.1.3 we discussed how a Higgs potential in which the Higgs field obtains a vacuum expectation value (vev), i.e. one with a minimum at a non-zero field value, leads to electroweak symmetry breaking to give masses to particles. We did, however, note that we had to simply construct a potential like the one in Eq. (1.14) in order for this to work.

We will now see how this symmetry breaking works in the MSSM, and how, with some assumptions, the MSSM can actually predict a potential leading to a Higgs vev. We begin by considering the Higgs scalar potential of the MSSM. Most of the terms contributing to this potential have been discussed already; including also contributions from the soft-breaking terms

$$\mathcal{L} \supset -bH_u H_d + \text{h.c.} - m_{H_u}^2 H_u^\dagger H_u - m_{H_d}^2 H_d^\dagger H_d, \quad (2.51)$$

the potential is given by [32]

$$\begin{aligned} V(H) = & \left(|\mu|^2 + m_{H_u}^2 \right) \left(|H_u^+|^2 + |H_u^0|^2 \right) + \left(|\mu|^2 + m_{H_d}^2 \right) \left(|H_d^0|^2 + |H_d^-|^2 \right) \\ & + [b(H_u^+ H_d^- + H_u^0 H_d^0) + \text{c.c.}] + \frac{1}{2} g^2 |H_u^+ H_d^{0*} + H_u^0 H_d^{-*}|^2 \\ & + \frac{1}{8} (g^2 + g'^2) \left(|H_u^0|^2 + |H_u^+|^2 - |H_d^0|^2 - |H_d^-|^2 \right)^2. \end{aligned} \quad (2.52)$$

For spontaneous electroweak symmetry breaking, we need this potential to have a (finite) minimum for non-zero field values; this is achieved by the simultaneous fulfillment of the criteria

$$2b < |\mu|^2 + m_{H_u}^2 + m_{H_d}^2, \quad (2.53)$$

$$b^2 > \left(|\mu|^2 + m_{H_u}^2 \right) \left(|\mu|^2 + m_{H_d}^2 \right). \quad (2.54)$$

This is indeed possible, so electroweak symmetry breaking is possible also in the MSSM. Note, however, that these constraints cannot be fulfilled without non-zero values for the soft parameters $m_{H_u}^2$, $m_{H_d}^2$, and b ; thus spontaneous electroweak breaking in the MSSM *requires* supersymmetry to be broken.

More interestingly, suppose that $m_{H_u}^2 = m_{H_d}^2$ at some high scale, e.g. at the scale at which supersymmetry is broken (the *input scale*). If it is assumed that some common mechanism causes all of the supersymmetry-breaking terms in the Lagrangian, this is a fairly reasonable starting point. We then allow these parameters to run with energy scale, by including loop corrections. Both $m_{H_u}^2$ and $m_{H_d}^2$ will increase with increasing energy scales, at a rate approximately proportional to their highest corresponding Yukawa coupling; y_t in the case of H_u , and y_b in the case of H_d , where y_t and y_b are the largest eigenvalues of Y_{ij}^u and Y_{ij}^d , from Eq. (2.38), respectively. Since $y_t \gg y_b$,

¹³This contribution comes from a diagram similar to the fermion loop diagram in Fig. 2.1, but with a scalar in the loop.

this means that at lower scales $m_{H_u}^2 \ll m_{H_d}^2$. If the input scale is sufficiently high, the first factor in Eq. (2.54) may even become negative, automatically fulfilling that constraint for positive b^2 . This does not guarantee electroweak symmetry breaking, but it helps significantly in widening the parameter space in which it is achieved.

This shows how spontaneous breaking of the electroweak symmetry can happen much more “organically” in the MSSM than in the Standard Model, as it can be achieved through quantum corrections, assuming universality of the soft-breaking parameters at the input scale.

One part of this argument is somewhat puzzling, though: In Eqs. (2.53) and (2.54), the three soft-breaking parameters are assumed to have some common origin at a high energy scale, and are effective parameters describing this process. The parameter μ , however, has an entirely different origin, coming from the superpotential as a part of the supersymmetric Lagrangian. Thus there is nothing to suggest that there would be any relation between μ and the soft-breaking parameters; nonetheless, μ has to be of the same order of magnitude as the soft parameters for the above argument to work out. This is referred to as the “ μ problem” of the MSSM.

2.4 Phenomenology of the MSSM

The MSSM predicts a number of new particles, called sparticles. Experimental evidence of supersymmetry would naturally include some signature of production of these particles at particle colliders like the LHC; for this reason, one of the most relevant observables to calculate theoretically in the MSSM is the production cross-section for supersymmetric particles.

Later in the thesis we will perform such a calculation for the pair-production of sleptons — the scalar partners of the Standard Model leptons — at hadron colliders. To establish some notation and conventions, we will here give a brief overview of the sparticles appearing in this process, before discussing how sleptons might hypothetically appear in results from hadron colliders.

2.4.1 Supersymmetric particles

For each Standard Model fermion f , the MSSM predicts two complex sfermions \tilde{f}_L and \tilde{f}_R , one from each of the scalar superfields needed to represent a Dirac fermion; leptons get slepton partners, while quarks get squark partners. Taking into account all possible sources for mass terms for these particles, including from auxiliary-field terms, soft-breaking terms, the superpotential, as well as from Higgs vev contributions like in the Standard Model, the masses are determined by the general form

$$\mathcal{L}_{\tilde{f}} = -(\tilde{f}_L^* \quad \tilde{f}_R^*) m_{\tilde{f}}^2 \begin{pmatrix} \tilde{f}_L \\ \tilde{f}_R \end{pmatrix}, \quad (2.55)$$

where $m_{\tilde{f}}^2$ is a generic 2×2 matrix. If this matrix is not diagonal, the mass eigenstates will differ from the chiral eigenstates;¹⁴ diagonalizing $m_{\tilde{f}}^2$, we can rewrite this in terms of the mass eigenstates \tilde{f}_1, \tilde{f}_2 as

$$\mathcal{L}_{\tilde{f}} = - \sum_{A=1}^2 m_{\tilde{f}_A}^2 |\tilde{f}_A|^2, \quad (2.56)$$

where now $m_{\tilde{f}_A}$ are numbers, $A = 1, 2$, and the mass eigenstates are related to the chiral eigenstates by

$$\begin{pmatrix} \tilde{f}_L \\ \tilde{f}_R \end{pmatrix} = \begin{pmatrix} \cos \theta_f & \sin \theta_f \\ -\sin \theta_f & \cos \theta_f \end{pmatrix} \begin{pmatrix} \tilde{f}_1 \\ \tilde{f}_2 \end{pmatrix}. \quad (2.57)$$

¹⁴Technically chirality has nothing to do with this; the L/R labels on the sfermions only denote the handedness of their associated Weyl spinors.

By convention, these eigenstates are usually defined so that $m_{\tilde{f}_2} \geq m_{\tilde{f}_1}$.

In our later calculations we will use this mass basis for sleptons and squarks, using their pole masses and mixing angles θ_f as the parameters of the theory.¹⁵ This helps keep the calculations as general as possible; for most of the sfermions this is rather overly cautious, as $\theta_f \approx 0$ for the first two generations of squarks and sleptons.¹⁶

Note that we have implicitly assumed that there is no mixing across slepton or squark flavors or generations; this is done to avoid large cross-sections for flavor-number violating processes. In practice this means restricting m_{ij}^2 in Eq. (2.40) to be approximately diagonal.

This mostly covers the sparticles that will appear in our later calculations; the sleptons obviously appear in the final state, while squarks appear in loop corrections to the quark-antiquark-electroweak gauge boson vertex. The only remaining particle is the gluino \tilde{g} , which is the fermion partner to the gluon.

As there are no other particles in the model with the same quantum numbers as the gluino it cannot mix with anything, making it somewhat simpler to discuss than the aforementioned sfermions; it is a Majorana fermion, originating from a single vector superfield g^a ; it is a color octet transforming in the adjoint representation of $SU(3)_C$, like its Standard Model counterpart; and its mass gets only one contribution at tree-level, from the soft-breaking term

$$\mathcal{L}_{\tilde{g}} = -\frac{1}{2}M_3\tilde{g}^a\tilde{g}^a + \text{c.c.}, \quad (2.58)$$

so that the gluino mass is simply $m_{\tilde{g}} = |M_3|$ at tree-level.

2.4.2 Slepton pair production at hadron colliders

The main candidates to discover sleptons are high-energy hadron or lepton (specifically electron-positron) colliders. The latter is more specifically suited for detecting slepton production, as there will be significantly less background at such colliders; furthermore, since one possible experimental signature of slepton production is missing momentum in the final state (see below), the analysis becomes much less complicated when the colliding particles are point particles, rather than the composite particles of hadron colliders.

However, leptons are much lighter than hadrons. In a circular accelerator, which is the most physically compact way of achieving the highest possible energies, the energy lost in bremsstrahlung would then be far larger for leptons than for hadrons. This makes a circular e^+e^- collider more or less completely unfeasible for high energies; to match the energies obtainable at hadron colliders, one would need a linear e^+e^- collider far larger than any currently existing.

Thus, we will focus on production at hadron colliders. The production of sleptons, which are not color-charged (and thus interact only weakly), will be suppressed compared to that of particles that do carry such charge (and interact strongly); but the energies obtainable still make hadron collider experiments a viable method for discovery of sleptons.

As we will discuss in the next chapter, hadron collisions are described by a partonic process of the hadron's constituent particles, i.e. quarks, antiquarks, and gluons, multiplied by a parton distribution function. The partonic process for slepton pair production is very similar to that of lepton pair production in the Drell-Yan process; the leading-order Feynman diagram can be seen in Fig. 2.2. Here A, B denote the mass eigenstates of the produced sleptons, while i denotes the flavor.

¹⁵In practice these have to be calculated from the other parameters in the theory, notably soft mass terms and the vevs of H_u^0, H_d^0 .

¹⁶The off-diagonal terms in Eq. (2.55) are proportional to the corresponding Yukawa couplings of Eq. (2.38). Since these couplings are in turn proportional to the (SM) particle masses, they are negligible for all but the stau, sbottom, and stop particles.

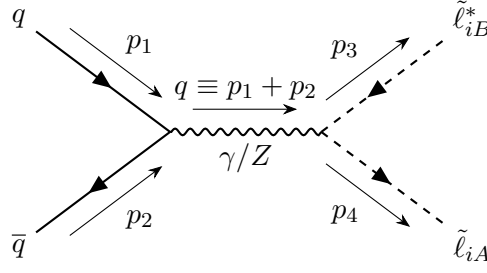


Figure 2.2: Tree-level partonic diagram for slepton pair production at a hadron collider

The intermediate state is either a Z boson or a photon; the latter is only possible for $A = B$. We will return to this diagram, and its higher-order corrections, in much greater detail in Chapter 4.

After the sleptons are produced they will rapidly decay. Following the conservation of R -parity and lepton number they will decay, possibly in several steps, down to the LSP and (at least) a lepton or neutrino of the same flavor as the produced slepton. As the LSP cannot decay further it will not be detected; thus the momentum of the detected final state will not match that of the initial state.

The amount of missing momentum can be deduced by momentum conservation on the detected final-state particles. However, since we do not know exactly the momenta of the colliding constituent particles of the hadron, this is not as straightforward as for lepton colliders. Still, since the collision energy is so large we can, to a very good approximation, assume that the incoming momentum is zero in the transverse direction. The LSP will therefore appear as missing momentum in the transverse direction, conventionally called *missing transverse energy*.

In other words, slepton pair production will contribute to the final state of two leptons or neutrinos and missing transverse energy. In addition to this there may be radiation of quarks and/or gluons from the initial state, which will show up as jets in the final state (more on this in the next chapter). To avoid discarding events that may be relevant for the discovery of new particles, we will also want to include processes with such radiation; hence we are looking for the *inclusive* cross-section for slepton production, cf. the discussion of Sec. 1.2.7.

Chapter 3

Quantum chromodynamics and the parton model

In this chapter we look the theory of strong interactions, called Quantum chromodynamics (QCD), and its implications for our later calculations.

We begin by discussing how the properties of the $SU(3)$ gauge group of QCD lead to significant physical consequences; namely the phenomena of *asymptotic freedom*, meaning that the strong force gets stronger at larger length scales and smaller energy scales, and vice versa; and *color confinement*, which is the observation that particles with color charge never appear freely, but instead in charge-neutral bound states called hadrons.

As a result of this, making theoretical predictions in QCD is challenging since at colliders we only know the precise momenta of the hadrons, not their constituent particles which are the ones directly appearing in the collision. This is dealt with in the parton model, wherein one assumes that a QCD observable factorizes into high- and low-energy components: The “hard” high-energy part is calculable perturbatively, since the strong coupling is smaller at these energies, while the “soft” low-energy part — assumed to be decoupled from the hard part as it happens on a much larger time scale — is not, but instead extracted from data by fitting theoretical predictions. The soft part is expressed in terms of parton distribution functions (PDFs), which function as probability distributions for finding a particular parton (fundamental color-charged particle) carrying a particular fraction of the momentum of the hadron.

After presenting the parton model, we note that the introduction of PDFs can aid in the renormalization of observables. The PDFs themselves are not directly observable, only through fitting data; this can be exploited by defining renormalized, energy scale-dependent PDFs, which will allow us to remove divergences from the calculation.

3.1 Structure of the $SU(3)$ gauge group

Quantum chromodynamics is based on invariance under the $SU(3)_C$ gauge group. As the name suggests, the group describes 3×3 unitary matrices with determinants equal to 1; in the fundamental representation it is generated by the Gell-Mann matrices λ^a [34]:

$$T^a \equiv \frac{1}{2}\lambda^a, \quad (3.1)$$

with $a = 1, 2, \dots, 8$. These generators satisfy

$$[T^a, T^b] = if^{abc}T^c, \quad (3.2)$$

where f^{abc} are the structure constants of the group. The fundamental representation describes the transformation properties of the quarks; these are arranged into color triplets ψ_i , $i = 1, 2, 3$, which transform according to

$$\psi_i \rightarrow \psi'_i = \left(e^{i\alpha^a(x)T^a} \right)_{ij} \psi_j, \quad (3.3)$$

where α^a are eight functions of x^μ .

The gluons are arranged into an octet transforming in the adjoint representation; the generators of this representation are defined by

$$(T_A^a)^{bc} = -if^{abc}. \quad (3.4)$$

3.1.1 Color sums

Calculations in QCD almost invariably involve taking products of the $SU(3)$ generators and summing over the various color states. To avoid having to do these calculations every time, using the explicit form of the representations, it is practical to categorize such sums in terms of the representation, and getting their value from group properties.

By Schur's lemma [35], any element in a group that commutes with all other elements in the group, for a given irreducible representation, are proportional to the identity. The proportionality factor is referred to as a Casimir invariant, and labels the representation. In $SU(3)$, one such Casimir invariant labeling a representation R is the quadratic Casimir $C(R)$, defined by

$$T_R^a T_R^a \equiv C(R)\mathbb{1}, \quad (3.5)$$

where as usual repeated indices are summed over. For the fundamental and adjoint representations, we label the quadratic Casimir by C_F and C_A , respectively.

Another useful quantity is the index $T(R)$ of a representation, which we encountered already in Sec. 2.2; for a representation R it is defined by

$$\text{tr} [T_R^a T_R^b] \equiv T(R)\delta^{ab}. \quad (3.6)$$

As for the quadratic Casimir, we label the index of the fundamental representation by T_F , and the adjoint representation by T_A .

Equations (3.5) and (3.6), together with the stated normalization of the generators and structure constants, imply the following relations, which we will be using repeatedly in our calculations:¹

$$T_{ik}^a T_{kj}^a = C_F \delta_{ij}, \quad (3.7)$$

$$T_{ij}^a T_{ji}^b = T_F \delta^{ab}, \quad (3.8)$$

$$f^{acd} f^{bcd} = C_A \delta^{ab}, \quad (3.9)$$

with the constants given by $C_F = \frac{N_C^2 - 1}{2N_C} = \frac{4}{3}$, $T_F = \frac{1}{2}$, and $C_A = N_C = 3$.² In a calculation where all color states of both representations are summed over, either of the first two relations can be used, giving

$$T_{ij}^a T_{ji}^a = C_F N_C = T_F (N_C^2 - 1). \quad (3.10)$$

¹Here and in the following, T^a with no subscript always refers to the generators of the fundamental representation.

²We usually write these quantities in terms of the number of color states N_C , keeping it as a variable; this makes it simpler to generalize calculations to other gauge groups.

3.2 Asymptotic freedom and color confinement

Many of the theoretical challenges of QCD stem from two principles called asymptotic freedom and color confinement. These can partially, at least qualitatively, be understood from the renormalization properties of the theory.

3.2.1 Renormalization of the strong coupling

The quark-gluon interaction term in the renormalized Lagrangian is given by

$$\mathcal{L}_{q\bar{q}g} = \mu^{\frac{4-d}{2}} g_s Z_1 A_\mu^a \bar{\psi}_i \gamma^\mu T_{ij}^a \psi_j, \quad (3.11)$$

where the bare and renormalized quantities are related by $g_{s0} = \mu^{\frac{4-d}{2}} Z_g g_s$, $A_0^a = \sqrt{Z_3} A^a$, $\psi_{i0} = \sqrt{Z_2} \psi_i$, and $Z_1 = Z_g Z_2 \sqrt{Z_3}$. As before we expand all of the renormalization constants around 1, $Z_i = 1 + \delta_i$. We can then find the 1-loop QCD β -function in the same way as for ϕ^4 theory in Sec. 1.2.5:

$$\beta(g_s) = \mu \frac{dg_s}{d\mu} = \epsilon g_s^2 \frac{\partial}{\partial g_s} \left(\delta_1 - \delta_2 - \frac{1}{2} \delta_3 \right). \quad (3.12)$$

Thus to find the β -function we need the renormalization of the gluon and quark 2-point functions, as well as for the quark-quark-gluon vertex.

The factor ϵ in Eq. (3.12) makes this much more straightforward than many other loop calculations, as only the divergent part of the counterterms will contribute in the limit $\epsilon \rightarrow 0$. Thus we can use the simplest possible renormalization scheme in defining the counterterm, namely the $\overline{\text{MS}}$ scheme, to remove only the terms proportional to $1/\bar{\epsilon}$. This in turn means that we only need to extract the parts of Passarino-Veltman coefficients³ that are proportional to $1/\bar{\epsilon}$. Assuming massless quarks, which does not impact the β -function but simplifies expressions, these are given by [36]

$$B_0(p^2, 0, 0) = \frac{1}{\bar{\epsilon}} + \text{finite}, \quad (3.13)$$

$$B_1(p^2, 0, 0) = -\frac{1}{2\bar{\epsilon}} + \text{finite}, \quad (3.14)$$

$$B_{00}(p^2, 0, 0) = -\frac{p^2}{12\bar{\epsilon}} + \text{finite}, \quad (3.15)$$

$$B_{11}(p^2, 0, 0) = \frac{1}{3\bar{\epsilon}} + \text{finite}, \quad (3.16)$$

$$C_{00} = \frac{1}{4\bar{\epsilon}} + \text{finite}. \quad (3.17)$$

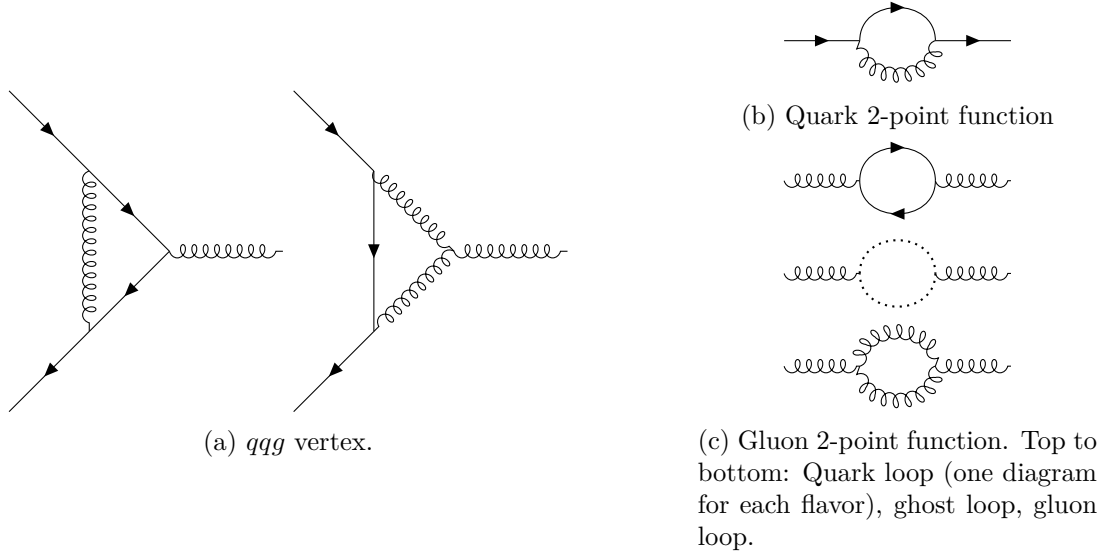
All other C functions are finite;⁴ the arguments of C_{00} are suppressed as they do not affect the divergence.

This makes it possible, through some fairly straightforward but tedious Dirac algebra, to calculate the necessary counterterms, always keeping only the terms that contribute to ultraviolet divergences. The quark-quark-gluon vertex gets two contributions at 1-loop, as shown in Fig. 3.1a; the quark 2-point function gets a contribution from the insertion of a quark-gluon loop shown in Fig. 3.1b; and the gluon 2-point function gets three (non-zero⁵) contributions, from insertions of

³These are defined in Sec. 1.3.

⁴“Finite” here really means UV-finite; there may be (and there are) infrared divergences, but these are irrelevant for counterterm purposes.

⁵There is also a contribution involving a 4-gluon vertex, but this vanishes in dimensional regularization.

Figure 3.1: 1-loop diagrams contributing to the QCD β -function.

quark, gluon, or ghost⁶ loops, shown in Fig. 3.1c. For completeness, and to give an example of how loop calculations are performed using Passarino-Veltman coefficients, we now carry out these calculations.

The simplest amplitude to renormalize, in the sense that it only gets one 1-loop correction, is the quark 2-point function. Following the notation of Eq. (1.74), we denote the sum of all 1PI insertions on the quark propagator by $i\Sigma^{ij}(\not{p})$, where i, j are in- and outgoing quark color states. At 1-loop with massless quarks we have

$$i\Sigma^{ij}(\not{p}) = i\left(\Sigma_2^{ij}(\not{p}) + \not{p}\delta_2\delta^{ij}\right) + \mathcal{O}(g_s^4), \quad (3.18)$$

where $i\Sigma_2^{ij}(\not{p})$ is given by the loop in Fig. 3.1b. Explicitly, we have

$$i\Sigma_2^{ij}(\not{p}) = (ig_s)^2 T_{jk}^a T_{li}^b \delta^{ab} \delta^{kl} \mu^{4-d} \int \frac{d^d k}{(2\pi)^d} \frac{\gamma^\mu (\not{k} + \not{p}) \gamma_\mu}{k^2 (k+p)^2}. \quad (3.19)$$

From Eq. (3.5) the color factor simplifies to $(T^a T^a)_{ij} = C_F \delta_{ij}$. The integral can be rewritten by using the contraction identities for γ matrices listed in Appendix A, and then factoring out as much as possible from the integrand; the remaining integral can be decomposed as described in Sec. 1.3. Dropping all terms that are finite as $\epsilon \rightarrow 0$, using Eqs. (3.13) and (3.14), we find

$$i\Sigma_2^{ij}(\not{p}) = \frac{ig_s^2}{16\pi^2} C_F \delta_{ij} \not{p} \frac{1}{\epsilon} + \text{finite}. \quad (3.20)$$

The quark self-energy counterterm in the $\overline{\text{MS}}$ scheme is then

$$\delta_2 = -\frac{g_s^2}{16\pi^2} C_F \frac{1}{\epsilon}. \quad (3.21)$$

⁶We have not discussed ghost particles in this thesis as they are not relevant for our purposes; they appear as a necessity when quantizing the gluon field in the path integral formalism, to avoid integrating over physically equivalent gauge configurations. In calculations, they mostly appear in loop corrections to gluon processes, like its propagator as seen here, or the 3- or 4-gluon vertex, since their only interactions are with gluons.

The calculation for the gluon self-energy works out in much the same way, with the obvious complication that there are three diagrams to add. We must also recall that the fermion loop must be added once for each quark flavor that can appear, giving N_F contributions; further, the anticommuting nature of the quarks and ghost particles demand a factor of (-1) in these diagrams, and that we take the trace of the fermion propagators in the loop. With all of these considerations, we can proceed as in the previous example. The sum of 1PI insertions on the gluon propagator at 1-loop is given by $\Pi^{\mu\nu ab}(p) = \Pi(p^2)(p^2 g^{\mu\nu} - p^\mu p^\nu)\delta^{ab}$,⁷ where a and b denote gluon color states, with

$$\Pi(p^2) = -\frac{g_s^2}{12\pi^2} \left[-N_F T_F + \frac{5}{4} C_A \right] \frac{1}{\bar{\epsilon}} - \delta_3 + \text{finite} + \mathcal{O}(g_s^4). \quad (3.22)$$

This immediately gives

$$\delta_3 = \frac{g_s^2}{12\pi^2} \left[\frac{5}{4} C_A - N_F T_F \right] \frac{1}{\bar{\epsilon}}. \quad (3.23)$$

We are then left with the quark-quark-gluon 3-point function. The full calculation of these diagrams is fairly cumbersome in the amount of Dirac matrices we have to keep track of; here it simplifies greatly, as we are only interested in the coefficient of the pole in $1/\bar{\epsilon}$. From Eq. (3.17) the only UV divergence in a generic 3-point tensor integral is in the coefficient of $g^{\mu\nu}$ in $C^{\mu\nu}$; all terms with less than two powers of the loop momentum in the numerator are UV-finite and can thus be dropped.

Adding together the diagrams in Fig. 3.1a, we find the following expression for the complete quark-quark-gluon vertex $ig_s \Gamma_{ij}^{a\mu}$ (a , i , and j denoting the color states of the gluon and quarks, respectively), including the tree-level result:

$$\Gamma_{ij}^{a\mu} = \gamma^\mu T_{ij}^a + \gamma^\mu T_{ij}^a \left(\frac{g_s^2}{16\pi^2} (C_F + C_A) \frac{1}{\bar{\epsilon}} + \delta_1 \right) + \text{finite} + \mathcal{O}(g_s^4), \quad (3.24)$$

giving, in the $\overline{\text{MS}}$ scheme,

$$\delta_1 = -\frac{g_s^2}{16\pi^2} (C_F + C_A) \frac{1}{\bar{\epsilon}}. \quad (3.25)$$

We now collect Eqs. (3.25), (3.21), and (3.23), and insert them into Eq. (3.12). With $T_F = \frac{1}{2}$, $N_F = 6$, and $C_A = 3$, we find

$$\beta(g_s) = \mu \frac{dg_s}{d\mu} = -\frac{g_s^3}{16\pi^2} \beta_0, \quad (3.26)$$

with

$$\beta_0 = \left[\frac{11}{3} C_A - \frac{4}{3} N_F T_F \right] = 7. \quad (3.27)$$

The fact that the β -function is negative is a very important property of QCD called *asymptotic freedom*. In practice this means that the strong coupling gets weaker at high energies, or equivalently at small distance or time scales; conversely the theory becomes unperturbative at small energies, or long distances and time scales, as it has an infrared Landau pole.

This property can also give a qualitative understanding of the observed phenomenon of *color confinement*, meaning that particles carrying color charge — quarks or gluons — are never seen as free states, only in bound states with net zero color charge, called hadrons. To extract a single particle from a bound state, due to asymptotic freedom, would require an infinite amount of energy, as the force between the color-charged particles grows with distance.

⁷Note that this satisfies the Ward identity $p_\mu \Pi^{\mu\nu ab} = 0$; this would not be the case without the ghost loop diagram. This illustrates the use of these particles; they are a mathematical tool to enforce gauge invariance in the quantized theory, and are not physically observable.

Note again that this is only a very qualitative explanation; the exact mechanism causing color confinement remains an open question in physics.

3.2.2 Jets

Color confinement is clearly evident in scattering processes in which a color-charged particle, i.e. a quark or a gluon, appears in the final state. Since this particle cannot exist in a free state, it must instead form bound states with other color-charged particles.

Even though there may initially be no such particles nearby in the final state, they can easily be created; as the strong coupling grows large for small energy transfers, the particle can readily emit a number of gluons moving in approximately the same direction. These in turn create quark-antiquark pairs. Eventually a large number of quarks and antiquarks will be moving together; these can then bind together in color-neutral hadronic states.

This process is called hadronization. Since this is a low-energy process, where the strong coupling is large, it cannot be calculated in perturbation theory; thus the exact process is not precisely understood.

In a detector, such a collection of hadrons is seen as a mostly localized signal called a *jet*. Each color-charged particle in the final state will manifest itself in the detector as an undetermined number of jets. Predicting the actual number is difficult for several reasons; for one, due to the size of the strong coupling it is likely that each outgoing parton will split one or more times in what is called a *parton shower*, creating several jets; furthermore, two jets may be approximately collinear, or one at a very low energy, so that they cannot be distinguished experimentally.

Such final states must be studied according to the discussion of Sec. 1.2.7. If we are looking for the production rate of, say, a pair of non-color-charged particles plus a jet, we can either restrict ourselves to final states with *exactly* one jet, cutting off processes with more jets according to some experimental resolution; or we can find the inclusive cross-section, where all processes wherein the colorless particles are produced along with *at least* one jet contribute.

3.3 Factorization and parton distribution functions

The properties of asymptotic freedom and color confinement significantly complicate calculations in QCD. For one, we never have direct access to the particles that are interacting in a collision; on a fundamental level, the interaction in a proton-proton collision is between quarks or gluons, but it is the proton that we can actually observe, and whose momentum we can control. The momentum of the proton is distributed among its constituent particles; classically these are just two u quarks and one d quark, but through low-energy gluon exchange it can also contain any other quark or antiquark, or even gluons.

The interactions governing this distribution of momentum happen on a much longer time scale than that of the collision. On the one hand, this allows us to assume that the two parts of the process — the long time-scale, low-energy *soft* part, and the short-time, high-energy *hard* scattering process — decouple, making it possible to factorize the result into hard and soft components. On the other hand, due to the running of the strong coupling, the soft part cannot be calculated in perturbation theory. In other words it becomes very complicated to calculate theoretically the process that determines which parton partakes in the interaction or what its momentum is; the soft part of the result needs to be extracted from experiments, by fitting to theoretical calculations.

This is summarized in the various factorization theorems of QCD, which state that cross-sections in the theory can be factorized into hard and soft parts. These have been proven for

several processes, e.g. the Drell-Yan process [37], whose hadronic part is identical to that of slepton pair production, to be discussed in detail in Chapter 4.

With factorization, we can write the cross-section as a convolution of a *partonic* cross-section, described by the fundamental interactions between constituent quarks and gluons — collectively called partons — and parton distribution functions (PDFs) $f_i(x)$, giving the probability density for a parton i to carry a fraction x of the momentum of the proton.^{8,9} The latter must be extracted from experiments. The resulting model is called the *parton model*.

Let us now consider a Drell-Yan-like process, in which two protons collide and produce a pair of particles A and B through a virtual electroweak boson, plus possible radiation of quarks or gluons from the initial state. This is described by a convolution of the partonic cross-section for the process $ij \rightarrow AB + X$, where i and j label a pair of partons and X any additional radiation, with two PDFs. With the incoming proton momenta given by P_1 and P_2 , the momenta of the interacting partons are

$$p_1 = x_1 P_1, \quad (3.28)$$

$$p_2 = x_2 P_2. \quad (3.29)$$

If the energy is large enough that incoming particles can be taken as approximately massless, so that $P_1^2 = P_2^2 = 0$, we can relate the partonic squared center-of-mass energy $\hat{s} = (p_1 + p_2)^2$, to the hadronic one $s = (P_1 + P_2)^2$ by

$$\hat{s} = x_1 x_2 s. \quad (3.30)$$

Furthermore, denoting the invariant mass of particles A and B by $(p_A + p_B)^2 = Q^2$, we can define a partonic threshold variable z , and a hadronic threshold variable τ , by

$$z \equiv \frac{Q^2}{\hat{s}} \in (0, 1), \quad (3.31)$$

$$\tau \equiv \frac{Q^2}{s} = x_1 x_2 z \in (0, 1). \quad (3.32)$$

These cannot be greater than 1 since no extra energy can come into the process in the initial state; we can only “lose” energy to radiation, making the invariant mass $Q^2 \leq \hat{s}$. With these constraints, we can write the hadronic cross-section, differential in Q^2 , as

$$\begin{aligned} & \frac{d\sigma}{dQ^2}(pp \rightarrow AB + X) \\ &= \sum_{ij} \int_{\tau}^1 \frac{dx_1}{x_1} \int_{\tau/x_1}^1 \frac{dx_2}{x_2} f_i(x_1) f_j(x_2) x_1 x_2 \frac{d\hat{\sigma}}{dQ^2}(ij \rightarrow AB + X), \end{aligned} \quad (3.33)$$

where the sum over partons i and j in principle includes all possible combinations of quarks, antiquarks, and gluons. σ and $\hat{\sigma}$ are called *hadronic* and *partonic* cross-sections, respectively. The factor of $\frac{x_1 x_2}{x_1 x_2}$ may seem odd when written on this form, but is due to the fact that the partonic cross-section is typically proportional to $1/\hat{s} = 1/x_1 x_2 s$. Thus we have in practice just preemptively just factored out $1/x_1$ and $1/x_2$ from the partonic cross-section, by shifting them over to the integration measure.

In practice, the conservation of baryon number and color charge greatly reduce the number of viable initial-state parton pairs. For Drell-Yan and similar processes, at next-to-leading order in

⁸In a high-energy scattering experiment any transverse momentum components of the partons will usually be negligible; thus their momenta p^μ can be approximated as $p^\mu = xP^\mu$, with P^μ being the momentum of the proton.

⁹One can of course also define PDFs for any other hadron, but hadron colliders almost exclusively collide protons.

the strong coupling the only options are a quark-antiquark pair, where a gluon may or may not be emitted, or a quark (or antiquark) with a gluon. In the latter case a quark (or antiquark) with the same flavor as the incoming one is emitted.

3.3.1 Integrating over PDFs

After calculating the partonic cross-section analytically, the PDF integration must be performed numerically. This can typically be made easier, and more computationally efficient, by exploiting that many of the terms in the partonic cross-section contain distributions in the threshold variable $z = \frac{\tau}{x_1 x_2}$. These might be delta functions $\delta(1 - z)$, which enforce momentum conservation in the case of no radiation; or so-called plus distributions $f_+(z)$. In both cases the distributions impose relations between x_1 and x_2 , lowering the dimensionality of the PDF integrals by one.

For the delta functions, this is straightforward; denoting a generic function of x_1 and x_2 by $g(x_1, x_2)$, we have

$$\int_{\tau/x_1}^1 \frac{dx_2}{x_2} g(x_1, x_2) \delta\left(1 - \frac{\tau}{x_1 x_2}\right) = g(x_1, x_2) \frac{x_1 x_2}{\tau} \Big|_{x_2=\tau/x_1} = g\left(x_1, \frac{\tau}{x_1}\right). \quad (3.34)$$

The treatment of the plus distributions requires some more care; in general, a plus distribution $f_+(z)$ is defined by its action in an integral with a function $g(z)$ so that

$$\int_0^1 dz g(z) f_+(z) \equiv \int_0^1 dz (g(z) - g(1)) f(z), \quad (3.35)$$

with $f_+(z < 1) = f(z)$. However, in our case the lower limit on the integral is non-zero, and we must also change variables. Again considering a general function $g(x_1, x_2)$, treating x_2 as a function of z while x_1 is independent, we get

$$\begin{aligned} \int_{\tau/x_1}^1 \frac{dx_2}{x_2} g(x_1, x_2) f_+\left(\frac{\tau}{x_1 x_2}\right) &= \int_{\tau/x_1}^1 \frac{dz}{z} g\left(x_1, \frac{\tau}{x_1 z}\right) f_+(z) \\ &= \int_0^1 \frac{dz}{z} g\left(x_1, \frac{\tau}{x_1 z}\right) f_+(z) - \int_0^{\tau/x_1} \frac{dz}{z} g\left(x_1, \frac{\tau}{x_1 z}\right) f(z) \\ &= \int_0^1 \frac{dz}{z} \left[g\left(x_1, \frac{\tau}{x_1 z}\right) - z g\left(x_1, \frac{\tau}{x_1}\right) \right] f(z) - \int_0^{\tau/x_1} \frac{dz}{z} g\left(x_1, \frac{\tau}{x_1 z}\right) f(z) \\ &= \int_{\tau/x_1}^1 \frac{dz}{z} \left[g\left(x_1, \frac{\tau}{x_1 z}\right) - z g\left(x_1, \frac{\tau}{x_1}\right) \right] f(z) - g\left(x_1, \frac{\tau}{x_1}\right) \int_0^{\tau/x_1} dz f(z). \end{aligned} \quad (3.36)$$

To summarize what we have just done: The first line is a simple change of integration variable; in the second we extend the lower integration limit, subtracting a “correction” integral on which we use the property $f_+(z < 1) = f(z)$; in the third we use the definition of the plus distribution under an integral; finally, we move the integration limit back up to τ/x_1 by re-absorbing the correction integral, but now leaving a “remainder” integral of the function $f(z)$.

In our calculations in the next chapter, we will encounter the cases $f(z) = 1/(1 - z)$ and $f(z) = \ln(1 - z)/(1 - z)$. For these cases, the remainder integral is fairly easy to evaluate analytically:

$$F(x_1) \equiv - \int_0^{\tau/x_1} dz f(z) = \begin{cases} \ln\left(1 - \frac{\tau}{x_1}\right), & f(z) = 1/(1 - z), \\ \frac{1}{2} \ln^2\left(1 - \frac{\tau}{x_1}\right), & f(z) = \ln(1 - z)/(1 - z), \end{cases} \quad (3.37)$$

leaving an expression which only has to be integrated over x_1 . For the first term, we transform the integration variable back to x_2 , leaving

$$\begin{aligned} \int_{\tau/x_1}^1 \frac{dx_2}{x_2} g(x_1, x_2) f_+ \left(\frac{\tau}{x_1 x_2} \right) \\ = \int_{\tau/x_1}^1 \frac{dx_2}{x_2} \left(g(x_1, x_2) - \frac{\tau}{x_1 x_2} g \left(x_1, \frac{\tau}{x_1} \right) \right) f \left(\frac{\tau}{x_1 x_2} \right) + F(x_1) g \left(x_1, \frac{\tau}{x_1} \right). \end{aligned} \quad (3.38)$$

For the first part of Eq. (3.38), and in terms where the integrand is a generic function of z , we still have to perform the integration over both variables.

3.4 Renormalized PDFs

So far we have discussed several types of divergence and how they are removed from calculations. Ultraviolet divergences are removed by renormalization of the parameters in the Lagrangian, and soft divergences typically cancel when adding cross-sections from different processes that contribute to the same observable. After all these are removed, however, there may still be remaining collinear divergences. These are dealt with by introducing renormalized, scale dependent PDFs.

This follows from the same principle as the “regular” renormalization discussed in Sec. 1.2: Collinear divergences are logarithmic, or alternatively proportional to $\frac{1}{\epsilon}$. This means that they can be removed by measuring the amplitude at some reference energy scale, and expressing results at other scales in terms of the difference from the reference scale.

This can also be viewed as a renormalization of the PDFs; we can do this since, as for the Lagrangian parameters, the PDFs themselves are not directly measurable. Instead, they are extracted from fitting theoretical calculations of cross-sections to experiment, so precisely how they are defined theoretically does not matter as long as they are convoluted with a finite theoretical partonic cross-section. This procedure leaves a scale dependence in the PDFs: Their scale dependences are governed by the DGLAP evolution equations [38–40], given by

$$\mu_F \frac{d}{d\mu_F} \begin{pmatrix} f_i(x, \mu_F) \\ f_g(x, \mu_F) \end{pmatrix} = \sum_j \frac{\alpha_s}{\pi} \int_x^1 \frac{d\xi}{\xi} \begin{pmatrix} P_{q_i q_j} \left(\frac{x}{\xi} \right) & P_{q_i g} \left(\frac{x}{\xi} \right) \\ P_{g q_j} \left(\frac{x}{\xi} \right) & P_{gg} \left(\frac{x}{\xi} \right) \end{pmatrix} \begin{pmatrix} f_j(\xi, \mu_F) \\ f_g(\xi, \mu_F) \end{pmatrix}, \quad (3.39)$$

where $\alpha_s = \frac{g_s^2}{4\pi}$, and i, j denote quark or antiquark flavors. The scale μ_F is called the *factorization scale*, as this renormalization can be seen as a re-factorization of the cross-section, where we absorb non-perturbative, low-energy parts of the process into the PDFs. It is in general separate from the scale we have discussed so far, which is called the *renormalization scale* μ_R ; however, they are often taken to be equal in calculations, so we will usually refer to them collectively as μ .

The P_{ij} functions appearing in Eq. (3.39) are called splitting functions; at leading order they

are given by

$$P_{qq}(z) = C_F \left[\frac{1+z^2}{(1-z)_+} + \frac{3}{2} \delta(1-z) \right], \quad (3.40)$$

$$P_{qg}(z) = T_F \left[z^2 + (1-z)^2 \right], \quad (3.41)$$

$$P_{gq}(z) = C_F \left[\frac{1+(1-z)^2}{z} \right], \quad (3.42)$$

$$P_{gg}(z) = 2C_A \left[\frac{z}{(1-z)_+} + \frac{1-z}{z} + z(1-z) \right] + \frac{\beta_0}{2} \delta(1-z), \quad (3.43)$$

with β_0 defined in Eq. (3.27). These can qualitatively be understood as (proportional to) the probability for an incoming parton j with momentum fraction (of the proton momentum) ξ to radiate off part of its energy, leaving a parton i with momentum fraction $x = z\xi$.

Splitting functions typically arise as the coefficients of collinear divergences in QCD calculations. We will see examples of this in the next chapter when calculating QCD corrections to the $q\bar{q}(\gamma/Z)$ vertex; the collinear divergences in the quark- and gluon-initiated processes are proportional to P_{qq} and P_{gg} , respectively.

We now look explicitly at how the collinear divergences of a partonic cross-section are absorbed into bare PDFs, leaving a finite partonic function and renormalized PDFs. First, recall that the hadronic cross-section can be written as

$$\frac{d\sigma}{dQ^2}(\tau) = \sum_{ij} \int_{\tau}^1 \frac{d\tilde{x}_1}{\tilde{x}_1} \int_{\tau/\tilde{x}_1}^1 \frac{d\tilde{x}_2}{\tilde{x}_2} \tilde{f}_i(\tilde{x}_1) \tilde{f}_j(\tilde{x}_2) \tilde{w}_{ij} \left(\tilde{z} = \frac{\tau}{\tilde{x}_1 \tilde{x}_2} \right). \quad (3.44)$$

This is just a restatement of Eq. (3.33), where we have placed tildes on the bare PDFs and partonic cross-section, here called w (with $1/\tilde{x}_1 \tilde{x}_2$ factored out as we alluded to previously). The latter generically contains collinear divergences.

We now assume that a similar relation can be made for the singular functions \tilde{w}_{ij} , i.e. that we can define functions $\Gamma_{ij}(x)$ and write

$$\tilde{w}_{ij}(z) = \sum_{kl} \int_{\tilde{z}}^1 \frac{dy_1}{y_1} \int_{\tilde{z}/y_1}^1 \frac{dy_2}{y_2} \Gamma_{ik}(y_1) \Gamma_{jl}(y_2) w_{kl} \left(\frac{\tilde{z}}{y_1 y_2} \right), \quad (3.45)$$

where w_{kl} is now finite. Inserting this into Eq. (3.44) and multiplying by 1 in the form of

$$1 = \int_{\tau}^1 \frac{dx_1}{x_1} \delta(x_1 - \tilde{x}_1 y_1) \tilde{x}_1 y_1 \int_{\tau/x_1}^1 \frac{dx_2}{x_2} \delta(x_2 - \tilde{x}_2 y_2) \tilde{x}_2 y_2, \quad (3.46)$$

we find

$$\frac{d\sigma}{dQ^2} = \sum_{kl} \int_{\tau}^1 \frac{dx_1}{x_1} \int_{\tau/x_1}^1 \frac{dx_2}{x_2} f_k(x_1, \mu) f_l(x_2, \mu) w_{kl} \left(z = \frac{\tau}{x_1 x_2} \right), \quad (3.47)$$

where we have defined the renormalized PDFs as

$$f_k(x, \mu) = \sum_i \int_0^1 d\tilde{x} dy \delta(x - \tilde{x}y) \tilde{f}_i(\tilde{x}) \Gamma_{ik}(y). \quad (3.48)$$

The μ scale dependence comes from the function Γ_{ij} and depends on renormalization scheme.

In practice, the divergences are removed by expressing the above quantities as perturbation series in the strong coupling α_s , so that

$$\tilde{w}_{ij} = \tilde{w}_{ij}^0 + \frac{\alpha_s}{\pi} \tilde{w}_{ij}^1 + \mathcal{O}(\alpha_s^2), \quad (3.49)$$

$$w_{ij} = w_{ij}^0 + \frac{\alpha_s}{\pi} w_{ij}^1 + \mathcal{O}(\alpha_s^2), \quad (3.50)$$

$$\Gamma_{ij} = \Gamma_{ij}^0 + \frac{\alpha_s}{\pi} \Gamma_{ij}^1 + \mathcal{O}(\alpha_s^2). \quad (3.51)$$

Inserting these into the above relations, and matching by order in α_s shows that the divergences in \tilde{w}_{ij} can systematically be cancelled by those of Γ_{ij} . In this way the Γ_{ij} functions perform the role of a generalized counterterm.

Exactly how the Γ_{ij} functions are defined, and consequently the renormalized PDFs, depends on the scheme used. The simplest choice, which we will adopt, is the $\overline{\text{MS}}$ scheme, which as before just corresponds to removing terms proportional to $\frac{1}{\epsilon}$. Since the collinear divergences are often proportional to the DGLAP splitting functions, as noted above, this typically means taking $\Gamma_{ij}^1(z) \propto \frac{1}{\epsilon} P_{ij}(z)$, with $\Gamma_{ij}^0(z) = \delta_{ij} \delta(1-z)$.

Chapter 4

Slepton pair production in QCD

In this chapter we make use of what we have covered in the previous chapters to calculate the theoretical cross-section for slepton pair production at hadron colliders.

We first establish the notation and kinematics of the process at the leading order, before adding QCD corrections. We consider the *inclusive* cross-section, meaning that we add all processes at the same order where a pair of sleptons are produced, regardless of the number of other color-charged particles (called jets) that are produced; to this end we calculate both the virtual loop diagrams, in regular QCD as well as including supersymmetric particles, and diagrams for emission of a single quark or gluon alongside the sleptons.

These calculations involve various divergences, which are dealt with according to their origin: Ultraviolet divergences from the loops are removed by field strength counterterms; soft divergences, from when the energies of emitted particles go to zero, cancel between diagrams; and collinear divergences, from when massless particles are emitted collinearly to the incoming partons, are dealt with by renormalized PDFs. After this procedure, we are left with a finite expression for the cross-section, to be integrated over parton momenta.

We then briefly discuss how the large logarithmic terms appearing at fixed orders can be dealt with using resummation. These terms grow large in the limit where the emitted momentum goes to zero, meaning that to compute such terms we can use the so-called eikonal approximation; this can be done efficiently by relating the cross-section to geometrical objects known as Wilson lines. Thus we will comment on how cross-sections in the eikonal limit can be calculated from Wilson lines, and resummed by taking advantage of the renormalization of these objects. In the interest of brevity we will not carry out the entire Wilson line calculation explicitly here — for details, the reader is referred to Refs. [41–47] — but we will demonstrate explicitly how loop corrections appear in the Wilson line formalism.

Finally, we combine the resummed results with the fixed-order ones. To avoid double-counting — the resummed cross-section automatically includes parts of the fixed-order results at all orders — we must use a technique called matching.

4.1 Kinematics and factorization

At leading order, the partonic process $q(p_1)\bar{q}(p_2) \rightarrow \tilde{\ell}_{iB}^*(p_3)\tilde{\ell}_{iA}(p_4)$ ¹ has two contributions, both s -channel diagrams; one with the exchange of a virtual Z boson, and one with a virtual photon. These are shown in Fig. 2.2. Their respective contributions to the S -matrix are as follows (all

¹Recall from Fig. 2.2 that $i = e, \mu, \tau$ denotes slepton flavor, while $A, B = 1, 2$ label mass eigenstates.

Feynman rules taken from Ref. [48]):²

$$i\mathcal{M}_Z = \bar{v}^r(p_2) \frac{-ie}{\sin\theta_W \cos\theta_W} \gamma^\mu [Z_{qL}(1 - \gamma^5) + Z_{qR}(1 + \gamma^5)] u^s(p_1) \\ \times \frac{-ig_{\mu\nu}}{Q^2 - m_Z^2 + im_Z\Gamma_Z} \frac{-ie}{\sin\theta_W \cos\theta_W} Z_{\ell_i}^{AB} (p_3 - p_4)^\nu, \quad (4.1)$$

$$i\mathcal{M}_\gamma = \bar{v}^r(p_2) (iQ_q e \gamma^\mu) u^s(p_1) \frac{-ig_{\mu\nu}}{Q^2} (-ie) (p_3 - p_4)^\nu \delta^{AB}, \quad (4.2)$$

where $q \equiv p_3 + p_4$ is the momentum of the exchanged gauge boson, with $Q \equiv \sqrt{q^2}$; in the case where there is no real emission from the initial state, $q = p_1 + p_2$ so that $Q^2 = \hat{s} \equiv (p_1 + p_2)^2$; s and r are the spins of the incoming quark and antiquark, respectively. The numerical factors in the Z exchange diagram are defined by $Z_{qL/R} \equiv -\frac{1}{2}(T_{qL/R}^3 - Q_q \sin^2\theta_W)$ and

$$Z_{\ell_i}^{AB} \equiv \begin{cases} \frac{1}{2}(\delta_1^A \cos^2\theta_\ell^i + \delta_2^A \sin^2\theta_\ell^i - 2\sin^2\theta_W) & A = B, \\ \frac{1}{2}\cos\theta_\ell^i \sin\theta_\ell^i & A \neq B, \end{cases} \quad (4.3)$$

and θ_ℓ^i is the left/right mixing angle (between the chiral and mass eigenstates) for slepton flavor i .³

The partonic differential cross-section is given by [6]

$$d\hat{\sigma} = \frac{1}{2\hat{s}} |\mathcal{M}|^2 d\Pi, \quad (4.4)$$

where $d\Pi$ is the differential phase space of the final-state particles. The phase space can be simplified in the center-of-mass frame, where the momenta of the different particles can be worked out fairly easily using conservation of momentum. We assume that $\sqrt{\hat{s}} \gg m_q$ so that the quarks can be assumed to be massless, while keeping the slepton masses. Using axial symmetry to define the coordinates so that all motion happens on a two-dimensional plane, the involved particle momenta can be parametrized as

$$p_1 = \left(\frac{\sqrt{\hat{s}}}{2}, 0, 0, \frac{\sqrt{\hat{s}}}{2} \right), \quad (4.5)$$

$$p_2 = \left(\frac{\sqrt{\hat{s}}}{2}, 0, 0, -\frac{\sqrt{\hat{s}}}{2} \right), \quad (4.6)$$

$$p_3 = (E_B, p \sin\theta, 0, p \cos\theta), \quad (4.7)$$

$$p_4 = (E_A, -p \sin\theta, 0, -p \cos\theta), \quad (4.8)$$

where θ is the center-of-mass scattering angle, and the slepton energies and (absolute value of) momentum are given by

$$E_{B,A} = \frac{Q^2 + m_{\ell_{iB,A}}^2 - m_{\ell_{iA,B}}^2}{2Q}, \quad (4.9)$$

$$p^2 = \frac{Q^2}{4} - \frac{m_{\ell_{iA}}^2 + m_{\ell_{iB}}^2}{2} + \frac{(m_{\ell_{iA}}^2 - m_{\ell_{iB}}^2)^2}{4Q^2}. \quad (4.10)$$

²Since A and B are just labels for mass eigenstates, not vector indices, we can allow ourselves to be somewhat haphazard with their placement for the sake of readability.

³Here we assume that the mixing is confined to the chiral eigenstates of individual flavors, so that the $\tilde{\ell}\tilde{\ell}^*$ pair must belong to the same flavor.

If there is real radiation from the initial state, these momenta will naturally change, but $p_{1,2}$ remain the same in the center-of-mass frame, while $p_{3,4}$ can also be written on the same form, but now in *their* center-of-mass-frame, or the rest frame of the virtual exchange boson.

At next-to-leading order, the cross-section gets contributions proportional to $\alpha_s = g_s^2/4\pi$; both via the exchange of virtual particles, and radiation of real ones. The latter technically describes a different process, but as we discussed previously we are looking for the *inclusive* cross-section for slepton pair production, i.e. that of the general hadronic process $pp \rightarrow \ell\bar{\ell}^* + X$, where X stands for anything that is produced along with the slepton pair.

Since particles with color charge only appear in the initial state, this is the only part that receives corrections at this order; it will therefore be convenient to factorize the cross-section into a hadronic current, which is where quantum corrections arise, and a slepton current and effective charge, both of which will remain unchanged at next-to-leading order.

To this end, we first look to factorize the phase space, in its most general form, i.e. including a third particle with momentum k (with $k^2 = 0$, $k^0 \equiv \omega$), that radiates off the initial state; in the case where no such particle appears, this momentum is trivially integrated out. In d dimensions, the phase space can be expressed as

$$d\Pi = (2\pi)^d \delta^d(k + p_3 + p_4 - p_1 - p_2) \frac{d^{d-1}k}{(2\pi)^{d-1}} \frac{1}{2\omega} \frac{d^{d-1}p_3}{(2\pi)^{d-1}} \frac{1}{2E_B} \frac{d^{d-1}p_4}{(2\pi)^{d-1}} \frac{1}{2E_A}. \quad (4.11)$$

Inserting two factors of unity (or more correctly, factors that integrate to unity), in the form of $(2\pi)^d \delta^d(k + q - p_1 - p_2) \frac{d^d q}{(2\pi)^d}$ and $\delta(q^2 - Q^2) dQ^2$, this can be factored as

$$d\Pi = \frac{1}{2\pi} d\Pi_L d\Pi_H dQ^2, \quad (4.12)$$

where now $d\Pi_H$ is the Lorentz-invariant phase space for the initial part of the interaction, with q being viewed as the momentum of a massive, on-shell boson with mass Q (when there is no radiation this phase space is trivial, as only q is integrated over and it is given exactly by momentum conservation), and $d\Pi_L$ similarly for the slepton part. Explicitly these are given by

$$d\Pi_H = (2\pi)^d \delta^d(q + k - p_1 - p_2) \frac{d^{d-1}q}{(2\pi)^{d-1}} \frac{1}{2q^0} \frac{d^{d-1}k}{(2\pi)^{d-1}} \frac{1}{2\omega}, \quad (4.13)$$

$$d\Pi_L = (2\pi)^d \delta^d(p_3 + p_4 - q) \frac{d^{d-1}p_3}{(2\pi)^{d-1}} \frac{1}{2E_B} \frac{d^{d-1}p_4}{(2\pi)^{d-1}} \frac{1}{2E_A}. \quad (4.14)$$

Using this factorization, the spin- and color-averaged tree-level cross-section can be written differential in the slepton invariant mass Q as

$$\frac{d\hat{\sigma}}{dQ^2} = \frac{4\pi\alpha^2}{\hat{s}} \left(P_\gamma H_{(\gamma)}^{\mu\nu} L_{(\gamma)\mu\nu} + P_Z H_{(Z)}^{\mu\nu} L_{(Z)\mu\nu} + P_Z \gamma H_{(Z\gamma)}^{\mu\nu} L_{(Z\gamma)\mu\nu} \right), \quad (4.15)$$

where $\alpha \equiv e^2/4\pi$. The three terms come from the expansion of the squared matrix element, $|\mathcal{M}|^2 = |\mathcal{M}_Z|^2 + |\mathcal{M}_\gamma|^2 + 2\text{Re}(\mathcal{M}_\gamma^* \mathcal{M}_Z)$. Here the P factors contain propagator factors and factors of Q_q , $1/\sin\theta_W \cos\theta_W$ in each term (as well as their sign); the L s are the slepton tensors, given by⁴

$$L_{(\gamma)}^{\mu\nu} = \delta^{AB} L^{\mu\nu}, \quad (4.16)$$

$$L_{(Z)}^{\mu\nu} = (Z_{\ell_i}^{AB})^2 L^{\mu\nu}, \quad (4.17)$$

$$L_{(Z\gamma)}^{\mu\nu} = Z_{\ell_i}^{AB} \delta^{AB} L^{\mu\nu}, \quad (4.18)$$

⁴There is no sum over A and B .

with

$$L^{\mu\nu} \equiv \int d\Pi_L (p_3 - p_4)^\mu (p_3 - p_4)^\nu. \quad (4.19)$$

The quark tensors are given by

$$H_{(\gamma)}^{\mu\nu} = \frac{1}{4N} \int d\Pi_H \text{Tr}[\not{p}_2 \gamma^\mu \not{p}_1 \gamma^\nu], \quad (4.20)$$

$$H_{(Z)}^{\mu\nu} = \frac{1}{4N} \int d\Pi_H \text{Tr}[\not{p}_2 \gamma^\mu (Z_{q_L}(1 - \gamma^5) + Z_{q_R}(1 + \gamma^5)) \\ \times \not{p}_1 \gamma^\nu (Z_{q_L}(1 - \gamma^5) + Z_{q_R}(1 + \gamma^5))], \quad (4.21)$$

$$H_{(Z\gamma)}^{\mu\nu} = \frac{1}{2N} \int d\Pi_H \text{Tr}[\not{p}_2 \gamma^\mu \not{p}_1 \gamma^\nu (Z_{q_L}(1 - \gamma^5) + Z_{q_R}(1 + \gamma^5))]. \quad (4.22)$$

The factor $1/4N$ comes from dividing by the number of possible initial spin states ($2^2 = 4$) and the number of color states N . At leading-order the initial state is restricted to be a color singlet, since the electroweak gauge bosons cannot carry color charge, so that $N = N_C = 3$; with radiation included this is no longer necessarily the case.

Using properties of the γ^5 matrix — specifically that its square is the identity, it anticommutes with all γ^μ , and that the trace of γ^5 times four other γ matrices is proportional to the Levi-Civita tensor — it is fairly straightforward to show that all of the quark tensors are actually proportional:

$$H_{(\gamma)}^{\mu\nu} \equiv H^{\mu\nu}, \quad (4.23)$$

$$H_{(Z)}^{\mu\nu} = 2(Z_{q_L}^2 + Z_{q_R}^2)H^{\mu\nu}, \quad (4.24)$$

$$H_{(Z\gamma)}^{\mu\nu} = 2(Z_{q_L} + Z_{q_R})H^{\mu\nu}. \quad (4.25)$$

This makes it possible to write a much simpler expression for the cross-section:

$$\frac{d\hat{\sigma}}{dQ^2} = \frac{4\pi\alpha^2}{\hat{s}Q^4} F_{q\ell_i}^{AB}(Q) H^{\mu\nu} L_{\mu\nu}, \quad (4.26)$$

with

$$F_{q\ell_i}^{AB}(Q) \equiv Q_q^2 \delta^{AB} - 2Q_q \delta^{AB} \frac{Z_{\ell_i}^{AB}}{\sin^2 \theta_W \cos^2 \theta_W} (Z_{q_L} + Z_{q_R}) \frac{Q^2(Q^2 - m_Z^2)}{(Q^2 - m_Z^2)^2 + m_Z^2 \Gamma_Z^2} \\ + 2 \frac{(Z_{\ell_i}^{AB})^2}{\sin^4 \theta_W \cos^4 \theta_W} (Z_{q_L}^2 + Z_{q_R}^2) \frac{Q^4}{(Q^2 - m_Z^2)^2 + m_Z^2 \Gamma_Z^2}, \quad (4.27)$$

$$L^{\mu\nu} \equiv \int d\Pi_L (p_3 - p_4)^\mu (p_3 - p_4)^\nu, \quad (4.28)$$

$$\epsilon_\mu \epsilon_\nu^* H^{\mu\nu} \equiv \int d\Pi_H \sum_X \langle |\mathcal{M}(q\bar{q} \rightarrow \gamma^* + X)|^2 \rangle. \quad (4.29)$$

Here ϵ_μ is the polarization of the virtual photon, and the matrix element in the last line is defined so that the $q\bar{q}\gamma^*$ vertex is given by γ^μ , i.e. not including coupling strength. $F_{q\ell_i}^{AB}$ can be viewed as an effective coupling induced by the interference between the γ and Z diagrams; with only the photon it would exactly equal the electromagnetic coupling.

The convenience of this factorization is that it is valid even beyond leading order, when taking into account QCD loop corrections, as these only affect the hadronic current $H^{\mu\nu}$; the slepton current $L_{\mu\nu}$ clearly does not receive any such corrections as the sleptons do not carry color charge,

while the effective charge $F_{q\ell_i}^{AB}$ remains the same as long as no supersymmetric particles appear in loops (see Sec. 4.4), since the above manipulations of Dirac traces remains valid.

The latter point can be seen since each higher-order correction introduces an even number of γ matrices; each loop gives two new vertices and two new fermion propagators, i.e. four new γ matrices, while initial-state radiation gives one vertex and one propagator, i.e. two γ matrices. Thus, the γ^5 matrices from the Z vertex will commute with everything else exactly like it did in the discussion above, and the same numerical factor $F_{\ell_i}^{AB}(Q)$ can be factored out.

The consequence of this is that when calculating 1-loop QCD corrections to the cross-section we will only have to consider corrections to the process $q\bar{q} \rightarrow \gamma^* + X$, where γ^* is a virtual photon with mass Q and X represents anything that can be radiated off of the initial state.

Since, as discussed, the slepton vertex receives no corrections at next-to-leading order in QCD, $L^{\mu\nu}$ always takes the same form, and can be calculated just once and re-used; as p_3 and p_4 are integrated over, $L^{\mu\nu}$ can only depend on q^μ , and from the available tensors and dimensional analysis it must then have the form

$$L^{\mu\nu} = L_1(Q)q^\mu q^\nu + L_2(Q)g^{\mu\nu}Q^2. \quad (4.30)$$

This can be contracted to make a pair of coupled equations:

$$q_\mu q_\nu L^{\mu\nu} = Q^4(L_1 + L_2), \quad (4.31)$$

$$g_{\mu\nu} L^{\mu\nu} = Q^2(L_1 + dL_2). \quad (4.32)$$

Since the integrands on the left-hand side of both equations (recall that $L^{\mu\nu}$ is defined to include a slepton phase space integral) are rotationally symmetric they can be factored out of the integral, making the system of equations straightforward to solve:

$$L_1(Q) = \frac{1}{1-d} \left[\frac{2(m_{\tilde{\ell}_{iA}}^2 + m_{\tilde{\ell}_{iB}}^2) - Q^2}{Q^2} - d \frac{(m_{\tilde{\ell}_{iB}}^2 - m_{\tilde{\ell}_{iA}}^2)^2}{Q^4} \right] \int d\Pi_L, \quad (4.33)$$

$$L_2(Q) = \frac{4}{1-d} \frac{p^2}{Q^2} \int d\Pi_L, \quad (4.34)$$

where the momentum p^2 is given in terms of the masses and Q^2 in Eq. (4.10). The total two-particle phase space of the sleptons is given by

$$\begin{aligned} \int d\Pi_L &= (2\pi)^d \int \delta^d(p_3 + p_4 - q) \frac{d^{d-1}p_3}{(2\pi)^{d-1}} \frac{1}{2E_B} \frac{d^{d-1}p_4}{(2\pi)^{d-1}} \frac{1}{2E_A} \\ &= \frac{p^{d-3}}{2^d \pi^{d-2} Q} \int d\Omega_{d-1} \\ &= \frac{p^{d-3}}{2^{d-1} \pi^{(d-3)/2} \Gamma(\frac{d-1}{2}) Q}, \end{aligned} \quad (4.35)$$

where Γ is the Euler gamma function. This is somewhat overly general; since the slepton part of the calculation receives no QCD corrections it is not divergent, so we can safely simplify it to $d = 4$. This gives a much simpler expression:

$$\int d\Pi_L = \frac{p}{4\pi Q}. \quad (4.36)$$

Note that $L^{\mu\nu}$ does not immediately satisfy the Ward identity; this is because $(p_3 - p_4)^\mu$ is not the full Feynman rule for the photon-slepton interaction, which also contains a Kronecker delta δ^{AB} ;

in the above factorization, this was instead included in the effective charge $F_{\ell_i}^{AB}$. The “Feynman rule” written on this form mixes left- and right-handed fields in the QED interaction term in the Lagrangian, which violates gauge invariance and thus the Ward identity. The full term including the Kronecker delta does satisfy the identity, as desired; this can be seen from setting $A = B$ in the above equations, which gives $L_1 = -L_2$.

Now that we have the slepton tensor on this form, we can use the Ward identity to simplify the final result further; since $q_\mu \mathcal{M}^\mu(q\bar{q} \rightarrow \gamma^* + X) = 0$, where $\epsilon_\mu^*(q) \mathcal{M}^\mu = \mathcal{M}$, by gauge symmetry,⁵ only the second term in Eq. (4.30) contributes when contracted with $H^{\mu\nu}$, so that the contraction of $H^{\mu\nu}$ with $L_{\mu\nu}$ reduces to a contraction with $g_{\mu\nu}$ and multiplication with a numerical factor. In other words, the entire slepton tensor can be encapsulated in taking

$$L_{\mu\nu} = \int d\Pi_L (p_3 - p_4)_\mu (p_3 - p_4)_\nu \rightarrow -\frac{p^3}{3\pi Q} g_{\mu\nu}. \quad (4.37)$$

Furthermore, since $-g_{\mu\nu}$ is equal to the sum of photon polarizations $\epsilon_\mu^* \epsilon_\nu$, the entire contraction can be written as

$$H^{\mu\nu} L_{\mu\nu} = \frac{p^3}{3\pi Q} \int d\Pi_H \sum_X \langle |\mathcal{M}(q\bar{q} \rightarrow \gamma^* X)|^2 \rangle. \quad (4.38)$$

Then, the final reference formula for the partonic cross-section is

$$\frac{d\hat{\sigma}}{dQ^2} = \frac{4\alpha^2 p^3}{3\hat{s} Q^5} F_{q\ell_i}^{AB}(Q) \int d\Pi_H \sum_X \langle |\mathcal{M}(q\bar{q} \rightarrow \gamma^* X)|^2 \rangle \quad (4.39)$$

4.2 Leading-order cross-section

At leading order there are no divergences to be regulated, so we can safely set $d = 4$. The tree-level diagram for $q\bar{q} \rightarrow \gamma^*$ is given by

$$i\mathcal{M}_0 = \bar{v}^r(p_2) \gamma^\mu u^s(p_1) \epsilon_\mu^*(q), \quad (4.40)$$

where a color-conserving Kronecker delta is implicit, since as discussed above, only color singlet initial quark states contribute. This gives a spin- and color-averaged matrix element (integrated over the phase space) of

$$\int d\Pi_H \langle |\mathcal{M}_0|^2 \rangle = -\frac{1}{4N_C} \int d\Pi_H \text{Tr}[\not{p}_2 \gamma^\mu \not{p}_1 \gamma_\mu] = \frac{d-2}{2N_C} \int d\Pi_H \hat{s}. \quad (4.41)$$

The phase space integral is trivial in this case:

$$\int d\Pi_H = \int \frac{d^{d-1}q}{(2\pi)^{d-1}} \frac{1}{2q^0} (2\pi)^d \delta^d(q - p_1 - p_2) = \frac{2\pi}{\hat{s}} \delta(1-z), \quad (4.42)$$

where $z \equiv Q^2/\hat{s}$. The cross-section is then, using Eq. (4.39) with $d = 4$:

$$\frac{d\hat{\sigma}_0}{dQ^2} = \frac{8\pi\alpha^2 p^3}{3N_C \hat{s} Q^5} F_{q\ell_i}^{AB}(Q) \delta(1-z) \quad (4.43)$$

$$\equiv \sigma_0 \delta(1-z). \quad (4.44)$$

⁵Unlike for the slepton tensor we are not factoring out anything that is necessary for gauge invariance from \mathcal{M} , so the Ward identity will actually hold.

For later reference, the cross-section in d dimensions is given by

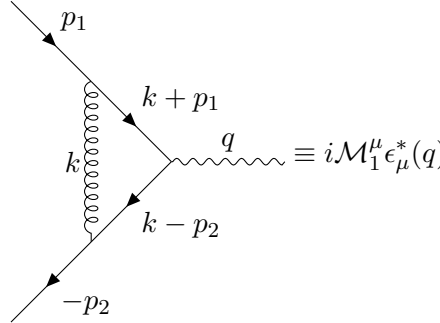
$$\frac{d\hat{\sigma}_0^d}{dQ^2} = (d-2) \frac{4\pi p^3}{3N_c \hat{s} Q^5} F_{q\ell_i}^{AB}(Q) \delta(1-z) \quad (4.45)$$

$$\begin{aligned} &= \left(\frac{d-2}{2} \right) \sigma_0 \delta(1-z) \\ &\equiv \sigma_0^d \delta(1-z). \end{aligned} \quad (4.46)$$

4.3 Standard Model corrections at NLO

4.3.1 Virtual loop correction

At one-loop order, so far not including any supersymmetry contributions, there is one virtual gluon diagram, given by



$$\equiv i\mathcal{M}_1^\mu \epsilon_\mu^*(q). \quad (4.47)$$

Here $\epsilon_\mu(q)$ is the polarization tensor of the virtual photon, and all fermion momenta are given in the direction of fermion flow as described by the arrows. At next-to-leading order (technically leading order in QCD) this contributes through their cross-term with the tree-level diagram.

The loop gives, not including photon polarization,

$$\begin{aligned} i\mathcal{M}_1^\mu &= \bar{v}_i^r(p_2) \left(i\mu^{(4-d)/2} g_s T_{ik}^a \right) \left(i\mu^{(4-d)/2} g_s T_{kj}^a \right) (-ig_{\rho\sigma}) \\ &\quad \times \int \frac{d^d k}{(2\pi)^d} \frac{\gamma^\rho i(\not{k} - \not{p}_2) \gamma^\mu i(\not{k} + \not{p}_1) \gamma^\sigma}{k^2 (k+p_1)^2 (k-p_2)^2} u_j^s(p_1) \\ &= -\delta_{ij} C_F i\mu^{4-d} g_s^2 \int \frac{d^d k}{(2\pi)^d} \frac{\bar{v}_i^r(p_2) N^\mu u_j^s(p_1)}{k^2 (k+p_1)^2 (k-p_2)^2}. \end{aligned} \quad (4.48)$$

Here we have used Eq. (3.7) to simplify the sum over the quark colors i, j ; the Kronecker delta δ_{ij} means that as in the tree-level case, only color singlet initial states contribute. Therefore, as before we only need to consider $N_C = 3$ different initial color states and can drop the color labels on the spinors.

The numerator can be simplified through contraction identities for γ matrices in d dimensions, the Dirac algebra, and using $\bar{v}(p_2)\not{p}_2 = \not{p}_1 u(p_1) = 0$ (for massless quarks):

$$\begin{aligned} N^\mu &= \gamma^\rho (\not{k} - \not{p}_2) \gamma^\mu (\not{k} + \not{p}_1) \gamma_\rho \\ &\rightarrow 2(2-d) \gamma_\nu k^\mu k^\nu - (2-d) \gamma^\mu g_{\rho\sigma} k^\rho k^\sigma + 4(\gamma^\mu (p_1 - p_2)_\nu - \gamma_\nu (p_1 - p_2)^\mu) k^\nu - 2\hat{s} \gamma^\mu. \end{aligned} \quad (4.49)$$

The arrow means that the two expressions are not equal, but evaluate to the same when placed between the two spinors. The matrix element can then be written as

$$i\mathcal{M}_1^\mu = C_F \mu^{4-d} g_s^2 \bar{v}^r(p_2) \Gamma^\mu u^s(p_1), \quad (4.50)$$

where Γ^μ can be expressed in terms of Passarino-Veltman functions. Suppressing arguments, which are the same for each function — $(p_1^2 = 0, \hat{s}, p_2^2 = 0, 0, 0, 0)$ — and following the LoopTools [26, 27] conventions for normalization of the loop integrals (again using the Dirac equation as above, as well as $p_1^2 = p_2^2 = 0$), we have

$$\begin{aligned} \frac{(4\pi)^{d/2} \mu^{4-d}}{r_\Gamma} \Gamma^\mu &= 2(2-d) \gamma_\nu C^{\mu\nu} - (2-d) \gamma^\mu g_{\rho\sigma} C^{\rho\sigma} \\ &\quad + 4(\gamma^\mu (p_1 - p_2)_\nu - \gamma_\nu (p_1 - p_2)^\mu) C^\nu - 2\hat{s} \gamma^\mu C_0 \\ &\rightarrow \left[(2-d)^2 C_{00} + (2-d) \hat{s} C_{12} - 2\hat{s} C_1 - 2\hat{s} C_2 - 2\hat{s} C_0 \right] \gamma^\mu. \end{aligned} \quad (4.51)$$

Here r_Γ is defined as

$$r_\Gamma \equiv \frac{\Gamma^2(1-\epsilon)\Gamma(1+\epsilon)}{\Gamma(1-2\epsilon)}, \quad (4.52)$$

with $d = 4 - 2\epsilon$.

The NLO contribution to the quark tensor is then (the phase space integral is the same as for the leading-order case)

$$\begin{aligned} H_1^{\mu\nu} &= \frac{1}{4N_C} \int d\Pi_H \sum_{\text{spins}} 2\text{Re}(\mathcal{M}_0^\mu \mathcal{M}_1^{\nu*}) \\ &= \text{Re}(f(\hat{s})) H_0^{\mu\nu}, \end{aligned} \quad (4.53)$$

where

$$f(\hat{s}) \equiv 2C_F \frac{r_\Gamma}{(4\pi)^{d/2}} g_s^2 \left[(d-2)^2 C_{00} - \hat{s}((d-2)C_{12} + 2(C_0 + C_1 + C_2)) \right], \quad (4.54)$$

and $H_0^{\mu\nu}$ is the leading-order hadronic current. The virtual correction to the cross-section is then given by

$$\frac{d\hat{\sigma}_v}{dQ^2} = \text{Re}(f(\hat{s})) \frac{d\hat{\sigma}_0^d}{dQ^2}, \quad (4.55)$$

with the leading-order cross-section given by Eq. (4.46).

To simplify keeping track of divergences, we expand each Passarino-Veltman function in terms of their divergences; for example,

$$\text{Re}(C_0) \equiv \frac{1}{\epsilon^2} C_0^2 + \frac{1}{\epsilon} C_0^1 + C_0^0, \quad (4.56)$$

where C_0^i are all finite, and the $1/\epsilon$ term contains both infrared and ultraviolet divergences. Expanding in ϵ , using

$$\Gamma(1-\epsilon)\Gamma(1+\epsilon) = 1 + \epsilon^2 \pi^2/6 + \mathcal{O}(\epsilon^3) \quad (4.57)$$

and $a^\epsilon = 1 + \epsilon \ln a + \frac{1}{2} \epsilon^2 \ln^2 a + \mathcal{O}(\epsilon^3)$, $f(\hat{s})$ can then be written as⁶

$$\begin{aligned} f(\hat{s}) &= \frac{\Gamma(1-\epsilon)}{\Gamma(1-2\epsilon)} \left(\frac{4\pi\mu^2}{Q^2} \right)^\epsilon C_F \frac{\alpha_s}{\pi} \left[\frac{1}{\epsilon^2} f^2 + \frac{1}{\epsilon} \left(f^1 + \ln \left(\frac{Q^2}{\mu^2} \right) f^2 \right) \right. \\ &\quad \left. + \left(f^0 + \frac{\pi^2}{6} f^2 + \frac{1}{2} \ln^2 \left(\frac{Q^2}{\mu^2} \right) f^2 + \ln \left(\frac{Q^2}{\mu^2} \right) f^1 \right) \right], \end{aligned} \quad (4.58)$$

⁶Terms of order $\mathcal{O}(\epsilon)$ go to zero in the limit $\epsilon \rightarrow 0$, and are dropped.

where

$$f^2 = 2C_{00}^2 - \hat{s}(C_{12}^2 + C_0^2 + C_1^2 + C_2^2), \quad (4.59)$$

$$f^1 = 2C_{00}^1 - 4C_{00}^2 - \hat{s}(C_{12}^1 - C_{12}^2 + C_0^1 + C_1^1 + C_2^1), \quad (4.60)$$

$$f^0 = 2C_{00}^0 - 4C_{00}^1 + 2C_{00}^2 - \hat{s}(C_{12}^0 - C_{12}^1 + C_0^0 + C_1^0 + C_2^0). \quad (4.61)$$

The $\ln(Q^2/\mu^2)$ terms appear since we have explicitly factored out $(\mu^2/Q^2)^\epsilon$. Note that this is written on a somewhat unnecessarily general form, as many of these coefficients are zero.

4.3.2 Renormalizing the virtual diagram

The renormalization of this diagram requires some care; we cannot simply subtract the ultraviolet divergence in the form of a vertex counterterm, since there is no parameter in the Lagrangian corresponding to a vertex like this, mixing QED and QCD interactions. What we can do instead is use the field renormalization of the quark field ψ ; the bare field can be written as $|\psi_0|^2 = Z_\psi |\psi|^2 = (1 + \delta_\psi) |\psi|^2$. Thus we can add the field renormalization $2\text{Re}(\delta_\psi) \frac{d\hat{\sigma}_0^d}{dQ^2}$ to the calculation.

We calculate the counterterm in the on-shell scheme, as discussed in Sec. 1.2.4; by Eq. (1.79) this means that

$$\delta_\psi = - \left. \frac{d}{d\not{p}} \Sigma_2(\not{p}) \right|_{\not{p}=0}, \quad (4.62)$$

where $i\Sigma_2(\not{p})$ is the gluon-quark loop correction to the quark propagator. Explicitly this is given by

$$\begin{aligned} i\Sigma_2(\not{p}) &= \text{diagram} \\ &= -g_s^2 \mu^{4-d} C_F \int \frac{d^d k}{(2\pi)^d} \frac{\gamma^\mu (\not{k} + \not{p}) \gamma_\mu}{k^2 (k+p)^2} \\ &= -g_s^2 \mu^{4-d} C_F (2-d) \int_0^1 dx \int \frac{d^d k}{(2\pi)^d} \frac{\not{p}(1-x)}{[k^2 + p^2 x(1-x)]^2}. \end{aligned} \quad (4.63)$$

Here we have introduced the Feynman parameter x and changed integration variables $k \rightarrow k - xp$, dropping the k^μ terms in the numerator which vanish due to symmetry. Differentiating with respect to \not{p} at $\not{p} = 0$ leaves the scaleless integral⁷

$$\int \frac{d^d k}{(2\pi)^d} \frac{1}{k^4} = \frac{i}{16\pi^2} \left(\frac{1}{\epsilon_{\text{UV}}} - \frac{1}{\epsilon_{\text{IR}}} \right). \quad (4.64)$$

Note that ϵ_{UV} and ϵ_{IR} are identical numerically; their subscripts are just meant to keep track of their origin, in that the former must be taken larger than zero, and the latter smaller than zero, when regulating the integral.

With this, the counterterm contribution to the cross-section is

$$2\text{Re}(\delta_\psi) \frac{d\hat{\sigma}_0^d}{dQ^2} = \sigma_0^d \delta(1-z) \frac{\alpha_s}{2\pi} C_F \left(\frac{1}{\epsilon_{\text{IR}}} - \frac{1}{\epsilon_{\text{UV}}} \right). \quad (4.65)$$

⁷This is solved by splitting the integral over the Euclidean k_E into low- and high-energy regions; the two integrals are solved using $d = 4 - 2\epsilon$, where $\epsilon < 0$ for the low-energy region, and $\epsilon > 0$ in the high-energy region.

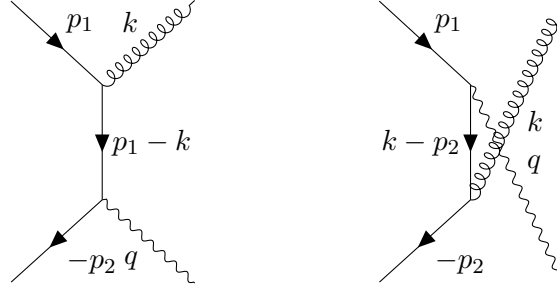


Figure 4.1: Real gluon emission diagrams that contribute at order α_s to the $q\bar{q} \rightarrow \tilde{\ell}\tilde{\ell}^* + X$ cross-section.

By evaluating the Passarino-Veltman coefficients of Eq. (4.58) in LoopTools [26, 27], we find that this exactly cancels the ultraviolet divergence from the virtual diagram, and adds an infrared one with the same coefficient. In this way, since $\epsilon_{\text{IR}} = \epsilon_{\text{UV}}$, nothing has really changed in the expression.

This means that in practice, when implementing Eq. (4.58) numerically, we actually obtain the renormalized expression when the UV-divergent terms are *not* actively removed; instead they are (heuristically) regarded as contributing to the IR-divergent ones.

4.3.3 Real gluon emission

The virtual correction to the cross-section is UV-finite when renormalized, but still contains infrared divergences. This can be amended by adding the cross-section for $q\bar{q} \rightarrow \tilde{\ell}\tilde{\ell}^* + g$, where g is a gluon, which at leading-order contributes at the same order in α_s as the above to the inclusive cross-section we are looking for.

As discussed in Sec. 4.1, the slepton part and intermediate propagator factorize in the cross-section, and we only have to consider the hadronic part of the process; in this case, the process $q_i\bar{q}_j \rightarrow \gamma^* g_a$ at leading-order. Here i, j denote the color states of the incoming quarks, and a the state of the gluon, which transforms in the adjoint representation. At this order there is one t -channel and one u -channel diagram, shown in Fig. 4.1. Their S -matrix element is given by

$$\begin{aligned}
 i\mathcal{M}_r &= \bar{v}_j^r(p_2) \left[\gamma^\mu \frac{\not{p}_1 - \not{k}}{(p_1 - k)^2} \left(i\mu^{\frac{4-d}{2}} g_s T_{ji}^a \right) \gamma^\nu + \left(i\mu^{\frac{4-d}{2}} g_s T_{ji}^a \right) \gamma^\nu \frac{\not{k} - \not{p}_2}{(k - p_2)^2} \gamma^\mu \right] u_i^s(p_1) \epsilon_\nu^{a*}(k) \epsilon_\mu^*(q) \\
 &\equiv \bar{v}_j(p_2) S^{\mu\nu} u_i^s(p_1) \epsilon_\nu^{a*}(k) \epsilon_\mu^*(q) T_{ji}^a,
 \end{aligned} \tag{4.66}$$

where k and q are the momenta of the gluon and virtual photon, respectively. Defining the partonic Mandelstam variables

$$\hat{s} \equiv (p_1 + p_2)^2 = (k + q)^2, \tag{4.67}$$

$$\hat{t} \equiv (p_1 - k)^2 = (p_2 - q)^2, \tag{4.68}$$

$$\hat{u} \equiv (p_1 - q)^2 = (p_2 - k)^2, \tag{4.69}$$

the spin- and color-averaged squared matrix element is given by

$$\begin{aligned}
 \langle |\mathcal{M}_r|^2 \rangle &= \frac{1}{4N_C^2} \text{Tr}[\not{p}_2 S^{\mu\nu} \not{p}_1 S^{\rho\sigma}] g_{\mu\sigma} g_{\nu\rho} T_{ji}^a T_{ij}^a \\
 &= \frac{C_F \mu^{4-d} g_s^2}{4N_C} \left\{ \frac{1}{\hat{t}^2} \text{Tr}[\not{p}_2 \gamma^\mu (\not{p}_1 - \not{k}) \gamma^\nu \not{p}_1 \gamma_\nu (\not{p}_1 - \not{k}) \gamma_\mu] + \frac{1}{\hat{t}\hat{u}} \text{Tr}[\not{p}_2 \gamma^\mu (\not{p}_1 - \not{k}) \gamma^\nu \not{p}_1 \gamma_\mu (\not{k} - \not{p}_2) \gamma_\nu] \right. \\
 &\quad \left. + (p_1 \leftrightarrow p_2) \right\}.
 \end{aligned} \tag{4.70}$$

The first term is fairly straightforward to evaluate using Dirac algebra in d dimensions:

$$\text{Tr}[\not{p}_2 \gamma^\mu (\not{p}_1 - \not{k}) \gamma^\nu \not{p}_1 \gamma_\nu (\not{p}_1 - \not{k}) \gamma_\mu] = 2(d-2)^2 \hat{u} \hat{t}. \quad (4.71)$$

The second requires a little more work, and using $\hat{s} + \hat{t} + \hat{u} = Q^2$, to simplify; in the end, it can be written as

$$\text{Tr}[\not{p}_2 \gamma^\mu (\not{p}_1 - \not{k}) \gamma^\nu \not{p}_1 \gamma_\mu (\not{k} - \not{p}_2) \gamma_\nu] = 2(d-4)(d-2) \hat{u} \hat{t} + 4(d-2) Q^2 \hat{s}. \quad (4.72)$$

Putting this together, the squared matrix element reduces to

$$\langle |\mathcal{M}_r|^2 \rangle = \frac{C_F \mu^{4-d} g_s^2}{2N_C} (d-2) \left[4 \frac{Q^2 \hat{s}}{\hat{t} \hat{u}} + 2(d-4) + (d-2) \left(\frac{\hat{u}}{\hat{t}} + \frac{\hat{t}}{\hat{u}} \right) \right]. \quad (4.73)$$

To carry out the phase space integral, it is convenient to express everything in terms of dimensionless variables. We use momentum conservation to eliminate one momentum integral and fix the absolute value of the spatial momenta, and the energy of the gluon, to $\omega = (1-z)\sqrt{\hat{s}}/2$; then, by axial symmetry, we can eliminate all but one angular integration variable. With this the differential phase space of the gluon and photon (as defined in Eq. (4.13)) can be simplified, in the center-of-mass frame, to

$$d\Pi_H = \frac{(1-z)^{d-3} (Q^2/z)^{(d-4)/2}}{2^{d-1} \pi^{(d-2)/2} \Gamma(\frac{d-2}{2})} [y(1-y)]^{\frac{d-4}{2}} dy, \quad (4.74)$$

where $y \equiv \frac{1}{2}(1 + \cos \theta) \in (0, 1)$ and as before $z = Q^2/\hat{s}$. The angle θ is the gluon emission angle in the center-of-mass frame. Using this, the Mandelstam variables can be rewritten in terms of y and z : From the definition of z , \hat{s} is immediately given by $\hat{s} = Q^2/z$. For the others,

$$\hat{t} = -\frac{Q^2}{z} (1-z)(1-y), \quad (4.75)$$

$$\hat{u} = -\frac{Q^2}{z} (1-z)y. \quad (4.76)$$

Inserted in Eq. (4.39), this gives (in $d = 4 - 2\epsilon$ dimensions)

$$\begin{aligned} \frac{d\hat{\sigma}_r}{dQ^2} &= \frac{C_F \mu^{2\epsilon} 2^{1+2\epsilon} \pi^\epsilon \alpha_s \alpha^2 (1-\epsilon) (1-z)^{1-2\epsilon} (Q^2/z)^{-\epsilon} p^3}{3N_C \hat{s} Q^5 \Gamma(1-\epsilon)} F_{q\ell_i}^{AB}(Q) \\ &\times \int_0^1 dy [y(1-y)]^{-\epsilon} \left[\frac{4z}{(1-z)^2 y(1-y)} - 4\epsilon + (2-2\epsilon) \left(\frac{y}{1-y} + \frac{1-y}{y} \right) \right]. \end{aligned} \quad (4.77)$$

The y integral can be performed through Euler beta functions;

$$\int_0^1 dy y^{a-1} (1-y)^{b-1} = B(a, b) = \frac{\Gamma(a)\Gamma(b)}{\Gamma(a+b)}. \quad (4.78)$$

This leaves⁸

$$\begin{aligned} \frac{d\hat{\sigma}_r}{dQ^2} &= \frac{8C_F \alpha_s \alpha^2 p^3}{3N_C \hat{s} Q^5} F_{q\ell_i}^{AB}(Q) \left(\frac{4\pi\mu^2}{Q^2} \right)^\epsilon (1-\epsilon) \frac{\Gamma(1-\epsilon)}{\Gamma(1-2\epsilon)} \\ &\times \left[-\frac{2}{\epsilon} z^{1+\epsilon} (1-z)^{-1-2\epsilon} - \frac{1}{1-2\epsilon} \left(\epsilon + \frac{1}{\epsilon} (1-\epsilon)^2 \right) z^\epsilon (1-z)^{1-2\epsilon} \right]. \end{aligned} \quad (4.79)$$

⁸Note that we must assume $\epsilon < 0$, i.e. $d > 4$, in using the beta functions, meaning that the divergences are infrared in nature

The terms in brackets can be expanded to first order in ϵ using $z^\epsilon = 1 + \epsilon \ln z + \mathcal{O}(\epsilon^2)$, and with plus distributions:⁹

$$(1-z)^{-1-2\epsilon} = -\frac{1}{2\epsilon}\delta(1-z) + \frac{1}{(1-z)_+} - 2\epsilon\left(\frac{\ln(1-z)}{1-z}\right)_+ + \mathcal{O}(\epsilon^2). \quad (4.80)$$

Then, discarding all terms of order higher than ϵ^1 , as well as setting $z = 1$ in all terms proportional to $\delta(1-z)$, the cross-section is given by

$$\frac{d\hat{\sigma}_r}{dQ^2} = \sigma_0^d C_F \frac{\alpha_s}{\pi} G(\epsilon) \left[\frac{1}{\epsilon^2} \delta(1-z) - \frac{1}{\epsilon} \frac{1+z^2}{(1-z)_+} - \frac{(1+z^2) \ln z}{1-z} + 2(1+z^2) \left(\frac{\ln(1-z)}{1-z} \right)_+ \right], \quad (4.81)$$

where

$$G(\epsilon) \equiv \left(\frac{4\pi\mu^2}{Q^2} \right)^\epsilon \frac{\Gamma(1-\epsilon)}{\Gamma(1-2\epsilon)} = 1 + \mathcal{O}(\epsilon). \quad (4.82)$$

We recognize this factor from the virtual diagram, in Eq. (4.58).

It is worth noting where the different divergences originate from; in the calculation above, they appear in the phase space integration for the region of phase space with $y \rightarrow 1$ or $y \rightarrow 0$, and in expanding $(1-z)^{-1-2\epsilon}$, which diverges for $z \rightarrow 1$. These are called collinear ($y \rightarrow 0, 1$ means $\cos \theta \rightarrow \pm 1$, i.e. the emitted gluon goes *collinear* to either of the quarks) and soft ($z \rightarrow 1$ means that the gluon energy $\omega \rightarrow 0$) divergences, respectively. The $1/\epsilon^2$ term has both of these contributions, while the other divergence is purely collinear, since the $\delta(1-z)$ part in the expansion of Eq. (4.80) cancels in all other terms.

Adding Eq. (4.55), evaluating the Passarino-Veltman coefficients in LoopTools [26, 27],¹⁰ the $q\bar{q}$ contribution to the partonic cross-section at NLO is given by

$$\begin{aligned} \frac{d\hat{\sigma}_{q\bar{q}\text{NLO}}}{dQ^2} = \sigma_0^d \frac{\alpha_s}{\pi} C_F G(\epsilon) & \left[\delta(1-z) \left(\frac{\pi^2}{3} - 4 \right) - \frac{(1+z^2) \ln z}{1-z} + 2(1+z^2) \left(\frac{\ln(1-z)}{1-z} \right)_+ \right. \\ & \left. - \frac{1}{\epsilon} \left(\frac{1+z^2}{(1-z)_+} + \frac{3}{2} \delta(1-z) \right) \right]. \end{aligned} \quad (4.83)$$

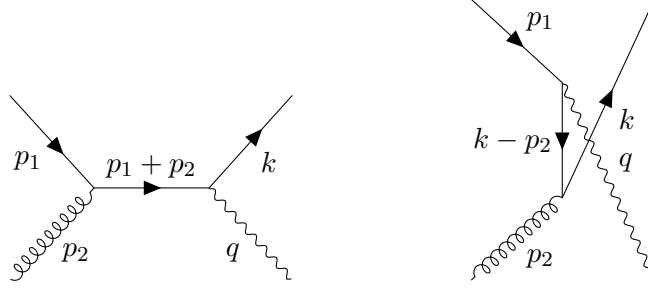
The ultraviolet divergence has been removed, so we drop the subscript on $\epsilon = \epsilon_{\text{IR}}$. Notice that as anticipated, the remaining collinear divergence is proportional to $P_{q\bar{q}}(z)$, as defined in Eq. (3.40).

Since the virtual loop contribution has a simple functional form, as verified by evaluating the coefficients in Eq. (4.58), it is not necessary to calculate these from Passarino-Veltman coefficients each time the cross-section is evaluated. Instead, it is more efficient to just use the above expression directly.

This changes when considering loop corrections from supersymmetric particles, as we will do in Sec. 4.4. There, since the particles in the loop are massive, the dependence on the scale μ and the physical energy scales will not factor out as neatly as here. This in turn makes the integrals over the Feynman parameters much more complicated, making it simpler to use Passarino-Veltman reduction.

⁹For the definition of plus distributions, see Sec. 3.3.1.

¹⁰This is done by evaluating the terms in Eq. (4.58) proportional to $1/\epsilon^2$, $1/\epsilon$, and finite ones, respectively, and verifying that the expression in the brackets $[\dots]$ of that equation evaluates to $-\frac{1}{\epsilon^2} - \frac{3}{2}\frac{1}{\epsilon} + \frac{\pi^2}{3} - 4$, regardless of the energy scales μ and Q (this only happens due to the massless nature of the particles in the loop; more complicated scale dependence is expected when the propagating particles are massive). Alternatively, one can explicitly perform the loop integral following the methods of Sec. 1.2.2, with the integrals over the Feynman parameters becoming Beta integrals similar to those of the real emission diagrams.

Figure 4.2: Leading-order diagrams for $qg \rightarrow q\gamma^*$.

4.3.4 Real quark emission

Next, we must consider the process $qg \rightarrow q\tilde{\ell}\tilde{\ell}^*$, or similarly with an antiquark instead of a quark. At the parton level this is obviously a very different process, but at the hadron level it contributes to the same observed process as the $q\bar{q}$ collision diagrams; a collision of two protons, leading to the production of a slepton pair, which manifests itself as missing transverse energy and a lepton pair in addition to a jet, since neither gluons nor quarks can be observed on their own. This process begins at order $\alpha^2\alpha_s$, and has no virtual contributions, so all divergences must cancel on their own.

As before, we only consider the hadronic part of the diagram, since the propagator and slepton pieces remain unchanged. Thus we need the S -matrix element for $qg \rightarrow q\gamma^*$, which at leading order has two contributions as shown in Fig. 4.2, and is given by

$$i\mathcal{M}_{qg} = \bar{u}_j^r(k) S_{(q)}^{\mu\nu} u_i^s(p_1) T_{ji}^a \epsilon_\nu^a(p_2) \epsilon_\mu^*(q), \quad (4.84)$$

where

$$S_{(q)}^{\mu\nu} \equiv \gamma^\mu \frac{i(\not{p}_1 + \not{p}_2)}{\hat{s}} \left(i\mu^{(4-d)/2} g_s \gamma^\nu \right) + \left(i\mu^{(4-d)/2} g_s \gamma^\nu \right) \frac{i(\not{k} - \not{p}_2)}{\hat{u}} \gamma^\mu, \quad (4.85)$$

with the Mandelstam variables defined exactly like in the gluon emission case, but now p_2 and k are the momenta of the incoming gluon and outgoing quark, respectively. Note that since the quarks are still taken to be massless the kinematics will work out in the same way as in the gluon emission calculation.

For the spin- and color-averaged squared matrix element we now have to take into account that the gluon has a different number of available states than the quark, as it transforms in the adjoint representation of $SU(3)_C$; since it is a massless vector it has 2 possible polarizations, like the quark, but the number of color states is given by the number of $SU(3)$ generators, namely $N_C^2 - 1$. The color factor remains the same, but here it is more convenient to use Eq. (3.8) to write it as $T_{ji}^a T_{ij}^a = T_F(N_C^2 - 1)$, where T_F is the index of the fundamental representation. With this, we have

$$\langle |\mathcal{M}_{qg}|^2 \rangle = \frac{T_F}{4N_C} \text{Tr} \left[\not{k} S_{(q)\mu\nu} \not{p}_1 S_{(q)}^{\nu\mu} \right]. \quad (4.86)$$

The trace calculation works out in a very similar fashion as for the gluon emission, leaving

$$\langle |\mathcal{M}_{qg}|^2 \rangle = \frac{T_F}{2N_C} \mu^{4-d} g_s^2 (d-2) \left[-4 \frac{4Q^2 \hat{t}}{\hat{u} \hat{s}} + 2(4-d) - (d-2) \left(\frac{\hat{u}}{\hat{s}} + \frac{\hat{s}}{\hat{u}} \right) \right]. \quad (4.87)$$

Expressing the Mandelstam variables as functions of z and y as in the previous section (again, because the kinematics are identical), one can see that this expression is regular for $z = 1$; this means that all divergences are collinear, and eliminates the need for plus distributions. Besides this

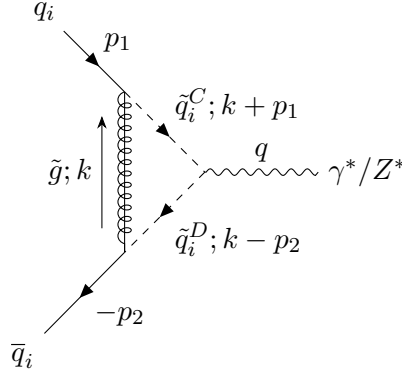


Figure 4.3: Supersymmetry correction to the $q\bar{q}\gamma/q\bar{q}Z$ vertex. For sparticles, both particle types and momenta (in the direction of the arrows) are given. C, D label the squark mass eigenstates, and i the quark/squark flavor.

the calculation is again similar to the gluon emission case, and gives a partonic cross-section of

$$\frac{d\hat{\sigma}_{qg}}{dQ^2} = \sigma_0^d T_F \frac{\alpha_s}{2\pi} G(\epsilon) \left[\left((1-z)^2 + z^2 \right) \left(\ln \frac{(1-z)^2}{z} - \frac{1}{\epsilon} \right) + \frac{1}{2} + 3z - \frac{7}{2}z^2 \right]. \quad (4.88)$$

Note that this also holds for gluon-antiquark scattering. Again, from Eq. (3.41) we are left with a collinear divergence proportional to the splitting function $P_{qg}(z)$, and the same prefactor $G(\epsilon)$ as defined in Eq. (4.82).

4.4 Supersymmetry correction

At order $\mathcal{O}(\alpha_s)$ there is just one contributing diagram involving supersymmetric particles, given by the loop shown in Fig. 4.3.

In the most general case,¹¹ the two squarks corresponding to one quark can have different masses, and the mass eigenstates are not necessarily the same as the chiral eigenstates. Thus the photon and Z exchange diagrams will no longer factor exactly like they have up to this point, since weak and QED interactions treat chirality differently; for example, the propagator factors from each contribution will then not be the same since different particles appear in the different processes (the squark- Z vertex allows for the two interacting squarks to not be in the same mass eigenstate, while the γ vertex does not), and mass mixing angles will appear differently as well. It is therefore necessary to evaluate the photon and Z exchange diagrams individually. The matrix element for the loop diagrams (including the slepton part and propagators) is given by

$$\begin{aligned} i\mathcal{M}_S = & \bar{v}^r(p_2) \frac{-ie}{c_W s_W} \Gamma_Z^\mu u^s(p_1) \frac{-ig_{\mu\nu}}{Q^2 - m_Z^2 + im_Z \Gamma_Z} \frac{-ie}{c_W s_W} Z_{\ell_i}^{AB} (p_3 - p_4)^\nu \\ & + \delta^{AB} \bar{v}^r(p_2) (iQ_q e) \Gamma_\gamma^\mu u^s(p_1) \frac{-ig_{\mu\nu}}{Q^2} (-ie) (p_3 - p_4)^\nu, \end{aligned} \quad (4.89)$$

¹¹Excluding mixing mass mixing across flavors, as discussed previously.

where $s_W, c_W \equiv \sin \theta_W, \cos \theta_W$. The vertices are given by [48]^{12,13}

$$\begin{aligned} \Gamma_Z^\mu = & \sum_{C,D=1}^2 \frac{i\mu^{(4-d)/2} g_s}{\sqrt{2}} T_{jk}^a [a(\tilde{q}_D)(1 - \gamma^5) + b(\tilde{q}_D)(1 + \gamma^5)] \\ & \times \int \frac{d^d k}{(2\pi)^d} \frac{i(-\not{k} + m_{\tilde{g}})}{k^2 - m_{\tilde{g}}^2} \frac{i}{(k + p_1)^2 - m_{\tilde{q}_C}^2} \frac{i}{(k - p_2)^2 - m_{\tilde{q}_D}^2} Z_q^{CD} (2k + p_1 - p_2)^\mu \\ & \times \frac{i\mu^{(4-d)/2} g_s}{\sqrt{2}} T_{ki}^a [a(\tilde{q}_C)(1 + \gamma^5) + b(\tilde{q}_C)(1 - \gamma^5)], \end{aligned} \quad (4.90)$$

and Γ_γ^μ is the same with $C = D$ and no factor Z_q^{CD} . The various numerical factors are defined by

$$a(\tilde{q}_C) \equiv -Q_{2C}, \quad (4.91)$$

$$b(\tilde{q}_C) \equiv Q_{1C}, \quad (4.92)$$

$$Z_q^{CD} \equiv -[T_{qL}^3 Q_{1C} Q_{1D} + T_{qR}^3 Q_{2C} Q_{2D} - Q_q s_W^2 \delta^{CD}], \quad (4.93)$$

with the mixing matrix given by

$$Q_{CD} = \begin{bmatrix} \cos \theta_q & \sin \theta_q \\ -\sin \theta_q & \cos \theta_q \end{bmatrix}. \quad (4.94)$$

note that without mass/chirality mixing, $Z_q^{11/22} = 2Z_{qL/R}$.

The reason that mixing angles and chirality projection operators appear even in the quark-squark-gluino vertex is that in the QCD Lagrangian, left- and right-handed fields are not mixed, which means that left-handed quark fields only interact with \tilde{q}_L , and vice versa. If there were no mixing and no mass difference between the two squark states one could simply sum over the chiralities with the γ^5 matrices canceling out, as in a regular QCD vertex, but in the general case we must keep track of the different squarks separately.

Since squarks are scalars, the Dirac matrix structure of these expressions is actually somewhat simpler than in the regular QCD case; apart from the loop integral, only γ^5 matrices appear, which are fairly straightforward to keep track of as they anti-commute with all γ^μ . This means that all terms proportional to \not{p}_1 or \not{p}_2 in the integral can be dropped, since they vanish when contracted with the external spinors.

Furthermore, these vertices contribute to the NLO cross-section through interference with the leading-order result, like the QCD loop did, giving terms proportional to e.g. $\text{Tr}[\not{p}_2 \Gamma_{Z/\gamma}^\mu \not{p}_1 \gamma^\nu]$. Such traces vanish for an odd number of γ matrices; in other words, all terms in $\Gamma_{Z/\gamma}^\mu$ not proportional to γ^μ , after rewriting the integral in terms of Passarino-Veltman functions, will not contribute to the trace. This makes it possible to simplify the loop integral in Eq. (4.90) (denoted by I_{CD}) considerably, dropping all terms containing \not{p}_1 and/or \not{p}_2 , as well as terms without γ^μ ; in the end, the only contributing part is

$$\begin{aligned} I_{CD} \equiv & -i\mu^{4-d} \int \frac{d^d k}{(2\pi)^d} \frac{(\not{k} - m_{\tilde{g}})(2k + p_1 - p_2)^\mu}{(k^2 - m_{\tilde{g}}^2)((k + p_1)^2 - m_{\tilde{q}_C}^2)((k - p_2)^2 - m_{\tilde{q}_D}^2)} \\ & \rightarrow 2 \frac{r_\Gamma}{(4\pi)^{d/2}} \gamma^\mu C_{00}(0, Q^2, 0, m_{\tilde{g}}^2, m_{\tilde{q}_C}^2, m_{\tilde{q}_D}^2). \end{aligned} \quad (4.95)$$

¹²Here C, D label the mass eigenstates of the intermediate squarks.

¹³As mentioned in Ref. [49] the treatment of gluinos, being Majorana fermions, requires some care in defining fermion flow directions, but the treatment for the quark-squark-gluino vertex is fairly straightforward.

For convenience, the list of arguments of C_{00} will henceforth be abbreviated to (C, D) , since only the squark mass eigenstates change from one term to another.

Writing out the terms in the C, D sum explicitly and using the anti-commutation of the γ^5 matrix, the vertex factors can be written as (as usual the color factors simplify to $C_F \delta_{ij}$; the Kronecker delta is left implicit below)

$$\begin{aligned} \Gamma_Z^\mu \rightarrow \frac{\alpha_s}{2\pi} (4\pi)^{(4-d)/2} r_\Gamma C_F \gamma^\mu [& C_{00}(1, 1) Z_q^{11} (\sin^2 \theta_q (1 + \gamma^5) + \cos^2 \theta_q (1 - \gamma^5)) \\ & - 2(C_{00}(1, 2) + C_{00}(2, 1)) Z_q^{12} \sin \theta_q \cos \theta_q \gamma^5 \\ & + C_{00}(2, 2) Z_q^{22} (\cos^2 \theta_q (1 + \gamma^5) + \sin^2 \theta_q (1 - \gamma^5))], \end{aligned} \quad (4.96)$$

$$\begin{aligned} \Gamma_\gamma^\mu \rightarrow \frac{\alpha_s}{2\pi} (4\pi)^{(4-d)/2} r_\Gamma C_F \gamma^\mu [& C_{00}(1, 1) (\sin^2 \theta_q (1 + \gamma^5) + \cos^2 \theta_q (1 - \gamma^5)) \\ & + C_{00}(2, 2) (\cos^2 \theta_q (1 + \gamma^5) + \sin^2 \theta_q (1 - \gamma^5))]. \end{aligned} \quad (4.97)$$

As we mentioned above, these diagrams contribute to the NLO cross-section through interference with the leading-order result. The phase space is identical to that of the leading-order case, with the hadronic part simply integrating to $\frac{2\pi}{s} \delta(1 - z)$ as in Sec. 4.2; and the slepton part contributing

$$\int d\Pi_L (p_3 - p_4)_\mu (p_3 - p_4)_\nu \rightarrow -\frac{p^3}{3\pi Q} g_{\mu\nu}, \quad (4.98)$$

like in Eq. (4.37). The cross-section can then be written as

$$\begin{aligned} \frac{d\hat{\sigma}_s}{dQ^2} &= \frac{1}{2\pi\hat{s}} \int d\Pi_H d\Pi_L \text{Re} \langle \mathcal{M}_0^* \mathcal{M}_s \rangle \\ &= -\frac{p^3 g_{\mu\nu} \delta(1 - z)}{12 N_C \pi Q \hat{s}^2} \left[\frac{e^4}{c_W^4 s_W^4} \frac{(Z_{\ell_i}^{AB})^2}{(Q^2 - m_Z^2)^2 + m_Z^2 \Gamma_Z^2} M_{ZZ}^{\mu\nu} \right. \\ &\quad \left. - \frac{Q_q e^4}{c_W^2 s_W^2} \frac{(Q^2 - m_Z^2) Z_{\ell_i}^{AB} \delta^{AB}}{Q^2 ((Q^2 - m_Z^2)^2 + m_Z^2 \Gamma_Z^2)} (M_{Z\gamma}^{\mu\nu} + M_{\gamma Z}^{\mu\nu}) + \frac{Q_q^2 e^4}{Q^4} \delta^{AB} M_{\gamma\gamma}^{\mu\nu} \right], \end{aligned} \quad (4.100)$$

where we have defined

$$M_{(Z/\gamma)(Z/\gamma)}^{\mu\nu} \equiv \text{Tr} [\not{p}_2 \Gamma_{Z/\gamma}^\mu \not{p}_1 \gamma_{Z/\gamma}^\nu], \quad (4.101)$$

with $\gamma_\gamma^\mu \equiv \gamma^\mu$ and

$$\gamma_Z^\mu \equiv \gamma^\mu (Z_{q_L} (1 - \gamma^5) + Z_{q_R} (1 + \gamma^5)). \quad (4.102)$$

Like in Sec. 4.1, all of the traces in Eq. (4.101) are proportional to $\text{Tr}[\not{p}_2 \gamma^\mu \not{p}_1 \gamma^\nu]$, which is equal to $2(4p_1^{(\mu} p_2^{\nu)} - \hat{s} g^{\mu\nu})$; once contracted with $g_{\mu\nu}$ from the slepton tensor, this gives $2(2 - d)\hat{s}$. The proportionality factors are again found by using properties of the γ^5 matrix.

The divergence in this expression (coming from C_{00}) is purely ultraviolet, meaning that it can be removed entirely by a counterterm without leaving any finite terms when expanding in $\epsilon = \frac{1}{2}(4 - d)$.¹⁴ Thus we can make this expression finite by effectively taking, when factoring out the usual prefactor $G(\epsilon)(1 - \epsilon)$,

$$\left(\frac{Q^2}{\mu^2} \right)^\epsilon \Gamma(1 + \epsilon) \Gamma(1 - \epsilon) \text{Re}(C_{00}) \rightarrow C_{00}^0 \equiv C, \quad (4.103)$$

¹⁴This is in contrast to what happened in Eq. (4.58), where the finite term contains contributions from IR-divergent functions.

where C_{00}^0 is, as before, the real part of the finite component of C_{00} . Since we are using the on-shell renormalization scheme for the particle masses there is, however, a finite contribution from the renormalization in this case, as we will see shortly.

In the end, the loop contribution to the cross-section, i.e. not including the counterterm, is given by

$$\begin{aligned} \frac{d\hat{\sigma}_s}{dQ^2} &= C_F G(\epsilon)(1 - \epsilon) \frac{8\alpha^2 \alpha_s}{3N_C \hat{s} Q^5} \delta(1 - z) F_{\hat{q}\ell_i}^{AB}(Q) \\ &= \sigma_0^d G(\epsilon) C_F \frac{\alpha_s}{\pi} \frac{F_{\hat{q}\ell_i}^{AB}(Q)}{F_{q\ell_i}^{AB}(Q)} \delta(1 - z), \end{aligned} \quad (4.104)$$

where

$$\begin{aligned} F_{\hat{q}\ell_i}^{AB} &= C(1, 1) \left[\frac{Q^4 (Z_{\ell_i}^{AB})^2 Z_q^{11}}{c_W^4 s_W^4 ((Q^2 - m_Z^2)^2 + m_Z^2 \Gamma_Z^2)} (2 \sin^2 \theta_q Z_{qR} + 2 \cos^2 \theta_q Z_{qL}) \right. \\ &\quad \left. - \frac{Q_q}{c_W^2 s_W^2} \frac{Q^2 (Q^2 - m_Z^2) Z_{\ell_i}^{AB} \delta^{AB}}{(Q^2 - m_Z^2)^2 + m_Z^2 \Gamma_Z^2} (Z_q^{11} + 2 \sin^2 \theta_q Z_{qR} + 2 \cos^2 \theta_q Z_{qL}) + Q_q^2 \delta^{AB} \right] \\ &\quad + C(2, 2) \left[\frac{Q^4 (Z_{\ell_i}^{AB})^2 Z_q^{22}}{c_W^4 s_W^4 ((Q^2 - m_Z^2)^2 + m_Z^2 \Gamma_Z^2)} (2 \cos^2 \theta_q Z_{qR} + 2 \sin^2 \theta_q Z_{qL}) \right. \\ &\quad \left. - \frac{Q_q}{c_W^2 s_W^2} \frac{Q^2 (Q^2 - m_Z^2) Z_{\ell_i}^{AB} \delta^{AB}}{(Q^2 - m_Z^2)^2 + m_Z^2 \Gamma_Z^2} (Z_q^{22} + 2 \cos^2 \theta_q Z_{qR} + 2 \sin^2 \theta_q Z_{qL}) + Q_q^2 \delta^{AB} \right] \\ &\quad - 2(C(1, 2) + C(2, 1)) \frac{Q^4 (Z_{\ell_i}^{AB})^2 Z_q^{12} (Z_{qR} - Z_{qL})}{c_W^4 s_W^4 ((Q^2 - m_Z^2)^2 + m_Z^2 \Gamma_Z^2)} \sin \theta_q \cos \theta_q. \end{aligned} \quad (4.105)$$

For the special case where $\theta_q = 0$ and $m_{\hat{q}_1} = m_{\hat{q}_2} = m_{\hat{q}}$, this reduces to $F_{\hat{q}\ell_i}^{AB} = 2C(0, Q^2, 0, m_g^2, m_{\hat{q}}^2, m_{\hat{q}}^2) F_{q\ell_i}^{AB}$, with $F_{q\ell_i}^{AB}$ as defined in Eq. (4.27).

4.4.1 Self-energy counterterm

As we alluded to above, the renormalization of the quark-squark-gluino vertex, when using the on-shell scheme for masses, leaves a finite contribution to the cross-section. Like in the QCD loop correction we add a field renormalization term $2\text{Re}(\delta_\psi^s) \frac{d\hat{\sigma}_0^d}{dQ^2}$; δ_ψ^s is given by

$$\delta_\psi^s = - \frac{d}{d\hat{p}} \Sigma_2^s(\hat{p}) \Big|_{\hat{p}=m_q=0}, \quad (4.106)$$

where Σ_2^s is the squark-gluino loop correction to the quark self-energy. Evaluating this diagram we find (as usual the color sum includes a color-conserving Kronecker delta, which we leave implicit)

$$\begin{aligned}
 i\Sigma_2^s(\not{p}) &= \text{Diagram: A quark line with momentum } p \text{ enters from the left, goes into a loop. The loop consists of a gluon (curly line) and a squark (dashed line). The gluon has momentum } k \text{ and the squark has momentum } p-k. \text{ The loop is labeled } g \text{ and } \tilde{q}_C. \text{ The quark line exits with momentum } p \text{ and continues to the right.} \\
 &= \sum_{C=1}^2 \mu^{4-d} g_s^2 T^a T^a \frac{1}{\sqrt{2}} [a(\tilde{q}_C)(1 - \gamma^5) + b(\tilde{q}_C)(1 + \gamma^5)] \\
 &\quad \times \int \frac{d^d k}{(2\pi)^d} \frac{\not{k} + m_{\tilde{g}}}{(k^2 - m_{\tilde{g}}^2) ((k-p)^2 - m_{\tilde{q}_A}^2)} \\
 &\quad \times \frac{1}{\sqrt{2}} [a(\tilde{q}_C)(1 + \gamma^5) + b(\tilde{q}_C)(1 - \gamma^5)]. \tag{4.107}
 \end{aligned}$$

The two terms in the integral are treated separately; the first is a tensor integral B^μ , while the other is a scalar 2-point function B_0 . The former can as discussed in section 1.3 be written as $B^\mu = -p^\mu B_1$, while B_0 is left as is. Differentiating this expression with respect to \not{p} ,¹⁵ as before dropping all terms that will vanish (meaning terms containing \not{p} , which is taken to zero in the definition of the counterterm, and the γ^5 terms that vanish when taking the trace with the leading-order result), and summing over the squark mass eigenstates, a similar trace calculation to the one leading to Eq. (4.104) gives the (finite) counterterm contribution to the cross-section:

$$\frac{d\hat{\sigma}_{\text{c.t.}}}{dQ^2} = \sigma_0^d G(\epsilon) C_F \frac{\alpha_s}{\pi} \frac{\delta F_{\tilde{q}\ell_i}^{AB}(Q)}{F_{q\ell_i}^{AB}(Q)} \delta(1-z), \tag{4.108}$$

with

$$\begin{aligned}
 \delta F_{\tilde{q}\ell_i}^{AB}(Q) &= B_1(0, m_{\tilde{g}}^2, m_{\tilde{q}_1}^2) \left[2 \frac{Q^4 (Z_{\ell_i}^{AB})^2 (\sin^2 \theta_q Z_{q_R}^2 + \cos^2 \theta_q Z_{q_L}^2)}{c_W^4 s_W^4 ((Q^2 - m_Z^2)^2 + m_Z^2 \Gamma_Z^2)} \right. \\
 &\quad \left. - 2 \frac{Q_q}{c_W^2 s_W^2} \frac{Q^2 (Q^2 - m_Z^2) Z_{\ell_i}^{AB} \delta^{AB}}{(Q^2 - m_Z^2)^2 + m_Z^2 \Gamma_Z^2} (\sin^2 \theta_q Z_{q_R} + \cos^2 \theta_q Z_{q_L}) + \frac{1}{2} Q_q^2 \delta^{AB} \right] \\
 &\quad + B_1(0, m_{\tilde{g}}^2, m_{\tilde{q}_2}^2) \left[2 \frac{Q^4 (Z_{\ell_i}^{AB})^2 (\cos^2 \theta_q Z_{q_R}^2 + \sin^2 \theta_q Z_{q_L}^2)}{c_W^4 s_W^4 ((Q^2 - m_Z^2)^2 + m_Z^2 \Gamma_Z^2)} \right. \\
 &\quad \left. - 2 \frac{Q_q}{c_W^2 s_W^2} \frac{Q^2 (Q^2 - m_Z^2) Z_{\ell_i}^{AB} \delta^{AB}}{(Q^2 - m_Z^2)^2 + m_Z^2 \Gamma_Z^2} (\cos^2 \theta_q Z_{q_R} + \sin^2 \theta_q Z_{q_L}) + \frac{1}{2} Q_q^2 \delta^{AB} \right]. \tag{4.109}
 \end{aligned}$$

With mass-degenerate, non-mixing squarks, this again simplifies considerably, reducing to $\delta F_{\tilde{q}\ell_i}^{AB} = B_1(0, m_{\tilde{g}}^2, m_{\tilde{q}}^2) F_{q\ell_i}^{AB}$.

Using Eqs. (3.14) and (3.17), we can verify that the divergences from the loop are in fact exactly canceled by the counterterm, as desired.

¹⁵For terms with no explicit \not{p} dependence we use $\frac{d}{d\not{p}} = 2\not{p} \frac{d}{dp^2}$.

4.5 Hadronic cross-section at NLO

Having computed the various contributions to the NLO partonic cross-section, we now want to collect them and calculate the hadronic cross-section. However, we are still left with collinear divergences which must first be dealt with; this is done by exploiting that what happens at the partonic level, in particular the very low-energy interactions that distribute momentum between the partons, is not physically observable.

We can therefore absorb the divergences into the *bare* parton distribution functions (PDFs), leaving finite, scale-dependent PDFs and a finite partonic contribution, as explained in Sec. 3.4. In terms of these bare PDFs $\tilde{f}_i(x)$, with x the fraction of the hadronic momentum carried by the parton, the hadronic cross-section is given by

$$\frac{d\sigma}{dQ^2} = \sigma_B \sum_{ij} \int_{\tau}^1 \frac{dx_1}{x_1} \int_{\tau/x_1}^1 \frac{dx_2}{x_2} \tilde{f}_i(x_1) \tilde{f}_j(x_2) \tilde{w}_{ij} \left(z = \frac{\tau}{x_1 x_2} \right), \quad (4.110)$$

where $\tau = Q^2/s$ so that $z = \tau/x_1 x_2$, and the Born cross-section $\sigma_B = x_1 x_2 \sigma_0^d$ has been factored out of the integral. The partonic functions \tilde{w}_{ij} are what has been calculated in the previous sections:

$$\tilde{w}_{q\bar{q}}(z) = \delta(1-z) + G(\epsilon) C_F \frac{\alpha_s}{\pi} \tilde{w}_{q\bar{q},\text{NLO}}, \quad (4.111)$$

$$\tilde{w}_{qg}(z) = G(\epsilon) T_F \frac{\alpha_s}{2\pi} \left[\left((1-z)^2 + z^2 \right) \left(\ln \frac{(1-z)^2}{z} - \frac{1}{\epsilon} \right) + \frac{1}{2} + 3z - \frac{7}{2} z^2 \right], \quad (4.112)$$

with the next-to-leading order $q\bar{q}$ function given by

$$\begin{aligned} \tilde{w}_{q\bar{q},\text{NLO}} = & -\frac{(1+z^2) \ln z}{1-z} + 2(1+z^2) \left(\frac{\ln(1-z)}{1-z} \right)_+ + \delta(1-z) \left(\frac{\pi^2}{3} - 4 + \frac{F_{q\bar{q}}^{AB}(Q)}{F_{q\bar{q}}^{AB}(Q)} + \frac{\delta F_{q\bar{q}}^{AB}(Q)}{F_{q\bar{q}}^{AB}(Q)} \right) \\ & + \frac{1}{\epsilon} \left[-\frac{1+z^2}{(1-z)_+} - \frac{3}{2} \delta(1-z) \right]. \end{aligned} \quad (4.113)$$

By the procedure outlined in Sec. 3.4 we can transform Eq. (4.110) into a convolution of renormalized PDFs and the finite functions w_{ij} . These still contain residual terms stemming from the divergences, since there are finite terms, that do not vanish for $\epsilon \rightarrow 0$, when expanding $G(\epsilon)$; explicitly, this prefactor gives

$$\begin{aligned} G(\epsilon) &= \left(\frac{4\pi\mu^2}{Q^2} \right)^{\epsilon} \frac{\Gamma(1-\epsilon)}{\Gamma(1-2\epsilon)} \\ &= 1 + \epsilon(\ln 4\pi - \gamma_E) + \epsilon \ln \frac{\mu^2}{Q^2} + \mathcal{O}(\epsilon^2). \end{aligned} \quad (4.114)$$

The $\ln 4\pi$ and γ_E terms are removed in the $\overline{\text{MS}}$ renormalization scheme, which we use for the PDFs; the remaining $\mathcal{O}(\epsilon)$ term leaves a finite contribution when multiplied by $1/\epsilon$. This leaves for the hadronic cross-section, now in terms of finite components,

$$\frac{d\sigma}{dQ^2} = \sigma_B \sum_{ij} \int_{\tau}^1 \frac{dx_1}{x_1} \int_{\tau/x_1}^1 \frac{dx_2}{x_2} f_i(x_1, \mu) f_j(x_2, \mu) w_{ij} \left(z = \frac{\tau}{x_1 x_2} \right). \quad (4.115)$$

The *finite* partonic functions w_{ij} are given by

$$w_{q\bar{q}}(z) = \delta(1-z) + C_F \frac{\alpha_s}{\pi} w_{q\bar{q},\text{NLO}}, \quad (4.116)$$

$$w_{qg}(z) = T_F \frac{\alpha_s}{2\pi} \left[\left((1-z)^2 + z^2 \right) \left(\ln \frac{(1-z)^2}{z} - \ln \frac{\mu^2}{Q^2} \right) + \frac{1}{2} + 3z - \frac{7}{2} z^2 \right], \quad (4.117)$$

with

$$w_{q\bar{q},\text{NLO}} = -\frac{(1+z^2)\ln z}{1-z} + 2(1+z^2)\left(\frac{\ln(1-z)}{1-z}\right)_+ + \delta(1-z)\left(\frac{\pi^2}{3} - 4 + \frac{F_{\bar{q}\ell_i}^{AB}(Q)}{F_{q\ell_i}^{AB}(Q)} + \frac{\delta F_{\bar{q}\ell_i}^{AB}(Q)}{F_{q\ell_i}^{AB}(Q)}\right) + \ln\frac{\mu^2}{Q^2}\left[-\frac{1+z^2}{(1-z)_+} - \frac{3}{2}\delta(1-z)\right]. \quad (4.118)$$

Extending Eq. (4.115) to find the *total* cross-section is trivial, by simply integrating over the invariant mass Q^2 . The limits of this integral are given by momentum conservation, $(m_{\tilde{\ell}_{iA}} + m_{\tilde{\ell}_{iB}})^2 \leq Q^2 \leq s$.

4.6 Cross-section in Mellin space

Equation (4.118) contains terms with plus distributions, which can grow very large in the threshold region $z \rightarrow 1$. In this region the emitted gluons are very low-energy, as most of the energy from the initial state is transferred to the intermediate gauge bosons.

These terms are called large logarithmic corrections. They can be dealt with by resummation; this means writing them on a form that when Taylor expanded, automatically includes contributions to all orders in the coupling constant. A simple example of resummation is the total fermion propagator in Eq. (1.74); this is obtained from summing together all diagrams with an arbitrary number of copies of the sum of 1PI insertions on the propagator.

When studying these logarithmic contributions, we will need an operation called the *Mellin transform*. The Mellin transform $F(N)$ of a function $f(z)$, where $z \in (0, 1)$, is defined by

$$F(N) \equiv \mathcal{F}(f) \equiv \int_0^1 dz z^{N-1} f(z). \quad (4.119)$$

Its inverse is given by

$$f(z) \equiv \mathcal{F}^{-1}(F) \equiv \frac{1}{2\pi i} \int_{c-i\infty}^{c+i\infty} dN z^{-N} F(N), \quad (4.120)$$

where $c \in \mathbb{R}$.

As we will see in Sec. 4.7, the soft-gluon emission contributions¹⁶ can be written on an exponentiated form in Mellin space.¹⁷ As a point of reference, as well as to see why the plus distributions are referred to as logarithmic corrections, it is constructive to calculate the Mellin transform of the cross-section we have just found.

Even without mentioning resummation, the Mellin transformed cross-section might be very useful, due to its effect on convolutions. The hadronic cross-section in Eq. (4.115) can be expressed as a convolution of the three functions $f_i(x_1)$, $f_j(x_2)$, and $w_{ij}(z)$ (leaving out scale dependence for simplicity), given by

$$\frac{d\sigma}{dQ^2} = \sigma_B \sum_{ij} \int_0^1 dx_1 dx_2 dz f_i(x_1) f_j(x_2) w_{ij}(z) \delta(\tau - x_1 x_2 z). \quad (4.121)$$

¹⁶Calculated in the so-called eikonal approximation, where emitted momenta are assumed to be small.

¹⁷The term ‘‘Mellin space’’ is used to denote that a function depends on the Mellin variable N . Conversely, functions of real variables such as $z = Q^2/\hat{s}$, that are *not* Mellin-transformed, are said to be in ‘‘ x -space’’ or ‘‘real space.’’

This can in principle allow for the numerical evaluation of the PDF integrals to be made much more efficient, by instead considering the Mellin moment of the cross-section, defined by

$$\frac{d\Sigma}{dQ^2}(N) \equiv \int_0^1 d\tau \tau^{N-1} \frac{d\sigma}{dQ^2}(\tau). \quad (4.122)$$

Inserting Eq. (4.121) into this definition and using the delta function to eliminate τ , this allows us to write the Mellin moment of the convolution as a simple product of the Mellin moments F_i , F_j , and W_{ij} , of f_i , f_j , and w_{ij} respectively, leaving

$$\frac{d\Sigma}{dQ^2}(N) = \sigma_B \sum_{ij} F_i(N) F_j(N) W_{ij}(N). \quad (4.123)$$

This shows the power of the Mellin transform; by considering Mellin moments of the various functions, it reduces the number of numerical integrations required to evaluate the cross-section. This is in particular helpful when taking resummed contributions into account; as noted above these are typically evaluated in Mellin space, meaning that conventionally we would need to solve a 3-dimensional integral: First the inverse Mellin transform of the partonic cross-section, then integrals over both of the PDFs.¹⁸ If we instead use the Mellin transformed PDFs, we only need one integral: The inverse Mellin transform of the convolution in Eq. (4.123).

This does, of course, require libraries to efficiently extract the Mellin moments of the PDFs, which currently does not exist for modern PDF sets. Still, as resummed contributions are calculated in Mellin space, it remains a useful exercise to calculate the Mellin moment of the partonic cross-section at next-to-leading order; both as a reference in Sec. 4.7 and in anticipation of future work, if one can efficiently use Mellin transformed PDFs.

4.6.1 Quark-gluon scattering

The quark-gluon scattering contribution in Eq. (4.117) is mostly straightforward to Mellin transform, as most of the terms are simple polynomials in z . These transform as

$$\int_0^1 dz z^{N-1} z^i = \frac{1}{N+i}. \quad (4.124)$$

Similarly, if the polynomial is multiplied by $\ln z$, the Mellin moment can be found using integration by parts:

$$\int_0^1 dz z^{N-1} z^i \ln z = - \int_0^1 dz z^{N-1} z^i = - \frac{1}{(N+i)^2}. \quad (4.125)$$

This leaves one term, containing the function $(z^2 + (1-z)^2) \ln(1-z)$. The Mellin moment of this function requires some more care, as the individual terms will diverge; thus, we introduce a regulator by writing the logarithm as $\ln(1-z) = \partial_\varepsilon (1-z)^\varepsilon$, where the limit $\varepsilon \rightarrow 0$ is implicit. The integral then becomes a Beta integral, giving

$$\begin{aligned} \partial_\varepsilon \int_0^1 dz z^{N-1} (z^2 + (1-z)^2) (1-z)^\varepsilon &= \partial_\varepsilon \left[\frac{\Gamma(N+2)\Gamma(1+\varepsilon)}{\Gamma(N+\varepsilon+3)} + \frac{\Gamma(N)\Gamma(3+\varepsilon)}{\Gamma(N+\varepsilon+3)} \right] \\ &= \partial_\varepsilon \left[\frac{N(N+1)\Gamma(N)}{(\varepsilon+1)(\varepsilon+2)\cdots(\varepsilon+N+2)} + \frac{\Gamma(N)}{(\varepsilon+3)(\varepsilon+4)\cdots(\varepsilon+N+2)} \right] \\ &= - \frac{N(N+1)\Gamma(N)}{(N+2)!} \sum_{k=1}^{N+2} \frac{1}{k} - \frac{2\Gamma(N)}{(N+2)!} \sum_{k=3}^{N+2} \frac{1}{k}, \end{aligned} \quad (4.126)$$

¹⁸This is for the differential cross-section; for the *total* cross-section we need another integral, over the invariant mass Q^2 .

where the regulator has been removed in the last step. Using that $\Gamma(N) = (N-1)!$ and reorganizing the sums in terms of the harmonic number $S_1(N) \equiv \sum_{k=1}^N 1/k$,¹⁹ and adding the previously calculated terms, we are left with

$$\begin{aligned} \frac{W_{qg}(N)}{T_F \frac{\alpha_s}{2\pi}} = & -2 \frac{N^2 + N + 2}{N(N+1)(N+2)} S_1(N) + \frac{N^4 + 11N^3 + 22N^2 + 14N + 4}{N^2(N+1)^2(N+2)^2} \\ & - \frac{N^2 + N + 2}{N(N+1)(N+2)} \ln \frac{\mu^2}{Q^2}. \end{aligned} \quad (4.127)$$

4.6.2 Quark-antiquark scattering

Many of the terms in Eq. (4.116) are proportional to delta functions; these transform trivially as $\delta(1-z) \rightarrow 1$. The remaining terms require similar manipulations as above; for the $1/(1-z)_+$ term we use the definition of the plus distribution, and also take $1/(1-z) = 1/(1-z)^{1-\varepsilon}$, as before in the limit $\varepsilon \rightarrow 0$. Expanding by order in ε to cancel divergences, we get

$$\frac{1+z^2}{(1-z)_+} \rightarrow -2S_1(N) + \frac{1}{N(N+1)}. \quad (4.128)$$

In the $(\ln(1-z)/(1-z))_+$ term we get rid of the logarithm as in the previous section; otherwise the calculation works out similarly to the other plus distribution, leaving

$$\begin{aligned} (1+z^2) \left(\frac{\ln(1-z)}{1-z} \right)_+ \rightarrow & 2S_1^2(N) - 2S_1(N) \frac{1}{N(N+1)} + \frac{1}{N^2} + \frac{1}{(N+1)^2} \\ & - 2 \sum_{k=1}^N \sum_{j=k+1}^N \frac{1}{jk} + \frac{1}{N(N-1)} - \frac{1}{N(N+1)}. \end{aligned} \quad (4.129)$$

For the remaining term, we use $\frac{d}{dN} z^N = \ln z z^N$ to rewrite

$$\int_0^1 dz z^{N-1} \frac{1+z^2}{1-z} \ln z = \partial_N \int_0^1 z^{N-1} \frac{1+z^2}{(1-z)^{1-\varepsilon}}. \quad (4.130)$$

Then, expanding in ε as before, as well as using the derivative of the harmonic number

$$\frac{d}{dN} S_1(N) = \zeta(2) - S_2(N), \quad (4.131)$$

with $\zeta(2) = \pi^2/6$, we get

$$\begin{aligned} \frac{1+z^2}{1-z} \ln z \rightarrow & 2S_1^2(N) - 2S_1(N) \frac{1}{N(N+1)} + \frac{1}{N^2} + \frac{1}{(N+1)^2} - \frac{\pi^2}{3} \\ & - 4 \sum_{k=1}^N \sum_{j=k+1}^N \frac{1}{jk} + \frac{2}{N(N-1)} - \frac{2}{N(N+1)}. \end{aligned} \quad (4.132)$$

By comparing Eqs. (4.129) and (4.132), we see that the awkward terms at the end will cancel when all contributions are added together according to Eq. (4.118).

Putting all of the terms together, the $q\bar{q}$ function in Mellin space is given by

$$W_{q\bar{q}}(N) = 1 + C_F \frac{\alpha_s}{\pi} W_{q\bar{q},\text{NLO}}, \quad (4.133)$$

¹⁹In general, $S_n(N) \equiv \sum_{k=1}^N 1/k^n$.

where

$$W_{q\bar{q},\text{NLO}} = 2S_1^2(N) - \frac{2S_1(N)}{N(N+1)} + \frac{1}{N^2} + \frac{1}{(N+1)^2} + \frac{2\pi^2}{3} - 4 + \frac{F_{\bar{q}\ell_i}^{AB}(Q)}{F_{q\ell_i}^{AB}(Q)} + \frac{\delta F_{\bar{q}\ell_i}^{AB}(Q)}{F_{q\ell_i}^{AB}(Q)} + \ln \frac{\mu^2}{Q^2} \left[2S_1(N) - \frac{1}{N(N+1)} - \frac{3}{2} \right]. \quad (4.134)$$

From the transformations of the plus distributions in Eqs. (4.128) and (4.129) we see that the divergence of the real-space partonic cross-sections for $z \rightarrow 1$ correspond to the limit $N \rightarrow \infty$ in Mellin space. Thus we find the behavior of the cross-section in the eikonal limit by the expansion

$$S_1(N) \simeq \ln \bar{N} + \frac{1}{2N} + \mathcal{O}\left(\frac{1}{N^2}\right), \quad (4.135)$$

where $\bar{N} \equiv Ne^{\gamma_E}$. In other words, we have a correspondence between plus distributions in z and logarithms of N , given by

$$\alpha_s \left(\frac{\ln(1-z)}{1-z} \right)_+ \leftrightarrow \alpha_s \ln^2 \bar{N}, \quad (4.136)$$

$$\alpha_s \frac{1}{(1-z)_+} \leftrightarrow \alpha_s \ln \bar{N}. \quad (4.137)$$

For later reference, the large- N limits of the NLO partonic cross-sections of Eqs. (4.127) and (4.133) are, keeping terms up to order $\sim 1/N$,

$$W_{qg}(N) \simeq -\frac{\alpha_s}{\pi} T_F \frac{\ln \bar{N} + \frac{1}{2} \ln \frac{\mu^2}{Q^2}}{N} + \mathcal{O}\left(\frac{1}{N^2}\right), \quad (4.138)$$

$$W_{q\bar{q}}(N) \simeq 1 + C_F \frac{\alpha_s}{\pi} \left(2 \ln^2 \bar{N} + 2 \ln \frac{\mu^2}{Q^2} \ln \bar{N} + \frac{2\pi^2}{3} - 4 - \frac{3}{2} \ln \frac{\mu^2}{Q^2} + \frac{F_{\bar{q}\ell_i}^{AB}(Q)}{F_{q\ell_i}^{AB}(Q)} + \frac{\delta F_{\bar{q}\ell_i}^{AB}(Q)}{F_{q\ell_i}^{AB}(Q)} + 2 \frac{\ln \bar{N} + \ln \frac{\mu^2}{Q^2}}{N} + \mathcal{O}\left(\frac{1}{N^2}\right) \right). \quad (4.139)$$

4.7 Resummation of large logarithms

The large logarithms in N we found above can be dealt with by all-order resummation. This is possible in the eikonal approximation, which can be represented by expectation values of Wilson lines, as we will discuss shortly.

The order to which we calculate the resummed result is denoted by the relation between the strong coupling and the logarithms: *Leading logarithmic* (LL) terms, e.g. the one in Eq. (4.136), are proportional to $\alpha_s^n \ln^{n+1} \bar{N}$, while *next-to-leading logarithmic* (NLL) terms, e.g. Eq. (4.137), are on the form $\alpha_s^n \ln^n \bar{N}$. To deal with the logarithms that appeared at NLO in perturbation theory, we will look to include the resummed result up to next-to-leading logarithmic accuracy.

As a first step, we will motivate how Wilson lines can be used to represent amplitudes in the eikonal limit.

4.7.1 Wilson lines and the eikonal approximation

Recall that from Eq. (1.7), we can construct a Wilson line from point y to x along a path P out of the gluon field $A_\mu^a(x)$, as

$$W_P(x, y) = P \left\{ \exp \left(ig_s \int_y^x A_\mu^a(z) T^a dz^\mu \right) \right\}. \quad (4.140)$$

The role of the path ordering operator can be seen by Taylor expanding this exponential; parametrizing the path P by $z^\mu(\lambda)$, $\lambda \in (a, b)$, with $z(a) = y$ and $z(b) = x$, the first few terms of the expansion are given by

$$\begin{aligned} W_P(x, y) = & 1 + ig_s \int_a^b d\lambda_1 \frac{dz^{\mu_1}(\lambda_1)}{d\lambda_1} \mathbf{A}_{\mu_1}(z(\lambda_1)) \\ & + \frac{(ig_s)^2}{2} \int_a^b d\lambda_1 \frac{dz^{\mu_1}(\lambda_1)}{d\lambda_1} \int_a^b d\lambda_2 \frac{dz^{\mu_2}(\lambda_2)}{d\lambda_2} \left[\mathbf{A}_{\mu_1}(z(\lambda_1)) \mathbf{A}_{\mu_2}(z(\lambda_2)) \theta(\lambda_1 - \lambda_2) \right. \\ & \left. + \mathbf{A}_{\mu_2}(z(\lambda_2)) \mathbf{A}_{\mu_1}(z(\lambda_1)) \theta(\lambda_2 - \lambda_1) \right] \\ & + \mathcal{O}(g_s^3), \end{aligned} \quad (4.141)$$

where $\theta(x)$ is the Heaviside step function.

In a generic term of the Taylor expansion with n gauge fields, each labeled by $i = 1, 2, \dots, n$, there are $n!$ different permutations in the ordering of the fields. We must sum over all of these permutations, and for each one the fields must be organized in order of decreasing path parameters λ_i . Denoting each possible permutation by π , letting $\pi(i)$ be a function that assigns a label to each field according to the specific permutation,^{20,21} the expansion can be written as

$$W_P(x, y) = \sum_{n=0}^{\infty} \frac{(ig_s)^n}{n!} \left(\prod_{i=1}^n \int_a^b d\lambda_i \frac{dz^{\mu_i}(\lambda_i)}{d\lambda_i} \right) \left[\sum_{\pi} \left(\prod_{i=1}^n \mathbf{A}_{\mu_{\pi(i)}}(z(\lambda_{\pi(i)})) \theta(\lambda_{\pi(i)} - \lambda_{\pi(i+1)}) \right) \right], \quad (4.142)$$

where $\lambda_{\pi(n+1)} = a$.

We can write out the sum over permutations by a re-labeling of indices, since all the indices appearing are just dummy indices that are summed over. For the second-order term in Eq. (4.141), this means that

$$\begin{aligned} & \frac{(ig_s)^2}{2} \int_a^b d\lambda_1 \frac{dz^{\mu_1}(\lambda_1)}{d\lambda_1} \int_a^b d\lambda_2 \frac{dz^{\mu_2}(\lambda_2)}{d\lambda_2} \left[\mathbf{A}_{\mu_1}(z(\lambda_1)) \mathbf{A}_{\mu_2}(z(\lambda_2)) \theta(\lambda_1 - \lambda_2) \right. \\ & \left. + \mathbf{A}_{\mu_2}(z(\lambda_2)) \mathbf{A}_{\mu_1}(z(\lambda_1)) \theta(\lambda_2 - \lambda_1) \right] \\ & = (ig_s)^2 \int_a^b d\lambda_2 \frac{dz^{\mu_2}(\lambda_2)}{d\lambda_2} \int_a^b d\lambda_1 \frac{dz^{\mu_1}(\lambda_1)}{d\lambda_1} \mathbf{A}_{\mu_2}(z(\lambda_2)) \mathbf{A}_{\mu_1}(z(\lambda_1)) \theta(\lambda_2 - \lambda_1). \end{aligned} \quad (4.143)$$

Here we have just switched the labels $1 \leftrightarrow 2$ in the first term, and swapped integration orders. We proceed similarly for the other terms in the expansion, using the step functions to restrict the

²⁰An explicit example can be seen in the $\mathcal{O}(g_s^2)$ term in Eq. (4.141), inside the brackets. The first term describes the permutation π_1 , which is defined so that $\pi_1(1) = 1$, $\pi_1(2) = 2$; the second describes π_2 , with $\pi_2(1) = 2$ and $\pi_2(2) = 1$.

²¹This notation is adapted from Ref. [7, p. 204].

integration limits; this allows us to write the Wilson line as

$$W_P(x, y) = \sum_{n=0}^{\infty} (ig_s)^n \int_a^b d\lambda_n \int_a^{\lambda_n} d\lambda_{n-1} \cdots \int_a^{\lambda_2} d\lambda_1 \frac{dz^{\mu_n}}{d\lambda_n} \cdots \frac{dz^{\mu_1}}{d\lambda_1} \mathbf{A}_{\mu_n}(z(\lambda_n)) \cdots \mathbf{A}_{\mu_1}(z(\lambda_1)), \quad (4.144)$$

or equivalently as

$$W_P(x, y) = \sum_{n=0}^{\infty} (ig_s)^n \int_a^b d\lambda_1 \int_{\lambda_1}^b d\lambda_2 \cdots \int_{\lambda_{n-1}}^b d\lambda_n \frac{dz^{\mu_n}}{d\lambda_n} \cdots \frac{dz^{\mu_1}}{d\lambda_1} \mathbf{A}_{\mu_n}(z(\lambda_n)) \cdots \mathbf{A}_{\mu_1}(z(\lambda_1)). \quad (4.145)$$

The former expression is convenient when the path is bounded from above, i.e. $a = -\infty$, b finite, while the latter is more useful when it is bounded from below, with $b = \infty$, a finite.

This series expansion for the Wilson line reveals a possible interpretation of these objects; it has the form of a standard perturbation expansion in the coupling constant, where each term can be viewed as a representation of a fermion moving from spacetime point y to x , emitting n gauge bosons (gluons in the case of $SU(3)$) in the process.

To make this correspondence clearer, and derive Feynman rules for these objects, we need to perform the integrals over the parameters λ_i . To this end, we Fourier transform the gauge fields using

$$A_\mu(z) = \int \frac{d^d k}{(2\pi)^d} A_\mu(k) e^{-ik \cdot z}, \quad (4.146)$$

and specify the parametrization of the path as $z^\mu(\lambda) = x^\mu + n^\mu \lambda$, $\lambda \in (-\infty, 0)$,²² so that $\frac{dz^\mu}{d\lambda} = n^\mu$. Here n^μ is a lightlike direction vector, $n^\mu n_\mu = 0$. Inserting this in Eq. (4.144), the integrals over the λ_i parameters (factoring out everything but the exponentials from the Fourier transform) can be written as

$$I_\lambda \equiv \left(\prod_{i=n}^1 \int_{-\infty}^{\lambda_{i+1}} d\lambda_i \right) \left(\prod_{i=1}^n \exp(-i\lambda_i n \cdot k_i - ix \cdot k_i) \right), \quad (4.147)$$

with $\lambda_{n+1} \equiv 0$. These integrals can be solved recursively; the innermost integral is given by

$$\int_{-\infty}^{\lambda_2} d\lambda_1 \exp\left(-i\lambda_1(n \cdot k_1 + i\varepsilon) - ix \cdot k_1\right) = \frac{i}{n \cdot k_1 + i\varepsilon} \exp\left(-i\lambda_2(n \cdot k_1 + i\varepsilon) - ix \cdot k_1\right), \quad (4.148)$$

where the $i\varepsilon$ was needed to regularize the integral. The exponential in this expression carries over to the integral over λ_2 :

$$\begin{aligned} \int_{-\infty}^{\lambda_3} d\lambda_2 \exp\left(-i\lambda_2(n \cdot (k_1 + k_2) + i\varepsilon) - ix \cdot (k_1 + k_2)\right) \\ = \frac{i}{n \cdot (k_1 + k_2) + i\varepsilon} \exp\left(-i\lambda_3(n \cdot (k_1 + k_2) + i\varepsilon) - ix \cdot (k_1 + k_2)\right). \end{aligned} \quad (4.149)$$

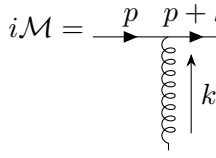
The remaining integrals are solved in exactly the same way, leaving

$$\begin{aligned} W_P(x, -\infty) = \sum_{n=0}^{\infty} (ig_s T^{a_n}) \cdots (ig_s T^{a_1}) \int \frac{d^d k_n}{(2\pi)^d} \cdots \int \frac{d^d k_1}{(2\pi)^d} (n \cdot A^{a_n}(k_n)) \cdots (n \cdot A^{a_1}(k_1)) \\ \times \exp\left(-ix \cdot \sum_{i=1}^n k_i\right) \prod_{i=1}^n \frac{i}{n \cdot \sum_{j=1}^i k_j + i\varepsilon}. \end{aligned} \quad (4.150)$$

²²This is for the case where the path is bounded from above; the calculation for the opposite case proceeds similarly.

Written on this form, we can see the correspondence to matrix elements. It closely resembles the perturbation series expansion for a fermion propagating from infinity to a point x on a lightlike path with $n^\mu = p^\mu$, $p^2 = 0$, while emitting a number of gluons with momenta $-k_i$ with the assumption that the k_i are small; this is called the *eikonal* approximation for the amplitude.

To see this, consider the $\mathcal{O}(g_s)$ term in the expansion for the aforementioned lightlike fermion. This term describes a massless fermion with momentum p , moving from infinity to x , while emitting or absorbing a gluon with momentum $k \ll p$. Denoting what happens at spacetime point x , be it an interaction with another fermion or something else, by M , and the completion of the gluon part of the diagram²³ by $G_\mu^a(k)$ the matrix element is given by

$$i\mathcal{M} = \text{diagram} = MG_\mu^a(k)ig_sT^a \frac{i(\not{p} + \not{k})\gamma^\mu}{(p+k)^2 + i\varepsilon} u(p), \quad (4.151)$$


where u is the spinor of the incoming fermion. The denominator reduces to $2p \cdot k + i\varepsilon$, since $p^2 = 0$ and $k^\mu \ll p^\mu$; for the numerator, dropping \not{k} , the Dirac algebra gives

$$\not{p}\gamma^\mu u(p) = 2p^\mu u(p) - \gamma^\mu \underbrace{\not{p}u(p)}_{=0}, \quad (4.152)$$

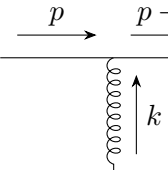
using the Dirac equation to eliminate the second term. Thus we have

$$i\mathcal{M} = Mig_sT^a \frac{i}{p \cdot k + i\varepsilon} p \cdot G^a(k) u(p). \quad (4.153)$$

This looks a lot like the $\mathcal{O}(g_s)$ term in Eq. (4.150), with some numerical differences that must be dealt with when connecting the Wilson line to cross-sections. Regardless, this illustrates that for soft-gluon processes, Wilson lines can be used as a proxy for matrix elements and cross-sections.

The Feynman rules for the perturbative expansion of Wilson lines can be deduced from Eq. (4.150) and our $\mathcal{O}(g_s)$ example (with p^μ now taking the role of n^μ in Eq. (4.150)):

- For each vertex with incoming gluon momentum k , a factor

$$\text{diagram} = ig_s \int \frac{d^d k}{(2\pi)^d} p \cdot A^a(k) T^a. \quad (4.154)$$


- For each fermion propagator with momentum $p+k$ in the direction of fermion flow, a factor

$$\text{diagram} = \frac{i}{p \cdot k + i\varepsilon}. \quad (4.155)$$


- For an external point x with momentum $p+k$ running into it, a factor

$$\text{diagram} = e^{-ik \cdot x}. \quad (4.156)$$


²³This can for example be the gluon polarization vector $\epsilon_\mu^a(k)$, or a propagator connecting to some other interaction.

Note that the direction of fermion flow only matters in the propagator, hence the fermion arrow on that diagram. In propagators we must take the momentum in the direction of fermion flow, while for the other elements only the direction of the momentum matters. This is seen from doing the above calculation for a Wilson line that is bounded from below, rather than from above (representing an outgoing fermion, or ingoing anti-fermion), which gives the same set of rules with the propagator momentum reversed.

4.7.2 Drell-Yan cross-section with Wilson lines

Having motivated Wilson lines as representations of soft-gluon processes and derived their Feynman rules, we can use this formalism to describe a collision between a quark and an antiquark, with incoming lightlike momenta p_1 and p_2 respectively, in the eikonal approximation. Setting up the coordinate system so that the collision happens at the spacetime origin, we can describe the incoming quark, on a classical²⁴ trajectory $z_1^\mu = p_1^\mu \lambda_1$, $\lambda_1 \in (-\infty, 0)$ by the Wilson line

$$W_{p_1}(0, -\infty) = P \left\{ \exp \left(ig \int_{-\infty}^0 \mathbf{A}_\mu(z_1) dz_1^\mu \right) \right\}, \quad (4.157)$$

and the antiquark, described as an outgoing particle with momentum $-p_2$, on the trajectory $z_2 = -p_2 \lambda_2$, $\lambda_2 \in (0, \infty)$, by the Wilson line

$$W_{-p_2}(\infty, 0) = P \left\{ \exp \left(ig \int_0^\infty \mathbf{A}_\mu(z_2) dz_2^\mu \right) \right\}. \quad (4.158)$$

These can be combined to construct the Drell-Yan Wilson line (also valid for slepton pair production, as the quark parts of these processes are identical), given by

$$U_{\text{DY}}(0) \equiv W_{-p_2}(\infty, 0) W_{p_1}(0, -\infty). \quad (4.159)$$

The eikonal quark-antiquark scattering cross-section (with the Born cross-section factored out as usual) is constructed from the vacuum expectation value of this quantity squared; it is given by [45]

$$w_{q\bar{q}}^{\text{eik}}(z) = \frac{Q}{2} \int_{-\infty}^{\infty} \frac{dy^0}{2\pi} e^{i \frac{Q}{2} (1-z)y^0} W_{\text{DY}}(y), \quad (4.160)$$

where $y^\mu = (y^0, \mathbf{0})$, and $W_{\text{DY}}(y)$ is the expectation value of a Wilson loop, integrated over the path C_{DY} as shown in Fig. 4.4. The loop is constructed from the product of the Wilson lines $U_{\text{DY}}(0)$, and its complex conjugate shifted from 0 to y , so that

$$W_{\text{DY}}(y) = \frac{1}{N_C} \left\langle 0 \left| \bar{T} U_{\text{DY}}^\dagger(y) T U_{\text{DY}}(0) \right| 0 \right\rangle, \quad (4.161)$$

where \bar{T} and T are anti-time- and time-ordering operators, respectively. This follows from the facts that the product of two Wilson lines makes another line, along their combined paths, and that the conjugate of a Wilson line is a Wilson line along the same path, but reversed.

²⁴This trajectory is assumed linear, as the emitted gluons are soft. In other words, the gluon momenta are sufficiently low that their emission does not affect the quark trajectory.

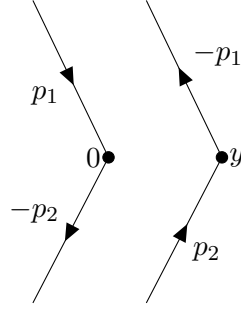


Figure 4.4: Integration path for the Wilson loop in Eq. (4.160), as well as the leading-order contribution to the same loop. Note that the lines extend to infinity, where the loop is closed. The dots at 0 and y are included to illustrate that these are external points as referenced in Eq. (4.156).

4.7.3 Calculation of W_{DY} to one-loop

In order to illustrate how loop corrections appear in this formalism, we now want to calculate $W_{\text{DY}}(y)$ to next-to-leading order in perturbation theory. The leading-order result is easily obtained from the Feynman rules listed Eqs. (4.154)–(4.156); since the leading-order Wilson loop shown in Fig. 4.4 has no propagators or vertices, the result is simply

$$W_{\text{DY}}^0(y) = 1. \quad (4.162)$$

Here we have removed the color factor $1/N_C$ which is absorbed into the Born cross-section, see Eq. (4.44).

At next-to-leading order, the loop gets four (non-zero) contributions as shown in Fig. 4.5. The calculation of these is made simpler by the fact that for each diagram we can use the so-called cut gluon propagator, i.e. we replace

$$\langle 0 | A_\mu^a(-k) A_\nu^b(k) | 0 \rangle \rightarrow -\delta^{ab} g_{\mu\nu} 2\pi\theta(k^0) \delta(k^2), \quad (4.163)$$

which turns the loop integral²⁵ over k into a phase space integral. To see why we can do this, it is helpful to consider the role of each diagram in Fig. 4.5, in light of Eq. (4.161). The two topmost diagrams represent the square of the Drell-Yan Wilson line with the emission of one gluon; in other words, they represent the squared matrix element for real gluon emission, and by the optical theorem and the Cutkosky cutting rules [50] this is proportional to the imaginary part of the amplitude shown in the topmost diagrams, which is obtained by using the cut gluon propagator.

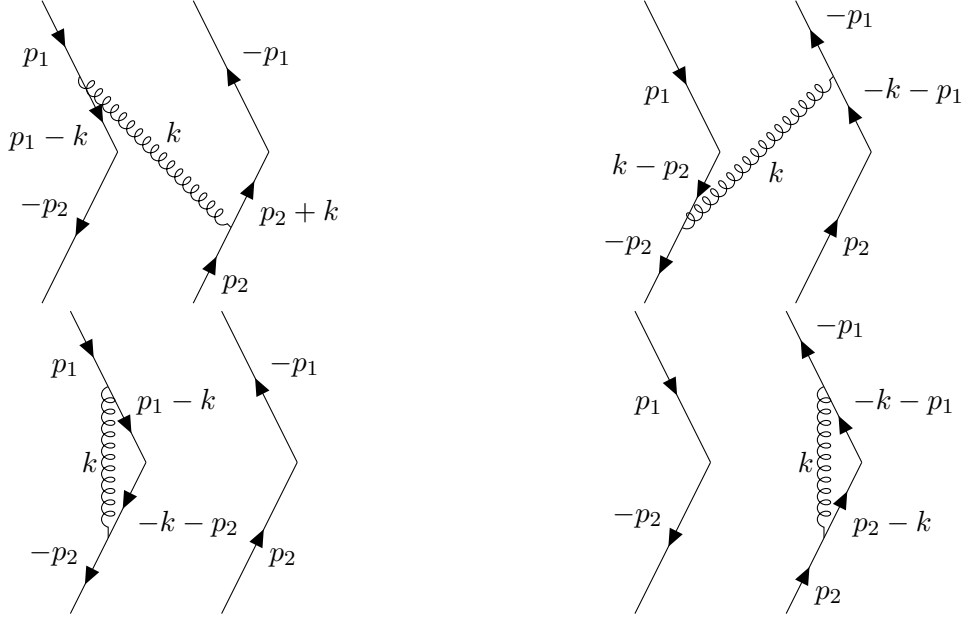
Meanwhile, the diagrams on the bottom represent interference terms between the leading-order result and virtual gluon exchange diagrams. Like in Sections 4.3.1 and 4.4 this is given by twice the real part of the amplitude; denoting the sum of the lower diagrams in Fig. 4.5 by W_V , we then have

$$2\text{Re}(W_V) = -2\text{Im}(-iW_V), \quad (4.164)$$

which is exactly what we get when using the cut gluon propagator.²⁶

²⁵This integral appears from the vertex rule of Eq. (4.154), along with the gluon fields in Eq. (4.163).

²⁶This is slightly different to how the cutting rules are usually stated, but it is equivalent; usually one uses the rules on the expression for $i\mathcal{M}$ to find the imaginary part of some amplitude \mathcal{M} , but here we use them on W_V to get the imaginary part of $-iW_V$.

Figure 4.5: One-loop contributions to W_{DY} .

Using this and the fact that $p_1^2 = p_2^2 = 0$, as well as making the usual replacement $g_s \rightarrow \mu^{(4-d)/2} g_s$ to keep the coupling dimensionless in d dimensions, again using the Feynman rules of Eqs. (4.154)–(4.156), we find that the 1-loop contribution is given by

$$W_{\text{DY}}^1 = 2g_s^2 C_F \mu^{4-d} \underbrace{\int \frac{d^{d-1}k}{(2\pi)^{d-1}} \frac{1}{2\omega} (e^{-iy_0\omega} - 1) \frac{p_1 \cdot p_2}{p_1 \cdot k p_2 \cdot k}}_{\equiv I}. \quad (4.165)$$

Here we have defined $\omega \equiv k^0$, and again removed a factor $1/N_C$. The integral I can be decomposed by parametrizing k in the center-of-mass frame as $k^\mu = \omega(1, \sin\theta, 0, \cos\theta)$, with p_1 and p_2 given by Eqs. (4.5) and (4.6), which means that

$$d^{d-1}k = \omega^{d-2} d\omega \sin^{d-4}\theta d(\cos\theta) d\Omega_{d-2}, \quad (4.166)$$

where due to symmetry, $d\Omega_{d-2}$ integrates to $2\pi^{(d-2)/2}/\Gamma(\frac{d-2}{2})$. The integral can then be rewritten as

$$I = \frac{1}{2^{d-3}\pi^{(d-2)/2}\Gamma(\frac{d-2}{2})} \underbrace{\int_0^\infty \frac{d\omega}{2\pi} \omega^{d-5} (e^{-iy_0\omega} - 1)}_{\equiv I_\omega} \underbrace{\int_{-1}^1 d(\cos\theta) \sin^{d-6}\theta}_{\equiv I_\theta}. \quad (4.167)$$

The two terms in I_ω are dealt with differently; for the term containing the exponential, we use a change of variables and the integral definition of the Gamma function to get

$$\int_0^\infty \frac{d\omega}{2\pi} \omega^{d-5} e^{-iy_0\omega} = \frac{1}{2\pi} (-y_0^2)^{(4-d)/2} \Gamma(d-4). \quad (4.168)$$

Note that in regulating the divergence in the Gamma function we must use $d > 4$, or $d = 4 - 2\epsilon$ with $\epsilon < 0$, making this an infrared divergence. This part of the integral can then be written as, using $\Gamma(1+x) = x\Gamma(x)$,

$$\int_0^\infty \frac{d\omega}{2\pi} \omega^{d-5} e^{-iy_0\omega} = -\frac{1}{2\epsilon} \frac{1}{2\pi} (iy_0)^{2\epsilon} \Gamma(1-2\epsilon). \quad (4.169)$$

The second term in I_ω has both infrared and ultraviolet divergences, but since it is scaleless it formally vanishes in dimensional regularization; more precisely it is proportional to $\frac{1}{\epsilon_{\text{UV}}} - \frac{1}{\epsilon_{\text{IR}}}$, where ϵ_{UV} and ϵ_{IR} are the dimensional regulators to remove the ultraviolet and infrared divergences, respectively. Then, since the Wilson loop is renormalizable [43], we can add a counterterm like we did in Sec. 4.3.1 to remove this term altogether.

For I_θ we make a variable change like the one in Sec. 4.3.3, defining $x \equiv \frac{1}{2}(1 + \cos \theta)$ to rewrite the integral as a Euler Beta integral, giving

$$I_\theta = 2^{d-5} \int_0^1 dx [x(1-x)]^{\frac{d-6}{2}} = 2^{d-5} \frac{\Gamma^2(\frac{d-4}{2})}{\Gamma(d-4)}. \quad (4.170)$$

To regulate the divergences in the Gamma functions we again use $d = 4 - 2\epsilon$, $\epsilon < 0$, and $\Gamma(1+x) = x\Gamma(x)$, resulting in

$$I_\theta = -\frac{1}{\epsilon} 2^{-2\epsilon} \frac{\Gamma^2(1-\epsilon)}{\Gamma(1-2\epsilon)}. \quad (4.171)$$

Then, collecting factors in Eq. (4.165) and rescaling $\mu^2 \rightarrow \mu^2 e^{\gamma_E}/4\pi$ according to the $\overline{\text{MS}}$ renormalization scheme, the (unrenormalized) expression is

$$W_{\text{DY}}^1 = C_F \frac{\alpha_s}{\pi} \frac{\Gamma(1-\epsilon)}{\epsilon^2} e^{-\epsilon\gamma_E} L^\epsilon, \quad (4.172)$$

where

$$L \equiv \left(\frac{i}{2} y_0 \mu e^{\gamma_E} \right)^2. \quad (4.173)$$

Expanding in ϵ and removing the poles, which is possible since the eikonal cross-section can be exponentiated and the divergences thus easily absorbed into bare distributions [51, 52], we get the final result for the expectation value of the Drell-Yan Wilson loop to order α_s :

$$W_{\text{DY}}(y) = 1 + C_F \frac{\alpha_s}{\pi} \left(\frac{1}{2} \ln^2 L + \frac{\pi^2}{12} \right) + \mathcal{O}(\alpha_s^2). \quad (4.174)$$

Next, in order to turn this into a cross-section, we need to calculate the Fourier transform as in Eq. (4.160). This can be made simpler by transforming to Mellin space, where we can make a few approximations; first, for large N , which will dominate the expression, we have $z^{N-1} \simeq e^{-N(1-z)}$. We then get

$$w_{q\bar{q}}^{\text{eik}}(N) = \frac{Q}{2} \int_0^1 dz \int_{-\infty}^{\infty} \frac{dy^0}{2\pi} e^{F(z, y^0)} W_{\text{DY}}(y), \quad (4.175)$$

with $F(z, y^0) \equiv \left(i \frac{Q}{2} y^0 - N \right) (1-z)$. Next we expand around the stationary point of $F(z, y^0)$, located at $z = 1$, $y^0 = -2i \frac{N}{Q} \equiv Y^0$; for the exponent this changes nothing, while $W_{\text{DY}}(y) \simeq W_{\text{DY}}(y^0 = Y^0) + \mathcal{O}(y^0 - Y^0)$. This makes the double integral simple; the y^0 is just the Fourier transform of a delta function, which in turn makes the z integral trivial. This leaves

$$\begin{aligned} w_{q\bar{q}}^{\text{eik}}(N) &= W_{\text{DY}} \left(y^0 = -2i \frac{N}{Q} \right) \\ &= 1 + C_F \frac{\alpha_s}{\pi} \left(2 \ln^2 \left(\bar{N} \frac{\mu}{Q} \right) + \frac{\pi^2}{12} \right) + \mathcal{O}(\alpha_s^2). \end{aligned} \quad (4.176)$$

Notice that since $\ln^2 \left(\bar{N} \frac{\mu}{Q} \right) = \ln^2 \bar{N} + \ln \frac{\mu^2}{Q^2} \ln \bar{N} + \mathcal{O}(1)$, we have reproduced the leading- and next-to-leading logarithmic behavior of Eq. (4.139).

4.7.4 Exponentiation

To upgrade this result to include corrections at all orders in α_s , it must be written on resummed form. This can be done according to the non-Abelian exponentiation theorem [51, 52], which states that the eikonal cross-section can be written as an exponential.

One way of obtaining this form is by the renormalization group. This is similar to what we did in finding the scale-dependent coupling in ϕ^4 theory, see Eq. (1.90), which when Taylor expanded contains an infinite number of orders in λ . In this case, we can solve the renormalization group equation for the Wilson loop $W_{\text{DY}}(N)$, which has the general solution [45]

$$W_{\text{DY}}\left(\frac{\mu\bar{N}}{Q}, \alpha_s(\mu^2)\right) = W_{\text{DY}}\left(1, \alpha_s\left(\frac{Q^2}{\bar{N}^2}\right)\right) \times \exp\left\{\int_{Q^2/\bar{N}^2}^{\mu^2} \frac{d\mu'^2}{\mu'^2} \left[\Gamma_{\text{cusp}}(\alpha_s(\mu'^2)) \log\left(\frac{\mu'^2 \bar{N}^2}{Q^2}\right) + \Gamma_{\text{DY}}(\alpha_s(\mu'^2))\right]\right\}, \quad (4.177)$$

with the universal cusp²⁷ anomalous dimension given at two-loop level by

$$\Gamma_{\text{cusp}}(\alpha_s) = \frac{\alpha_s}{\pi} C_F + \left(\frac{\alpha_s}{\pi}\right)^2 C_F \left[C_A \left(\frac{67}{36} - \frac{\pi^2}{12}\right) - N_F \frac{5}{18}\right] + \mathcal{O}(\alpha_s^3), \quad (4.178)$$

and the Drell-Yan anomalous dimension

$$\Gamma_{\text{DY}}(\alpha_s) = 0 + \mathcal{O}(\alpha_s^2). \quad (4.179)$$

$W_{\text{DY}}\left(1, \alpha_s\left(\frac{Q^2}{\bar{N}^2}\right)\right)$ is determined by boundary conditions.

To verify that this contains our fixed-order calculation of Eq. (4.176), we expand to first order in α_s (including the running coupling itself, i.e. we set $\alpha_s(\mu'^2) \simeq \alpha_s(\mu^2)$ which is accurate to leading order), assumming $W_{\text{DY}}\left(1, \alpha_s\left(\frac{Q^2}{\bar{N}^2}\right)\right) = 1$, to get

$$W_{\text{DY}} = 1 + 2 \frac{\alpha_s}{\pi} C_F \ln^2\left(\frac{\mu\bar{N}}{Q}\right) + \mathcal{O}(\alpha_s^2), \quad (4.180)$$

reproducing the leading- and next-to-leading-logarithmic behavior of Eq. (4.176). The $\frac{\pi^2}{12}$ term is missing, but this is unproblematic; the main purpose of the soft-gluon resummation is taking care of the logarithms that grow large for large N , so constant terms are negligible. Furthermore, the full cross-section can like before be factorized into hard and soft parts, the soft factor being this exponentiated function, so “missing” factors in the soft part can be included in the hard part.

4.7.5 Resummed cross-section at NLL

With the exponentiated Wilson loop, we can proceed to calculate the resummed $q\bar{q}$ partonic cross-section for the Drell-Yan process (or similar processes, such as slepton pair production). We need the eikonal cross-section as stated in Eq. (4.177),²⁸ QCD factorization theorems, and the two-loop results for the cusp anomalous dimension and QCD beta function; the latter are given by

$$\Gamma_{\text{cusp}}(\alpha_s) = \frac{\alpha_s}{\pi} \Gamma_{\text{cusp}}^1 + \left(\frac{\alpha_s}{\pi}\right)^2 \Gamma_{\text{cusp}}^2 + \mathcal{O}(\alpha_s^3), \quad (4.181)$$

²⁷A cusp is a non-smooth point on a Wilson line, like the ones at 0 and y in $W_{\text{DY}}(y)$.

²⁸As we showed at the end of Sec. 4.7.3, W_{DY} in Mellin space is identical to the eikonal partonic cross-section, also in Mellin space.

with coefficients given in Eq. (4.178), and

$$\beta(\alpha_s) = \mu \frac{d}{d\mu} \alpha_s = -2\alpha_s [\alpha_s b_0 + \alpha_s^2 b_1 + \mathcal{O}(\alpha_s^3)], \quad (4.182)$$

with $4\pi b_0 = \frac{11}{3}C_A - \frac{4}{3}T_F N_F$ and $(4\pi)^2 b_1 = \frac{34}{3}C_A^2 - \frac{20}{3}C_A T_F N_F - 4C_F T_F N_F$. Then, performing the integral over μ' in Eq. (4.177) gives [53]²⁹

$$\frac{d\hat{\sigma}_{q\bar{q}}^{\text{res}}}{dQ^2} = \sigma_0^d \exp\left(\frac{\alpha_s}{\pi} C_{q\bar{q}}^1(\alpha_s)\right) \exp[S(N, \alpha_s)], \quad (4.183)$$

with³⁰

$$\frac{C_{q\bar{q}}^1}{C_F} = \frac{2\pi^2}{3} - 4 - \frac{3}{2} \ln \frac{\mu^2}{Q^2}, \quad (4.184)$$

$$S(N, \alpha_s) = g_1(\lambda) \ln \bar{N} + g_2(\lambda). \quad (4.185)$$

The functions $g_1(\lambda)$ and $g_2(\lambda)$, where $\lambda \equiv b_0 \alpha_s \ln \bar{N}$, contain the LL and NLL contributions, respectively. They are given by

$$g_1(\lambda) = \frac{\Gamma_{\text{cusp}}^1}{\pi b_0 \lambda} (2\lambda + (1 - 2\lambda) \ln(1 - 2\lambda)), \quad (4.186)$$

$$g_2(\lambda) = -\frac{\Gamma_{\text{cusp}}^2}{\pi^2 b_0^2} [2\lambda + \ln(1 - 2\lambda)] + \frac{\Gamma_{\text{cusp}}^1 b_1}{\pi b_0^3} \left[2\lambda + \ln(1 - 2\lambda) + \frac{1}{2} \ln^2(1 - 2\lambda) \right] - \frac{\Gamma_{\text{cusp}}^1}{\pi b_0} \ln \frac{\mu^2}{Q^2} \ln(1 - 2\lambda). \quad (4.187)$$

This result can be improved by including collinear effects in the so-called *collinear-improved* resummation formalism [54]; in practice this amounts to taking [55]

$$S(N, \alpha_s) \rightarrow S(N, \alpha_s) + \frac{\alpha_s}{2\pi} \int_0^1 dz z^{N-1} \int_{\mu^2}^{(1-z)^2 Q^2} \frac{dq^2}{q^2} P_{qq}^{\text{reg}}(z), \quad (4.188)$$

in Eq. (4.183). Here $P_{qq}^{\text{reg}} = -C_F(1+z)$ is the regular part of the splitting function given in Eq. (3.40), i.e. after subtracting singularities at $z = 1$. The q^2 integral is trivial; the remaining Mellin transform is performed using the methods described in Sec. 4.6, keeping only terms up to order $\sim 1/N$. Carrying out the integral, the result of this extra term is effectively encapsulated in the modification

$$C_{q\bar{q}}^1 \rightarrow \tilde{C}_{q\bar{q}}^1 = C_{q\bar{q}}^1 + 2C_F \frac{\ln \bar{N} + \frac{1}{2} \ln \frac{\mu^2}{Q^2}}{N}, \quad (4.189)$$

in Eq. (4.183).

4.7.6 Matching with fixed-order calculations

With the resummed cross-section now at hand, we can combine it with our earlier fixed-order calculations. This must be done carefully, as the naive approach of simply adding the resummed calculation to the fixed-order one would lead to double-counting.

²⁹Here we have taken $\mu_F \equiv \mu_R \equiv \mu$, as discussed in Sec. 3.4.

³⁰The resummed contribution is calculated in pure QCD, i.e. not including sparticle loop corrections.

This happens because the resummed result contains corrections from soft gluon radiation at all orders in the strong coupling. These corrections are already included in the fixed-order result, as shown in Eq. (4.139); thus, when adding the resummed cross-section to our fixed-order one we must take care to only include those parts of the expression that are at a higher order in α_s than the fixed-order result. This procedure is called matching.

In practice, we match the resummed result to a given order in perturbation theory, in our case the next-to-leading order, by subtracting the power series expansion of the resummed result up to the given order in α_s . Explicitly, matching to NLO, this means that for incoming partons i, j ,

$$\frac{d\hat{\sigma}_{ij}^{\text{match}}}{dQ^2} = \frac{d\hat{\sigma}_{ij}^{\text{res}}}{dQ^2} - \frac{d\hat{\sigma}_{ij}^{\text{exp}}}{dQ^2}. \quad (4.190)$$

The expansion is found by using the Taylor series $\ln(1-x) = -\sum_{n=1}^{\infty} \frac{1}{n} x^n$ to expand $g_{1,2}$, as defined in Eqs. (4.186) and (4.187), in terms of λ ; with this we can Taylor expand the expression in Eq. (4.183) in α_s , giving

$$\frac{1}{\sigma_0^d} \frac{d\hat{\sigma}_{q\bar{q}}^{\text{exp}}}{dQ^2} = 1 + \frac{\alpha_s}{\pi} \left[C_F \left(2 \ln^2 \bar{N} + 2 \ln \frac{\mu^2}{Q^2} \ln \bar{N} \right) + \tilde{C}_{q\bar{q}}^1 \right]. \quad (4.191)$$

This reproduces the large- N limit of the NLO partonic cross-sections, given in Eq. (4.139).³¹

Adding Eq. (4.190) to our NLO result gives the cross-section at what is called NLO+NLL accuracy.

4.7.7 Evaluating the inverse Mellin transform

Finally, we must convolute the resummed partonic cross-section with PDFs, and calculate the inverse Mellin transform, to add to the fixed-order result. Ideally, as we discussed in Sec. 4.6, we would like to evaluate the PDFs in Mellin space and then take the inverse Mellin transform, as this would reduce the PDF convolution into a simple product; this is made problematic in practice by the fact that easily available Mellin moments of modern PDF sets do not currently exist.³² Therefore we must make do with calculating the inverse Mellin transform of just the partonic cross-section, and then the convolution with the PDFs in x -space.

There is one simplification we can make, however. From the discussion in Sec. 4.6, the resummed contribution to the hadronic cross-section, after matching orders with the fixed-order result, is (denoting the Mellin transform by \mathcal{F} and its inverse by \mathcal{F}^{-1})

$$\begin{aligned} \frac{d\sigma^{\text{match}}}{dQ^2} &= \sigma_B \sum_{ij} \mathcal{F}^{-1} \left[\mathcal{F}(f_i)(N, \mu) \mathcal{F}(f_j)(N, \mu) W_{ij}^{\text{match}} \right] \\ &= \sigma_B \sum_{ij} \int_0^\infty dz \int_0^1 dx_1 dx_2 f_i(x_1, \mu) f_j(x_2, \mu) \mathcal{F}^{-1} \left(W_{ij}^{\text{match}} \right) (z) \delta(\tau - x_1 x_2 z), \end{aligned} \quad (4.192)$$

with $\frac{d\hat{\sigma}_{ij}^{\text{match}}}{dQ^2} = \sigma_0^d W_{ij}^{\text{match}}$. Note the increased upper limit on z ; this is because, as discussed in Ref. [56], a Landau pole in Mellin space causes the function in z -space not to vanish for $z > 1$.

³¹Not including the supersymmetry contributions; as noted previously the resummed result contains only QCD corrections.

³²The ideal way to do this would be to calculate the Mellin moments just once and store them in a grid; but since the inverse Mellin requires N to be complex, and over an infinite range, the dimensionality of such a grid makes this cumbersome.

However, as noted in Ref. [56] the $z > 1$ region gives only a very small contribution; thus, as a fairly good approximation we will simply assume $z \in (0, 1)$ to simplify the numerical evaluation.

The integrand may oscillate rapidly for large N when taking the inverse Mellin transform; these oscillations may be reduced by extracting a factor N^2 . This factor can be absorbed into the PDFs by using that for any function $f(x)$ that vanishes at $x = 1$, such as the PDFs, integration by parts gives

$$\mathcal{F}\left(-x \frac{df}{dx}\right) = - \int_0^1 dx x^N \frac{df}{dx} = N \int_0^1 x^{N-1} f(x) = N \mathcal{F}(f). \quad (4.193)$$

Defining $\bar{f}_i \equiv -x \frac{df_i}{dx}$ for the PDFs, this means that we can rewrite the resummed contribution to the hadronic cross-section as

$$\frac{d\sigma^{\text{match}}}{dQ^2} = \sigma_B \sum_{ij} \int_{\tau}^1 \frac{dx_1}{x_1} \int_{\tau/x_1}^1 \frac{dx_2}{x_2} \bar{f}_i(x_1, \mu) \bar{f}_j(x_2, \mu) \mathcal{F}^{-1}\left(\frac{W_{ij}^{\text{match}}}{N^2}\right)\left(z = \frac{\tau}{x_1 x_2}\right). \quad (4.194)$$

This does require us to calculate derivatives of the PDFs, but as these have the same arguments as the PDFs themselves they can be stored on the same type of grid, making them much simpler to calculate and store than the Mellin moments.

We now turn to the actual form of the inverse Mellin transform, and how it can be calculated numerically. From Eq. (4.120), the inverse Mellin transform of a general Mellin moment $F(N)$ is given by

$$\mathcal{F}^{-1}(F) \equiv f(z) = \frac{1}{2\pi i} \int_{c-i\infty}^{c+i\infty} dN z^{-N} F(N), \quad (4.195)$$

where c is a real number. The integration path can be deformed as long as we do not change the number of singularities within it; following Ref. [56] we choose the *minimal prescription* (MP) path, parametrized as

$$N(x) = C_{MP} + |x| e^{\text{sgn}(x)\phi}, \quad (4.196)$$

$x \in (-\infty, \infty)$, with $C_{MP} = 2$, $\phi = \frac{3\pi}{4}$, and x real. Note that $N^*(x) = N(-x)$. Using this parametrization we have

$$\begin{aligned} f(z) &= \frac{1}{2\pi i} \left[- \int_{-\infty}^0 dx e^{-i\phi} z^{-N(x)} F(N(x)) + \int_0^{\infty} dx e^{i\phi} z^{-N(x)} F(N(x)) \right] \\ &= \frac{1}{2\pi i} \int_0^{\infty} dx \left[e^{i\phi} z^{-N(x)} F(N(x)) - e^{-i\phi} z^{-N(-x)} F(N(-x)) \right]. \end{aligned} \quad (4.197)$$

We now notice that the integrand has the form of $2i$ times the imaginary part of a function, i.e. $2i\text{Im}a = a - a^*$, since

$$F(N(-x)) = F(N^*(x)) = F^*(N(x)). \quad (4.198)$$

Thus we have

$$f(z) = \frac{1}{\pi} \int_0^{\infty} dx \text{Im} \left(e^{i\phi} z^{-N(x)} F(N(x)) \right). \quad (4.199)$$

Lastly, to make this expression more practical to implement numerically, removing the need to cut off the integration for large x , we define $x \equiv -\ln y$, $y \in (0, 1)$ and change integration variables, to obtain

$$f(z) = \frac{1}{\pi} \int_0^1 \frac{dy}{y} \text{Im} \left(e^{i\phi} z^{-N(y)} F(N(y)) \right), \quad (4.200)$$

where now

$$N(y) = C_{MP} - \ln y e^{i\phi}. \quad (4.201)$$

As long as we use a numerical integration method that avoids the endpoints of the integration range, the fact that N is singular at $y = 0$ will not be an issue.

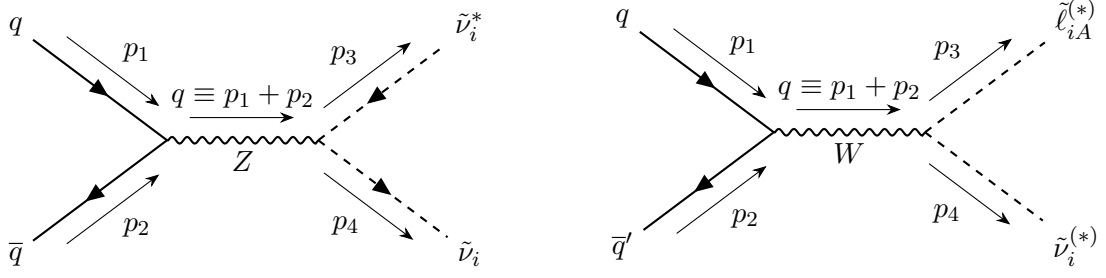


Figure 4.6: Tree-level production of sneutrinos at a hadron collider, either in a pair (left) or along with a slepton (right). $i = e, \mu, \tau$ denotes flavor; $A = 1, 2$ is the mass eigenstate of the slepton. The charges in the slepton-sneutrino diagram are left ambiguous for generality; the final state can be either $\tilde{\ell}_i \tilde{\nu}_i^*$ or $\tilde{\ell}_i^* \tilde{\nu}_i$.

4.8 Generalizing to other particles

With our NLO+NLL cross-section now at hand for slepton pair production, it is fairly straightforward to generalize to other final states. The most immediate generalization is to also include the production of sneutrinos; either a pair of these particles, or a sneutrino along with a slepton. The leading-order diagrams for both of these cases are shown in Fig. 4.6. In both processes the loop corrections are mostly identical to the ones we have calculated above; the difference only appears in the effective couplings.

The simplest case is that of sneutrino pair production. Being uncharged, this pair can only be created from a Z boson; furthermore there is only one mass eigenstate to consider as the MSSM only contains left-handed neutrino superfields. This makes the effective couplings simpler than those of slepton pair production; they are given by

$$F_{q\nu_i}(Q) = \frac{(Z_{qL}^2 + Z_{qR}^2)Q^4}{2\sin^4\theta_W \cos^4\theta_W \left((Q^2 - m_Z^2)^2 + m_Z^2 \Gamma_Z^2 \right)}, \quad (4.202)$$

$$F_{\tilde{q}\nu_i}(Q) = \frac{Q^4}{2\sin^4\theta_W \cos^4\theta_W \left((Q^2 - m_Z^2)^2 + m_Z^2 \Gamma_Z^2 \right)} \left[C(1,1)Z_q^{11}(\cos^2\theta_q Z_{qL} + \sin^2\theta_q Z_{qR}) \right. \\ \left. + C(2,2)Z_q^{22}(\sin^2\theta_q Z_{qL} + \cos^2\theta_q Z_{qR}) \right. \\ \left. - (C(1,2) + C(2,1))Z_q^{12}(Z_{qR} - Z_{qL})\sin\theta_q \cos\theta_q \right], \quad (4.203)$$

$$\delta F_{\tilde{q}\nu_i}(Q) = \frac{Q^4}{2\sin^4\theta_W \cos^4\theta_W \left((Q^2 - m_Z^2)^2 + m_Z^2 \Gamma_Z^2 \right)} \left[B_1(0, m_{\tilde{g}}^2, m_{\tilde{q}_1}^2)(\cos^2\theta_q Z_{qL} + \sin^2\theta_q Z_{qR}) \right. \\ \left. + B_1(0, m_{\tilde{g}}^2, m_{\tilde{q}_2}^2)(\sin^2\theta_q Z_{qL} + \cos^2\theta_q Z_{qR}) \right], \quad (4.204)$$

with all constants the same as in the slepton case, and i denoting flavor. These replace $F_{q\ell_i}^{AB}$, $F_{\tilde{q}\ell_i}^{AB}$, and $\delta F_{\tilde{q}\ell_i}^{AB}$, respectively, in the cross-section.

For the slepton-sneutrino final state the modification is slightly more complicated, due to the fact that this process is mediated by a charged W^\pm boson. This means that the initial-state quarks

are not a simple quark-antiquark pair like before, but instead a quark q and an antiquark \bar{q}' with the opposite SU(2) isospin.³³ The amplitudes for the different pairings are then multiplied by a factor $|V_{qq'}|^2$, where $V_{qq'}$ are CKM matrix elements as referenced in Sec. 1.1.4.

The loop corrections are mostly the same as before. We do have to be careful in adding counterterms; here the self-energy counterterms we add are averages of the respective counterterms for the two quarks, as there are two different particles in the initial state. In the end, the effective couplings are given by

$$F_{qq'\ell_i}^A(Q) = \frac{|V_{qq'}|^2 (W_{\ell_i}^A)^2 Q^4}{8 \sin^4 \theta_W \left((Q^2 - m_W^2)^2 + m_W^2 \Gamma_W^2 \right)}, \quad (4.205)$$

$$F_{\bar{q}\bar{q}'\ell_i}^A(Q) = \frac{|V_{qq'}|^2 (W_{\ell_i}^A)^2 Q^4}{4 \sin^4 \theta_W \left((Q^2 - m_W^2)^2 + m_W^2 \Gamma_W^2 \right)} \left[C'(1, 1) \cos \theta_q \cos \theta_{q'} + C'(2, 2) \sin \theta_q \sin \theta_{q'} \right. \\ \left. + C'(1, 2) \cos \theta_q \sin \theta_{q'} + C'(2, 1) \sin \theta_q \cos \theta_{q'} \right], \quad (4.206)$$

$$\delta F_{\bar{q}\bar{q}'\ell_i}^A(Q) = \frac{|V_{qq'}|^2 (W_{\ell_i}^A)^2 Q^4}{16 \sin^4 \theta_W \left((Q^2 - m_W^2)^2 + m_W^2 \Gamma_W^2 \right)} \left[B_1(0, m_{\tilde{g}}^2, m_{\tilde{q}_1}^2) \cos^2 \theta_q + B_1(0, m_{\tilde{g}}^2, m_{\tilde{q}_2}^2) \sin^2 \theta_q \right. \\ \left. + B_1(0, m_{\tilde{g}}^2, m_{\tilde{q}'_1}^2) \cos^2 \theta_{q'} + B_1(0, m_{\tilde{g}}^2, m_{\tilde{q}'_2}^2) \sin^2 \theta_{q'} \right], \quad (4.207)$$

where A denotes the slepton mass eigenstate. Here we have defined

$$W_{\ell_i}^A \equiv \delta_1^A \cos \theta_\ell + \delta_2^A \sin \theta_\ell, \quad (4.208)$$

and

$$C'(B, D) \equiv \text{Re} C_{00} \left(0, Q^2, 0, m_{\tilde{g}}^2, m_{\tilde{q}_B}^2, m_{\tilde{q}'_D}^2 \right) \Big|_{\text{finite}}. \quad (4.209)$$

For reference, the corresponding effective couplings of slepton pair production are listed in Eqs. (4.27), (4.105), and (4.109).

³³Which is the quark and which is the antiquark depends on the charge of the produced slepton, and consequently the W boson; a W^+ boson requires an initial state of $u\bar{d}$ or similar pairings, while W^- requires a $\bar{u}d$ -type pair.

Chapter 5

Numerical results

In this chapter we implement our analytical calculations numerically, to demonstrate the actual impact that the higher-order corrections have on the results. Among the most important of the expected effects is a decreased dependence upon the arbitrary scale μ ; this reduces the theoretical uncertainty, making comparisons to experimental data more reliable.

We evaluate the cross-section for a wide range of MSSM parameters — taking advantage of our very general calculations, which for example allows us to give different values to masses and mixing angles for each squark flavor — to examine how the results depend on the various parameters.

To verify our calculations, we perform some tests. In order to evaluate the resummed results we need to transform from Mellin space to x -space, using differentiated PDFs; to check that this works as desired we compare the NLO hadronic cross-section obtained from the Mellin-space results of Sec. 4.6 to the standard x -space ones. We also compare our results to those of some widely used numerical packages for supersymmetry calculations — RESUMMINO [53, 57–61] and PROSPINO [62] — including the speed of different programs.

All results in this chapter were obtained using the VEGAS integration algorithm [63, 64]. Passarino-Veltman coefficients were evaluated in LoopTools [26, 27],¹ and PDFs and the strong coupling in LHAPDF [65].

5.1 Conventions and technical details

When evaluating the cross-section, a number of choices must be made regarding conventions. Here we comment on some of these choices, and how they may differ from other sources.

The first choice is that of the scale μ .² Being an arbitrary parameter, this can in principle take any value; the most conventional approach is setting it to some energy scale that is representative of the observable we are calculating. For the differential cross-section we therefore set $\mu = Q$, i.e. the invariant mass of the slepton pair. If we are calculating the total cross-section, meaning that the invariant mass is integrated over, it is instead set equal to the average mass of the two sleptons; $\mu = (m_{\tilde{\ell}_{iA}} + m_{\tilde{\ell}_{iB}})/2$. This keeps the scale fixed, rather than implicitly integrating over it as we would have done with $\mu = Q$.

The theoretical uncertainty due to missing orders in the perturbation expansion is, by convention, defined as the difference between the cross-section evaluated at $\mu' = 2\mu$ and at $\mu' = \mu/2$, μ being the central scale as defined above.

¹We used the analytical expressions for the virtual QCD loop as explained at the end of Sec. 4.3.3; for the supersymmetric contributions the Passarino-Veltman functions were used.

²Technically there are two such parameters, both the renormalization scale μ_R and the factorization scale μ_F ; but as we noted in Sec. 3.4, we take them to be equal, $\mu_R \equiv \mu_F \equiv \mu$, in all of our calculations.

As we have discussed previously, the renormalization scheme varies depending on the quantity in question. Following the conventions of PROSPINO and RESUMMINO we renormalize couplings and PDFs in the $\overline{\text{MS}}$ scheme, while masses (and as a consequence, fields) are renormalized in the on-shell scheme. The latter is mainly for practical purposes, to avoid having to convert from pole masses to $\overline{\text{MS}}$ masses in propagators.

However, there is a potential ambiguity in the electroweak sector when renormalizing the masses of the W and Z bosons, the electromagnetic fine-structure constant $\alpha = e^2/4\pi$, and the Weinberg angle θ_W . From Sec. 1.1.3, denoting the electroweak couplings by g and g' , and the Higgs vacuum expectation value by v , these quantities are related by

$$m_W = \frac{1}{2}vg, \quad (5.1)$$

$$m_Z = \frac{1}{2}v\sqrt{g^2 + g'^2}, \quad (5.2)$$

$$e = \frac{gg'}{\sqrt{g^2 + g'^2}}, \quad (5.3)$$

$$\sin \theta_W = \frac{g'}{\sqrt{g^2 + g'^2}}. \quad (5.4)$$

Since all of these quantities depend on the same set of parameters g , g' , and v (which in turn is determined by the Higgs potential), we must choose a consistent scheme in which to renormalize them. One possibility, if one insisted on keeping the fine-structure constant in the $\overline{\text{MS}}$ scheme, would be to calculate the RG running of the electroweak couplings g and g' in the $\overline{\text{MS}}$, and from that calculate the $\overline{\text{MS}}$ running of the above quantities; here we choose the simpler option, keeping to the conventions of PROSPINO and RESUMMINO, of instead evaluating all of these quantities in the on-shell scheme.

In practice this means using the pole masses [19] $m_W = 80.379$ GeV and $m_Z = 91.188$ GeV, and then relating the Weinberg angle and fine-structure constant to these by

$$\sin^2 \theta_W = 1 - \frac{m_W^2}{m_Z^2}, \quad (5.5)$$

$$\alpha = \sqrt{2} \frac{G_F m_W^2 \sin^2 \theta_W}{\pi}, \quad (5.6)$$

where $G_F = 1.16638 \times 10^{-5}$ GeV⁻² is Fermi's constant. Note that the actual numerical difference between one scheme and the other should not be terribly large, as the RG running of the electroweak parameters is much lesser than that of the strong coupling and the PDFs; the important part is consistency in the renormalization of quantities that are closely related.

The strong coupling and the PDFs are still allowed to run with scale according to the $\overline{\text{MS}}$ scheme; the dependence of these upon the scale is calculated in LHAPDF.

Where our conventions differ from those commonly used in software for supersymmetry calculations, is in our inclusion of the decay widths of the weak bosons in their propagators. These are often neglected in such packages, as the produced sparticles are expected to be sufficiently heavy that the impact of the widths is fairly small; we choose to include them here as it leads to somewhat more precise results, and makes the calculations more generalizable to the case where the produced particles are light.

Unless otherwise stated, all calculations were done using the PDF4LHC21_40_pdfas [66] Hessian PDF sets to evaluate both PDFs and the strong coupling. Being a fairly modern set, this is expected to give more reliable results in the region where the partonic momentum fractions x approach 1.

This is relevant for calculations with heavy sleptons, as a large initial-state momentum is then needed to produce the sleptons with any significant phase space.

This set contains PDFs for 5 flavors or quarks and antiquarks, plus the gluon; the top quark PDF is presumably low enough that it can be neglected in these calculations. This means taking $N_F = 5$ in the beta function coefficients appearing in Eq. (4.183).

The error in the result due to uncertainty in the PDFs is calculated according to the process described in Ref. [66]. The PDF set contains 43 total members indexed from $i = 0, 1, 2, \dots, 42$: $i = 0$ gives the central cross-section; $i = 1, 2, \dots, 40$ give the PDF error; and $i = 41, 42$ give the error from uncertainty in α_s by using different values for α_s . Denoting the cross-section calculated from PDF member i by σ^i , the PDF error is given by

$$\delta\sigma_{\text{PDF}} = \sqrt{\sum_{i=1}^{40} (\sigma^i - \sigma^0)^2}, \quad (5.7)$$

while the α_s error is

$$\delta\sigma_{\alpha_s} = \frac{1}{2}(\sigma^{42} - \sigma^{41}). \quad (5.8)$$

These two are combined to give the “PDF+ α_s ” uncertainty:

$$\delta\sigma_{\text{PDF}+\alpha_s} = \sqrt{(\delta\sigma_{\text{PDF}})^2 + (\delta\sigma_{\alpha_s})^2}. \quad (5.9)$$

All calculations are made with center-of-mass energy $\sqrt{s} = 13$ TeV unless otherwise stated, matching the energy at the LHC in run II.

5.2 Verification and comparisons

Before moving on to our main results, we need to verify the consistency of our calculations and numerical techniques. To do this, we first compare our results to those obtained from other sources. Obviously the comparison will depend on the choices of conventions discussed in the previous section, so we take care to keep track of what conventions are used to make comparisons consistent.

5.2.1 Comparisons to other sources

In Fig. 5.1 we compare our NLO results for left-handed selectrons (with no left-right mixing in the mass eigenstates), for various choices of these conventions, to those obtained from PROSPINO. We evaluated the results for two different PDF sets; the aforementioned PDF4LHC21_40_pdfas set (with 40 members to determine the PDF uncertainty), and the PDF4LHC15_nlo_30_pdfas [67] set (with 30 members) which was used in the PROSPINO calculations. We also tested the impact of excluding the b quark when summing over initial-state partons, hypothesizing that PROSPINO, an older software, may not include it. Finally, as we noted in the previous section, we have so far chosen to include the Z boson width in our calculations, whereas many programs do not; to see how much this changes results we also made our calculations with $\Gamma_Z = 0$. Fig. 5.1 shows the results for all combinations of these three settings.

The largest impact is made by the choice of PDF set, fairly unsurprisingly; as we will see in Sec. 5.4 the PDF error, which is not included in this plot, is one of the main sources of theoretical uncertainty at NLO. Thus the central values of the cross-section evaluated with different sets should be expected to be different, within the PDF uncertainty. The difference from whether the b quark is included or not is smaller, but still exhibits a clear trend in reducing the relative difference to

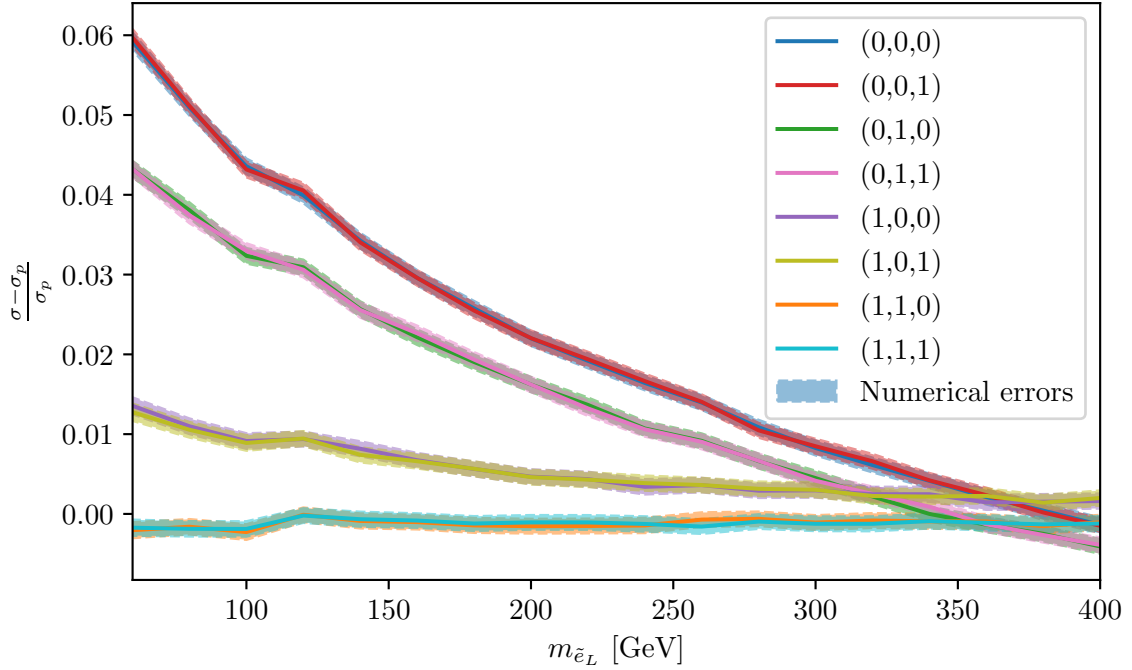


Figure 5.1: Comparison of numerical results for the cross-section for pair-production of left-handed selectrons at NLO, σ , obtained from the expressions in Chapter 4, relative to those obtained from PROSPINO, σ_p . The parentheses (a, b, c) are used as a shorthand for what conventions are used in our calculations: $a = 0, 1$ denotes the use of the PDF set with 40 or 30 members, respectively; $b = 0, 1$ means that 5 or 4 quarks, respectively, were summed over in the initial state; and $c = 0, 1$ means that the Z boson width is included or set to zero, respectively.

the PROSPINO results when it is *not* included. The Z boson width, as anticipated in the previous section, has little consequence on the results when the final-state masses are so far above m_Z ; its impact will mostly show up for final-state invariant masses around m_Z .

In the end, when using the same PDF set as PROSPINO, and not including the b quark or Z width, the results are in good agreement up to numerical errors, though this agreement is fairly dependent on conventions.

For a more general comparison to PROSPINO, we show our NLO results for a collection of different final states (including the previous left-handed selectron pair, for comparison purposes), obtained with the “standard” conventions as described in Sec. 5.1, compared to those obtained with PROSPINO, in Fig. 5.2. The behavior is mostly the same in all cases, with some deviations in the charged-current processes.³

These deviations might be due to differences in how the (squared) CKM matrix elements are dealt with. In Eqs. (4.205), (4.206), and (4.207), they are kept general as $|V_{qq'}|^2$, for any up-type quark q and down-type q' . Using experimentally obtained absolute values of the entries of the CKM matrix, allowing for interactions across quark generations, will lead to the most accurate results; it may also, however, take significantly longer to evaluate than simply keeping the matrix diagonal. The latter allows us to sum over only one incoming quark flavor, the other being required to belong to the same generation, instead of summing over both as in the former case. In Fig. 5.2 we have evaluated the expressions in both cases; when the CKM matrix is kept diagonal, the charged-current

³These are mediated by W^\pm bosons, with a slepton and sneutrino in the final state.

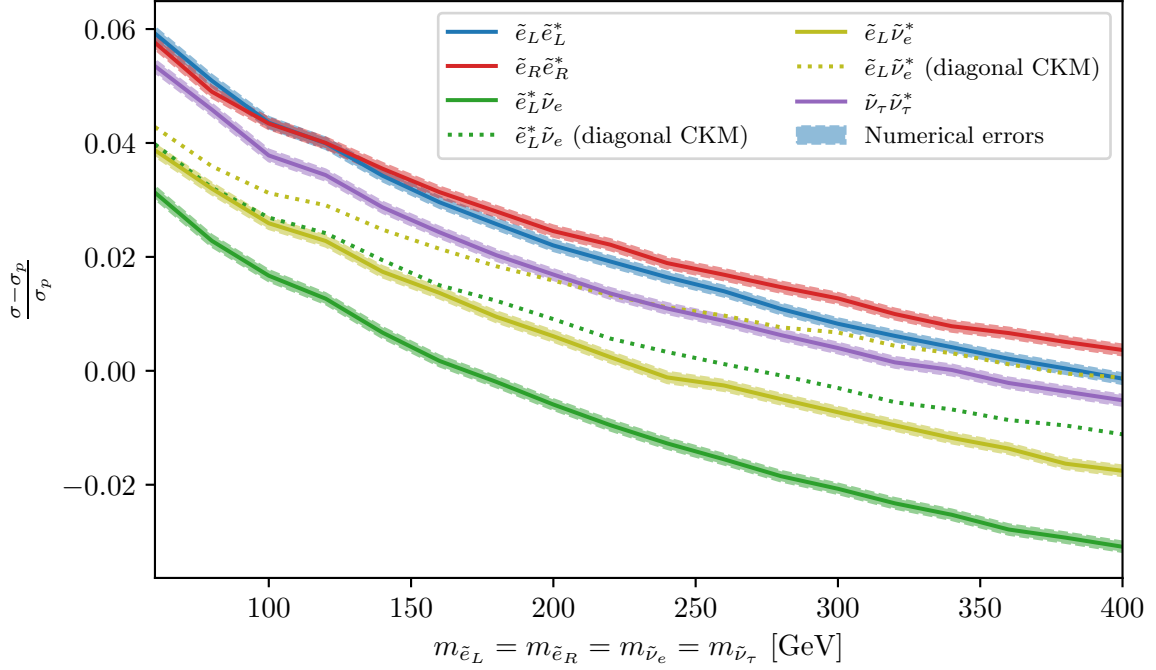


Figure 5.2: Comparison of our NLO results, σ , to those obtained in PROSPINO, σ_p , for a variety of different final states. For the charged-current process we also show the result when the CKM matrix is taken to be diagonal, shown by dotted lines.

results are similar to the neutral-current ones, suggesting that PROSPINO may indeed be using a diagonal CKM matrix.

A similar comparison to RESUMMINO, but now comparing the results at NLO+NLL, is shown in Fig. 5.3. This shows largely the same behavior as in Fig. 5.2, suggesting that any major differences between the calculations stem from differences in convention also in this case.

This comes with a slight caveat, though. Even though the final NLO+NLL results from our calculations and from RESUMMINO are similar, and well within the PDF uncertainties as shown in Sec. 5.4, there is a somewhat notable difference in that our cross-section increases slightly when adding resummed contributions (again, see Sec. 5.4), whereas it decreases, also slightly, in the RESUMMINO results. There are several reasons why this may be happening, notably possible differences in exactly how the improved resummation formalism, as discussed in Sec. 4.7.5, is defined, or in the matching procedure. RESUMMINO also treats the PDFs differently for resummed contributions, using a fitting and evolution procedure in Mellin space [59]. Regardless, as we noted the NLO+NLL results from the two sources are still in fairly good agreement.

Again, like in the comparison to PROSPINO, the behavior for the charged-current process is markedly different from the other cases. This suggests that also RESUMMINO may be using a diagonal version of the CKM matrix.⁴ Our numerical implementation thus represents an improvement on the current standard for slepton-sneutrino production, in terms of accuracy.

Lastly we make a note on the efficiency of the different codes, specifically in comparing our results to those of RESUMMINO. A comparison of the time elapsed when evaluating the cross-section for left-handed selectron pair production at NLO+NLL, for a set of 100 randomly chosen

⁴This can be verified in the RESUMMINO source code; as of version 3.1.1, the diagonal version is used as the standard.

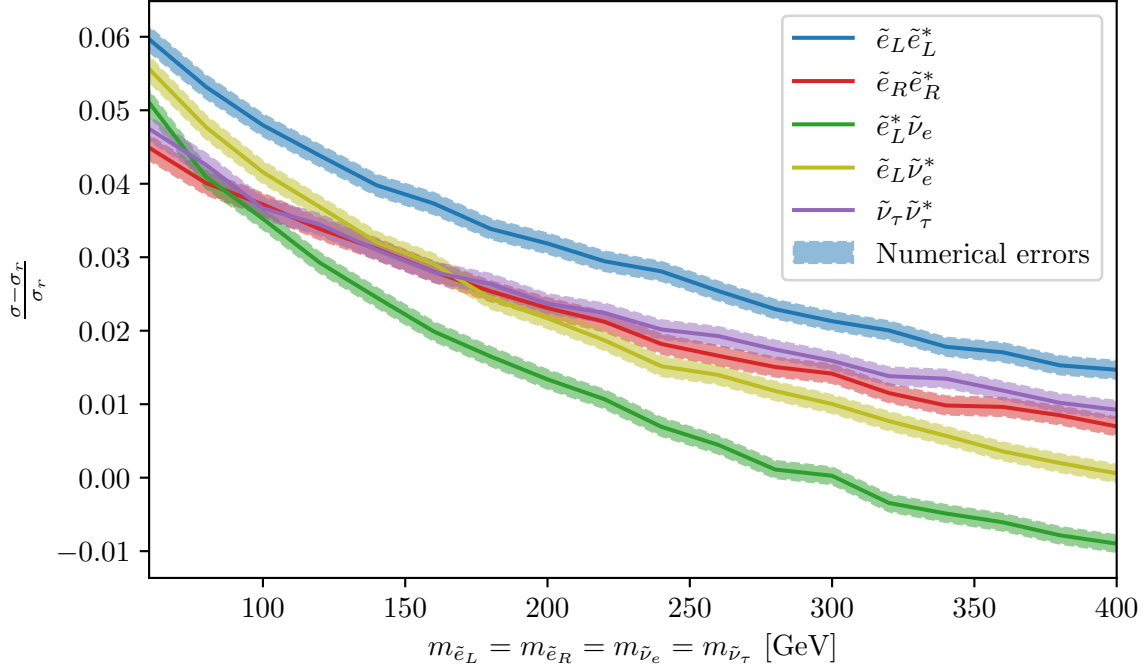


Figure 5.3: Similar to Fig. 5.2, but now comparing our NLL results, σ , to those from RESUMMINO, σ_r . Our charged-current results were obtained keeping the off-diagonal terms in the CKM matrix.

parameter points,⁵ is shown to the left in Fig. 5.4 along with the relative numerical error. We see that our calculations lead to significant speed-up, without sacrificing numerical precision.

This is likely due in large part to the fact that we have made our expressions analytical to the extent that it is possible, thus reducing the need to load external packages. We do rely on LoopTools for the supersymmetric QCD contributions, and on LHAPDF for the PDFs and strong coupling, but everything else is analytical. In particular this includes the virtual QCD loop as explained previously, which is computed significantly faster with the analytical expression rather than having to evaluate all of the Passarino-Veltman functions of Eq. (4.58). We were also able to reduce the dimensionality of many of the integrals with the manipulations of Sec. 3.3.1.

Another difference, which we noted already in comparing the NLO+NLL cross-sections to RESUMMINO, is how the PDFs and inverse Mellin transform are dealt with. As explained in Sec. 4.7.7 we opted to use differentiated PDFs in x -space, which were calculated once and then stored, to reduce oscillations in the resummed expressions for large N . This should make the convergence of integrals quicker, with better stability in the partonic cross-section, and does not require any additional calculations at run-time. In comparison, RESUMMINO evaluates PDFs in Mellin space through a least-squares fitting procedure at run-time [59], which may both be time-consuming and vulnerable to numerical uncertainty.

A similar comparison for the production of $\tilde{e}_L^* \tilde{\nu}_e$, via a W^+ boson, is shown to the right in Fig. 5.4. As we noted above, the fact that we chose to include the full form of the CKM matrix, and not assume that it is diagonal, is expected to slow down the evaluation by requiring a sum over more quarks. This is reflected in the times, as our evaluation now takes slightly longer than that of RESUMMINO for most of the points;⁶ still, our evaluation is more consistent in speed, and has a

⁵These were generated by random sampling on the MSSM parameter space.

⁶Notice also that the RESUMMINO calculation is faster than for the neutral-current process, since the charged W^+ boson, restricts each incoming quark flavor to be either a quark or antiquark, depending on isospin, as opposed to

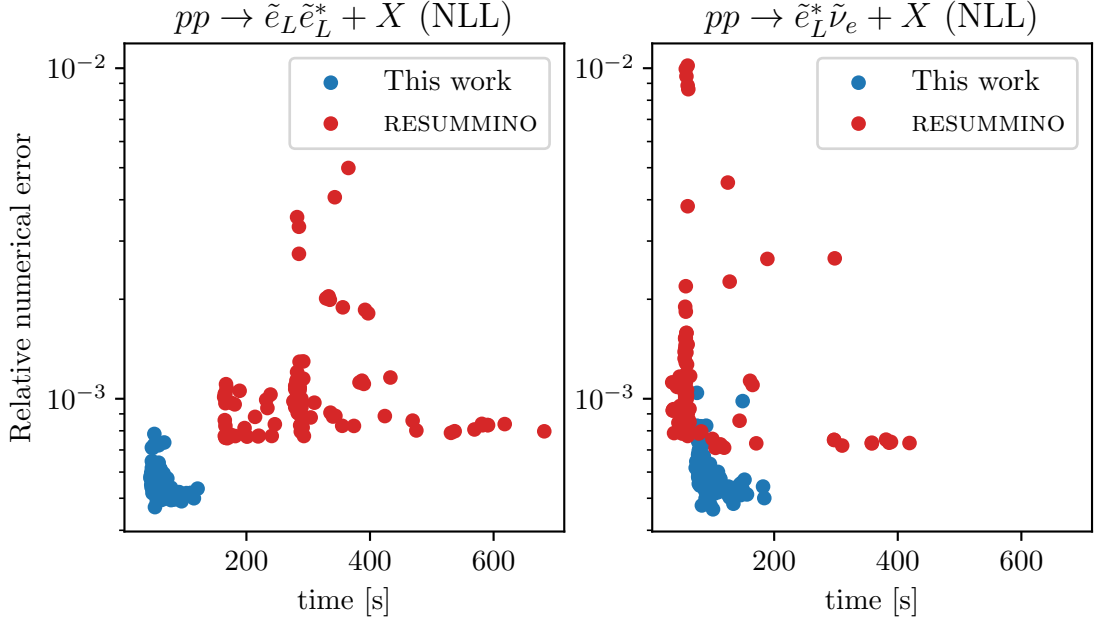


Figure 5.4: Comparison of time elapsed and relative numerical error for neutral- and charged-current processes, both in the evaluation of the cross-section at NLO+NLL, for our code and RESUMMINO. For both processes, 100 MSSM parameter points were randomly selected. All calculations were done on the same machine.

lower numerical uncertainty. Thus, since the difference in speed is not very large, we would argue that it is a fair trade-off in achieving better accuracy with the more general CKM matrix form.

5.2.2 Inverse Mellin transform

Lastly, we check the consistency of the numerical inverse Mellin transform as described in Sec. 4.7.7. To do this, we calculate the total cross-section at NLO for left-handed selectron pair production as a function of selectron mass, both conventionally and from the Mellin-space partonic cross-section of Sec. 4.6, and compare the two. This is shown in Fig. 5.5.

The uncertainty shown is purely numerical, from the integration. We note that the agreement is good, if not necessarily perfect; better agreement might be reached using more integration points than we have done here.⁷ Furthermore, to evaluate the harmonic numbers $S_1(N) \equiv \sum_{n=1}^N \frac{1}{n}$ for complex N , we used the series expansion

$$S_1(N) \sim \ln \bar{N} + \frac{1}{2N} - \sum_{k=1}^{\infty} \frac{B_{2k}}{2k N^{2k}}, \quad (5.10)$$

where B_i are the Bernoulli numbers, up to $\mathcal{O}(\frac{1}{N^{10}})$. Thus the agreement will never be perfect. When taking the inverse Mellin transform of resummed results, which are given exactly in terms of logarithms of N , no such approximation is necessary, so the precision is likely better in that case.

the γ, Z bosons that allow both. Thus RESUMMINO only needs to fit half as many PDFs in Mellin space.

⁷The purpose of the calculation from Mellin space partonic expressions was mainly to get a rough comparison to the real-space results, so the numerical routine can likely be refined.

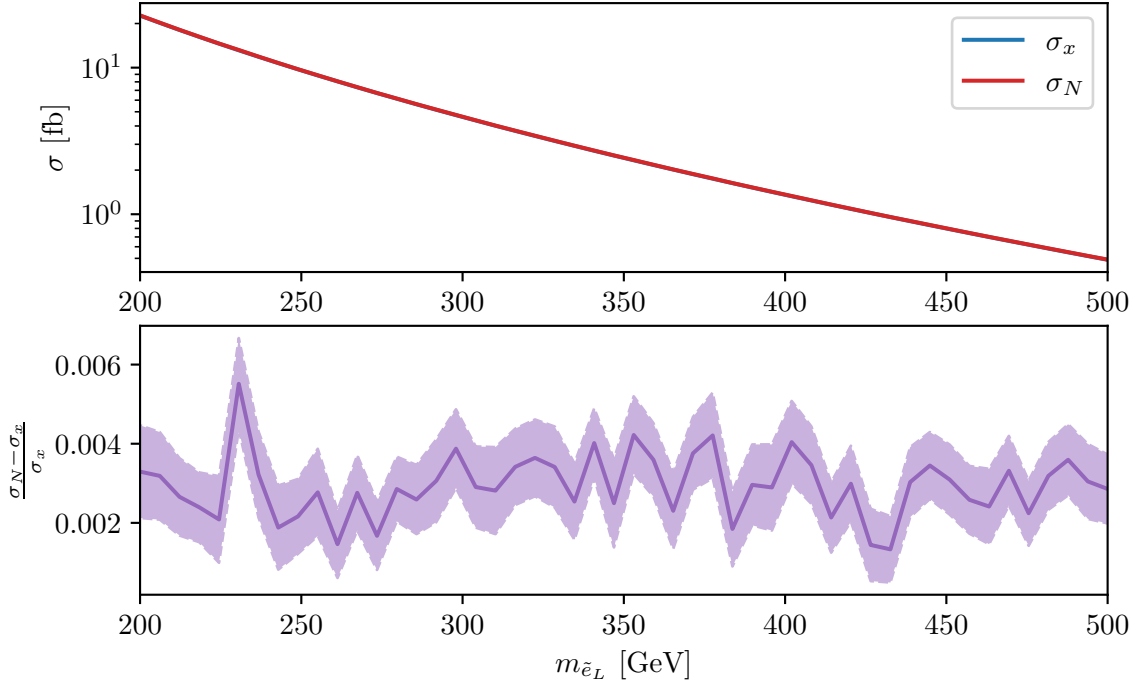


Figure 5.5: Comparison of the total cross-section at NLO for left-handed selectron pair production obtained from the conventional x -space expressions of Eqs. (4.116) and (4.117), denoted by σ_x , to those obtained from the Mellin moments of the partonic cross-section, Eqs. (4.133) and (4.127), denoted by σ_N . The upper plot shows both results as functions of the selectron mass (the difference is too small to be visible here), while the lower shows their relative difference. All squark masses are set equal at $m_{\tilde{q}} = 1$ TeV, with all squark mixing angles $\theta_q = 0$; the gluino mass is set to $m_{\tilde{g}} = 2$ TeV.

There could also be a small uncertainty in the numerical differentiation of the PDFs,⁸ cf. the discussion in Sec. 4.7.7, as the numerical uncertainty from the differentiation is not included. Regardless, the difference is of the same order of magnitude as the numerical uncertainty and far smaller than the scale and PDF uncertainties, so the agreement is good enough for our purposes.

5.3 Scale dependence

One of the most important motivations for calculating higher-order corrections to cross-sections is the expected reduction in dependence upon the unphysical energy scale μ . Being an arbitrary unphysical parameter it must drop out of any exact computation; in other words, if we could somehow calculate all of the contributions to a process in perturbation theory, we would expect the μ dependence to cancel entirely. Any higher-order correction to a perturbative result represents a step toward this idealized scenario; thus we expect the μ dependence to gradually decrease as we include more contributions.

This is also the logic behind defining the theoretical uncertainty from missing higher orders by varying the scale between 2 and 1/2 times the central scale; as μ is expected to drop out when including all contributions one expects the exact result to lie somewhere in the range reached when

⁸The derivative was calculated using cubic spline interpolation, using the grid on which the PDF values are stored as reference points.

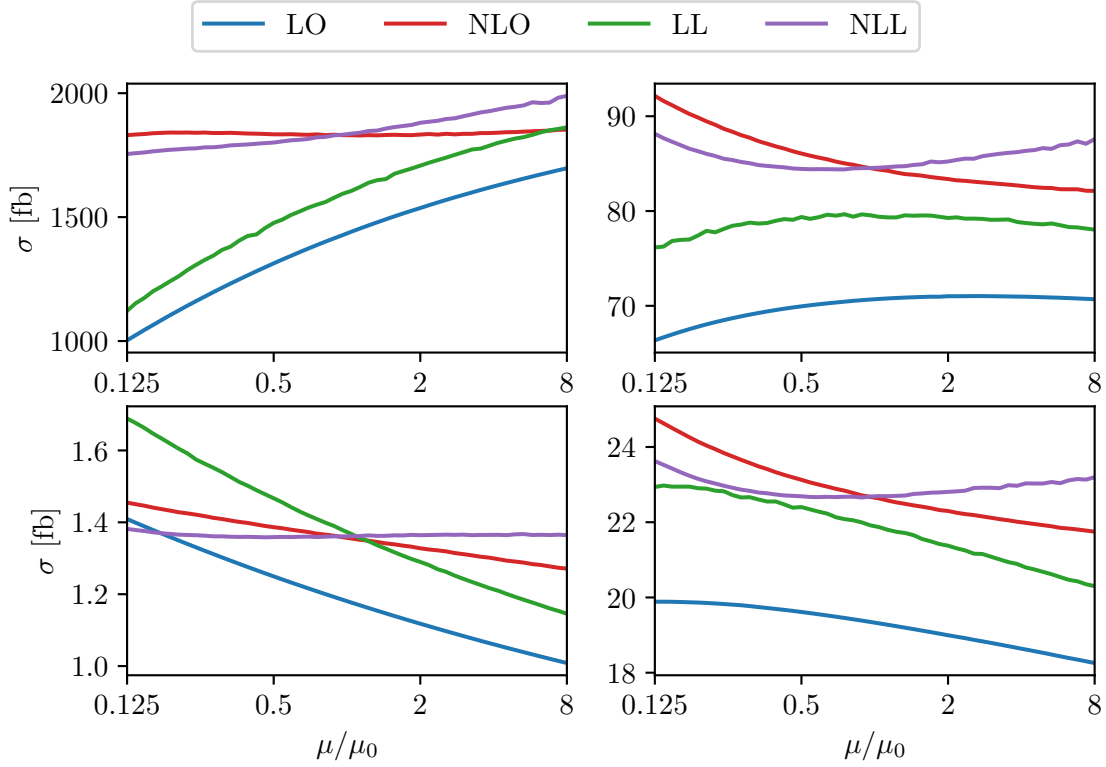


Figure 5.6: Scale-dependence of the total cross-section for pair production of left-handed selectrons, given as a function of the ratio of the scale to the central scale $\mu_0 = m_{\tilde{e}_L}$. Selectron masses (clockwise from top-left) $m_{\tilde{e}_L} = 60$ GeV, $m_{\tilde{e}_L} = 140$ GeV, $m_{\tilde{e}_L} = 200$ GeV, $m_{\tilde{e}_L} = 400$ GeV. All other parameters are identical to those used for Fig. 5.5.

varying the scale. From this perspective we can also understand the choice of μ as some energy scale representative of the interaction, as higher-order corrections will presumably contribute around this scale.

A selection of plots showing the cross-section as a function of the scale are shown in Fig. 5.6.⁹ These exhibit roughly the expected behavior, notably that the scale dependence generally decreases as we go from NLO to NLO+NLL.

Where the behavior clearly differs from the naively expected one is when we add higher-order corrections to the leading-order result; in this case the scale dependence can actually increase, and the higher-order results often lie outside of the expected range obtained by varying the scale. This shows an example of what we discussed at the end of Sec. 1.2.1. At the leading order this is purely an electroweak process, meaning that the only notable scale dependence is from the PDFs; but when including loop corrections the strong coupling also appears, which runs much more rapidly.

This illustrates one of the main flaws of the conventional definition of theoretical uncertainties by scale dependence; the scale dependence at a certain order does not “know” what new couplings may appear at higher orders, thus potentially underestimating the effect of these higher-order terms.

⁹These include results at LO+LL; we obtain these by adding the g_1 term of Eq. (4.185), matched to leading-order (i.e. by taking $\exp(\dots) \approx 1$ in the expansion of Eq. (4.183)), to the leading-order result of Eq. (4.46). In the rest of our figures the LO+LL results are mostly not included, as they mainly just make the figures more cluttered without revealing anything too interesting.

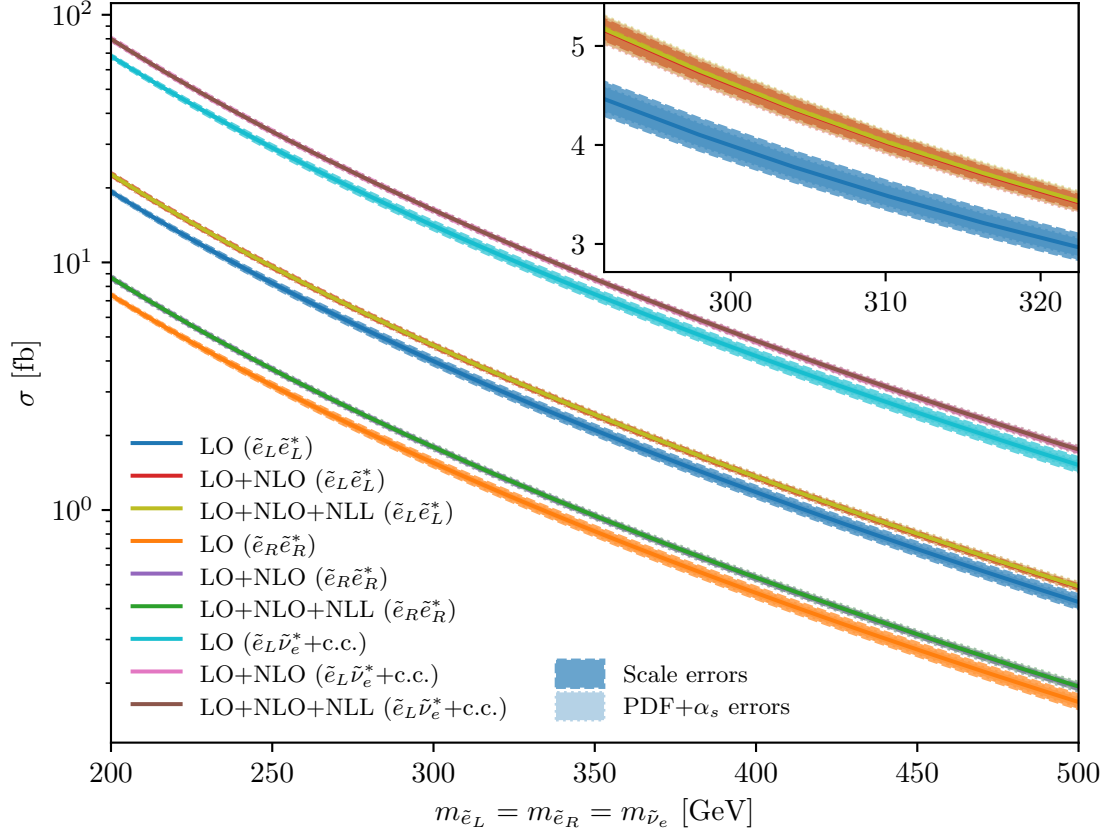


Figure 5.7: Total cross-section for production of either a pair or selectrons, or a selectron-sneutrino pair, as a function of their mass. All MSSM parameters are identical to those used for Fig. 5.5.

5.4 Dependence upon MSSM parameters

Having verified the consistency of our calculations, and seen that higher-order corrections perform as expected in reducing the dependence upon the arbitrary renormalization scale, we can now move on to implement our results for a range of MSSM parameters. This will allow us to investigate how sensitive the cross-section is to variations of the parameters; conversely, it shows what parameters will be the most sensitive to measurements at colliders.

5.4.1 Final-state masses and PDF uncertainty

The most obvious parameter to test is the mass of the produced particles, which will have a significant impact on the available phase space of the particles. Fig. 5.7 shows the total cross-section for selectron production as a function of their mass, with uncertainties from scale variation and PDFs as defined previously. We include all processes with at least one selectron in the final state, be it in a pair of either chirality, or along with a sneutrino. In other words, the processes taken into account are

$$pp \rightarrow \tilde{e}_L \tilde{e}_L^* + X; \quad pp \rightarrow \tilde{e}_R \tilde{e}_R^* + X; \quad pp \rightarrow \tilde{e}_L \tilde{\nu}_e^* + X + \text{c.c.}, \quad (5.11)$$

where X denotes any collection of particles that can be created along with the sleptons, contributing to the inclusive cross-section. To represent all of these cross-sections in the same figure, all final-state particle masses are assumed equal.

The results seen here confirm much of what we have discussed previously; firstly, including QCD corrections to the leading-order cross-section gives a fairly large numerical enhancement, significantly more than what we would naively expect from the scale uncertainty of the LO result. Adding resummed results on top of the fixed-order ones does not give that much of an enhancement, but it does reduce the scale uncertainty by a fair amount. Reduced theoretical uncertainty is invaluable in comparing theoretical calculations to experiments, as it allows us to make far more definitive predictions, and be more stringent in excluding regions of parameter space.

The behavior as a function of the final-state masses is also as expected from kinematical considerations. By momentum and energy conservation, the invariant mass Q of the final-state particles must at least equal their total mass, meaning that the available phase space to be integrated over decreases as the total mass increases. This further means that the Born cross-section becomes increasingly suppressed, as seen from the Q -dependence in Eq. (4.44).

A larger required invariant mass will also suppress the cross-section through the PDFs; from Eq. (4.115) a larger $\tau = Q^2/s$ increases the lower limit on the momentum fractions of the incoming partons, towards regions where their PDF values are significantly smaller.¹⁰

This suppression for large momentum fractions also explains why the PDF uncertainty¹¹ increases with the final-state mass, as seen in Fig. 5.7, simply from a lack of sufficient data. This happens since as we just noted, the larger required invariant mass forces the momentum fractions of the partons to increase. Conversely, however, to fit PDFs in this region to experiment we need measurements obtained for large momentum fractions. This is difficult in practice if the produced particles are light, since the production cross-section will then be dominated by regions of lower invariant mass and momentum fractions. Thus, since all currently discovered particles have masses below 200 GeV, i.e. to the left of the range shown in Fig. 5.7, it is a challenge to gather enough experimental data to precisely determine PDFs in the large- x region, and consequently to precisely compare theoretical cross-sections for production of heavy particles to experiment.

This comparison can potentially be made simpler, even without improving the PDFs, with higher center-of-mass energies in colliders. This can be understood from our above discussion; as stated, the lower limit on the partonic momentum fractions is $\tau = Q^2/s$. A higher center-of-mass energy \sqrt{s} will then allow the momentum fractions to be low even if the invariant mass Q is large, allowing regions of phase space with lower PDF uncertainties to be the dominant contribution to the cross-section.

A recent increase in center-of-mass energy from $\sqrt{s} = 13$ TeV to $\sqrt{s} = 13.6$ TeV at the LHC can help improve the uncertainty, as shown in Fig. 5.8. Here we compare the relative PDF uncertainty (*not* including α_s uncertainty this time) for (selectron-) sneutrino pair production as a function of sneutrino mass for the two center-of-mass energies; the relative uncertainty is clearly reduced, especially for larger masses. To further illustrate the point we also include results for a hypothetical 20 TeV collider, in which the relative PDF error is further reduced.

5.4.2 Mass mixing

As we discussed in Sec. 2.4, for stau particles we in general expect the mass eigenstates not to correspond to the chiral eigenstates. The mixing between these eigenspaces is described by the parameter θ_τ . As we have done our calculations with mass eigenstates, a non-zero mixing angle will not affect the phase space, since the final-state masses are unchanged. This further means that the relative enhancement from LO to NLO (with just QCD) and NLO+NLL should not be affected, as the preferred region of phase space — and hence the preferred values of $z = Q^2/\hat{s}$ —

¹⁰The PDFs $f_i(x)$ decrease drastically as x increases. This is largely owing to the running of the strong coupling, which causes low momenta to be preferred.

¹¹Really the combined PDF and α_s uncertainty, but this is dominated by the PDF.

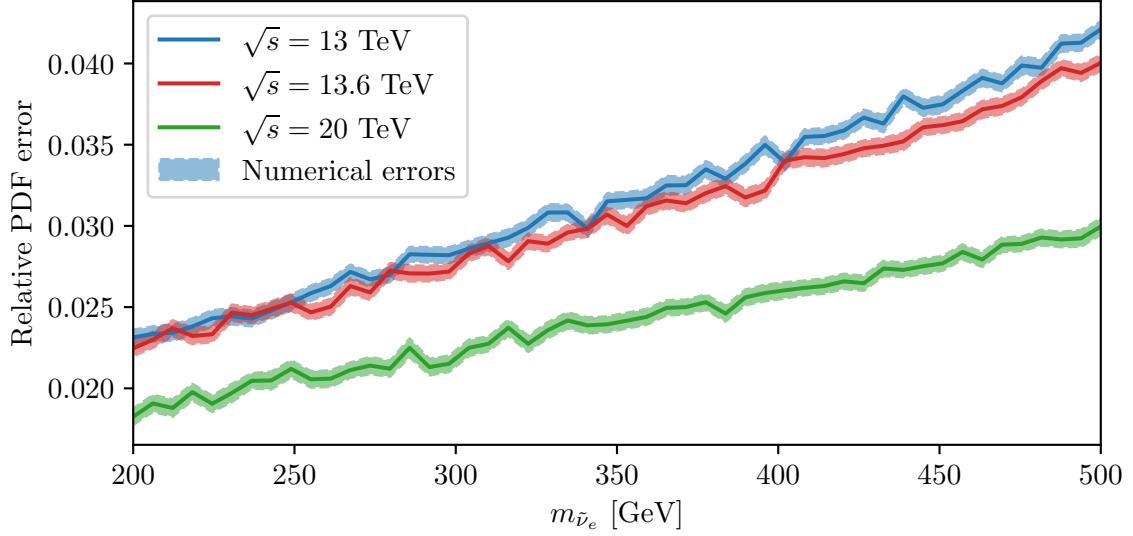


Figure 5.8: Relative PDF uncertainty for $\tilde{\nu}_e \tilde{\nu}_e^*$ production at NLL, for varied center-of-mass energies.

are unchanged. The entire effect of the mixing angle will show up in the effective coupling $F_{q\ell}^{\alpha\beta}$, defined in Eq. (4.27), and its 1-loop versions, where it appears since the Z boson couples differently to left- and right-handed particles.

In Fig. 5.9 we show the dependence of the NLL cross-section upon the mixing angle, as well as the so-called K -factor $K = \sigma/\sigma_{\text{LO}}$, i.e. the relative enhancement from the leading-order result. The latter supports the above discussion, as the K -factor is roughly constant with respect to the mixing angle, except for a few fluctuations of the order of magnitude of the numerical uncertainty.

The mixing angle can, not unexpectedly, have a significant impact on the value of the cross-section. For particle-antiparticle pairs, configurations where the produced sleptons approximately correspond to the left-handed chiral eigenstate (meaning $\cos\theta_\tau = 1$ for $\tilde{\tau}_1 \tilde{\tau}_1^*$ production, and $\cos\theta_\tau = 0$ for $\tilde{\tau}_2 \tilde{\tau}_2^*$ production) are preferred, simply because the $\text{SU}(2)_L$ gauge group only couples to left-handed fields. For the mixed final state $\tilde{\tau}_1 \tilde{\tau}_2^*$ (or its complex conjugate) there is no production at all for the extreme cases of $\cos\theta_\tau = 0, 1$, as in these cases the mass eigenstates correspond exactly to chiral eigenstates, and production of unequal-chirality pairs is not possible. When there *is* mixing between the two eigenspaces, the maximum cross-section is achieved when $Z_\tau^{\alpha\beta}$, as defined in Eq. (4.3), is maximized, i.e. for $\cos\theta_\tau = 1/\sqrt{2}$ or $\theta_\tau = 45^\circ$.

To further investigate this maximum-mixing case, we look at how the cross section for $\tilde{\tau}_1 \tilde{\tau}_2^* + \text{c.c.}$ production depends on the two stau masses, in the case of $\theta_\tau = 45^\circ$. The cross-section as a function of both masses, under the restriction $m_{\tilde{\tau}_2} \geq m_{\tilde{\tau}_1}$, is shown in Fig. 5.10; keeping their average mass fixed at $(m_{\tilde{\tau}_1} + m_{\tilde{\tau}_2})/2 = 200$ GeV, the cross-section as a function of the mass difference is shown in Fig. 5.11.

In both cases, the dependence is largely just a question of kinematics, since the final-state masses do not have any direct influence on the QCD corrections.¹² As we discussed in the previous section, an overall increase in the final-state mass reduces the cross-section, exactly as shown in Fig. 5.10. What is more interesting is that even though the total mass stays the same, so that the available phase space is not affected, a larger mass difference between the stau eigenstate causes the cross-section to decrease. This is again just a consequence of energy and momentum conservation,

¹²They do *indirectly* have some influence on these corrections, through the dependence on $z = Q^2/\hat{s}$, where Q^2 is necessarily increased by a larger final-state mass.

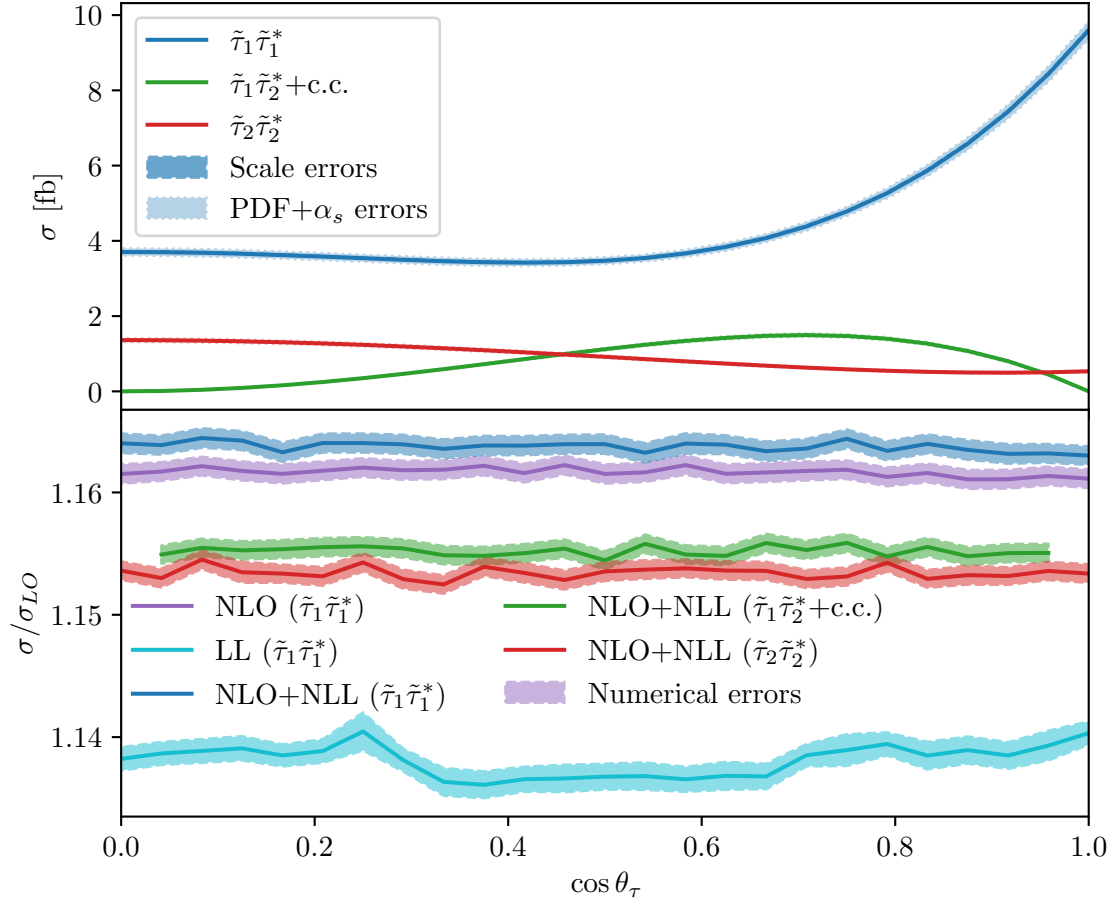


Figure 5.9: Top: NLL total cross-section for production of a pair of stau particles, for all combinations of mass eigenstates, as a function of mixing angle θ_τ . Stau masses are set to $m_{\tilde{\tau}_1} = 250$ GeV, $m_{\tilde{\tau}_2} = 400$ GeV; for other parameters, see Fig. 5.5. Bottom: Relative enhancement compared to leading-order results.

which causes the momentum factor of Eq. (4.10) to decrease for unequal masses.

5.4.3 Squark and gluino masses

In the theoretical calculations of the last chapter, in particular when adding loop effects from supersymmetric particles, we emphasized generality, in principle allowing for separate values for each of the 12 squarks, and the 6 squark mixing angles. In this way as many parameters as possible can be specified when evaluating the expression, enabling a more complete scan of the parameter space of the theory.

Of course, the squark sector parameters are not expected to have an awfully large impact on the cross-section; the squark-loop contributions only appear at 1-loop level, and are not the main contribution even at this level, as the loop corrections are dominated by soft-gluon effects. Still, with sufficient precision in the theory predictions and the PDFs, these variations can still have a non-negligible impact, at least for the first generation of squarks; these will presumably have the largest impact on the result since the u and d quarks have the largest PDFs.

The total cross-section for left-handed selectron pair production at NLL, as a function of \tilde{u} and \tilde{d} squark masses, are shown in Fig. 5.12. As anticipated the effect is fairly small, smaller

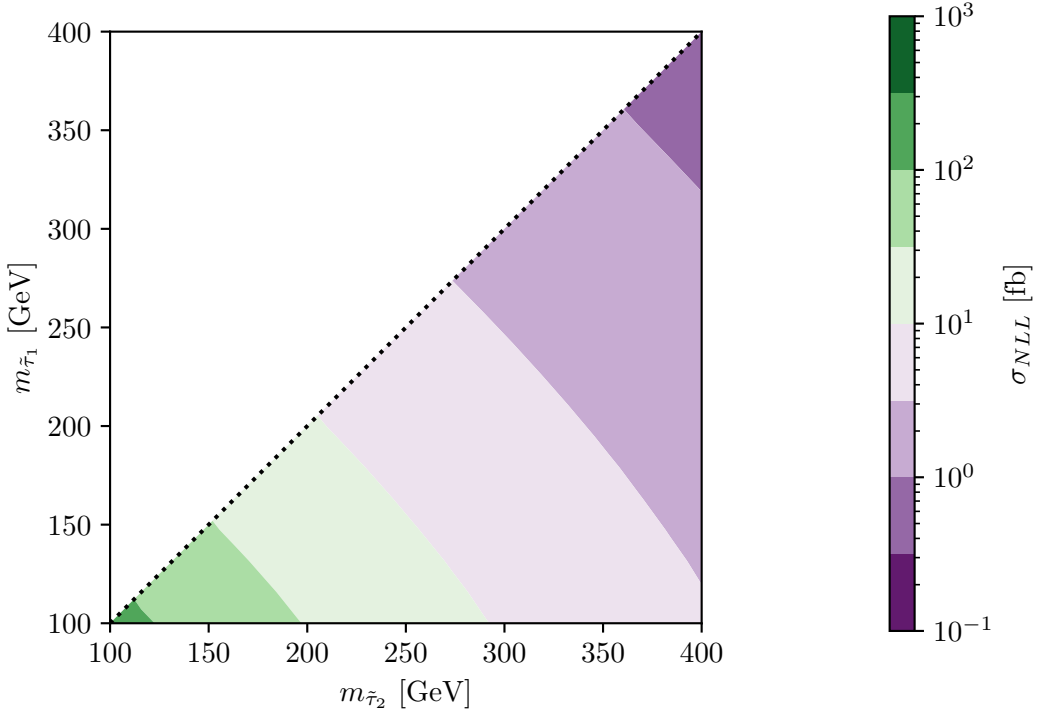


Figure 5.10: Inclusive cross-section for $pp \rightarrow \tilde{\tau}_1 \tilde{\tau}_2^* + \text{c.c.}$ at NLO+NLL accuracy, as a function of the stau masses. Maximum mixing between mass and chiral eigenstates are assumed, i.e. $\theta_\tau = 45^\circ$. Squark and gluino sector parameters are the same as for Fig. 5.5.

than the theoretical uncertainty. Still, as noted above, with improved theoretical precision the effect can be non-negligible in comparison with experimental data. Not surprisingly the largest effect is seen for \tilde{u} masses, simply because the $u\bar{u}$ initial state, which is where this loop appears, is the main contribution to the cross-section. Furthermore, as we noted previously the left-handed particles generally dominate as they have $SU(2)_L$ couplings; as a consequence the cross-section is more sensitive to changes in the left-handed squark masses than right-handed ones.

The cross-section can also depend on the gluino mass, albeit more weakly; on the one hand they appear in every squark-gluino loop, independent of flavor, but each loop only has one power of the gluino propagator, versus two for the squarks. The cross-section as a function of squark and gluino masses, assuming all squark masses are equal, is shown in Fig. 5.13. Here we see a more pronounced dependence than before, due to the fact that we are now varying masses in every squark-gluino loop regardless of flavor. As anticipated the cross-section is more strongly dependent on the squark mass than the gluino mass.

A few things in Fig. 5.13 are worth commenting on. For one, we see clearly in the upper right-hand corner that as the particles in the loop become significantly heavier than the sleptons, and thus far above the dominant invariant mass contributions, they *decouple*. This means that the loop makes barely any contribution to the cross-section, and is seen from the fact that the cross-section becomes nearly independent of the squark and gluino masses.

As an aside, this behavior illustrates the usefulness of effective field theories, in which particles that are far more massive than experimental energy scales are integrated out. If the heavy particles are sufficiently heavy they *decouple* and do not affect observables at lower energy scales. Conversely, this explains the experimental challenge of discovering heavy particles from their appearances in loops, since they affect observables at lower energies only very weakly.

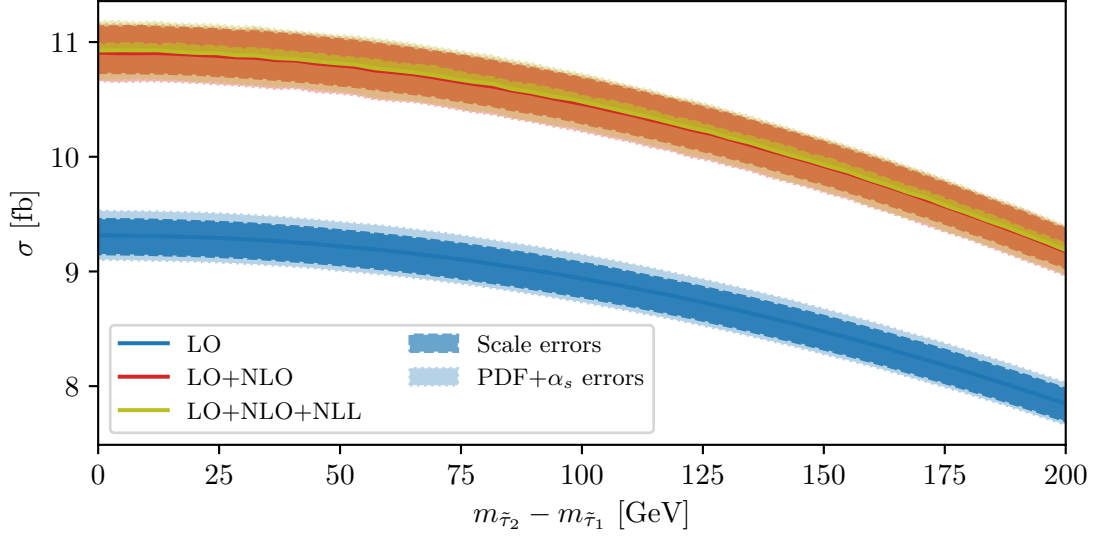


Figure 5.11: Inclusive cross-section for $pp \rightarrow \tilde{\tau}_1 \tilde{\tau}_2^* + \text{c.c.}$ at NLO+NLL accuracy, as a function of the mass separation between the stau eigenstates, $m_{\tilde{\tau}_2} - m_{\tilde{\tau}_1}$, with $(m_{\tilde{\tau}_1} + m_{\tilde{\tau}_2})/2 = 200$ GeV and $\theta_\tau = 45^\circ$. Squark and gluino sector parameters are the same as for Fig. 5.5.

The behavior for small squark and gluino masses, seen in the lower left-hand corner of Fig. 5.13, is also interesting. As the masses drop below the selectron mass, $m_{\tilde{q}}, m_{\tilde{g}} \lesssim m_{\tilde{e}_L}$, the total cross-section *decreases* by a fairly significant amount.

The fact that the dominant behavior, as a function of the masses, happens in this region is not that surprising. After all, as we have argued from the Q -dependence of the Born cross-section, the dominant contribution in the space of slepton invariant masses Q^2 is when the invariant mass is as low as possible, while still giving the sleptons a reasonably-sized phase space. In other words the region where $Q^2 \sim m_{\tilde{e}_L}^2$, meaning that the two are on the same order of magnitude, dominates the phase space integration.

Meanwhile, in the virtual loop contributions to the cross-section, including the one including supersymmetric particles, the invariant mass Q^2 is exactly equal to the center-of-mass energy of the partonic initial state, since nothing is radiated off. Q^2 thus represents the relevant energy scale in the loop, as seen from the arguments of the Passarino-Veltman function of Eq. (4.95), so contributions where the masses are around the same scale, i.e. all masses $m \sim Q \sim m_{\tilde{e}_L}$, are preferred.

What is somewhat more surprising is the fact that the cross-section decreases in this region, suggesting negative interference between the leading-order result and the supersymmetric loop correction. It should be noted, however, that the scenario where this happens, i.e. where $m_{\tilde{q}}, m_{\tilde{g}} \lesssim m_{\tilde{e}_L}$, is not terribly relevant from a phenomenological perspective, since squarks and gluinos are typically assumed to be heavier than sleptons in most supersymmetric models.

5.4.4 Weak boson widths

As we saw in Sec. 5.2, whether or not the decay width of the mediating gauge boson is included in the calculation does not make much of a difference when the final-state mass is significantly above the gauge boson mass. Where it will have a large impact is if conservation of energy allows the invariant mass of the sleptons to pass below m_Z ; in other words, if $m_{\tilde{\ell}_{i\alpha}} + m_{\tilde{\ell}_{i\beta}} < m_Z$. Admittedly this is somewhat of a contrived scenario, as it is unlikely that the slepton masses could be that low

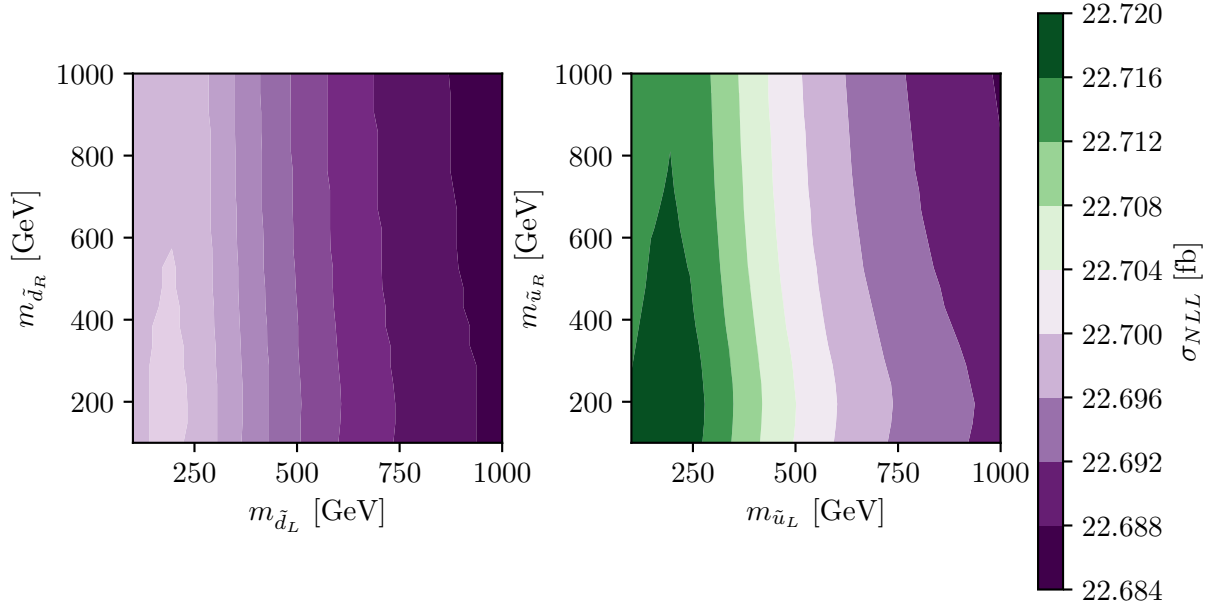


Figure 5.12: Total cross-section for left-handed selectron pair production at NLL, as a function of first-generation squark masses. The selectron mass is set to 200 GeV; the gluino mass $m_{\tilde{g}} = 2$ TeV. All squark masses except \tilde{d} in the left-hand plot and \tilde{u} in the right-hand one, are kept constant at 1 TeV; mass and chiral eigenstates are assumed equal.

without having been discovered already, but more generality in the expressions, and slightly better accuracy, is still an advantage.

Assuming for the sake of the argument that the left-handed selectron has the mass $m_{\tilde{e}_L} = 40$ GeV, we can calculate the invariant mass distribution around $Q = m_Z$ as shown in Fig. 5.14.¹³ The distribution is peaked at $Q = m_Z$ as one would expect, and finite everywhere due to the non-zero decay width. Note also that since the invariant mass is so much lower than in the previously shown results, the PDF ($+\alpha_s$) error is far lower than the scale variation error, even for the NLL results.

¹³This figure shows $\frac{d\sigma}{dQ}$, whereas we have usually stated the differential cross-section as $\frac{d\sigma}{dQ^2}$. The transformation between the two is a simple application of the chain rule for differentiation, that just amounts to $\frac{d\sigma}{dQ} = 2Q \frac{d\sigma}{dQ^2}$.

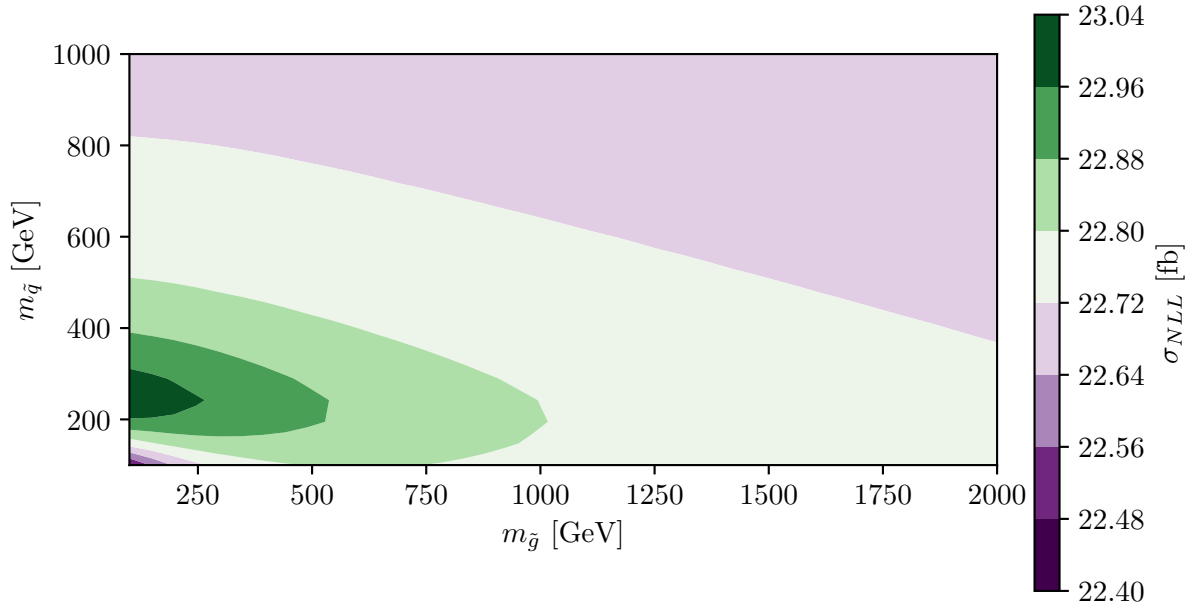


Figure 5.13: Total cross-section for left-handed selectron pair production at NLL, as a function of gluino and squark masses. The selectron mass is set to 200 GeV; all squark masses are assumed equal, with no mixing between mass and chiral eigenstates.

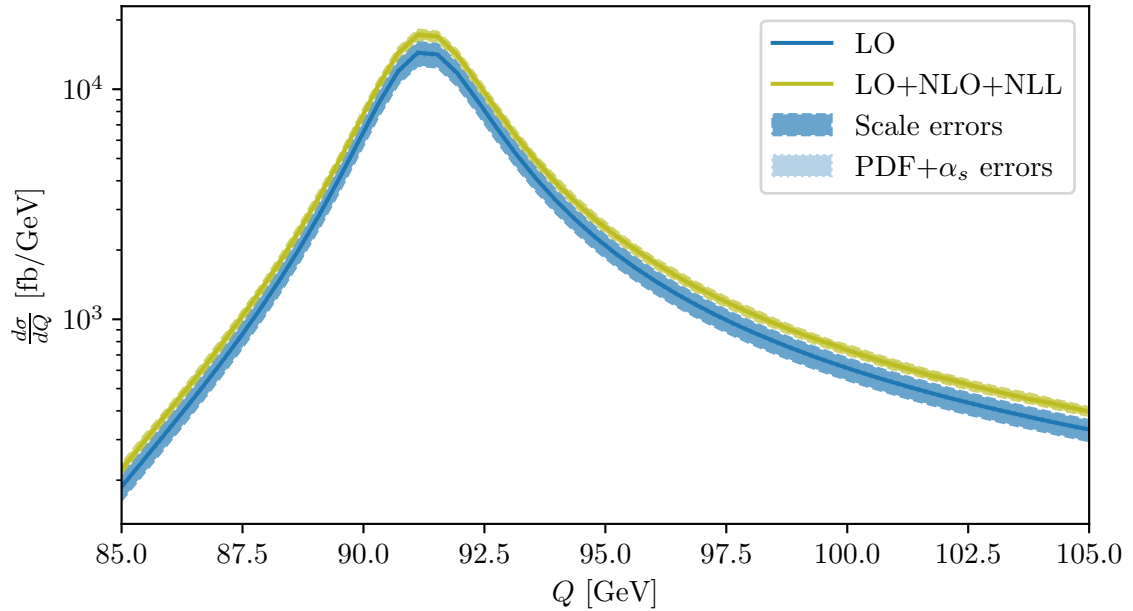


Figure 5.14: Differential cross-section for left-handed selectron pair production as a function of slepton invariant mass Q , for $m_{\tilde{e}_L} = 40$ GeV. Squark and gluino parameters are the same as in Fig. 5.5.

Conclusion

In this thesis we have studied slepton pair production at hadron colliders, and how higher-order corrections affect the inclusive cross-section for this process. First, we presented some theoretical background needed to do calculations in Quantum Chromodynamics with supersymmetric particles.

We reviewed the techniques of regularization and renormalization to remove divergences in perturbative Quantum Field Theory, as well as how momentum integrals can be systematically kept track of using Passarino-Veltman reduction; we gave a brief introduction to supersymmetry as an extension to the symmetry groups of the Standard Model, and to the construction of a minimal supersymmetric extension to the Standard Model (MSSM); and we discussed some technicalities arising when doing calculations in perturbative Quantum Chromodynamics (QCD), in particular the concepts of asymptotic freedom and color confinement, and how they relate to parton distribution functions and the renormalization thereof.

Using these concepts, we calculated the inclusive cross-section for slepton pair production to next-to-leading order. The quantum corrections arising at this order include virtual loop corrections — both from supersymmetric particles, namely squarks and gluinos, and from Standard Model quarks and gluons. Both of these contain ultraviolet divergences, which were removed through renormalization of the quark field; the latter correction also has infrared divergences. These were largely removed when adding all diagrams contributing to the *inclusive* cross-section, i.e. also diagrams with emission of real gluons or quarks; the remaining collinear divergences were removed by renormalization of the PDFs, as discussed in Chapter 3.

With this all divergences have been removed, leaving the finite cross-section at NLO. However, in cancelling the infrared divergences we were left with logarithmic terms that can grow very large in the limit where the energy of the emitted gluons is low, called the eikonal limit. These logarithms were handled by resummation. As we discussed, the cross-section in the eikonal limit can be represented by Wilson lines, which through renormalization can be written on an exponentiated form, thus including the large logarithmic contributions to all orders in perturbation theory. With this we obtained the cross-section at NLO+NL precision.

Upon completion of our analytical calculations, we show some representative results from a numerical implementation of our calculations. These show that the inclusion of QCD corrections to the leading-order cross-section gives a fairly significant increase to the cross-section; far larger, in particular, than the naive estimate obtained from varying the renormalization and factorization scales of the leading-order result, which contains no QCD interactions. The numerical effect of also including resummed results is less dramatic; the main effect here is a reduction in the dependence upon the unphysical scales compared to the fixed-order result, meaning that the theoretical uncertainty is lowered. This is invaluable in comparisons of theoretical models to experiment, as it allows us to be more stringent in excluding regions of the parameter space of the model.

In our results we also include a comparison to standard numerical tools for cross-section calculations in supersymmetry, namely PROSPINO and RESUMMINO. We were able to improve

existing results in several respects. In terms of accuracy, we included off-diagonal contributions from the CKM matrix, and the decay widths of the W and Z bosons, neither of which are done in the existing packages. We also saw that our implementation was quicker than that of RESUMMINO in calculating resummed contributions, while also being more reliable in terms of relative numerical error. Thus it can be used more efficiently in a scan of the parameter space of the MSSM.

There are many paths open for future work on this subject. One possibility is what we just mentioned, using these results in a precise scan of the parameter space of the MSSM, by comparing their predictions to experiment. Even though the results as stated here can be implemented fairly efficiently, being given analytically to a large extent, evaluating the cross-section at a single point can still take over a minute; thus, due to the sheer number of parameters in the model, a straightforward evaluation of every single parameter point is so time-consuming that it becomes completely unfeasible. Instead, it could be more efficient to use machine learning techniques to interpolate on the parameter space.

It is also possible to speed up the numerical evaluation in a number of ways, to potentially aid in such a parameter scan. In particular, as we noted in Sec. 4.6, evaluating the PDFs in Mellin space can simplify and speed up the numerical integration significantly, by reducing the dimensionality of the PDF integrals. To do this efficiently one would ideally need some way of storing PDFs in Mellin space; this is made challenging by the fact that the Mellin variable N is complex, and should be sampled over an infinite range when calculating the inverse Mellin transform. A possible solution is restricting oneself to a particular parametrization of the integration contour, e.g. the one we chose in Eq. (4.200). With such a parametrization N is fixed by a single real parameter, that runs over a finite range; thus it might be possible to store Mellin space PDF values on a grid in this variable. The drawback of this approach is that it does not allow for other integration contours, which might be useful for optimization purposes.

Another possibility is applying the same theoretical methods we have used here to other processes. An obvious generalization is the production of *gauginos* or *Higgsinos* — the fermion supersymmetric partners of gauge bosons and the Higgs particle, respectively — which have production mechanisms similar to those of sleptons. The alternative is looking at production of color-charged particles, like squarks or gluinos, which have larger cross-sections due to their strong interactions. Since both the initial- and final-state particles in such a process are strongly interacting, QCD corrections can arise in both the initial and final state. As a consequence there are many more contributions, both making the calculations more complicated and presumably the higher-order effects more significant.

Appendices

Appendix A

Dirac algebra in d dimensions

Here we note some important relations of Dirac γ matrices that are used in our calculations. These matrices are ubiquitous in amplitude calculations with fermions, so it is very useful to derive a set of reference formulae for them rather than repeat similar calculations endlessly. These can all be derived from the Dirac algebra, given by¹

$$\{\gamma^\mu, \gamma^\nu\} = 2g^{\mu\nu} \mathbb{1}_{4 \times 4}. \quad (\text{A.1})$$

A.1 Contraction identities

From Eq. (A.1) it is fairly straightforward to find expressions for products of several γ matrices, in which one or more pairs of indices are contracted. Such products commonly appear in processes with gauge bosons, where the propagator of the gauge boson contains a factor $g_{\mu\nu}$, forcing a contraction of two indices. Exploiting this contraction and the Dirac algebra will allow us to remove two of the matrices, significantly simplifying calculations.

These expressions can be found recursively; for the case of just two matrices, Eq. (A.1)

$$\gamma^\mu \gamma_\mu = g_{\mu\nu} \gamma^\mu \gamma^\nu = \frac{1}{2} g_{\mu\nu} \{\gamma^\mu, \gamma^\nu\} = g_{\mu\nu} g^{\mu\nu} = d. \quad (\text{A.2})$$

Then, for a product of three matrices, this leads to

$$\gamma^\mu \gamma^\nu \gamma_\mu = 2g^{\mu\nu} \gamma_\mu - \gamma^\nu \gamma^\mu \gamma_\mu = (2 - d) \gamma^\nu. \quad (\text{A.3})$$

Here we first used Eq. (A.1) to swap the order of the first two matrices, and then inserted our result from Eq. (A.2). The calculations for higher numbers of matrices multiplied proceed similarly; assuming that the contraction $\gamma^\nu \gamma^{\mu_1} \gamma^{\mu_2} \dots \gamma^{\mu_{n-1}} \gamma_\nu \equiv A^{\mu_1 \mu_2 \dots \mu_{n-1}}$ is known, we find the next result by

$$\gamma^\nu \gamma^{\mu_1} \gamma^{\mu_2} \dots \gamma^{\mu_n} \gamma_\nu = 2\gamma^{\mu_2} \dots \gamma^{\mu_n} \gamma^{\mu_1} - \gamma^{\mu_1} A^{\mu_2 \dots \mu_n}. \quad (\text{A.4})$$

More specifically, this leads to the following set of identities, used repeatedly in the thesis:

$$\gamma^\mu \gamma_\mu = d, \quad (\text{A.5})$$

$$\gamma^\mu \gamma^\nu \gamma_\mu = (2 - d) \gamma^\nu, \quad (\text{A.6})$$

$$\gamma^\mu \gamma^\nu \gamma^\lambda \gamma_\mu = 4g^{\nu\lambda} + (d - 4) \gamma^\nu \gamma^\lambda, \quad (\text{A.7})$$

$$\gamma^\mu \gamma^\nu \gamma^\lambda \gamma^\rho \gamma_\mu = (4 - d) \gamma^\nu \gamma^\lambda \gamma^\rho - 2\gamma^\rho \gamma^\lambda \gamma^\nu. \quad (\text{A.8})$$

¹The dimensionality of the Dirac matrices is unrelated to the number of spacetime dimensions, so they remain 4×4 matrices even when $d = 4 - 2\epsilon$.

A.2 Trace relations

Our calculations with fermions also typically include taking the trace of products of Dirac matrices, from summing over the spins of the fermions. Such traces actually vanish in many cases, specifically when the number of multiplied matrices is odd. To show this we use $\gamma^5 \equiv i\gamma^0\gamma^1\gamma^2\gamma^3$, which satisfies $\gamma^5\gamma^5 = \mathbb{1}$ and $\{\gamma^\mu, \gamma^5\} = 0$; then, for any product of $n = 2m - 1$ matrices, where $m = 1, 2, 3, \dots$, we have

$$\begin{aligned}
 \text{Tr}[\gamma^{\mu_1} \dots \gamma^{\mu_n}] &= \text{Tr}[\gamma^{\mu_1} \dots \gamma^{\mu_n} \gamma^5 \gamma^5] \\
 &= -\text{Tr}[\gamma^5 \gamma^{\mu_1} \dots \gamma^{\mu_n} \gamma^5] \\
 &= -\text{Tr}[\gamma^5 \gamma^5 \gamma^{\mu_1} \dots \gamma^{\mu_n}] \\
 &= -\text{Tr}[\gamma^{\mu_1} \dots \gamma^{\mu_n}] \\
 &= 0.
 \end{aligned} \tag{A.9}$$

Breaking it down step by step, this is what we have just done: In the first line we multiply by the identity in the form of $\gamma^5\gamma^5$; in the second, we commute the leftmost γ^5 past the n others, picking up a factor $(-1)^{2m-1} = -1$; in the third we use that $\text{Tr}[ABC] = \text{Tr}[CAB]$; and in the fourth we remove the identity. This leaves an expression that is equal to its own negative, i.e. zero.

For products of an even number of matrices, we can find the trace by using the Dirac algebra. The most useful cases are those of two or four matrices multiplied together; if there are more, the expression can often be simplified through the use of our above contraction identities. For two Dirac matrices, we have

$$\text{Tr}[\gamma^\mu \gamma^\nu] = \frac{1}{2} \text{Tr}[\{\gamma^\mu, \gamma^\nu\}] = 4g^{\mu\nu}, \tag{A.10}$$

using again the cyclic property of the trace as well as $\text{Tr}[\mathbb{1}_{4 \times 4}] = 4$. This can in turn be used for the product of four γ matrices; explicitly, through repeated use of the Dirac algebra we find

$$\begin{aligned}
 \text{Tr}[\gamma^\mu \gamma^\nu \gamma^\rho \gamma^\sigma] &= 2g^{\mu\nu} \text{Tr}[\gamma^\rho \gamma^\sigma] - \text{Tr}[\gamma^\nu \gamma^\mu \gamma^\rho \gamma^\sigma] \\
 &= 2g^{\mu\nu} \text{Tr}[\gamma^\rho \gamma^\sigma] - 2g^{\mu\rho} \text{Tr}[\gamma^\nu \gamma^\sigma] + \text{Tr}[\gamma^\nu \gamma^\rho \gamma^\mu \gamma^\sigma] \\
 &= 2g^{\mu\nu} \text{Tr}[\gamma^\rho \gamma^\sigma] - 2g^{\mu\rho} \text{Tr}[\gamma^\nu \gamma^\sigma] + 2g^{\mu\sigma} \text{Tr}[\gamma^\nu \gamma^\rho] - \underbrace{\text{Tr}[\gamma^\nu \gamma^\rho \gamma^\sigma \gamma^\mu]}_{=\text{Tr}[\gamma^\mu \gamma^\nu \gamma^\rho \gamma^\sigma]}.
 \end{aligned} \tag{A.11}$$

We can now solve for $\text{Tr}[\gamma^\mu \gamma^\nu \gamma^\rho \gamma^\sigma]$, and use Eq. (A.10) to get

$$\text{Tr}[\gamma^\mu \gamma^\nu \gamma^\rho \gamma^\sigma] = 4g^{\mu\nu} g^{\rho\sigma} - 4g^{\mu\rho} g^{\nu\sigma} + 4g^{\mu\sigma} g^{\nu\rho}. \tag{A.12}$$

Bibliography

- [1] C.N. Yang and R.L. Mills, *Conservation of Isotopic Spin and Isotopic Gauge Invariance*, *Phys. Rev.* **96** (1954) 191.
- [2] F. Englert and R. Brout, *Broken Symmetry and the Mass of Gauge Vector Mesons*, *Phys. Rev. Lett.* **13** (1964) 321.
- [3] P.W. Higgs, *Broken Symmetries and the Masses of Gauge Bosons*, *Phys. Rev. Lett.* **13** (1964) 508.
- [4] G.S. Guralnik, C.R. Hagen and T.W.B. Kibble, *Global Conservation Laws and Massless Particles*, *Phys. Rev. Lett.* **13** (1964) 585.
- [5] The ATLAS Collaboration, *Observation of a new particle in the search for the Standard Model Higgs boson with the ATLAS detector at the LHC*, *Physics Letters B* **716** (2012) 1.
- [6] M.D. Schwartz, *Quantum Field Theory and the Standard Model*, Cambridge University Press, 1 ed. (2014).
- [7] M.E. Peskin and D.V. Schroeder, *An Introduction to Quantum Field Theory*, Westview Press, 1 ed. (1995).
- [8] S.L. Glashow, *The renormalizability of vector meson interactions*, *Nuclear Physics* **10** (1959) 107.
- [9] S. Weinberg, *A model of leptons*, *Phys. Rev. Lett.* **19** (1967) 1264.
- [10] A. Salam, *Weak and Electromagnetic Interactions*, *Conf. Proc. C* **680519** (1968) 367.
- [11] K.G. Wilson, *Confinement of Quarks*, *Phys. Rev. D* **10** (1974) 2445.
- [12] S.M. Carroll, *Spacetime and Geometry*, Cambridge University Press (7, 2019).
- [13] N. Cabibbo, *Unitary symmetry and leptonic decays*, *Phys. Rev. Lett.* **10** (1963) 531.
- [14] M. Kobayashi and T. Maskawa, *CP Violation in the Renormalizable Theory of Weak Interaction*, *Prog. Theor. Phys.* **49** (1973) 652.
- [15] Z. Maki, M. Nakagawa and S. Sakata, *Remarks on the unified model of elementary particles*, *Prog. Theor. Phys.* **28** (1962) 870.
- [16] R.D. Peccei and H.R. Quinn, *CP Conservation in the Presence of Instantons*, *Phys. Rev. Lett.* **38** (1977) 1440.
- [17] W. Pauli and F. Villars, *On the invariant regularization in relativistic quantum theory*, *Rev. Mod. Phys.* **21** (1949) 434.

- [18] G. 't Hooft and M. Veltman, *Regularization and renormalization of gauge fields*, *Nuclear Physics B* **44** (1972) 189.
- [19] PARTICLE DATA GROUP collaboration, *Review of Particle Physics*, *PTEP* **2020** (2020) 083C01.
- [20] C.G. Callan, Jr., *Broken scale invariance in scalar field theory*, *Phys. Rev. D* **2** (1970) 1541.
- [21] K. Symanzik, *Small distance behavior in field theory and power counting*, *Commun. Math. Phys.* **18** (1970) 227.
- [22] N.N. Bogoliubov and O.S. Parasiuk, *On the Multiplication of the causal function in the quantum theory of fields*, *Acta Math.* **97** (1957) 227.
- [23] K. Hepp, *Proof of the Bogolyubov-Parasiuk theorem on renormalization*, *Commun. Math. Phys.* **2** (1966) 301.
- [24] W. Zimmermann, *Convergence of Bogolyubov's method of renormalization in momentum space*, *Commun. Math. Phys.* **15** (1969) 208.
- [25] G. Passarino and M. Veltman, *One-loop corrections for e^+e^- annihilation into $\mu^+\mu^-$ in the Weinberg model*, *Nuclear Physics B* **160** (1979) 151.
- [26] T. Hahn and M. Pérez-Victoria, *Automated one-loop calculations in four and D dimensions*, *Computer Physics Communications* **118** (1999) 153.
- [27] G.J. van Oldenborgh and J.A.M. Vermaseren, *New algorithms for one-loop integrals*, *Zeitschrift für Physik C Particles and Fields* **46** (1990) 425.
- [28] G. 't Hooft and M. Veltman, *Scalar one-loop integrals*, *Nuclear Physics B* **153** (1979) 365.
- [29] H.J.W. Müller-Kirsten and A. Wiedemann, *Introduction to Supersymmetry*, World Scientific, 2 ed. (2010).
- [30] S.R. Coleman and J. Mandula, *All Possible Symmetries of the S Matrix*, *Phys. Rev.* **159** (1967) 1251.
- [31] R. Haag, J.T. Lopuszanski and M. Sohnius, *All Possible Generators of Supersymmetries of the S -matrix*, *Nucl. Phys. B* **88** (1975) 257.
- [32] S.P. Martin, *A Supersymmetry primer*, *Adv. Ser. Direct. High Energy Phys.* **18** (1998) 1 [[hep-ph/9709356](#)].
- [33] L. Girardello and M.T. Grisaru, *Soft Breaking of Supersymmetry*, *Nucl. Phys. B* **194** (1982) 65.
- [34] M. Gell-Mann, *Symmetries of baryons and mesons*, *Phys. Rev.* **125** (1962) 1067.
- [35] I. Schur, *Neue Begründung der Theorie der Gruppencharaktere*, Sitzungsberichte der Königlich-Preussischen Akademie der Wissenschaften zu Berlin (1905).
- [36] G. Sulyok, *A closed expression for the UV-divergent parts of one-loop tensor integrals in dimensional regularization*, *Phys. Part. Nucl. Lett.* **14** (2017) 631 [[hep-ph/0609282](#)].
- [37] J.C. Collins, D.E. Soper and G.F. Sterman, *Factorization of Hard Processes in QCD*, *Adv. Ser. Direct. High Energy Phys.* **5** (1989) 1 [[hep-ph/0409313](#)].

- [38] G. Altarelli and G. Parisi, *Asymptotic Freedom in Parton Language*, *Nucl. Phys. B* **126** (1977) 298.
- [39] Y.L. Dokshitzer, *Calculation of the Structure Functions for Deep Inelastic Scattering and e^+e^- Annihilation by Perturbation Theory in Quantum Chromodynamics.*, *Sov. Phys. JETP* **46** (1977) 641.
- [40] V.N. Gribov and L.N. Lipatov, *Deep inelastic ep scattering in perturbation theory*, *Sov. J. Nucl. Phys.* **15** (1972) 438.
- [41] S. Catani and L. Trentadue, *Resummation of the QCD Perturbative Series for Hard Processes*, *Nucl. Phys. B* **327** (1989) 323.
- [42] G.F. Sterman, *Summation of Large Corrections to Short Distance Hadronic Cross-Sections*, *Nucl. Phys. B* **281** (1987) 310.
- [43] G.P. Korchemsky and A.V. Radyushkin, *Renormalization of the Wilson Loops Beyond the Leading Order*, *Nucl. Phys. B* **283** (1987) 342.
- [44] G. Korchemsky and G. Marchesini, *Partonic distributions for large x and renormalization of Wilson loop*, *Nuclear Physics B* **406** (1993) 225.
- [45] G.P. Korchemsky and G. Marchesini, *Resummation of large infrared corrections using Wilson loops*, *Phys. Lett. B* **313** (1993) 433.
- [46] A.V. Belitsky, *Two loop renormalization of Wilson loop for Drell-Yan production*, *Phys. Lett. B* **442** (1998) 307 [[hep-ph/9808389](#)].
- [47] E. Laenen, K.J. Larsen and R. Rietkerk, *Position-space cuts for Wilson line correlators*, *JHEP* **07** (2015) 083 [[1505.02555](#)].
- [48] P. Richardson, *Simulations of R-parity Violating SUSY Models*, Ph.D. thesis, Oxford U., 2000. [hep-ph/0101105](#).
- [49] M. Bolz, *Thermal Production of Gravitinos*, Ph.D. thesis, Hamburg U., 2000. 10.3204/DESY-THESIS-2000-013.
- [50] R.E. Cutkosky, *Singularities and discontinuities of Feynman amplitudes*, *J. Math. Phys.* **1** (1960) 429.
- [51] J.G.M. Gatheral, *Exponentiation of Eikonal Cross-sections in Nonabelian Gauge Theories*, *Phys. Lett. B* **133** (1983) 90.
- [52] J. Frenkel and J.C. Taylor, *Nonabelian Eikonal Exponentiation*, *Nucl. Phys. B* **246** (1984) 231.
- [53] G. Bozzi, B. Fuks and M. Klasen, *Threshold Resummation for Slepton-Pair Production at Hadron Colliders*, *Nucl. Phys. B* **777** (2007) 157 [[hep-ph/0701202](#)].
- [54] M. Kramer, E. Laenen and M. Spira, *Soft gluon radiation in Higgs boson production at the LHC*, *Nucl. Phys. B* **511** (1998) 523 [[hep-ph/9611272](#)].
- [55] S. Catani, D. de Florian and M. Grazzini, *Higgs production in hadron collisions: Soft and virtual QCD corrections at NNLO*, *JHEP* **05** (2001) 025 [[hep-ph/0102227](#)].

- [56] S. Catani, M.L. Mangano, P. Nason and L. Trentadue, *The Resummation of soft gluons in hadronic collisions*, *Nucl. Phys. B* **478** (1996) 273 [[hep-ph/9604351](#)].
- [57] G. Bozzi, B. Fuks and M. Klasen, *Transverse-momentum resummation for slepton-pair production at the CERN Large Hadron Collider*, *Phys. Rev. D* **74** (2006) 015001.
- [58] G. Bozzi, B. Fuks and M. Klasen, *Joint resummation for slepton pair production at hadron colliders*, *Nuclear Physics B* **794** (2008) 46.
- [59] B. Fuks, M. Klasen, D.R. Lamprea and M. Rothering, *Precision predictions for electroweak superpartner production at hadron colliders with Resummino*, *Eur. Phys. J. C* **73** (2013) 2480 [[1304.0790](#)].
- [60] J. Fiaschi and M. Klasen, *Neutralino-chargino pair production at NLO + NLL with resummation-improved parton density functions for LHC Run II*, *Phys. Rev. D* **98** (2018) 055014.
- [61] J. Fiaschi, M. Klasen and M. Sunder, *Slepton pair production with aNNLO+NNLL precision*, *JHEP* **04** (2020) 049 [[1911.02419](#)].
- [62] W. Beenakker, R. Hopker and M. Spira, *PROSPINO: A Program for the production of supersymmetric particles in next-to-leading order QCD*, [hep-ph/9611232](#).
- [63] G.P. Lepage, *A New Algorithm for Adaptive Multidimensional Integration*, *J. Comput. Phys.* **27** (1978) 192.
- [64] G.P. Lepage, *VEGAS: An Adaptive Multi-dimensional Integration Program*, .
- [65] A. Buckley, J. Ferrando, S. Lloyd, K. Nordström, B. Page, M. Rüfenacht et al., *LHAPDF6: parton density access in the LHC precision era*, *Eur. Phys. J. C* **75** (2015) 132 [[1412.7420](#)].
- [66] R.D. Ball et al., *The PDF4LHC21 combination of global PDF fits for the LHC Run III*, [2203.05506](#).
- [67] J. Butterworth et al., *PDF4LHC recommendations for LHC Run II*, *J. Phys. G* **43** (2016) 023001 [[1510.03865](#)].